

Evaluation of Bridge Performance and Rating through Non-destructive Load Testing

Final Report

Prepared by:

Andrew Jeffrey, Sergio F. Breña, and
Scott A. Civjan
University of Massachusetts Amherst
Department of Civil and Environmental Engineering
232A Marston Hall
130 Natural Resources Rd
Amherst, MA 01003

Prepared for:

Vermont Agency of Transportation
One National Life Drive
Montpelier, VT 05633

January 2009

1. Report No.	2. Government Accession No.	3. Recipient's Catalog No.	
4. Title and Subtitle Evaluation of Bridge Performance and Rating through Non-destructive Load Testing		5. Report Date January 2009	
		6. Performing Organization Code	
7. Author(s) Andrew Jeffrey, Sergio F. Breña, and Scott A. Civjan		8. Performing Organization Report No. 2009-1	
9. Performing Organization Name and Address University of Massachusetts Amherst Dept. of Civil & Environmental Engineering Marston Hall 232A – 130 Natural Resources Rd Amherst, MA 01003		10. Work Unit No.	
		11. Contract or Grant No.	
12. Sponsoring Agency Name and Address Vermont Agency of Transportation One National Life Drive Montpelier, VT 05633		13. Type of Report and Period Covered Research	
		14. Sponsoring Agency Code	
15. Supplementary Notes None			
16. Abstract Non-destructive load testing can be used as a tool to better understand the field behavior of bridges. Equipment to conduct non-destructive load testing was acquired and used to test two distinctly different bridges that are part of the bridge infrastructure in Vermont. One of the bridges, an old (1920s) reinforced concrete bridge had deteriorated over many years in service and currently carries heavy quarry trucks along its three spans. The other bridge, a non-composite steel bridge on interstate 91, was locally damaged by an over height truck as it passed underneath it. Results from the field tests in these two bridges were used to assess the effects of deterioration and damage on the bridge behavior. Additionally, the results were used to estimate a load rating number for these two bridges consistent with the field measurements taken during the load tests. No detrimental effects of damage or deterioration on bridge performance could be inferred from the non-destructive field test results.			
17. Key Words Non-destructive bridge testing, load rating.		18. Distribution Statement	
19. Security Classif. (of this report)	20. Security Classif. (of this page)	21. No. Pages 271	22. Price

“The information contained in this report was compiled for the use of the Vermont Agency of Transportation. Conclusions and recommendations contained herein are based upon the research data obtained and the expertise of the researchers, and are not necessarily to be construed as Agency policy. This report does not constitute a standard, specification, or regulation. The Vermont Agency of Transportation assumes no liability for its contents or the use thereof.”

TABLE OF CONTENTS

TABLE OF CONTENTS.....	IV
LIST OF TABLES.....	X
LIST OF FIGURES	XIII
ABSTRACT.....	1
CHAPTER 1 - INTRODUCTION.....	2
1.1 Background.....	2
1.1 Bridge Inspection and Load Rating.....	3
1.3 Scope of Work.....	3
1.4 Organization of Report.....	5
CHAPTER 2 - LITERATURE REVIEW.....	6
2.1 Background.....	6
2.2 Proof Load Testing.....	6
2.3 Diagnostic Testing.....	6
2.4 Analysis and Finite Element Modeling.....	9
2.5 Summary of Literature Review.....	10
CHAPTER 3 - DESCRIPTION OF TEST BRIDGES.....	11
3.1 Roylton Bridge VT 14 Br. 28.....	11
3.1.1 Historical Significance.....	12
3.1.2 The Surrounding Area.....	14
3.1.3 Average Daily Traffic.....	15
3.1.4 Overall Geometry.....	16
3.1.5 T-beams.....	17
3.1.5.1 T-Beam Construction Plans.....	17
3.1.5.2 T-Beam Current Condition.....	19
3.1.6 Deck.....	21
3.1.7 Scupper Holes.....	21
3.1.8 Guard Rail.....	22
3.1.9 Abutments.....	24
3.1.10 Piers/Bent caps.....	25
3.1.11 Load Rating and Current Condition.....	26
3.2 Weathersfield Bridge I-91 Br. 30.....	26
3.2.1 History.....	27
3.2.2 Geometry.....	27
3.2.3 Average Daily Traffic.....	28
3.2.4 Abutments.....	28

3.2.5 Piers	29
3.2.6 Girders	29
3.2.6.1 Support Conditions	30
3.2.6.2 Damage From Vehicle Collision	32
3.2.7 Diaphragms.....	32
3.2.8 Deck.....	33
3.2.9 Joints.....	33
3.2.10 Curb and Railing.....	34
3.2.11 Load Rating and Current Condition	34
CHAPTER 4 - TESTING PROCEDURE.....	35
4.1 Testing Equipment.....	35
4.1.1 Strain Gauges.....	35
4.1.2 Strain Gauge Attachment	36
4.1.3 Recording Strain Data	37
4.1.4 Load Vehicle	37
4.1.5 Auto Clicker	38
4.2 Royalton Bridge.....	38
4.2.1 Objective of Load Testing.....	38
4.2.2 Strain Gauge Placement	39
4.2.2.1 Longitudinal and Transverse Placement of Strain Gauges	39
4.2.2.1.1 Placement for Goal #1: Moment Distribution in Beams	41
4.2.2.1.2 Placement for Goal #2: Load Transfer Around Damage	41
4.2.2.1.3 Placement for Goal #3: Load Distribution in Bridge Deck	42
4.2.2.1.4 Placement for Goal #4: Moment Transfer Across Interior Piers.....	42
4.2.2.1.5 Placement for Goal #5: Structural Contribution of Concrete	
Guard Rails	43
4.2.2.2 Vertical Location of Gauges on Beams	43
4.2.2.3 Vertical Location of Gauges on Guard Rail	44
4.2.2.4 Use of Gauge Extensions on Reinforced Concrete.....	45
4.2.2.5 Attaching Gauges to Bridge.....	45
4.2.3 Condition and Weather the During Testing.....	45
4.2.4 Load Vehicle	46
4.2.5 Load Vehicle Position	47
4.2.5.1 Transverse Position and Lanes	47
4.2.5.2 Longitudinal Position.....	47
4.2.6 Repetition of Loading.....	48
4.2.7 Record of Quarry Trucks Crossing Bridge.....	48
4.3 Weathersfield.....	49
4.3.1 Objective of Load Testing.....	49
4.3.2 Strain Gauge Placement	50
4.3.2.1 Longitudinal and Transverse Placement of Strain Gauges.....	50
4.3.2.1.1 Placement for Goal #1: Negative Moment Over Piers	51
4.3.2.1.2 Placement for Goal #2: Composite Action Between Deck And	
Girders	52

4.3.2.1.3 Placement for Goal #3: Effect of Truck Strike on Load Distribution	52
4.3.2.1.4 Placement for Goal #4: Distribution Factor of Deck	52
4.3.2.2 Vertical Placement of Gauges on Girders	52
4.3.2.3 Attaching Gauges to Bridge	53
4.3.3 Condition and Weather During Testing	53
4.3.4 Load Vehicle	53
4.3.5 Load Vehicle Position	55
4.3.5.1 Transverse Position and Lanes	56
4.3.5.2 Longitudinal Position	58
4.3.6 Repetition of Loading	58
CHAPTER 5 - DATA REDUCTION	60
5.1 Data Records	60
5.1.1 Initial Steps of Data Reduction	60
5.2 Royalton Bridge Data Reduction	60
5.2.1 Assessment of Elastic Bridge Response from Raw Strain History Data	61
5.2.2 Repeatability of Data	63
5.2.3 Neutral Axis Calculation	63
5.2.4 Moment Calculation	65
5.2.4.1 Deck in Positive Bending	65
5.2.4.2 Deck in Negative Bending	67
5.2.4.3 Effective Deck Width	68
5.3 Weathersfield Bridge Data Reduction	73
5.3.1 Linear Bridge Response Determined from Raw Strain History Data	73
5.3.2 Repeatability of Data	75
5.3.3 Averaging Data Runs	75
5.3.4 Neutral Axis Calculation	75
5.3.5 Moment Calculation	77
5.3.5.1 Moment of Inertia and Centroid of Steel Girder	78
5.3.5.2 Effective Deck Width	78
5.3.5.3 Deck in Positive Bending	78
5.3.5.4 Deck in Negative Bending	80
CHAPTER 6 - DATA ANALYSIS	85
6.1 Royalton Bridge	85
6.1.1 Transverse Distribution of Strain	85
6.1.1.1 Transverse Strain Distribution at Mid-Span	85
6.1.1.2 Transverse Strain Distribution Near Span Ends	93
6.1.2 Contribution of Guard Rails	98
6.1.2.1 Span 1 - Upstream Guard Rail	99
6.1.2.2 Span 2 - Upstream Guard Rail	100
6.1.2.3 Span 2 - Downstream Guard Rail	102
6.1.2.4 Analysis of Guardrail Contribution	104
6.1.3 Neutral Axis Depth	105

6.1.4	Modulus of Concrete in Moment Calculation	113
6.1.5	Concrete Areas in Tension in Moment Calculation	113
6.1.6	Beam Line Analysis of Span Moments	116
6.1.7	Measured Positive Moment Transverse Distribution	118
6.1.7.1	Global Moment Comparison with Beam Line Analysis	124
6.1.7.2	Guardrail Contribution to Moment	125
6.1.7.3	AASHTO Distribution Factors Comparison	126
6.1.8	Transverse Negative Moment Distribution	128
6.2	Weathersfield Bridge	134
6.2.1	Negative Bending Strain Distribution at Pier Support Sections	134
6.2.2	Positive Bending Strain Distribution at Sections within Middle Span	140
6.2.3	Effect of Truck Impact Damage on Strain Distribution	145
6.2.4	Neutral Axis Depth	150
6.2.4.1	Neutral Axis Depth at Mid-Span	150
6.2.4.2	Neutral Axis Depth Near Pier Support	156
6.2.4.3	Neutral Axis Depth at Damaged Sections	168
6.2.5	Transverse Moment Distribution	175
6.2.5.1	Positive Moment Transverse Distribution	175
6.2.5.2	Negative Moment Transverse Distribution	178
6.2.6	Beam Line Analysis	182
6.2.7	AASHTO Distribution Factor Comparison	183
CHAPTER 7 - BRIDGE MODELING		187
7.1	Model Description	187
7.1.1	Elements	187
7.1.2	Material Properties	189
7.1.3	Support Conditions	189
7.1.4	Rigid Links	189
7.1.5	Lane Definition	190
7.1.6	Truck Configuration and Loading	191
7.1.7	Moments	191
7.2	Finite Element Model Comparison with Beam Line Analysis	193
7.3	Model Comparison with Field Results	194
7.3.1	Positive Moment Comparison with Field Results	194
7.3.2	Negative Moment Comparison with Field Results	197
7.4	Summary of Finite Element Modeling	200
CHAPTER 8 - BRIDGE LOAD RATING		201
8.1	Background	201
8.2	Description of Load Rating Procedure	201
8.3	Analysis and Rating Trucks	203
8.4	Royalton Bridge Rating	204
8.4.1	Selected Bridge Model	204
8.4.2	Flexural Strength Assumptions	205
8.4.3	Royalton Bridge Rating based on Diagnostic Field Tests	206

8.5 Weathersfield Bridge Rating	209
8.5.1 Selected Bridge Model	209
8.5.2 Weathersfield Bridge Rating based on Diagnostic Field Tests	212
 CHAPTER 9 - SUMMARY AND CONCLUSIONS	 218
9.1 Summary	218
9.2 Conclusions	220
9.2.1 Royalton Bridge	220
9.2.2 Weathersfield Bridge	221
9.3 Methodology for instrumentation and data reduction on site specific bridges	222
Limitations on use of equipment and software	224
 APPENDIX A - TESTING OF FIELD EQUIPMENT	 225
A.1 Testing Procedure	226
A.2 Load and Strain Measurement	227
A.3 Analysis and Test Results	228
A.4 Strain Calculation	230
 APPENDIX B - TESTING OF GAUGE EXTENSIONS	 232
B.1 Testing Procedure	232
B.2 Analysis and Test Results	233
 APPENDIX C - GUIDE FOR CONDUCTING LOAD TESTS	 235
C.1 Pre-Inspection Planning	235
C.2 Attaching Strain Gauges	235
C.3 Load Vehicle	236
C.4 Use of More Than One Load Vehicle	237
C.5 Equipment Setup	238
 APPENDIX D - DATA FORMATTING AND VISUAL BASIC	 239
D.1 Formatting Raw Data	239
D.2 Organization of Modified Data	239
D.3 Main Visual Basic Macro	240
D.3.1 Load Truck Position and Time	240
D.3.2 Organization of Data into Gauge Pairs	240
D.3.3 Comparing Data From Repeated Test Runs	241
D.3.4 Calculation of Neutral Axis Depth	241
D.3.5 Strain and Neutral Axis at Incremental Distances	242
D.4 Moment Visual Basic Macro	242
D.4.1 Royalton Moment Calculation	242
D.4.1.1 Royalton Positive Moment Calculation with Neutral Axis in T-Beam Stem	244
D.4.1.2 Royalton Positive Moment Calculation with Neutral Axis in T-beam Slab	245

D.4.1.3 Royalton Negative Moment Calculation	246
D.4.2 Weathersfield Moment Calculation	248
D.4.2.1 Positive Bending Moment of Inertia	248
D.4.2.2 Negative Bending Moment of Inertia	250
D.4.2.3 Weathersfield Moment Equations	252

LIST OF TABLES

Table 4.1: Gauge Combinations of Figure 4.4.....	40
Table 4.2: Royalton Truck Weight (pounds)	47
Table 4.3: Test Record for Royalton Bridge.....	49
Table 4.4: List of Gauge Locations in Weathersfield Load Test.....	51
Table 4.5: Weight of Weathersfield Trucks.....	54
Table 4.6: Test Record for Weathersfield Bridge.....	59
Table 5.1: Gauge Pair Properties Used in Royalton Calculations	70
Table 5.2: Deck Slab Properties Used in Royalton Calculations	71
Table 5.3: Beam Properties Used in Royalton Calculations.....	72
Table 5.4: Properties of Weathersfield Girder Used to Calculate Moment.....	82
Table 5.5: Properties of Weathersfield Deck in Positive Bending	83
Table 5.6: Properties of Weathersfield Deck in Negative Bending.....	84
Table 6.1: Maximum Strain Peaks and Truck Location Cross Section 2 (Lane 1).....	86
Table 6.2: Bottom Gauge Strain for Transverse Distribution Evaluation	89
Table 6.3: Number of Engaged Beams in Bridge Response at Mid-Span.....	92
Table 6.4: Number of Engaged Beams in Bridge Response at Beam Ends	98
Table 6.5: Guardrail Strain Readings	100
Table 6.6: Variation of Neutral Axis Depth at Mid-Span in Interior Beams.....	106
Table 6.7: Stress and Moment in Cross Section (Gauge Pair #23 – Truck at 108 ft).....	116
Table 6.8: Moments from Beam Line Analysis in Cross-Sections at Mid- Span.....	118
Table 6.9: Comparison of Modulus and Cross Sectional Moment.....	119

Table 6.10: Calculated Moments from Field Measurements.....	125
Table 6.11: Calculated Moment in Instrumented Guard Rail Sections	126
Table 6.12: AASHTO Distribution Factors and Design Moment for Royalton Bridge Girders.....	127
Table 6.13: Comparison of Measured Moment to AASHTO Design Moment.....	128
Table 6.14: Moment Comparison of End Span to Mid-Span	129
Table 6.15: Weathersfield Transverse Strain at Pier Supports	135
Table 6.16: Weathersfield Transverse Strain Measurement and Distance	141
Table 6.17: Bottom Gauge Strain for Girder Damage Evaluation	146
Table 6.18: Neutral Axis Depth at Mid-Span	151
Table 6.19: Neutral Axis Depth at Pier Support Cross Sections	157
Table 6.20: Neutral Axis Depth at Damaged Cross Section.....	168
Table 6.21: Calculated Positive Moment in Cross Section 4 from Field Measurement.....	176
Table 6.22: Calculated Negative Moments at Pier Locations from Field Measurement.....	179
Table 6.23: Beam Line Analysis Moment Comparison.....	183
Table 6.24: AASHTO Distribution Factors and Design Moment for Weathersfield Bridge Girders	185
Table 6.25: Comparison of Measured Moment to AASHTO Design Moment.....	186
Table 7.1: Element Material Properties	189
Table 7.2: Effect of Including Shell Moments in Finite Element Model	193
Table 7.3: Comparison of Beam Line Analysis to Finite Element Model Moment.....	193
Table 7.4: Comparison of Finite Element and Field Moments in Positive Moment Region (Girders II-V).....	195
Table 7.5: Comparison Finite Element and Field Moments in Negative Moment Region	197

Table 8.1 – Selection of Bridge Parameters for Load Rating	203
Table 8.2 – Rating Trucks.....	204
Table 8.3 – Interior Girder Dead and Live-Load Moments (Impact factor not included) Calculated Using Beam Line Model.....	206
Table 8.4 – Ratio of Test to Calculated Rating Factor (K) Based on Non-composite Section Bottom Strains	207
Table 8.5 – Operating Rating Based on Uncracked Section Properties ($f_y = 33$ ksi)	207
Table 8.6 – Inventory Rating Based on Uncracked Section Properties ($f_y = 33$ ksi)	208
Table 8.7 –Posting Values Based on Uncracked Section Properties ($f_y = 33$ ksi)	208
Table 8.8 – Summary Rating Table: Royalton Bridge (tons) *	209
Table 8.9 – Dead and Live-Load Moments Calculated Using 3D-FEM Model	212
Table 8.10 – Ratio of Test to Calculated Rating Factor (K) Based on Non-composite Section Bottom Strains	214
Table 8.11 – Operating Rating Based on Non-composite Section Properties	215
Table 8.12 – Inventory Rating Based on Non-composite Section Properties	216
Table 8.13 –Posting Values Based on Non-composite Section Properties.....	217
Table 8.14 – Summary Rating Table: Weathersfield Bridge (tons) *	217
Table A.1: Reference Loads Applied to Beam	229
Table A.2: Comparison of Theoretical Calculated and Measured Strain	230
Table D.1: Input Parameters for Positive Bending Moment Calculation	244
Table D.2: Input Parameters for Moment Calculation with Positive bending.....	247
Table D.3: Input Parameters for Composite Sections in Positive bending.....	249
Table D.4: Input Parameters for Composite Sections in Negative Bending	250

LIST OF FIGURES

Figure 1.1: Photographs of Subject Bridges	4
Figure 3.1: Diagram of Spaulding Bridge	11
Figure 3.2: Picture of Spaulding Bridge taken in 1927	12
Figure 3.3: Photograph of Electric Generating Plant Just Below Bridge	13
Figure 3.4: Line of Trucks from Quarry Stopped During Load Test	15
Figure 3.5: Quarry Truck Crossing Birdge	16
Figure 3.6: Royaltan Bridge Cross Section with Beam Seat Steps	17
Figure 3.7: Cross Section of T-Beam Reinforcement.....	18
Figure 3.8: Profile View of T-Beams	19
Figure 3.9: Detailed Map and Photographs of Damage to Structure.....	20
Figure 3.10: Cross Section of Deck With 3 T-beams	21
Figure 3.11: Map with scupper Hole Locations	22
Figure 3.12: Cross Section of Guard Rail.....	23
Figure 3.13: Photograph of Downstream Guard Rail	24
Figure 3.14: Cross Section of Piers	25
Figure 3.15: Aerial Photograph of Bridge Taken at Load Test	26
Figure 3.16: Plan View of Weathersfield Bridge	28
Figure 3.17: Weathersfield Bridge Profile View	28
Figure 3.18: Photograph of South Pier (Facing North)	29
Figure 3.19: Weathersfield Framing Plan.....	30
Figure 3.20: Girder and Deck Connection Detail	30
Figure 3.21: Bearings Supporting W36x170 Beams	31

Figure 3.22: Photographs of Damage to Flange Girders From Truck Strike	32
Figure 3.23: Joints in Bridge Deck	33
Figure 4.1: Picture of BDI Strain Gauge	36
Figure 4.2: Attachment of Strain Gauges	37
Figure 4.3: Photographs of AutoClicker Attached to Load Vehicle.....	38
Figure 4.4: Gauge Locations for All Tests in Royalton Bridge.....	39
Figure 4.5: Strain Gauges Attached to Deteriorated and Adjacent Beams.....	42
Figure 4.6: Diagram of Strain Gauge Locations on T-beams.....	43
Figure 4.7: Drawing and Photograph of Gauge Pair Attached to Guardrail.....	44
Figure 4.8: Dimensions of Royalton Load Vehicle	46
Figure 4.9: Diagram of Truck Lane Locations	48
Figure 4.10: Diagram of Weathersfield Bridge Gauge Locations	50
Figure 4.11: Diagram and Photograph of Gauge Pair Placement.....	53
Figure 4.12: Dimensions of Weathersfield Load Vehicles.....	56
Figure 4.13: Weathersfield Lane Positions.....	57
Figure 5.1: Strain History Gauge Pair #20 (Lane 2).....	62
Figure 5.2: Strain Histories of Repeated Test Runs Plotted Together Gauge Pair #20 (Lane 2)	63
Figure 5.3: Royalton Strain Profile.....	64
Figure 5.4: Neutral Axis Depths Calculated for Gauge Pair #20 (Lane 2).....	64
Figure 5.5: T-Beam Stem Dimensions and Rebar Configuration.....	66
Figure 5.6: Strain Profile and Force Diagram of Royalton Cross Section in Positive Bending	67
Figure 5.7: Stain Profile and Force Diagram of Royalton Cross Section in Negative Bending	68
Figure 5.8: Strain History of Gauge Pair #4 (Lane 2)	74

Figure 5.9: Combined Plot of Strain History of Gauge Pair #4 (Lane 2).....	75
Figure 5.10: Weathersfield Strain Profile.....	76
Figure 5.11: Calculated Neutral Axis Depth Gauge Pair #4 (Lane 2).....	76
Figure 5.12: Calculated Moment of Gauge Pair #4 (Lane 2).....	77
Figure 5.13: Weathersfield Cross Section in Positive Bending.....	79
Figure 5.14 Weathersfield Cross Section in Negative Bending.....	80
Figure 6.1: Royalton Bridge (Plan View) Cross-Sections and Gauge Numbering.....	85
Figure 6.2: Strain Histories Measured at Cross-Section 2 (Truck on Lane 1).....	88
Figure 6.3: Measured Strain in Bottom Gauge in Cross Section 2.....	90
Figure 6.4: Measured Strain in Bottom Gauge in Cross Section 5.....	91
Figure 6.5: Centroid of Load in Vehicle.....	93
Figure 6.6: Centroid of Load Producing Maximum Response at Cross Sections.....	93
Figure 6.7: Measured Strain in Bottom Gauge in Cross Section 1.....	94
Figure 6.8: Measured Strain in Bottom Gauge in Cross Section 3.....	95
Figure 6.9: Measured Strain in Bottom Gauge in Cross Section 4.....	96
Figure 6.10: Measured Strain in Bottom Gauge in Cross Section 6.....	97
Figure 6.11: Strain Histories on Exterior Girder and Upstream Guardrail in Span 1 (Lane 1).....	99
Figure 6.12: Strain in Guard Rail Gauge Pair #31 (Lane 1 – 72 ft).....	100
Figure 6.13: Strain Histories on Exterior Girder and Upstream Guardrail in Span 2 (Lane 1).....	101
Figure 6.14: Strain in Guard Rail Gauge Pair #32 (Lane 1 – 106 ft).....	102
Figure 6.15: Strain Histories on Exterior Girder and Downstream Guardrail in Span 2 (Lane 3).....	103
Figure 6.16: Strain in Guard Rail Gauge Pair #33 (Lane 1 –109 ft).....	104

Figure 6.17: Cross Section of Royalton Bridge with Load Truck Lanes	106
Figure 6.18: Beam II Span 1	107
Figure 6.19: Beam III Span 1	108
Figure 6.20: Beam V Span 1	109
Figure 6.21: Beam II Span 2	110
Figure 6.22: Beam III Span 2	111
Figure 6.23: Beam V Span 2	112
Figure 6.24: Strain and Stress Profile (Gauge Pair #23 – Truck at 108 ft).....	114
Figure 6.25: Beam Line Analysis of Span 1 (Load Vehicle at 70 ft)	117
Figure 6.26: Beam Line Analysis of Span 2 (Load Vehicle at 108 ft)	117
Figure 6.27: Calculated Moment in Cross Section 2 with $E_c=3,122$ ksi	120
Figure 6.28: Calculated Moment in Cross Section 5 with $E_c=3,122$ ksi	121
Figure 6.29: Calculated Moment in Cross Section 2 with $E_c=4,415$ ksi	122
Figure 6.30: Calculated Moment in Cross Section 5 with $E_c=4,415$ ksi	123
Figure 6.31: Moment in Cross Section 1 (Truck at 70 ft).....	130
Figure 6.32: Moment at Cross Section 3 (Truck at 70 ft).....	131
Figure 6.33: Moment at Cross Section 4 (Truck at 108 ft).....	132
Figure 6.34: Moment at Cross Section 6 (Truck at 108 ft).....	133
Figure 6.35: Weathersfield Bridge (Plan View) Cross-Sections and Gauge Numbering	134
Figure 6.36: Measured Strain in Gauge Cross Section 1	136
Figure 6.37: Lower Gauge Strain in Cross Section 7 (Lane 3 – 183 ft)	137
Figure 6.38: Plan View of Bridge with Load Trucks at 200 ft in Lane 1	138
Figure 6.39: Plan View of Bridge with Load Trucks at 200 ft in Lane 3	139
Figure 6.40: Plan View of Bridge with Load Trucks at 183 ft in Lane 3	140

Figure 6.41: Measured Bottom Gauge Strain in Cross Section 2.....	142
Figure 6.42: Measured Bottom Gauge Strain in Cross Section 4.....	143
Figure 6.43: Measured Bottom Gauge Strain in Cross Section 6.....	144
Figure 6.44: Measured Strain in Bottom Gauge of Girder I with Truck in Lane 1.....	147
Figure 6.45: Measured Strain in Bottom Gauge of Girder II with Truck in Lane 1.....	148
Figure 6.46: Measured Strain in Bottom Gauge of Girder IV with Truck in Lane 3.....	149
Figure 6.47: Neutral Axis Depth in Cross Section 4 Beam II	152
Figure 6.48: Neutral Axis Depth in Cross Section 4 Beam III.....	153
Figure 6.49: Neutral Axis Depth in Cross Section 4 Beam IV.....	154
Figure 6.50: Neutral Axis Depth in Cross Section 4 Beam V	155
Figure 6.51: Neutral Axis Depth in Cross Section 1 Beam I.....	158
Figure 6.52: Neutral Axis Depth in Cross Section 1 Beam II	159
Figure 6.53: Neutral Axis Depth in Cross Section 1 Beam III.....	160
Figure 6.54: Neutral Axis Depth in Cross Section 1 Beam IV.....	161
Figure 6.55: Neutral Axis Depth in Cross Section 1 Beam V	162
Figure 6.56: Neutral Axis Depth in Cross Section 7 Beam I.....	163
Figure 6.57: Neutral Axis Depth in Cross Section 7 Beam II	164
Figure 6.58: Neutral Axis Depth in Cross Section 7 Beam III.....	165
Figure 6.59: Neutral Axis Depth in Cross Section 7 Beam IV.....	166
Figure 6.60: Neutral Axis Depth in Cross Section 7 Beam V	167
Figure 6.61: Neutral Axis Depth in Cross Section 3 Beam I.....	169
Figure 6.62: Neutral Axis Depth in Cross Section 3 Beam II	170
Figure 6.63: Neutral Axis Depth in Cross Section 3 Beam IV.....	171

Figure 6.64: Neutral Axis Depth in Cross Section 5 Beam I.....	172
Figure 6.65: Neutral Axis Depth in Cross Section 5 Beam II	173
Figure 6.66: Neutral Axis Depth in Cross Section 5 Beam IV.....	174
Figure 6.67: Calculated Moment in Cross Section 4.....	177
Figure 6.68: Calculated Moment in Cross Section 1	180
Figure 6.69: Calculated Moment in Cross Section 7	181
Figure 7.1 Geometry of Elements used in Finite Element model of Weathersfield Bridge	188
Figure 7.2: Truck Load Lanes in Model (Southbound - Left to Right).....	190
Figure 7.3: Captured Images of Moments Finite Element Model (Truck at 189 feet in lane 2)	192
Figure 7.4: Comparison between Measured and Calculated Moments in Cross Section 4	196
Figure 7.5: Comparison of Measured and Calculated Moments in Cross Section 1	198
Figure 7.6: Comparison of Measured and Calculated Moments in Cross Section 7	199
Figure 8.1 – Model used for Royalton Bridge Rating Calculations (Span 2).....	205
Figure 8.2 – Typical Midspan Cross Section for Span 2	206
Figure 8.3 – Detail of Connection Between Deck and Girders and Application of Support Conditions	210
Figure 8.4 – General View of 3D Model of Weathersfield without Deck Elements.....	210
Figure 8.5 – Underside View of 3D-Finite Element Model of Weathersfield Bridge.....	211
Figure 8.6 – Detail of Cover Steel Girders over Interior Support in Weathersfield Bridge Model.....	212
Figure A.1: Photograph of Beam in Four Point Load Test.....	225
Figure A.2: Drawing of Test Setup.....	226

Figure A.3: 2 BDI Gauges and Laboratory Gauge Attached to Top Flange	227
Figure A.4: Record of Strain History Tested In Load Frame	228
Figure A.5: Neutral Axis of Bending Calculation	229
Figure B.1: Photograph of Gauges Attached to W12x30 Beam.....	232
Figure B.2: Raw Strain Data.....	233
Figure B.3: Raw 3-in Gauge Strain and One-Sixth of 18-in Extension Strain.....	234
Figure B.4: Raw 3-in Gauge Strain and Corrected 18-in Extension Strain.....	234
Figure C.1: Photo of Load Truck Being Pulled With Chain	238
Figure D.1: Cross Section in Positive Bending with Neutral Axis Below Slab	245
Figure D.2: Cross Section in Positive Bending with Neutral Axis in Slab	246
Figure D.3: Cross Section in Negative Bending.....	247
Figure D.4: Cross Section of Typical Composite Section in Positive Bending	249
Figure D.5: Cross Section of Typical Composite Section in Negative Bending.....	251
Figure D.6: Strain Profile of Weathersfield Bridge.....	252

ABSTRACT

Non-destructive load testing can be used as a tool to better understand the field behavior of bridges. Equipment to conduct non-destructive load testing was acquired and used to test two distinctly different bridges that are part of the bridge infrastructure in Vermont. One of the bridges, an old (1920s) reinforced concrete bridge (Royalton Bridge) had deteriorated over many years in service and currently carries heavy quarry trucks along its three spans. The second bridge, a non-composite steel bridge on interstate 91 (Weathersfield Bridge), was locally damaged by an over height truck as it passed underneath it. Results from the field tests in these two bridges were used to assess the effects of deterioration and damage on the bridge behavior.

Particular behavioral aspects were of interest for each of the bridges. The following main parameters were investigated in the Royalton Bridge: (1) the contribution of heavy reinforced concrete parapets (guardrails) to the load carrying capacity of exterior girders; (2) moment continuity across expansion joints generated by partially filled joints with concrete and pavement debris; and (3) effects of observed concrete spalling due to localized corrosion in some girders on bridge behavior. In general no detrimental effects of deterioration could be determined from the results of the bridge load tests. The rotational restraint induced by debris accumulation in bridge joints had little effect on moments determined along the bridge girders. The heavy reinforced concrete parapet behaved compositely (partially) with exterior girders as determined from measured strain profiles during the field tests.

In the Weathersfield Bridge load testing was planned to identify the following key aspects of the bridge behavior: (1) determination of composite action at negative and positive moment sections; (2) evaluation of effects of girder damage due to truck impact on the overall bridge behavior; and (3) transverse live-load moment distribution among girders in the critical positive and negative moment sections of the bridge. The load testing results revealed no evidence of detrimental behavior of the truck impact on the overall behavior of the bridge. The tests also showed that composite action was apparent at positive moment sections of the bridge but only a small effect of composite behavior was observed at negative moment sections. Transverse distribution of live-load moments among girders was conservatively estimated using current AASHTO equations.

Finally, the load testing results were used to estimate a load rating number for the two bridges consistent with the field measurements taken during the load tests. The load rating numbers obtained through load testing were consistently higher than those determined through normal rating procedures for both bridges.

CHAPTER 1 - INTRODUCTION

1.1 Background

Traditional evaluations of a bridge behavior are based upon assumptions of material properties, load distributions in the bridge deck, any quantified structural damage from visual inspections, and the accuracy of as-built construction drawings. As a result of these assumptions, analytical calculations often differ from actual bridge behavior. Field testing of a bridge can reveal its integrity, structural deficiency, composite behavior, and stiffness of non-structural elements; it is the only means that in situ performance can be verified.

Material properties of concrete, steel, and reinforcing steel are not known precisely and may vary throughout the structure. Therefore it is often necessary to assume that the material is continuous and homogeneous, and that behavior will be both linear and elastic. To ensure conservative results of these assumptions, reduction factors are used when calculations are performed involving the strength of materials.

Variations in reinforced concrete construction such as the effect of concrete hardening, corrosion of reinforcing bars, or the appearance of a large crack in a structural member or bridge deck is difficult to quantify. Engineers also find similar difficulties in steel construction with corrosion of steel girders or beams. It is often impossible for an engineer to correlate the affect of material property variation throughout a bridge to original design performance.

Analytical techniques used in the calculation of bridge behavior are often founded on simplifying assumptions that are used generically depending on bridge type, but do not necessarily reflect the condition of a bridge in the field. Assumptions of bridge behavior can include the existence of composite action that can occur between a concrete bridge deck and steel girders, material properties, and live load distribution factors specified guidelines of the American Association of State Highway Transportation Officials (AASHTO). As a result, bridge behavior observed in the field often differs from analytical predictions.

Bridge load ratings determined by a highway official are not trivial, and have important safety and economic implications. If a bridge capacity determined by field testing is found to be higher than standard design calculations would imply, the service life may be extended; delaying bridge repairs or replacement resulting in a significant economic benefit. In some cases where overload permits are routinely needed for vehicles to cross a bridge, an increased capacity might allow more overload vehicles to cross without having to apply for a permit or be detoured around a bridge. This could create additional cost benefit for both the owner and public.

If transportation officials have a better understanding of the load carrying mechanisms of a bridge they will be able to calculate more accurate load ratings. Aware of the need for a better understanding of bridge behavior under loading, this project focuses on field testing procedures and data analysis that can be used to improve the understanding of load distribution in bridge decks, composite action between steel and concrete, and the effect on load distribution among members where there is evidence of damage.

By performing in situ field tests of bridges with known loads while measuring strains in structural members, many of the simplifying assumptions of load distribution and material properties can be replaced with accurate models of bridge behavior. The objective of this project was to develop a load test methodology and demonstrate it through diagnostic field tests of two bridges in the State of Vermont. The two bridges were selected, in the Vermont towns of Royalton and Weathersfield, in coordination with the Vermont Agency of Transportation (VTrans) personnel to achieve specific goals in each test.

1.1 Bridge Inspection and Load Rating

Currently VTrans inspects bridges longer than 20 feet in their inventory on a two year cycle following national bridge inspection safety guidelines. The inspection is intended to identify and document any damage or deterioration found on the structure. Documentation may include photos of the present condition as well as notes describing any damage or material deterioration. While inspections are typically scheduled on a two-year cycle, bridges in poor condition are monitored every six to twelve months. Bridge inspections are a major source of resource allocation (human and economic) in most state highway agencies. Currently both the Royalton and Weathersfield bridges are scheduled to be inspected on two-year cycles.

New load ratings are calculated using load factor design by VTrans after any structural improvement work such as the replacement of a bridge deck or steel beam. Load ratings performed by VTrans are often based on bridge inspections and prior ratings, using both hand calculations and computer analysis. Load capacity calculations are performed using AASHTO guidelines.

1.3 Scope of Work

The focus of this project is to load test two bridges in the state of Vermont that Vermont Agency of Transportation (VTrans) officials have identified as having common details of many other bridges. VTrans officials would like to improve their understanding of bridge behavior through non-destructive load testing.

The first bridge is a three span reinforced concrete structure constructed in Royalton, Vermont in the 1920s (Figure 1.1a). The second is a continuous 3 span steel girder designed with a non-composite reinforced concrete deck located in Weathersfield, Vermont, constructed in 1965 (Figure 1.1b). Both of these bridges are described in detail in Chapter 3.



(a) Royalton Bridge



(b) Weathersfield Bridge

Figure 1.1: Photographs of Subject Bridges

1.4 Organization of Report

A review of existing literature on load testing was conducted and is listed and summarized in Chapter 2. In the remaining chapters, information pertinent to both the Royalton and Weathersfield bridges is listed in the first section, with additional details specific to the Royalton and Weathersfield Bridges in subsequent sections. Chapter 3 presents a detailed description of each test bridge, including historical context and existing conditions documented during the field test and by inspection reports received from the Vermont Agency of Transportation. Chapter 4 includes a detailed field report of procedures performed during the load tests as well as a description of load test goals and corresponding load test methodology. Chapter 5 describes methods of reducing strain data measured during the field tests and lists equations used to calculate neutral axis depth and moments. Chapter 6 presents the analysis performed of bridge behavior using strain data and calculated bending moments, and compares results with analytical models. Comparisons of bridge behavior with AASHTO guidelines for load distribution are also included. Chapter 7 describes the comparison of a three-dimensional finite element model of the Weathersfield Bridge with field measurements. Finally, Chapter 8 contains a project summary and conclusions.

Appendices provide additional information and reference. Appendix A and B summarize laboratory testing and verification of field equipment. Appendix C is intended as a guide to plan and conduct future load tests. Appendix D contains the background and equations derived to organize raw strain data and calculate results for each bridge. Appendix E contains plots of measured strain data, calculated neutral axis depths, and calculated moments.

CHAPTER 2 - LITERATURE REVIEW

2.1 Background

Prior to the investigation into the characteristics of the Royalton and Weathersfield Bridges, a review of relevant literature was conducted to assess similar projects that have been done in the past by others. A number of diagnostic and proof load tests have been performed with varying results. Some methodologies used to assess bridge conditions have changed over time with improvements in available technology.

Before the age of computers and sophisticated electronic measuring instruments, bridges were often proof load tested. Proof load tests simply prove that a bridge can support a specified load greater than the service limit. When proof load tests are employed today, one or more parameters such as strain or deflection are usually monitored. The loading is increased until the truck reaches a limit based on a calculated load rating.

2.2 Proof Load Testing

Saraf et al (1996) studied four bridges, including both concrete and steel, in the state of Michigan using a proof load testing to check highway bridges with severe corrosion and deterioration to structural members. To pass the State of Michigan proof load test, a load must generate a moment in the structure almost twice what the legal load limit would produce. The loads are incrementally applied under the supervision of engineers while monitoring strain and deflection.

The authors used results from an analytical model to compare measured strains and deflection in the field during the test. The in situ performance of all the bridges was found to be stiffer than analytical predictions, and all passed the proof load testing.

The benefit of a proof load test is that bridge behavior beyond the service range of the structure can be checked and verified with certainty. There is some risk however, that the bridge could be loaded into a non-linear range and cause permanent damage. Another drawback of a proof load test is that it may not answer questions about whether a vehicle with different axle configuration or loading, such as a special permit vehicle can safely cross the structure. To answer complex questions about bridge behavior, diagnostic testing methods have been developed with a goal of better understanding bridge behavior.

2.3 Diagnostic Testing

Diagnostic tests can be designed to only load the bridge within service limits, and have been performed while monitoring deflection, acceleration, or strain. The tests may be either destructive or non-destructive. Destructive tests require repairs to the structure after testing, such re-painting steel or patching of concrete cover where foil strain gauges were attached to steel. Non-destructive tests by design do not require any

repair work after the test. Since the focus of this study is non-destructive testing, the following will only discuss this type of testing method.

Non-destructive load testing equipment and techniques developed by Bridge Diagnostics, Inc (BDI) were selected to test the bridges in this project. The BDI method uses pairs of strain gauges placed at discrete locations on the top and bottom of a beam. The BDI manufactured strain gauges can be attached to both concrete and steel structural members. The bridge is loaded by a load truck which is driven across the bridge at crawl speed, while strains are recorded. The position of the load truck is monitored and correlated to the strain history when the data is reduced.

Schultz et al., (1995) developed the BDI investigation methods of bridge behavior with diagnostic testing and calibrated finite element modeling. The authors note that measurements of deflection or acceleration are not as useful when the goal of a test is to determine stresses in the structure and ultimately a load rating.

A diagnostic load test can be performed using strain gauges attached to structural components of the bridge in select locations to measure strain, while a load of less than the legal limit is driven onto the bridge. Strain gauges can be attached to the surface of a structural member using mechanical anchors, clamps, and/or adhesive. Strain measurements from the top and bottom of a cross section can be used to determine directly the location of the neutral axis of bending.

After testing, gauges can be removed without causing damage to the structure. Depending on the goals of the testing, a finite element model of the bridge is calibrated to the measured bridge behavior in the field; it is then used to estimate the bridge response to different load configurations and weights.

Bridge Diagnostics, Inc (BDI) conducted a load test on reinforced concrete approach spans of the University Bridge in Seattle, Washington. To collect field data, 40 strain gauges were attached to the bridge. During the test a load truck followed four marked lanes, with each run repeated twice for repeatability. The truck traversed the bridge at 5 mph, while wheel revolutions were recorded to measure travel distance using an AutoClicker, a device that sends a signal of truck position to the data recorder in real time.

By using a moving vehicle as opposed to a static test, the influence of truck position at all gauge locations can be analyzed at any point along the trucks' path. By plotting the strain history versus load position, the truck position causing maximum moment at gauge positions on the bridge was determined. The load rating for the bridge, based on a calibrated finite element model from the tests, was increased using both a conventional beam analysis and American Association of State Highway and Transportation Officials (AASHTO) guidelines, primarily due to lateral and longitudinal load distribution in the structure.

Bridge Diagnostics, Inc (2002) completed load testing and load rating of a girder bridge with concrete deck that was rehabilitated with a hollow core fiber reinforced polymer (FRP) deck and asphalt overlay. Strain gauges were attached to the top and bottom flanges of steel support girders with 18 strain gauges pair locations. To analyze the structure strain data plots from the bridge were first plotted for visual inspection to check for accuracy. A finite element model of the bridge was calibrated using the test results to verify satisfactory behavior of the new FRP deck.

Jáuregui and Barr (2004) used a non-destructive testing evaluation of the I-40 Bridge over the Rio Grande River, a pre-cast pre-stressed concrete bridge. The objective of the test was to determine if the capacity of the bridge could be increased, so that overload permits would not have to be denied, and would save truckers from a detour around the bridge.

The authors used 32 strain gauges placed at both the top and bottom of the girder at each location creating 16 pairs of gauges. The gauge pairs were attached at both center span and at a pier. A loaded tri-axle water truck of 52.4 kips was driven across the bridge along three pre-determined load paths. Each pass of the truck was repeated three times for averaging.

After creating a finite element model of the bridge in SAP 2000, Jáuregui and Barr were able to verify that the bridge inventory and operating rating could be increased to allow special permit vehicles to cross the span.

Cai and Shahawy (2004) have found that stresses measured in the field during bridge tests are often lower than predicted by analysis methods. The authors had attributed this to the concrete strengths and contributions of non-structural components.

Barker (1999) studied a systematic method for conducting diagnostic load tests of bridges and load rating of the bridge using analytical models. The research identified differences between assumed factors in analysis that contribute to bridge response such as the actual dead load, impact factor, and stiffness of non-structural components.

Barker found that increases in load capacity from analytical calculations can be related to different attributes in a bridge. Barker isolated the calculation of each factor to present a bridge owner with useful information about the load rating, such that the owner can decide how to change a rating by including or ignoring certain factors. While understanding of which components were beneficial to the load rating was reported to be complicated, the load rating of a subject bridge was increased as a result of a test following the outlined procedure.

Zhou (1996) tested a non-composite steel plate girder bridge with a concrete deck. Strains were measured at the top and bottom of girders, with most instruments in cross sections in the positive moment region to determine neutral axis depth. Loading trucks with multiply axle configuration and known weights were used during the test. Using a calibrated finite element model, Zhou determined that the bridge could be analyzed as a composite structure. Live load distribution factors were also determined from the test. Because of the load tests and models, a 50% increase in the load rating was possible.

Sartor et al. (1999) studied four bridges with short term strain monitoring and finite element modeling. The goal of the testing was to determine the effects of live loads on bridges with observed damage. Using portable strain recording equipment, areas of interest in the bridge were instrumented and monitored for one to two days with unrestricted traffic. The recorded data strain was then correlated with stress to determine if corrective maintenance action would be needed in the bridges.

Jáuregui et al. (2002) studied a non-composite steel girder bridge using diagnostic testing by measuring strain in girders and the deflection at mid-span. The bridge was loaded with concrete blocks placed on the bridge and a load truck until yielding occurred in girders. Testing revealed that positive moment regions had

partially composite action. Negative moment regions acted non-compositely although curbing did increase the stiffness around exterior girders.

2.4 Analysis and Finite Element Modeling

A finite element analysis of a bridge is often performed to verify bridge behavior with diagnostic field tests. Finite element models may be calibrated to match bridge behavior based on field results, and is particularly useful when a bridge has irregular geometry or variable material properties. Unusual loadings from an overload permit vehicle may also be input to a calibrated finite element model to check bridge response. The following researchers have created finite element models of bridges with similar attributes to the two bridges selected for this project.

Jáuregui et al (2002) studied a pre-cast girder bridge with concrete slab modeled using frame elements to represent girders and shell elements to represent the slab. The girders were modeled at their geometric centroid with rigid body constraints connected to the centroid of deck shells to model composite behavior. The model was used to determine live load distribution factors and to increase the load rating of the bridge.

Huang et. al (2004) investigated the effect of deck and diaphragm stiffness on a steel girder bridge with 60-degree angle of skew using a load tested and finite element modeling the authored compared results with AASHTO LRFD specifications

From the modeling, it was found that varying the modulus of elasticity of the concrete deck within 10 percent of nominal values had little effect on the load distribution. By increasing diaphragm stiffness, it was found that load distribution was increased among girders. The difference in strain among members however, was not proportional to the relative stiffness of diaphragms.

The authors found that diaphragms in a bridge significantly influence the girder strains by reducing the strain directly under a load while increasing the strain in girders away from a load. It was also found that diaphragms connected between girders at pin supports create negative strains in girders near the obtuse corner of the bridge and that maximum strains at mid-span were reduced. Additionally, the authors found that AASHTO was conservative for positive moments, but not conservative in for negative moment areas.

Chajes et al. (1997) studied a three-span simply supported bridge with steel girders and a non-composite concrete slab. By measuring strain during a diagnostic test and calibrating a finite element model, restraint in the supports was determined to be significant and composite behavior in the bridge was verified. A grillage finite element model was created in the analysis that correlated the measured bridge performance. Rotational springs in the model were used to estimate the amount of stiffness in the bridge. As a result of the tests and modeling, the load rating of the bridge was increased.

2.5 Summary of Literature Review

Diagnostic field tests are valuable to the understanding of bridge behavior and can be used to support engineers and bridge owners when making decisions regarding load rating and overload permits of existing bridges. Past diagnostic tests have successfully been performed on steel, concrete, and pre-cast concrete bridges. Load testing is commonly conducted in combination with other engineering tools such as simple analytical models or finite element models to verify that field performance is in accord with acceptable bridge models. Models can also be used to extrapolate results to other loading conditions such standard AASHTO design vehicles or special permit vehicles with irregular axle configurations.

CHAPTER 3 - DESCRIPTION OF TEST BRIDGES

3.1 Royalton Bridge VT 14 Br. 28

Known locally as the Spaulding Bridge in Royalton, Vermont, bridge #28 carries vehicular traffic across the White River on state highway 14. It has three spans supported with reinforced concrete T-beams: (Figure 3.1) outer spans are 33 feet (10.06 m) with a center span of 38 feet (11.58 m). Geometrically the bridge is on an 18-degree horizontal curve and is super elevated.

Constructed in the late 1920's, it has significant deterioration to some structural members. This damage poses a challenge to verifying assumed load distribution and calculating bridge capacity. Bridge #28 has been selected by VTrans officials as a representative bridge with similar attributes to a number of other bridges in the state; many of these bridges are in equally poor condition. Therefore, bridge #28 is an ideal test candidate for this project. Figure 3.2 below shows a photograph taken shortly after construction.

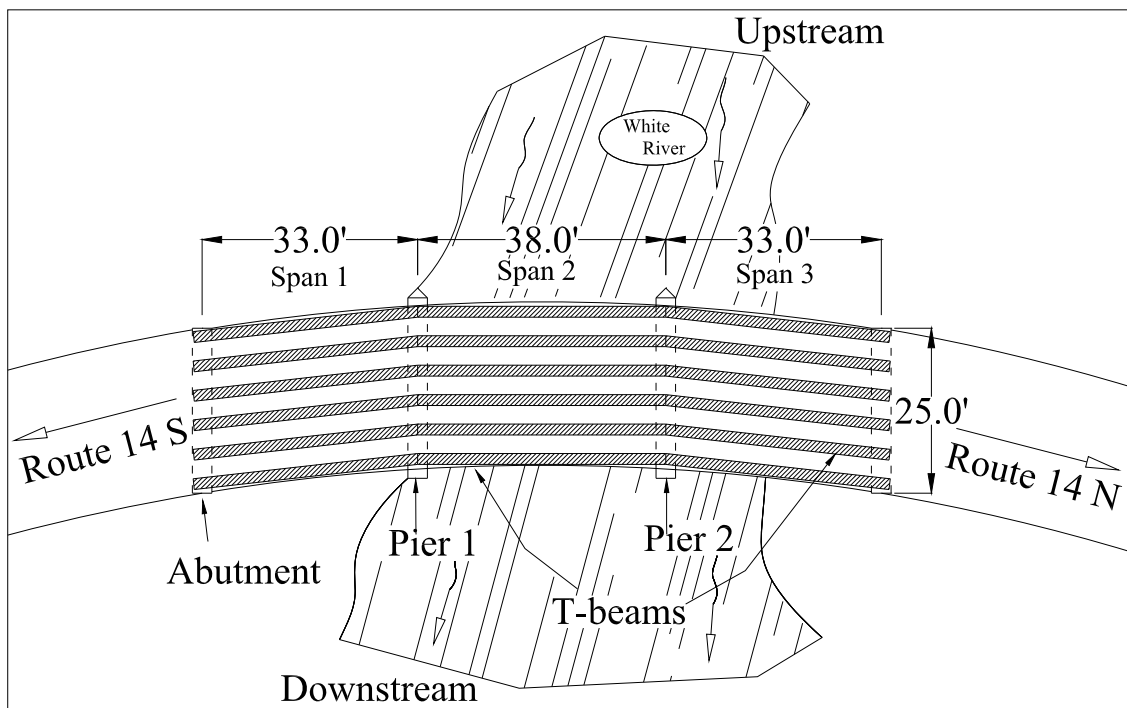


Figure 3.1: Diagram of Spaulding Bridge



Figure 3.2: Picture of Spaulding Bridge taken in 1927¹

3.1.1 Historical Significance

Circa 1789 a mill operated in the Northwest corner of Royalton, VT along the second branch of the White River, damming the water flowing over a small ledge outcropping. In 1836 a road was built along and across the river next to the mill, the present location of Vermont State Route 14. This new road required the construction of two wooden bridges spanning the second branch of the White River (Nash, 148-9).

The second crossing was completed with the construction of a covered multiple king post bridge. The covered bridge was located next to the mill and at the intersection of two main roads and four houses, an area that is recorded to have become a center of activity by the 1850s. The mill contained a grindstone to mill corn, saws to cut logs into lumber, and produced paint until the buildings were destroyed by a fire in 1893. In 1899 an electric generating plant was constructed on the site, selling power to local villages (photograph of Figure 3.3). Today only the barn structure (to the right of the smokestack) still stands (Nash, 149).

¹ Courtesy Vermont State Archives

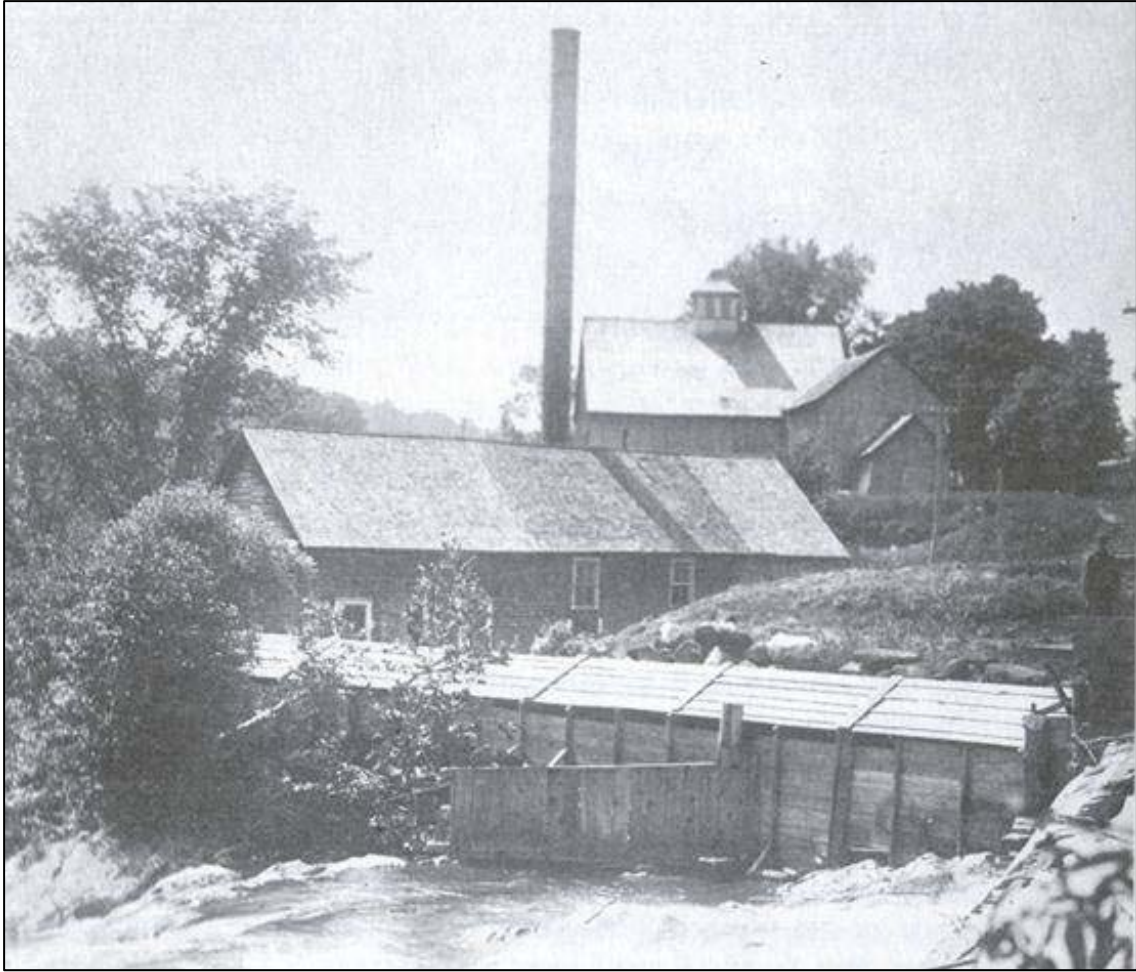


Figure 3.3: Photograph of Electric Generating Plant Just Below Bridge²

In November of 1927 heavy rain caused river levels to rise in the White River, resulting in extensive flooding that washed away several homes, roads, railroads, culverts, bridges, destroyed telephone lines, and resulted in seven deaths in the White River valley (Johnson, 15). Along the main branch of White River through Royalton, all of the town's bridges, with the exception of a railroad crossing, were destroyed by the force of water and debris. Bridges along the tributaries of the White River fared somewhat better, including the covered bridge near the mill that suffered damage during the flood but did not wash away (Nash, 63-4).

Approximately one mile (1.6 km) downstream from the mill, a metal bridge under construction to replace the 1836 original was washed away during the flood (Nash, 149). It is estimated that as a result of the flooding in 1927, over 1200 bridges needed replacement across the State of Vermont. A large amount of construction soon followed, necessitating the use of standardized bridge plans created by state highway engineers, with reinforced concrete the new building material of choice (McCullough, 133-4).

² Reproduced with permission of Dr. Holly Nash Wolfe

Following the state's long history of using timber, stone, and cast iron, reinforced concrete was introduced to build arch bridges around the turn of the twentieth century. Since arches work in compression, concrete was an ideal building material for this use. The heyday of concrete arch construction in Vermont lasted from about 1908 to 1925, at which time new designs with flat slabs or T-beams were found to be a more economical choice (McCullough, 172).

The new age of bridge construction with reinforced concrete in Vermont is noted by McCullough who writes that “during the years 1924 and 1925, 192 bridges were built; ninety slab structures, thirty-three T-beam bridges, and thirty-two reinforced concrete boxes...Thus almost 85 percent of all new bridges were reinforced concrete” (McCullough, 207). Around 1920, designers began to use T-beam construction, in which the beam is cast monolithically with the bridge deck. They found these designs to be more economical than arch designs because of the cost savings with formwork and ease of construction. The use of T-beam popularity in construction was short lived however, after steel support beams became a more economical choice in the 1930s (McCullough, 172).

Although several variations in the design of T-beam construction existed, standardized plans were created by the state highway department engineers and distributed free to towns, which undoubtedly led to their growing popularity. The advantage of having standardized plans was not lost on engineers, who used them in 75 percent of more than 1600 bridges constructed between 1928 and 1930 (McCullough, 196).

Much of the funding for new bridges was provided by state legislatures. In the post World War I era, federal money became available in an effort to create better roads (McCullough 134). The Federal Highway Aid Project, which began in 1916 and was continued in 1921 by Congress, authorized federal monies to be used for state highway construction provided that the roads met set design standards. As a result of these Federal Aid funds, plans were drawn in 1925 for a replacement of the wooden king post bridge next to the mill in Royalton with a concrete T-beam structure. Completed a year later in 1926 as shown in Figure 3.2 above, the new bridge became known as the Spaulding Bridge after the family who owns an adjacent farm on the former site of the old mill. While other structures along the river suffered damage in the flood in the fall of 1927, the newly constructed concrete bridge apparently remained unharmed.

Subsequently, the first bridge on the second branch (that had been reconstructed using metal and destroyed in the flood) was re-built using a two span bridge with concrete T-beam design of a similar standardized plan (Nash, 149). Today, both bridges survive and are still in service.

3.1.2 The Surrounding Area

The countryside surrounding the Spaulding Bridge appears to have changed little over the years since its construction. While trees may have overgrown some farmland, grassy fields and pastures still surround the bridge. However, the river channel under the bridge has been altered. In its current state the flow of the river has been restricted through span 1 by approximately 8 feet (2.44 m) of fill on the upstream

side of the bridge that is partially retained by the first pier. The fill height is within a few feet (1000 mm) of the exterior T-beam below the bridge deck. It is unclear if this fill was purposely placed across span 1 or is a result of erosion.

Additionally, a large stone rip-rap extends from the abutment wall 3 to about mid-span of span 3. Therefore the width of the river channel passing under the bridge is approximately the width of the center span and one-half of span 3.

The height of water and flow in the White River varies with precipitation in the watershed. On the day of the field test, the depth of the channel below the bridge was between knee and waist deep, with a swift current.

3.1.3 Average Daily Traffic

As of the last traffic estimate in 1998, the average daily traffic over the Spaulding Bridge on Route 14 is 1400 vehicles per day with six percent truck traffic. The truck traffic along this road on the day of the test included a number of flatbed tractor-trailer trucks transporting heavy slabs of granite from a nearby quarry as shown in Figure 3.4 and Figure 3.5. Through verbal communication with VTrans officials, Route 14 and the Spaulding bridge are a main trucking route for this quarry. It was noted by an officer with the State of Vermont Department of Motor Vehicles, onsite to weigh the load vehicles, that when checked on previous occasions the quarry trucks have never exceeded legal load limits.



Figure 3.4: Line of Trucks from Quarry Stopped During Load Test



Figure 3.5: Quarry Truck Crossing Birdge

3.1.4 Overall Geometry

The bridge was constructed with a curved geometry to conform to the horizontal alignment of Route 14 as it switches banks of the river (Figure 3.1). As part of the federal aid project to build better roads and construct the Spaulding Bridge, the alignment of Route 14 was changed to help motorists travel at higher speeds along the route. Previously, a 90-degree bend in the alignment existed for motorists crossing the wooden bridge.

The current concrete bridge is set on an 18-degree horizontal curve with a 2.5% downward grade from span 1 to span 3. The deck is also super elevated at five degrees with the outer radius of curvature of the deck raised on the upstream side of the bridge.

3.1.5 T-beams

3.1.5.1 T-Beam Construction Plans

Six reinforced concrete T-beams in each span support the bridge deck, spaced 54 inches (1372 mm) on center. The beams run parallel between supports in a straight line, and support the curved geometry of the deck above. All of the beams are 20 inches (508 mm) in width and 28 inches (711 mm) in height including the 7 inch (178 mm) deck slab. Additionally, beam seats on abutment walls and pier bent caps are stepped at $2\frac{3}{4}$ inches (70 mm) to create the super elevation as shown in Figure 3.6.

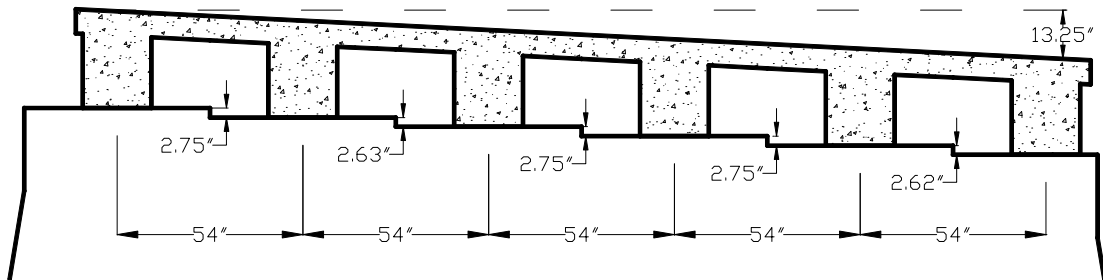


Figure 3.6: Royalton Bridge Cross Section with Beam Seat Steps

The reinforcement schedule described below is taken from original construction plans of the bridge, and unfortunately could not be fully verified in the field as a destructive bridge investigation was not performed. The reinforcement in spans 1 and 3 (Figure 3.7 and Figure 3.8) include seven longitudinal $1\frac{1}{8}$ inch (29 mm) square reinforcing bars in two layers. The bottom layer includes four bars centered $2\frac{1}{2}$ inches (64 mm) above the beam seat. The second layer contains three bars centered $5\frac{1}{2}$ inches (140 mm) above the beam seat. In the top of the beam, two $\frac{1}{2}$ inch (13 mm) square longitudinal reinforcing bars are centered $2\frac{1}{8}$ inches (54 mm) below the top of the deck slab. Open vertical stirrups of $\frac{1}{2}$ inch (13 mm) square rebar loop around the bottom reinforcement and are hooked over top reinforcement with a 45-degree bend as shown in Figure 3.7.

The reinforcement schedule in span 2 includes eight $1\frac{1}{4}$ inches (32 mm) square longitudinal reinforcing bottom bars spaced in two layers. The bottom layer includes four bars centered $2\frac{1}{2}$ inches (64 mm) above the beam seat. The second bottom layer contains four bars centered $5\frac{1}{2}$ inches (140 mm) above the beam seat. In the top of the beam two longitudinal reinforcing bars located $2\frac{1}{8}$ inches (54 mm) below the top of the slab are $\frac{1}{2}$ inch (13 mm) square. Open vertical stirrups of $\frac{1}{2}$ inch (13 mm) square rebar loop around the bottom reinforcement and are hooked over top reinforcement with a 45-degree bend as shown in Figure 3.7.

Original bridge construction plans specify that “[r]einforcing steel shall conform to standard specifications for structural steel grade billet steel concrete reinforcing bars of A.S.T.M. serial designation A-15-14.” From these specifications and the date of construction, the reinforcing steel yield point is approximately 33 ksi (228 MPa) and ultimate strength between 55 and 70 ksi (379 and 483 MPa) (Hool, 36). The specified concrete strength for construction is not specified in bridge plans provided by VTrans.

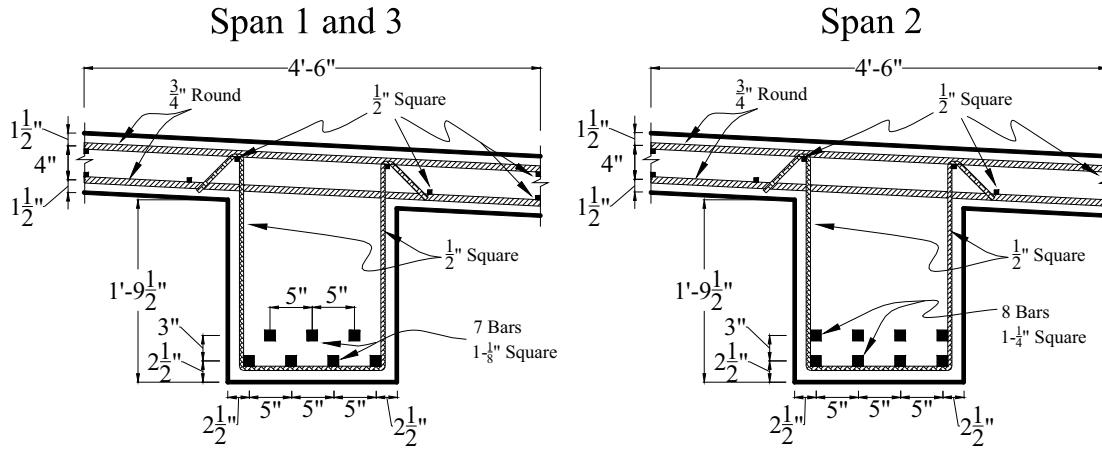


Figure 3.7: Cross Section of T-Beam Reinforcement

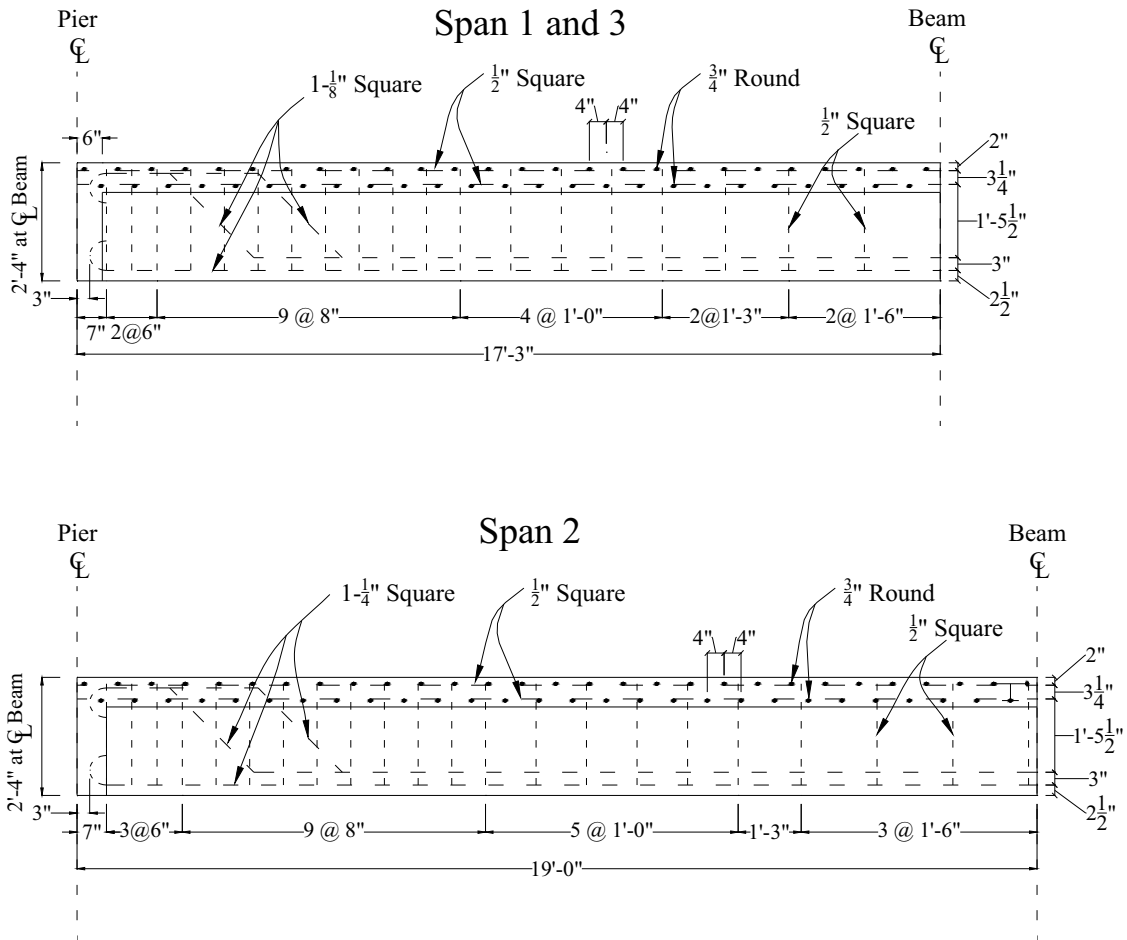


Figure 3.8: Profile View of T-Beams

3.1.5.2 T-Beam Current Condition

In its current condition some of the concrete cover has spalled along the bottom of the T-beams in select locations caused by heavily corroded reinforcing bars. Concrete near both abutment walls has also fallen away, and reinforcing bars are visibly missing due to exposure and corrosion. Figure 3.9 illustrates mapped locations of some documented deterioration of the bridge.

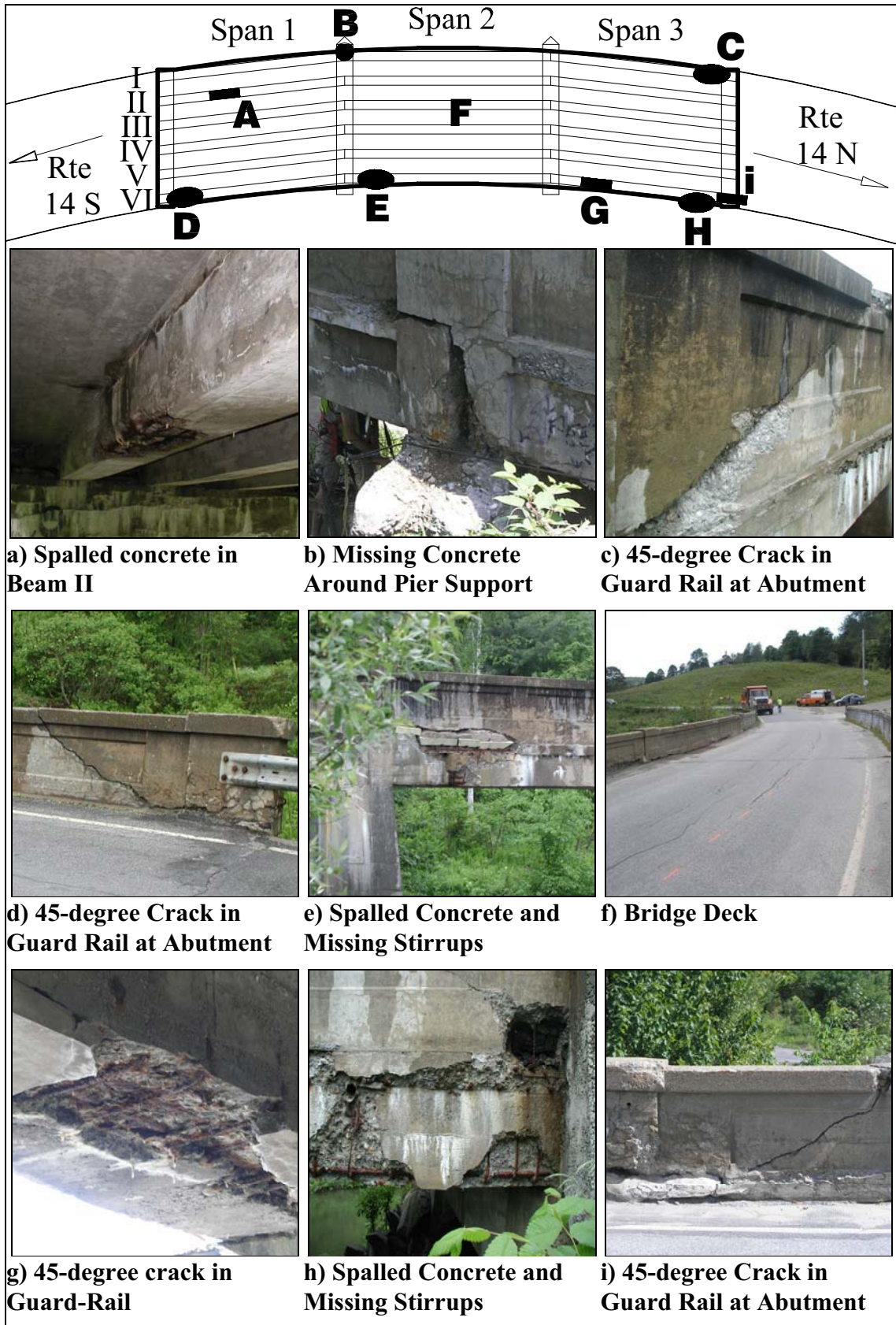


Figure 3.9: Detailed Map and Photographs of Damage to Structure

3.1.6 Deck

The concrete deck slab is 7 inches (178 mm) thick and conforms to the super elevation and roadway grade described above. The deck was designed with the T-beams to be simply supported with joints over piers and at each abutment. A wearing surface of bitumen pavement covers the concrete, and the expansion joint appears to have been covered by the crew applying the pavement. As a result, there are transverse cracks in the wearing surface at joint locations above both piers and abutments.

Steel reinforcement in the deck include transverse $\frac{3}{4}$ inch (19 mm) round rebar spaced at 8 inches (203 mm), located in two layers $1\frac{1}{2}$ inches (38 mm) from both the top and bottom of the slab. Longitudinal reinforcement was placed in two layers using $\frac{1}{2}$ inch (13 mm) square bars placed inside the transverse reinforcement. Longitudinal bars are located in the deck at the edge of each T-beam and midway between beams (Figure 3.10).

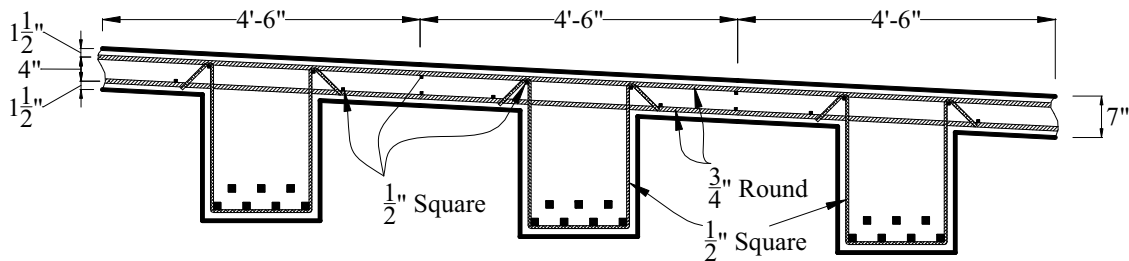


Figure 3.10: Cross Section of Deck With 3 T-beams

3.1.7 Scupper Holes

Four scupper holes of 3 inch (76 mm) galvanized pipe were built into the bridge for drainage of the superstructure to the river below (Figure 3.11). The super elevated design of the bridge superstructure creates sheet drainage across the deck toward scupper holes from the upstream side to downstream curb. One pipe was installed in each of the exterior spans near abutments, and two were placed in the center span near the piers. Set at an angle, the holes extend from the curb on the downstream side of the bridge and daylight beside the top of exterior T-beams.

It was observed during the site investigation that much of the deterioration of the bridge including spalled concrete and locations of heavily corroded or missing rebar are concentrated in the areas where the scupper holes drain water from the bridge deck. It is assumed that some of this deterioration is due to the use of de-icing chemicals in the winter and the drainage path of the superstructure through the scupper holes. Photographs in Figure 3.9 (e and h), show existing damage near scupper holes.

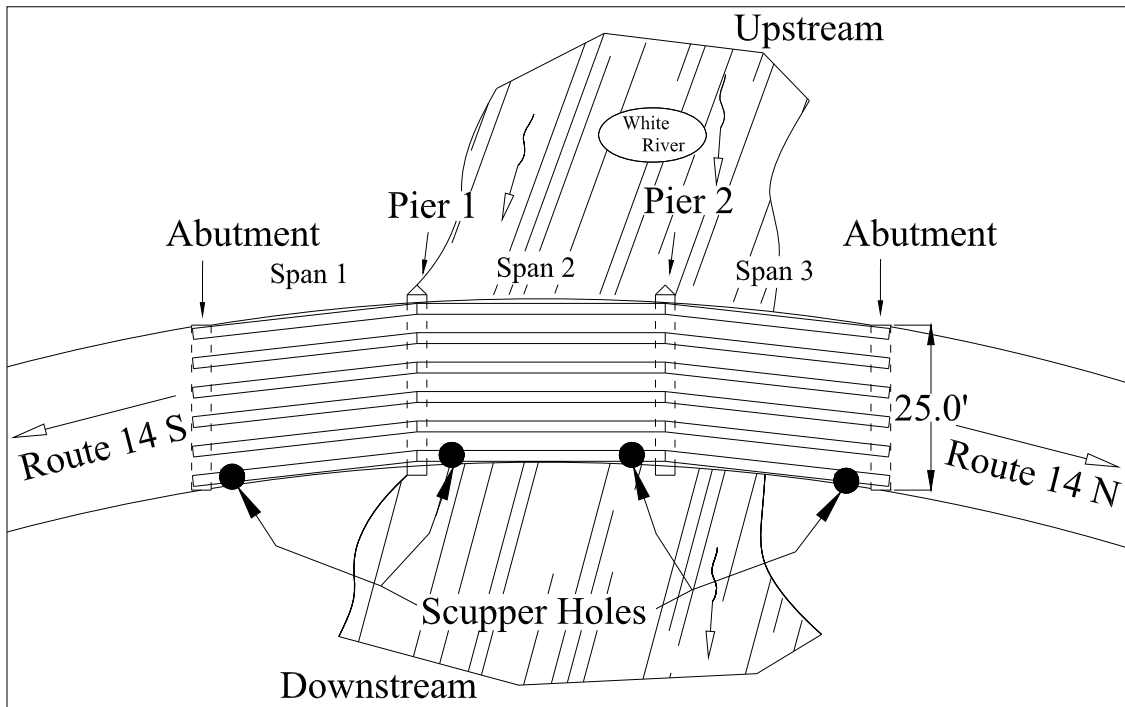


Figure 3.11: Map with scupper Hole Locations

3.1.8 Guard Rail

Reinforced concrete guardrails were cast on the bridge deck that are 46 inches (1168 mm) in height and 16 inches (406 mm) in width at the widest point. Gaps at interior supports were provided to prevent restraint at simple support conditions of each span. The design, as shown in the photograph of Figure 3.13 is typical for many of the standardized bridge plans constructed in this era with recessed panels to add aesthetic appeal. The guardrails follow the 18-degree horizontal curve of the road along the edge of the bridge deck.

The guardrails were likely cast in place after the bridge deck was completed and were not designed to add structural rigidity. The guardrails have two longitudinal $\frac{1}{2}$ inch (13 mm) square bars at the top of the railing, and one $\frac{1}{2}$ inch (13 mm) bar toward the bottom of the section. Additionally, $\frac{1}{2}$ inch (13 mm) square vertical reinforcement spaced at 18 inch (457 mm) link the guardrail to the exterior T-beams. Although the beams are straight, the guardrail is curved to conform to the horizontal geometry. Therefore, the horizontal position of the guardrail relative to the exterior T-beam changes along each span, with the inside edge of the guardrail always above the beam along its cross section.

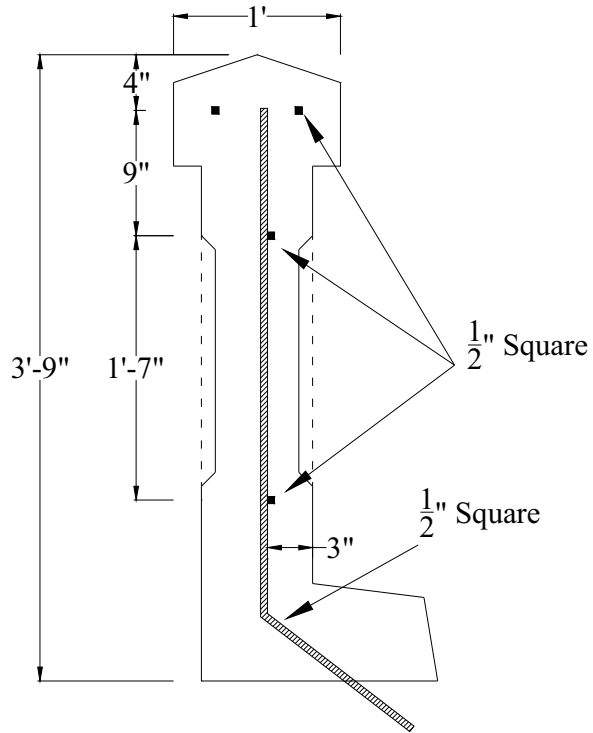


Figure 3.12: Cross Section of Guard Rail



Figure 3.13: Photograph of Downstream Guard Rail

In their current state the guardrails have sections with spalled concrete and exposed rebar. Large shear cracks have also formed at a 45-degree angle at three of four ends, extending up from abutments toward the center of the bridge, as shown in Figure 3.9 (c, d, and i).

It was also noticed that around one scupper hole that a large patch of concrete and insulation type foam had been used to repair a hole near the bottom of the rail as documented in Figure 3.9h.

3.1.9 Abutments

As-built construction plans of abutments could not be found for this bridge, and an extensive site investigation of the abutment construction could not be conducted during field testing. However, the general size and placement of abutment construction can be ascertained from the original construction plans.

Both abutments are three feet in width at beam end supports and increase in width vertically with a slope of 2 inches per foot (51 mm per 305 mm) vertically downward. Notes on the construction plans require that footings be constructed when excavation reached rock or a suitable foundation material.

The abutment under span 3 is protected by stone riprap while span 1 is currently protected by a large amount of fill as described above. The backfill material behind each abutment and below the roadway surface is unknown.

3.1.10 Piers/Bent caps

Both piers were constructed in the river with battered points on the upstream face. While pier construction is expensive, the engineering design of T-beam construction at the time of the Spaulding bridge could only achieve spans of 30 to 40 feet (9.14 to 12.19 m) in length (McCullough, 210). Since the White River at this crossing is 104 feet (31.70 m), three spans and two piers were required. The excavation for the pier footings would have been dug until a suitable base material could be found in the river. Considering the ledge outcropping next to the bridge, deep excavations below the waterline may not have been necessary.

Construction plans show the footings are 62 inches (1575 mm) wide at the base and about 25 feet (7.62 m) in length. The sides of the piers taper slightly at $\frac{1}{2}$ inch per foot (13 mm per 305 mm), with a 3 foot (914 mm) width at the top to support the beams (Figure 3.14).

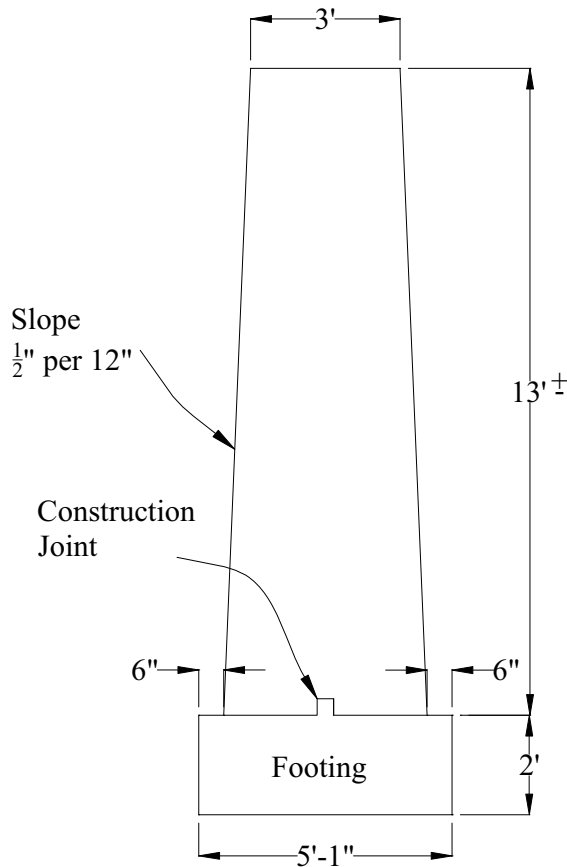


Figure 3.14: Cross Section of Piers

3.1.11 Load Rating and Current Condition

The current load rating for the Royalton Bridge in this project has been reduced due to severe deterioration of reinforced concrete from cracking, spalling of concrete, and severe rust scale and loss of reinforcing bars. The reduction is based on the assumption of a 10% section loss of T-beam reinforcement.

During the last inspection in May of 2005, the bridge deck, superstructure, and substructure all received a “poor” condition rating and the bridge was listed as “structurally deficient” in the Vermont bridge inventory. Using load factors, the bridge received an inventory rating of HS-30 and operating rating HS-51. The bridge in its current state is open to the public without load posting or vehicle restrictions.

3.2 Weathersfield Bridge I-91 Br. 30

Two identical three span continuous steel girder bridges sharing number 30 on Interstate 91 in Vermont were constructed as highway overpasses in 1965. Each carries two lanes of traffic on Interstate 91 North and Southbound over route 131 at exit 8, in the town of Weathersfield, Vermont. Neither has an emergency pull off or breakdown lane. The bridge carrying southbound traffic was selected for testing.

This bridge was selected because when calculating moments generated in the bridge assuming non-composite behavior, the controlling factor is negative moments over the piers. Conducting a field test of the bridge is the only means of verifying actual bridge behavior. Because this bridge is similar to many of the highway bridges constructed in Vermont, it is an ideal candidate for testing non-destructive methods.



Figure 3.15: Aerial Photograph of Bridge Taken at Load Test

3.2.1 History

The creation of the National Interstate and Defense Highway System in Vermont spurred the creation of the Interstate 91 (I-91) corridor. With the majority of funding for interstates raised by the federal government, states were able to construct modern limited access highways for safe high-speed travel. The strict design requirements for highways necessitate construction of bridges for not only crossing rivers, streams, and railroads but also secondary roads to maintain grade separation. Development of interstates was a major undertaking for the engineers of Vermont's Department of Transportation who were tasked to design many of the interstate bridges in-house.

The majority of the bridge plans completed for interstates in Vermont in the early 1960s were simply supported structures, as they were easier to analyze than continuous girder bridges. The first computer to perform complex bridge calculations was not purchased until 1965 by the department, leaving engineers in a time before the popularity of electronic calculators to complete work using slide rules (McCullough, 257-9).

Considering the amount of time and effort necessary to complete a bridge design, it is not surprising that more than one bridge might be built from the same plan. This is the case for the design in Weathersfield at exit 8 on Interstate 91, where both north and southbound bridges are mirror images of each other, with the exception of a minor difference in roadway grade. Designed in 1962, both bridges were constructed in 1965.

3.2.2 Geometry

The bridge has three spans and a straight horizontal alignment, with a total length of 214 feet 6 inches (65.38 m) and skew angle of 41° 54' 39". The abutment wall, interior piers, and deck joints are configured with this skew angle. The center span is 84 feet 6 inches (25.76 m) and side spans are 65 feet (19.81 m). The bridge deck is 30 feet (9.14 m) wide with two travel lanes. The grade of the roadway across the bridge is 2.8%, decreasing in the southbound direction (Figure 3.16 and Figure 3.17).

Route 131 below the bridge is 44 feet (13.41 m) in width and with a centerline symmetric about the centerline of the bridge at the 41° 54' 39" angle of skew. The traffic configuration on route 131 includes two twelve foot travel lanes and two 10 foot (3.05 m) paved shoulders.

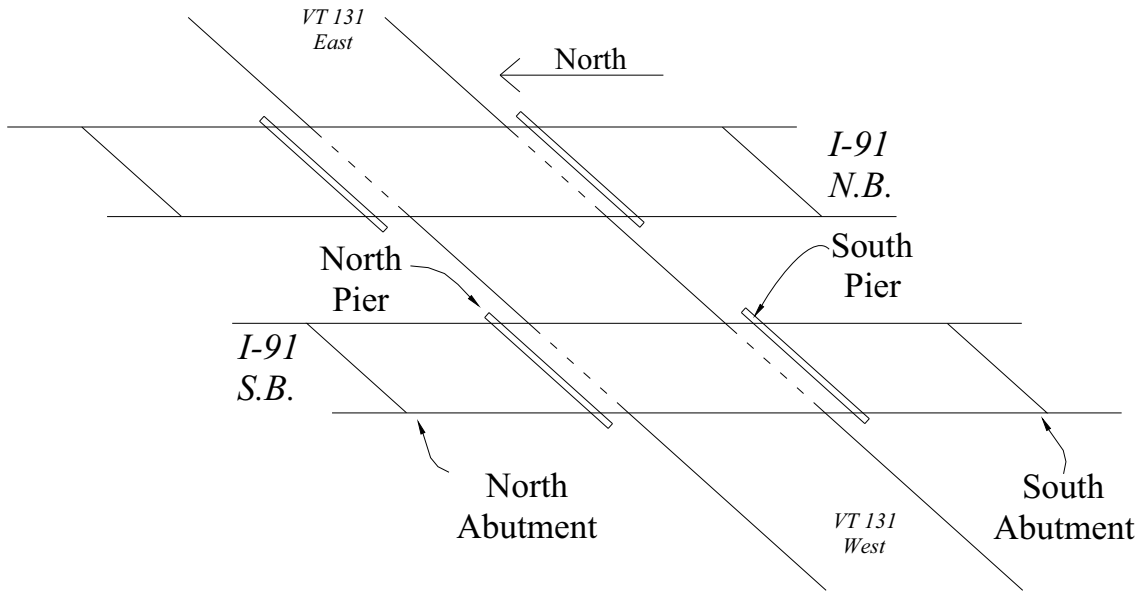


Figure 3.16: Plan View of Weathersfield Bridge

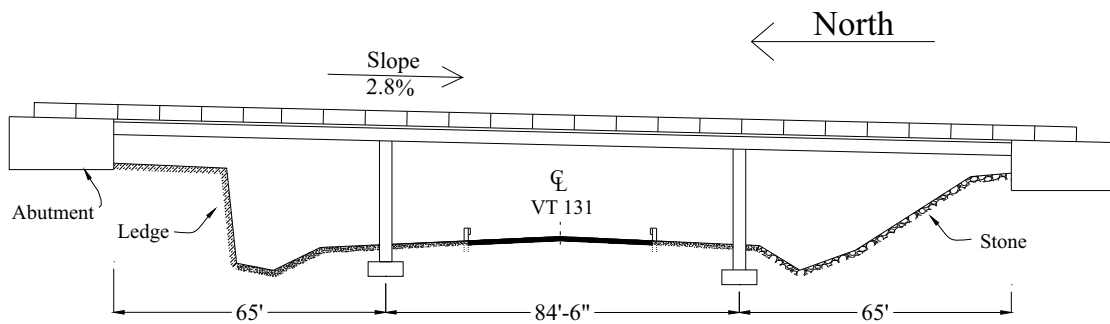


Figure 3.17: Weathersfield Bridge Profile View

3.2.3 Average Daily Traffic

As of the last traffic estimate in 1998 the average daily traffic over the southbound bridge is 5250 vehicles per day with thirteen percent truck traffic. The bridge is currently in open and service with no load postings.

3.2.4 Abutments

Both abutments are constructed with reinforced concrete and backfilled with a granular material. The roadway was built in a cut section that has a ledge outcropping. The north abutment is directly supported by the ledge, while the south abutment required H-piles. Stone protects the steep slope extending from face of the south abutment toward route 131; while a blasted ledge outcropping surrounds the front face of the north abutment.

The front edge of each abutment is skewed at $41^{\circ} 54' 39''$ to conform to the geometry described above. The face walls of each abutment have a shelf to support ends of all five girders, with stepped seats to provide create slight crown to the deck.

3.2.5 Piers

Two interior piers set at a skew angle of $41^{\circ} 54' 39''$ as described above in the geometry, divide the bridge into three spans. Each pier, constructed with reinforced concrete, consists of a bent cap supported by two columns. The columns are supported by footings placed below grade. Please see Figure 3.18 below.



Figure 3.18: Photograph of South Pier (Facing North)

3.2.6 Girders

The main structural elements consist of five continuous rolled W36x170 members of A36 steel that are 214 feet 6 inches (65.38 m) in length. The members are set parallel to the direction of Interstate 91 traffic with a spacing of 7 feet 6 inches (2286 mm) (Figure 3.19). Diaphragms that connect girders are described below in a following section.

Two splice plates join girder sections in the center span, 17 feet (5.18 m) from pier supports. The spliced connections include plates $11'' \times \frac{1}{16}'' \times 42.5''$ (279 x 17 x 1080 mm) on outside flanges, $4'' \times 1'' \times 42.5''$ (102 x 25 x 1080 mm) on inside flanges, and plates $30'' \times \frac{7}{16}'' \times 18.5''$ (762 x 11 x 470 mm) attached to each side of the web. Hi-tensile bolts of $\frac{7}{8}$ inch (22 mm) diameter are used throughout the connection.

The girders directly support the bottom of the concrete deck, with a 1 inch (25 mm) lip of concrete placed between the top flange of the beam and bottom of the 7½ inch (191 mm) slab (Figure 3.20). There are no shear connectors placed on the top of the steel beam, as the beams were not designed to act compositely with the deck.

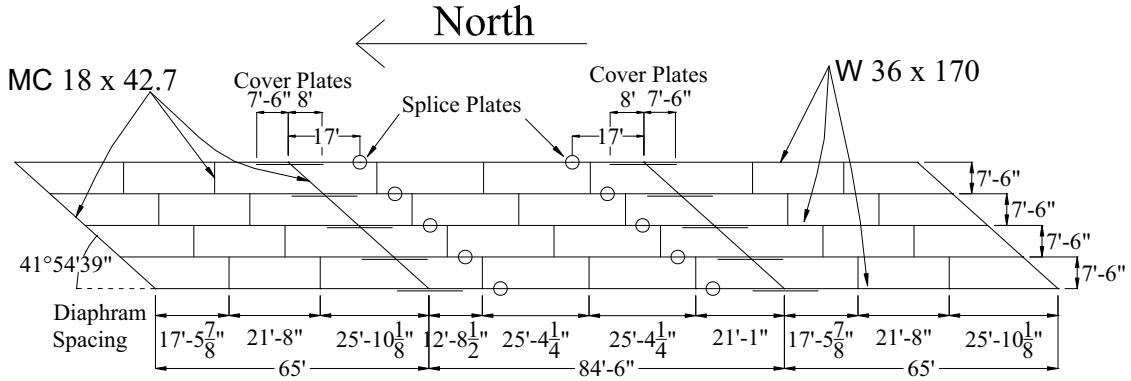


Figure 3.19: Weathersfield Framing Plan

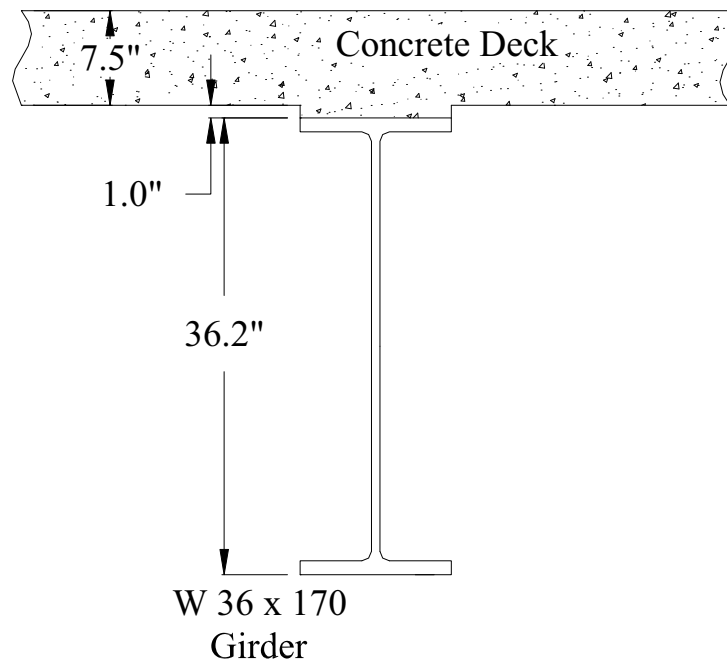


Figure 3.20: Girder and Deck Connection Detail

3.2.6.1 Support Conditions

The girders are supported at each end by abutment walls and above each pier. The south abutment has a rocker type connection designed to allow rotation but not translation as shown in Figure 3.21a. The piers and north abutment have a rocker type bearing that allows some translation.

As shown in Figure 3.21b the steel between the bottom rocker and lower flange of the I-beam can physically deform to allow expansion as well as rotation at the support. The interior piers have a similar bearing type as the north abutment as shown in Figure 3.21c.



a) Bearing South Abutment



b) Bearing North Abutment



c) Bearing Over Interior Pier



d) Cover Plate Over Interior Pier

Figure 3.21: Bearings Supporting W36x170 Beams

Cover plates were also added to the beam section above interior piers. Typically cover plates are used as a way to increase the moment capacity of the beam without using a larger section shape along the entire span. Extending 15 feet 6 inches (4.72 m) in length, the $\frac{1}{2}$ " x 10" (13 mm x 254 mm) cover plates were welded to top and bottom flanges of the W36x170 members.

3.2.6.2 Damage From Vehicle Collision

It was noted during the last state engineers' bridge inspection in May of 2004 that the bridge had been struck by an over-height vehicle in 2003. Marking on the bridge by inspectors indicate that the collision took place on or before June 28, 2003. Damage was caused to three of the five girders above the westbound travel lane of route 131, and was still present at the time of the load test. The extent of the damage to two of the girders is limited to a localized section where the lower flange has been bent (Figure 3.22). The third girder (Figure 3.22b) suffered a bent lower flange, a 21 ¼ inch (540 mm) crack at the flange-web interface, as well as permanent deformation to the entire cross section that was pushed visibly out of alignment due to the force of the collision. Inspectors monitoring the crack have not noticed any crack growth.



a) Lower Flange Bent Upward Crack

b) Lower Flange Bent Upward and Between Web and Flange

Figure 3.22: Photographs of Damage to Flange Girders From Truck Strike

3.2.7 Diaphragms

The five girders are connected to C18x35 diaphragm members, through a connection plate that is welded to the web of the girder and bolted to the channel. Seven rows of diaphragms are connected perpendicularly to the girders, with three in the center span and two in each side span. Additional C18x35 members are connected at the skew angle of 41° 54' 39" to each girder above interior pier supports and abutment supports (Figure 3.19).

3.2.8 Deck

The bridge has a 7 ½ inch (191 mm) thick reinforced concrete deck slab. The original plans indicate 1 ½ inch (38 mm) of bitumen concrete wearing surface, however in 1989 a 2 inch(51 mm) overlay of bitumen concrete wearing surface was placed on the deck.

3.2.9 Joints

An open finger joint with a trough near the north abutment allows for expansion and contraction of the bridge, shown in Figure 3.23a. The joint is located near the bearing support in Figure 3.21b that allows translation. A trough below the joint is installed to collect and shed water away from structural steel below.

A closed joint, shown below in Figure 3.23b of the south end of the bridge is designed to be impermeable to water. From the design of the bearing below the joint (Figure 3.21a) is not designed for translation, but may allow for some rotation.



A) Finger Expansion Joint (north)

B) Closed joint (south)

Figure 3.23: Joints in Bridge Deck

3.2.10 Curb and Railing

Curbing composed of concrete and granite, is provided along the entire length of the bridge. The curb cantilevers past the centerline of the exterior girder for a distance of 29 in (737 mm). The exterior 23 in (548 mm) portion of the 15 in (381 mm) thick curb is constructed using reinforced concrete. The concrete anchors a metal railing and backs a 6" x 12" (152 mm x 305 mm) granite curb face. Railings are fashioned from metal using posts and railings.

3.2.11 Load Rating and Current Condition

The current load rating for this bridge after an inspection in May of 2004 finds that the bridge is overall in "satisfactory" condition, and does not require a posting or restriction. Using load factors, the bridge received an inventory rating of HS-35 and operating rating HS-58. The negative moment over interior piers, however, controls the load rating, which prevents some overload permits from being granted. Without the capacity for overload vehicles, they must exit the highway and detour around the bridge. Additionally, when inspected in May of 2004, both the deck and superstructure received a "satisfactory" rating while the substructure was recorded to be in "good" condition.

CHAPTER 4 - TESTING PROCEDURE

This chapter outlines the engineering background and testing procedure followed to conduct the Royalton and Weathersfield Bridge field tests. Additional information including more detailed procedures and methods for conducting field tests can be found in Appendix C.

The testing of both bridges is designed to capture the bridges' response to applied loads, so a finite element model can be calibrated. By measuring strains at calculated positions along a bridge structure with a moving semi-static load, the load carrying characteristics of the bridge can be recorded in a relatively short period.

Testing for the Royalton and Weathersfield Bridges followed similar procedures, utilizing the same equipment with minor modifications. Each test required the attachment of strain gauges to the structural members of each bridge, followed by the recording of strain measurements as a load truck traversed that bridge following a set path.

4.1 Testing Equipment

The testing equipment used in this project was purchased from Bridge Diagnostics Inc. (BDI). Included with the BDI materials were strain gauges, wiring, software to record strain data on a portable laptop computer, and a device to track the load truck location. Additional equipment such as the load vehicle and traffic control was supplied by VTrans on the day of testing.

4.1.1 Strain Gauges

The BDI manufactured strain gauges utilize a full Wheatstone bridge with four 350 Ω foil gauges to measure both tension and compression along its axis of orientation, within two percent accuracy. The BDI strain gauge shown in Figure 4.1 is 3 inches (72.2 mm) long between mounting holes. Each gauge is reusable and has an individual serial number used to correlate recorded strain data during analysis.

Typical strain gauges are attached to structural members to record the strain between the two points it is mounted. In this study, at least two gauges are placed at the same cross section of a member in a pair. The ideal placement of gauges is at both the top and bottom of the cross section to record maximum strain values, either in tension or compression. Assuming a linear strain profile, a strain diagram of the member can be created and moment calculated at the gauge pair location as is discussed in Chapter 6.

The holes at each end of a gauge allow attachment to structural members with $\frac{1}{4}$ inch (6.4 mm) bolts. A one-sixteenth inch (1.6 mm) pad under the mounting holes

ensures the gauge does not contact the structural member and that measured deformation occurs entirely over the across 3 inch (72.2 mm) gauge length.



Figure 4.1: Picture of BDI Strain Gauge

BDI also manufactures aluminum gauge extensions for testing reinforced concrete structures, which increase the gauge length beyond 3 inches (72.2 mm). A gauge extension is useful when testing heterogeneous materials such as reinforced concrete, in which flexural cracks occur under loading. Because deformation concentrates around flexural cracks in the concrete, the extensions allow an average strain over a longer distance. The BDI extensions extend the effective length of the gauge in 3 inch (72.2 mm) increments between 6 and 24 inches (152 to 610 mm). The actual strain can be determined during data reduction by dividing the measured strain by one-third of the extended gauge length.

4.1.2 Strain Gauge Attachment

Gauges can be attached to structural members using either C-clamps or a bolt and nut through the holes of each gauge as shown in Figure 4.2. The selection of an attachment method is governed by the material of the attached member, ease of installation, and access to structural members. C-clamps, which are easiest to install and remove, can be only be used in steel structures where they can be attached to a beam flange or side of an angle section. As noted in Appendix A, no significant differences in measured strains were observed during tests in the laboratory with different attachment methods.

For reinforced concrete or steel structures where clamps cannot be attached, the alternative is to pass $\frac{1}{4}$ inch (6.4 mm) bolts through the mounting holes on the gauge and secure with a nut. The bolt can then be attached to a structural member using either an adhered tab or mechanical anchor drilled into concrete. When using a strain gauge extension, one end of the gauge is bolted to the extension while the other end is adhered to the member using a bolt. A second bolt then attaches the gauge extension to the structural member.



a) Clamped Strain Gauge



b) Adhered With Tab



c) 1/4" Mounting Tabs



d) Gauge With Extension

Figure 4.2: Attachment of Strain Gauges

4.1.3 Recording Strain Data

Gauges are wired to a single power supply box that interfaces with a portable laptop computer. The computer operator must balance all strain gauges before load testing begins and can control data recording. The frequency that strain data points are recorded can be set with software. All tests with this project were conducted at 33.33 Hertz, that is 33.33 points were recorded per second. During a test, continuous strain data is recorded from all gauges connected to the system.

4.1.4 Load Vehicle

Testing requires the use one or more heavy trucks to generate a response from the bridge structure. As the test is non-destructive, the truck weight is necessarily below the service limit. It is important to record each axle weight, or if possible the load applied at each tire to calibrate an analytical model with recorded strain data.

Both of the load tests conducted for this project utilized a load vehicle provided by VTrans. An official from the Vermont motor vehicle enforcement unit used portable scales to weigh each tire load.

For the majority of runs, the truck was driven across the bridge at approximately 5 mph (8 km/hr). This speed eliminates effects of dynamic impact and simulates a semi-static loading. Additional test runs at higher speeds were also conducted for comparison purposes.

4.1.5 Auto Clicker

Calibration of a finite element model also requires knowledge of the truck position on the bridge paired with each strain history. To track the longitudinal truck position along the bridge, BDI developed the AutoClicker, a device shown in Figure 4.3.



Figure 4.3: Photographs of AutoClicker Attached to Load Vehicle

Using a reflective paddle attached to the truck tire, an infrared camera mounted over the wheel senses the paddle at each tire revolution and emits a signal with a portable radio. The signal is instantaneously received at the power supply box and the time is marked on the raw data recorded by the laptop. Knowing the distance traveled per revolution of the truck tire, the longitudinal position of the vehicle can be calculated during data analysis.

4.2 Royalton Bridge

4.2.1 Objective of Load Testing

The objective of the load test of the Royalton bridge is to determine the load carrying characteristics of the bridge structure, given the deterioration of structural components and uncertainties of material properties. To accomplish the objective, five goals were set that governed placement of the strain gauges during the testing:

- 1) Determine moment distribution in beams under load.
- 2) Determine load transfer around adjacent beams with observed damage.

- 3) Determine load distribution in bridge deck.
- 4) Determine moment transfer across interior piers.
- 5) Determine the structural contribution of concrete guardrails to supporting loads.

Accomplishing these individual goals increases the understanding of behavior for each bridge component under loading. Because the T-beams, bridge deck, and guard rails all affect bridge behavior, each component is important to achieving the objective.

4.2.2 Strain Gauge Placement

Controlling factors in the placement of the gauges were access to the structure and the number of tests that could be completed in one day. While span 1 could be accessed easily using ladders, the location over the White River made span 2 and portions of span 3 difficult to access. Before the instrumentation, movable staging was installed under span 2 that could be pulled across the river so members of the research team could attach the gauges and run wires. Because of time constraints put on the project and limited access to span 3 it was assumed that spans 1 and 3 act similarly due to symmetry.

4.2.2.1 Longitudinal and Transverse Placement of Strain Gauges

To collect enough data to satisfy the five main goals, 33 locations for gauge pairs were created in locations shown in Figure 4.4. Because only ten gauge pairs can be connected to testing equipment during each test, four test setups A, B, C, and D were required. The gauge pairs attached in each of these four test setups are listed in Table 4.1.

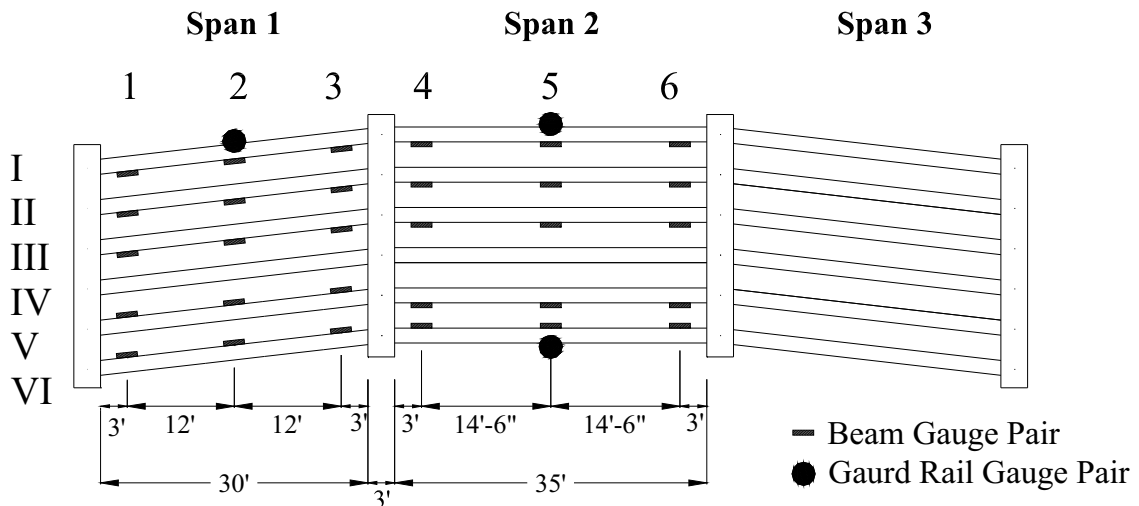


Figure 4.4: Gauge Locations for All Tests in Royalton Bridge

Table 4.1: Gauge Combinations of Figure 4.4

Test Setup	Gauge Pair	Girder Type	Distance From Span 1 Abutment	
			(feet)	(meters)
A	I-1	Exterior	3	1.04
	I-2	Exterior	15	5.22
	I-3	Exterior	27	9.40
	II-1	Interior	3	1.04
	II-2	Interior	15	5.22
	II-3	Interior	27	9.40
	III-1	Interior	3	1.04
	III-2	Interior	15	5.22
	III-3	Interior	27	9.40
	GR I-2	Guardrail	15	5.22
B	V-1	Interior	3	1.04
	V-2	Interior	15	5.22
	V-3	Interior	27	9.40
	V-4	Interior	36	12.53
	V-5	Interior	51	17.57
	VI-1	Exterior	3	1.04
	VI-2	Exterior	15	5.22
	VI-3	Exterior	27	9.40
	VI-4	Exterior	36	12.53
	VI-5	Exterior	51	17.57
C	III-4	Interior	36	12.53
	III-5	Interior	51	17.75
	III-6	Interior	65	22.62
	V-4	Interior	36	12.53
	V-5	Interior	51	17.75
	V-6	Interior	65	22.62
	VI-4	Exterior	36	12.53
	VI-5	Exterior	51	17.75
	VI-6	Exterior	65	22.62
	GR V-5	Guardrail	51	17.75
D	I-4	Exterior	36	12.53
	I-5	Exterior	51	17.75
	I-6	Exterior	65	22.62
	II-4	Interior	36	12.53
	II-5	Interior	51	17.75
	II-6	Interior	65	22.62
	III-4	Interior	36	12.53
	III-5	Interior	51	17.75
	III-6	Interior	65	22.62
	GR I-5	Guardrail	51	17.75

4.2.2.1.1 Placement for Goal #1: Moment Distribution in Beams

To calculate the moment along a beam gauge pairs are placed at select locations. If it is assumed that the shape of the moment diagram is approximately linear between gauge pairs, a moment diagram for each beam can be created.

For each of the beams tested, three gauge pairs were spaced along each beam. Pairs were placed at mid-span near the maximum positive moment region, and at each end. Gauge pairs ends of each beam were located 36 inches (914 mm) from the face of the abutment to avoid problems with shear and zero moment of the simply supported spans.

4.2.2.1.2 Placement for Goal #2: Load Transfer Around Damage

From a prior inspection of the structure two areas of interest with severe deterioration (such as spalled concrete cover with heavily corroded rebar) were mapped (a and e) on a plan view diagram of the bridge shown in Figure 3.9. It was determined that both of these deteriorated beams and the adjacent beams should be instrumented with strain gauges to understand load distribution around damaged sections. These results can then be compared to similarly instrumented beams with no visible signs of damage.

The first area of deterioration with spalled concrete and corroded rebar is located on beam II as shown in Figure 3.9a. Beams I and III on either side of the damaged beam II in span 1 were instrumented to determine load distribution as shown in Figure 4.5. For comparison, beams I, II, and III in span 2 were also instrumented as they show no outward signs of deterioration.

The second area of deterioration is located near the scupper hole on beam VI as shown in Figure 3.9e. Beam VI and adjacent beam V in span 2 were instrumented. For comparison, beams V and VI in span 1 were also instrumented as they did not exhibit visible signs of damage.

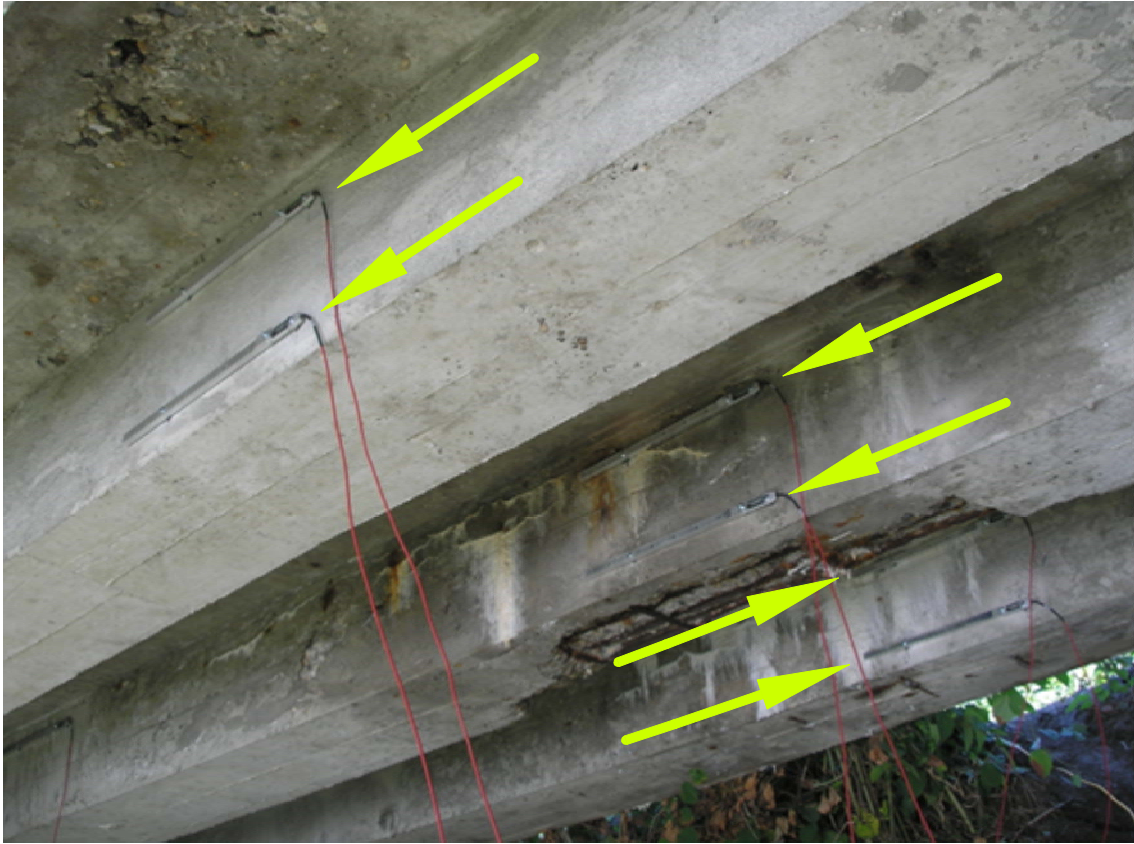


Figure 4.5: Strain Gauges Attached to Deteriorated and Adjacent Beams

4.2.2.1.3 Placement for Goal #3: Load Distribution in Bridge Deck

The load from a truck supported by the bridge deck is similar to a set of point loads applied at tire locations. The point loads are distributed by the deck to nearby beams. Parallel T-beams were instrumented to determine the concentrated force distribution from the deck to individual beams across the bridge.

T-beams I, II, and III in span 2 were instrumented for this purpose. They are in relatively good condition without visible signs of deterioration or problems that might contribute to changes in load distribution.

4.2.2.1.4 Placement for Goal #4: Moment Transfer Across Interior Piers

While the bridge is designed with simply supported spans, it has been found in past studies that unintended moment transfer can occur through piers (Jáuregui and Barr 2004). Ideally, with simply supported conditions there would be zero moment at the ends of each beam.

End gauges were attached 36 inches (914 mm) from the end of the beam at both sides of pier 1 to calculate moment. If moment is transferred through the piers, it will be indicated by strain recorded by gauge pairs when the truck loading lies outside the span.

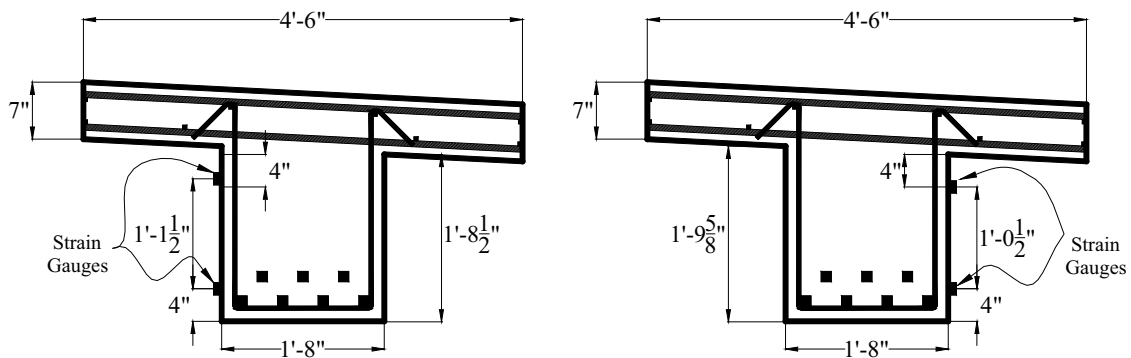
4.2.2.1.5 Placement for Goal #5: Structural Contribution of Concrete Guard Rails

To investigate any structural stiffness contribution from the guardrails, gauge pairs were mounted at mid-span in three sections on the guardrail to measure any moment transfer (Figure 4.4). Because there were clear gaps at expansion joints between the spans of the rail, it was assumed that there would be low moment at ends of the guardrail sections near interior piers, and instrumentation at mid-span would produce the most tangible results.

4.2.2.2 Vertical Location of Gauges on Beams

The lower gauge in each beam stem was placed 4 in (102 mm) from the bottom to position the gauge parallel to reinforcing bars as shown in Figure 4.6. All of the top gauges were positioned 4 in (102 mm) from the bottom of the concrete deck on the side of the beam stem, a distance chosen that would allow gauges to be easily attached and removed. The top and bottom gauges of each pair were placed on the same side of each beam.

While the ideal location for the top gauge might be an attachment to the top of the T-beam, placing a gauge at this location was not possible. Layers of asphalt paving above the reinforced concrete would not be a suitable material to attach the gauges, nor could the layers be removed for the test. Additionally, the gauges would be damaged if accidentally run over by the load truck or traffic while bridge lanes were open between tests.



a) Gauges Attached to Upstream Face b) Gauges Attached to Downstream Face

Figure 4.6: Diagram of Strain Gauge Locations on T-beams

While only placing gauges on one side of the beam will not capture the effects of any torsion resulting from the load, these effects are considered minimal. Having

both gauges in the pair located on the same side of the beam is advantageous for installation and measuring the vertical distance between the pair.

As shown in Figure 4.6 gauges were attached to either the upstream or the downstream face of the beam at different sections. Due to the super elevation of the concrete deck, this had an effect on the gauge spacing, with gauges located on the upstream side of the bridge having a slightly greater spacing.

4.2.2.3 Vertical Location of Gauges on Guard Rail

Gauge pairs attached to guardrail sections were all attached on the roadway side at center span. The top gauge was located 4 inches (102 mm) below the top of the guardrail and the bottom gauge was located five inches above the road deck as shows in Figure 4.7. Spacing between pairs was 31 inches (787 mm).

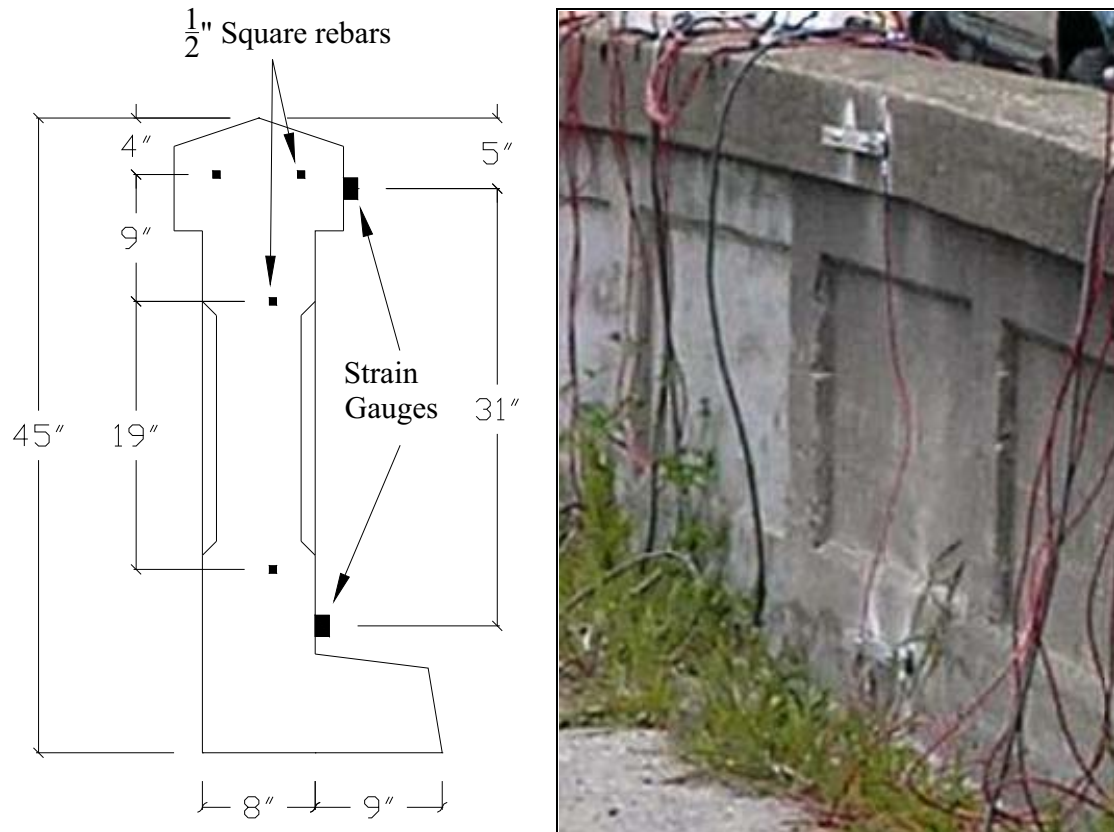


Figure 4.7: Drawing and Photograph of Gauge Pair Attached to Guardrail

4.2.2.4 Use of Gauge Extensions on Reinforced Concrete

Because the structure is constructed of reinforced concrete, aluminum extensions designed by BDI were used to extend the strain gauge length and average deformations over several flexural cracks.

A strain gauge length of 18 inches (467 mm) was determined from recommended strain gauge length by BDI, which is based on beam theory that flexural cracks form at approximately 45-degree angles in concrete. Additional recommendations from the gauge manufacturer were that the gauge length not exceed $L/20$ and is not less than 1.5 times the beam depth, where L is span length. Maximum gauge lengths of 18 and 21 inches (457 and 533 mm) were therefore recommended based on the $L/20$ ratio for the 30 and 35-foot (9.14 and 10.67 m) spans, respectively. In theory, if a crack propagates at a 45-degree angle in the beam, an 18-inch (457 mm) gauge length would ensure that the gauge would span at least one crack; the strain measured over the gauge and extension length is then averaged. Therefore, all gauge extensions were set to create a total gauge length of 18 inches (457 mm) for the test.

4.2.2.5 Attaching Gauges to Bridge

It was quickly determined on site that holes could not be drilled into the structure using masonry concrete drill bits or hammer drills due to the hardness of the concrete and large aggregate found near the surface. As an alternative, steel tabs and adhesive were used to bond both the extensions and strain gauges to the bridge.

Prior to attaching the gauges, the approximate location of the tabs was marked with a permanent marker on the concrete by measuring with a tape from a pier or abutment wall to the location of the gauge. A level was used to transfer marks from the bottom of the beam to the top so that the gauges were correctly positioned at the same beam cross section. The area where the tab would be attached was then ground with an electric grinder to smooth the area in preparation for the tab. The spot was then vigorously cleaned of dust using a small hand held brush. A permanent marker was then used to mark the exact point where the tab would be adhered to the beam.

Before each run of the load truck, the strain readings from all strain gauges were monitored to ensure that the initial strain readings at the start of the test were close to zero. If there were any noticeable strain readings, the bridge was checked for any approaching traffic and all of the gauges were re-balanced before the truck made another pass.

4.2.3 Condition and Weather the During Testing

Setup and testing for the Royalton Bridge took place on August 21st, 2006 when the load vehicle was weighed and the research team began to mark and grind the concrete surface where tabs would be attached using tabs and epoxy. The team returned

early in the morning on August 22nd to attach gauges, run wires, mark out lanes, and conduct the load tests. The weather condition on both days was partly cloudy skies with highs near 80°F (14°C).

4.2.4 Load Vehicle

The load vehicle provided by VTrans was a tandem axle dump truck (Figure 4.8), loaded with sand from a nearby highway garage that was stockpiled for use on icy roads in the winter. The truck weight was measured using portable scales by the Vermont enforcement agency by a certified officer the day prior to the test. The scales allowed individual tire loads to be measured and recorded. The total weight was found to be 63.7 kips (28,894 kg); the individual tire loads are listed in

Table 4.2.

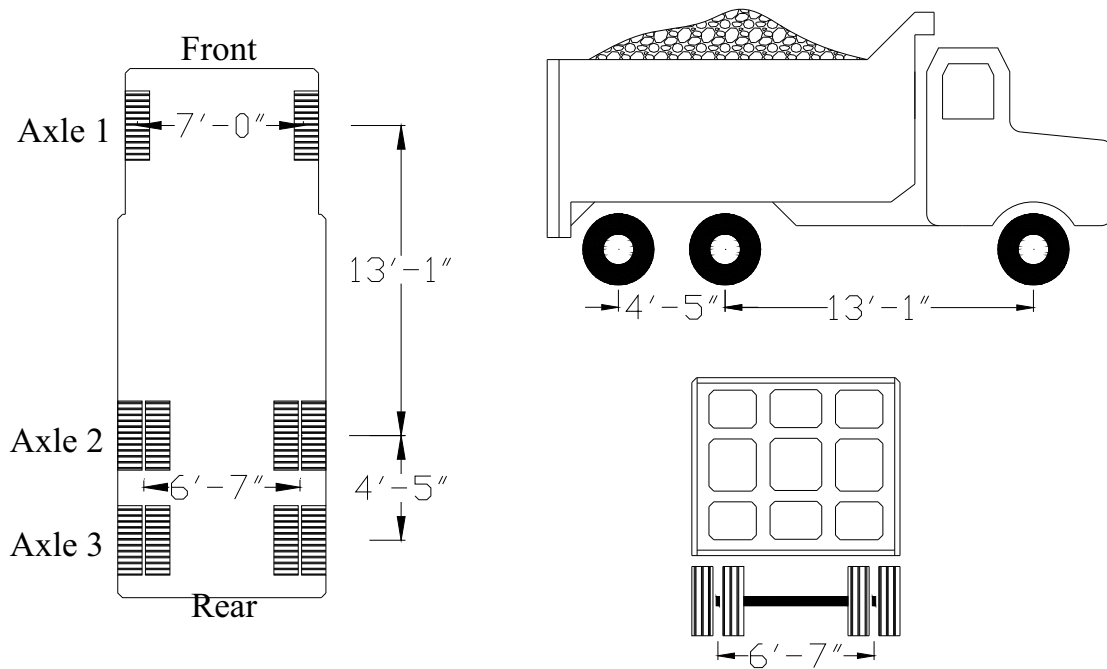


Figure 4.8: Dimensions of Royalton Load Vehicle

The truck was stored indoors overnight to prevent any precipitation from significantly changing the moisture conditions of the sand that could affect its weight. It was recognized that due to moisture loss there might be a weight change during the testing, however these changes were considered negligible. It was not possible to re-weigh the truck after the testing, however any weight change was thought to be insignificant compared to the overall truck weight.

Table 4.2: Royalton Truck Weight (pounds)

	Left		Right		Total	
	(lb)	(kg)	(lb)	(kg)	(lb)	(kg)
Axle 1	7,200	(3,266)	6,700	(3,039)	13,900	(6,305)
Axle 2	12,600	(5,715)	12,500	(5,670)	25,100	(11,385)
Axle 3	11,400	(5,171)	13,300	(6,033)	24,700	(11,204)
Total	31,200	(14,152)	32,500	(14,742)	63,700	(28,894)

4.2.5 Load Vehicle Position

A record of the load vehicle position is critical to accurately model the bridge response. Therefore, time was taken to ensure that both the transverse and longitudinal position of the truck was recorded for each test.

4.2.5.1 Transverse Position and Lanes

Three lanes were established prior to testing for the driver to follow that were designed to produce maximum strain in gauges. With a 20 foot (6 m) wide bridge deck, two lanes were created as close to either guardrail as the driver could position the truck, and one lane was created in the center of the bridge as shown in Figure 4.9. The truck axle width measured as the center-to-center distance between dual tires was 6 feet 7 inch (2 m). Lane 1 was established on the left side of the bridge (upstream). Lane 2 was centered on the bridge deck straddling the two center beams. A third lane on the far right side (downstream) side of the bridge was used for the final pass.

4.2.5.2 Longitudinal Position

The longitudinal truck position was monitored with the use of the AutoClicker attached over the rear wheel of the load truck. A distance of 10.8 feet (3.29 m) was measured per revolution of the tire with the attached AutoClicker. A line painted on the roadway 40 feet (12.19 m) from the bridge abutment, served as a reference point for the truck to start each run.

Before each test started, the truck was aligned with the front tire positioned over the painted line to ensure that the load vehicle would always start from the same position. Additionally, the paddle for the AutoClicker was positioned just before the infrared camera so that the first click would be recorded as the truck began to move forward. Data was recorded while the truck continued to cross the bridge following each lane until the rear axle was off the bridge.

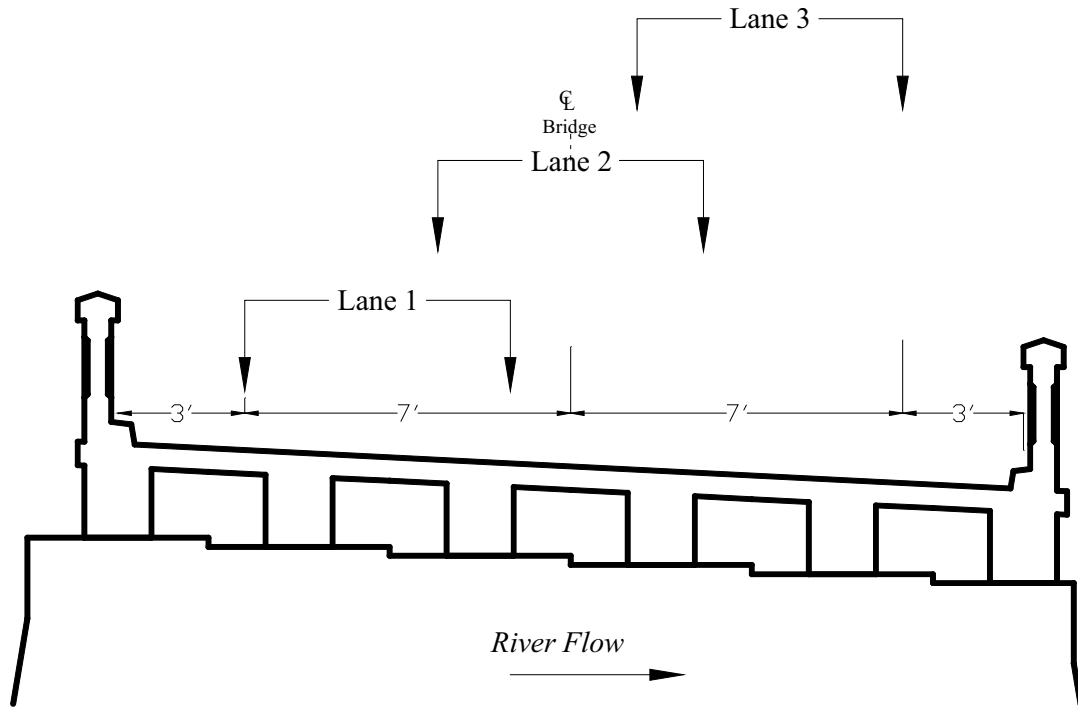


Figure 4.9: Diagram of Truck Lane Locations

4.2.6 Repetition of Loading

For each configuration of the strain gauges under the structure, two passes were made and recorded in each lane as listed in Table 4.3. In cases where there was a problem with the data recording system or when the truck not properly positioned in the lane, the pass was repeated. Duplicating each pass of the truck reduced the chance of any error and verified linear behavior of bridge elements.

4.2.7 Record of Quarry Trucks Crossing Bridge

During the initial strain gauge configuration, four heavily loaded trucks from a quarry (Figure 3.4) which frequently cross the bridge were stopped in traffic as the load vehicle was crossing the bridge. The crossing of these four trucks at their normal crossing speed was recorded for review and analysis comparison. As the trucks were crossing the span, a portable radio was used to record clicks as the trucks crossed the bridge at approximately 25 mph (40 km/hr). The first click was made at approximately the same starting point for the load vehicle 40 feet (12.19 m) before the bridge, with subsequent clicks as the front of each truck reached either an abutment wall or interior pier.

Additional information, including the data recorded during the Royalton and Weathersfield Bridge tests, is presented and discussed in Chapter 5.

Table 4.3: Test Record for Royalton Bridge

Setup	Run ID	Lane
A	1	1
	2	1
	Granite Truck Record	
	3	2
	4	2
	5	3
B	6	3
	1	1
	2	1
	3	2
	4	2
	5	3
C	6	3
	1	1
	2	1
	3	2
	4	2
	5	3
D	6	3
	1	1
	2	1
	3	2
	4	2
	5	3
	6	3
	7	3
	8	High Speed
9	High Speed	

4.3 Weathersfield

4.3.1 Objective of Load Testing

The objective of the Weathersfield bridge test is to determine the load carrying characteristics of the bridge structure, given the large angle of skew, damage to girders from a truck strike, and the possibility of composite action. VTrans officials were most interested in the negative moment region over each pier because this was the controlling factor for bridge rating. To accomplish the objective, four goals were set that governed placement of the strain gauges during the testing:

- 6) Determine controlling factors for negative moment over piers.
- 7) Determine if composite action exists between deck and girders.
- 8) Determine possible effect of truck strike damage on load distribution.
- 9) Determine transverse distribution factors of bridge given the large skew angle and diaphragms.

4.3.2 Strain Gauge Placement

The controlling factors in the placement of the gauges were access to the structure and the number of tests that could be completed in one day. Since all critical areas of interest to achieve the objective were located in the center span, side spans were not instrumented.

4.3.2.1 Longitudinal and Transverse Placement of Strain Gauges

To collect enough data to satisfy the four main goals, 30 locations for gauge pairs were created in locations shown in Figure 4.10. Three test setups (A, B, and C) were required because only ten gauge pairs could be connected to the available equipment during each test. Details of the gauge pair locations used in each test setup are listed in Table 4.4.

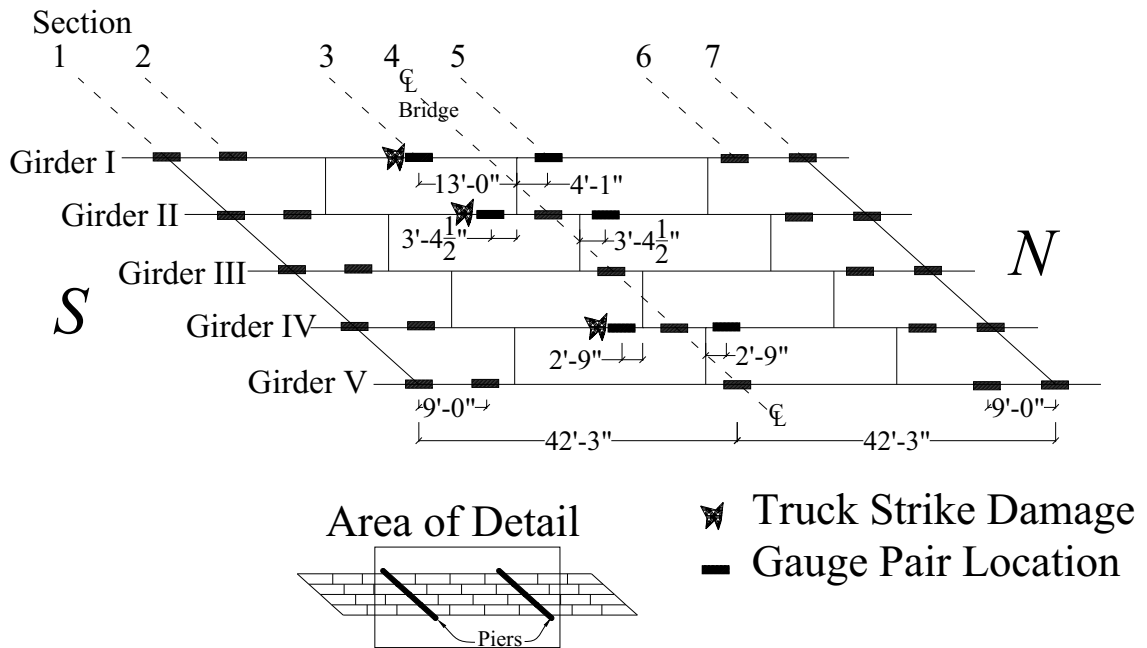


Figure 4.10: Diagram of Weathersfield Bridge Gauge Locations

Table 4.4: List of Gauge Locations in Weathersfield Load Test

Test Setup	Gauge Pair	Girder Type	Distance From North Pier	
			(feet)	(meters)
A	I-3	Exterior	51.1	17.77
	I-5	Exterior	34.0	11.82
	II-3	Interior	49.8	17.33
	II-4	Interior	42.3	14.70
	II-5	Interior	34.7	12.07
	III-4	Interior	42.3	14.70
	IV-3	Interior	49.2	17.11
	IV-4	Interior	42.3	14.70
	IV-5	Interior	35.3	12.29
	V-4	Exterior	42.3	14.70
B	I-6	Exterior	9.0	3.13
	I-7	Exterior	0.5	0.17
	II-6	Interior	9.0	3.13
	II-7	Interior	0.5	0.17
	III-6	Interior	9.0	3.13
	III-7	Interior	0.5	0.17
	IV-6	Interior	9.0	3.13
	IV-7	Interior	0.5	0.17
	V-6	Exterior	9.0	3.13
	V-7	Exterior	0.5	0.17
C	I-1	Exterior	214.0	74.47
	I-2	Exterior	205.5	71.51
	II-1	Interior	214.0	74.47
	II-2	Interior	205.5	71.51
	III-1	Interior	214.0	74.47
	III-2	Interior	205.5	71.51
	IV-1	Interior	214.0	74.47
	IV-2	Interior	205.5	71.51
	V-1	Exterior	214.0	74.47
	V-2	Exterior	205.5	71.51

4.3.2.1.1 Placement for Goal #1: Negative Moment Over Piers

Load tests B and C were designed to determine the negative bending moments at interior piers. Gauge pairs were placed 6 inches (152 mm) from the support bearing

plate, because the plate prevented the gauge from being attached directly at the support (sections 1 and 7 of Figure 4.10). Gauge pairs were also located 9 feet (2.74 m) from bearing plates of both piers supports, a distance equal to ten percent of the center span length (sections 2 and 6 of Figure 4.10).

4.3.2.1.2 Placement for Goal #2: Composite Action Between Deck And Girders

The effects of composite action will be determined by plotting the neutral axis of beam sections based on strain data in Chapter 6. Plots that show a neutral axis of bending above half of the beam depth will indicate the presence of composite action, which can be verified from all gauge pairs.

4.3.2.1.3 Placement for Goal #3: Effect of Truck Strike on Load Distribution

In order to quantify the effect of damage caused by a truck strike, gauge pairs I-3, II-3, and IV-3 in Figure 4.10 were placed adjacent to damage on the lower flange of the girders. Gauges were located adjacent to damage and not directly at the point of impact as shown in Figure 3.22a because a flat section of steel is required to attach gauges without causing permanent harm to the whetstone bridge.

Gauges pairs were also placed symmetrically about the centerline of the bridge to compare strain histories with the damaged gauges (I-5, II-5, and IV-5 in Figure 4.10). To ensure symmetric loading given the angle of skew, trucks also traversed the bridge in opposite directions with test setup A for data comparison.

4.3.2.1.4 Placement for Goal #4: Distribution Factor of Deck

The gauge pairs in sections 1, 2, 4, 6, and 7 of Figure 4.10 were aligned longitudinally along the bridge in members based on the angle of skew. By comparing the truck position with moments in each of the members, the distribution of loads by the bridge deck and diaphragms may be determined.

The gauges were placed in sections 1, 2, 6, and 7 of Figure 4.10 to investigate transverse distribution factors in negative moment regions in test setup B and C. Gauges placed at the centerline on the bridge span in section 4 can be used to investigate transverse distribution factors in positive moment regions in test setup A.

4.3.2.2 Vertical Placement of Gauges on Girders

For each gauge pair, gauges were placed as close as possible to the flanges of the steel girders. One gauge was attached to the bottom of the lower flange and a second gauge was attached to the bottom of the top flange as shown in Figure 4.11.

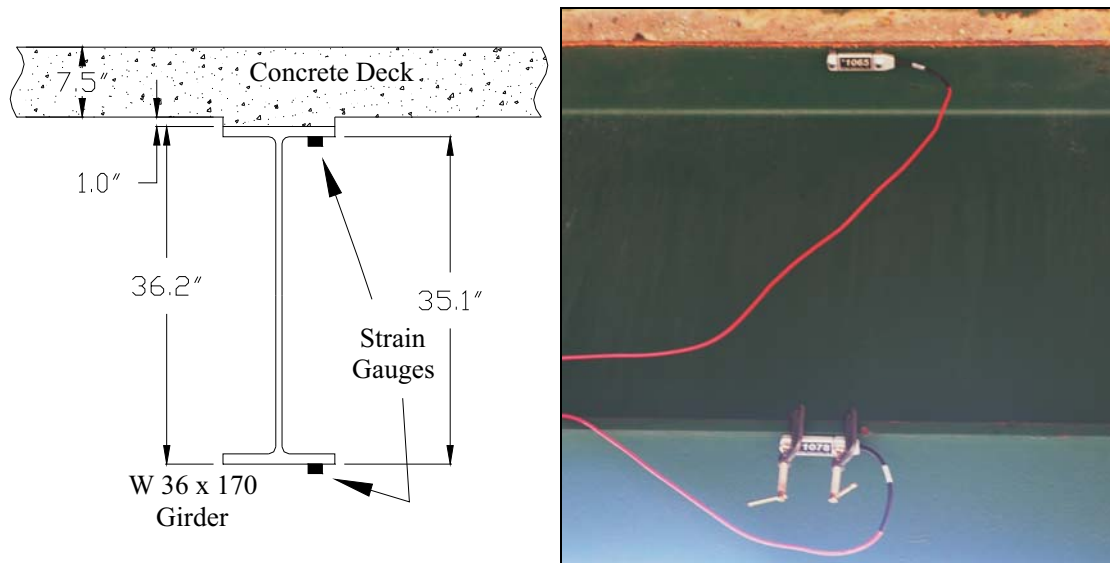


Figure 4.11: Diagram and Photograph of Gauge Pair Placement

4.3.2.3 Attaching Gauges to Bridge

The top flange gauge was secured using a tab and adhesive method. The gauges on the lower flange were attached using a C-clamp around the flange, with the exception of gauges placed 6 inches (152 mm) from interior piers. It was found that next to the piers C-clamps were not large enough to fit over cover plates, so the tabs and adhesive were used.

4.3.3 Condition and Weather During Testing

Testing for the Weathersfield bridge took place on September 20, 2006. Temperatures ranged from a low of 50°F (10°C) in the morning to near 70°F (21°C) in the afternoon, with fog giving way to partly cloudy skies. Work began at 7:00 am and concluded around 4:00 pm, with three test setups completed.

4.3.4 Load Vehicle

To achieve the objective of attaining the highest negative moment over the piers and generate a large response from the bridge, careful consideration was given to the load vehicle. Based on the weight of the highway department dump truck used in the Royalton test, an estimate of the negative moment over both piers was calculated by plotting an influence function. The influence function was used to calculate the expected moment generated in the bridge and analyze load vehicle configurations that could increase the moment.

The possibility of using two trucks during the load test was considered to increase both positive and negative moments. Further calculations determined two optimal truck spacing that could increase the negative moment over piers by

approximately 70 percent, without exceeding service limits. The first configuration was to align trucks in the same lane with 45 feet (13.72 m) between the rear bumper of the front truck and the front bumper of the rear truck. The second configuration was to space trucks in the same lane as close together as possible.

An influence function was also created for the positive moment in the center span. Through calculations, it was found that the maximum positive moment is generated with the second configuration above, with two trucks spaced bumper to bumper.

Because both tests produced approximately the same increase in negative moment, and the second configuration generated the largest positive moment, the second configuration with back-to-back spacing was selected for the load testing.

VTrans provided two tandem axle dump trucks loaded with sand for the day of testing to achieve the desired moment values. The truck weights were measured using portable scales by the Vermont enforcement agency by a certified officer the day of the test. The scales allowed individual tire loads to be measured and recorded. The total weight of the two trucks used in the test was found to be 57.5 and 59.2 kips (26,082 and 26,853 kg) (Table 4.5).

The trucks were aligned back to back, with approximately 13 feet 5 inches (4.09 m) between the rear axle of the front truck and the front axle of the rear truck as shown in Figure 4.12. This distance was maintained throughout the load test by chaining the two trucks together. As the front truck moved forward, it towed the rear truck which was in neutral gear. The AutoClicker was attached to the rear axle of the front truck to record the truck positions while crossing the bridge.

Table 4.5: Weight of Weathersfield Trucks

Truck ID		Left		Right		Total	
		(lb)	(kg)	(lb)	(kg)	(lb)	(kg)
T16031	Axle 1	8100	(3,674)	7100	(3,221)	15,200	(6,895)
	Axle 2	9400	(4,264)	11500	(5,216)	20,900	(9,480)
	Axle 3	9300	(4,218)	12100	(5,488)	21,400	(9,707)
	Total	26,800	(12,156)	30,700	(13,925)	57,500	(26,082)
T16040	Axle 1	6600	(2,994)	8000	(3,629)	14,600	(6,622)
	Axle 2	10300	(4,672)	11600	(5,262)	21,900	(9,934)
	Axle 3	10300	(4,672)	12400	(5,625)	22,700	(10,297)
	Total	27,200	(12,338)	32,000	(14,515)	59,200	(26,853)

4.3.5 Load Vehicle Position

The standard truck run direction was north to south (Southbound). However, trucks were also run in both directions (northbound and southbound) for test setup A so that strain readings among damaged sections could be compared. In the standard loading the trucks were aligned back-to-back.

Additional loadings with trucks moving at a higher speed of approximately 20 mph (32 km/hr) were recorded with each load setup. The purpose of testing the bridge with vehicles moving at a higher speed is to compare (in a general way) the bridge response with dynamic loading to the low speed testing. In these high-speed runs, drivers positioned the trucks side-by-side and followed the painted travel lanes of the interstate across the bridge. The side-by-side configuration of the two trucks was selected because a close back-to-back spacing would not have been safe during these runs.

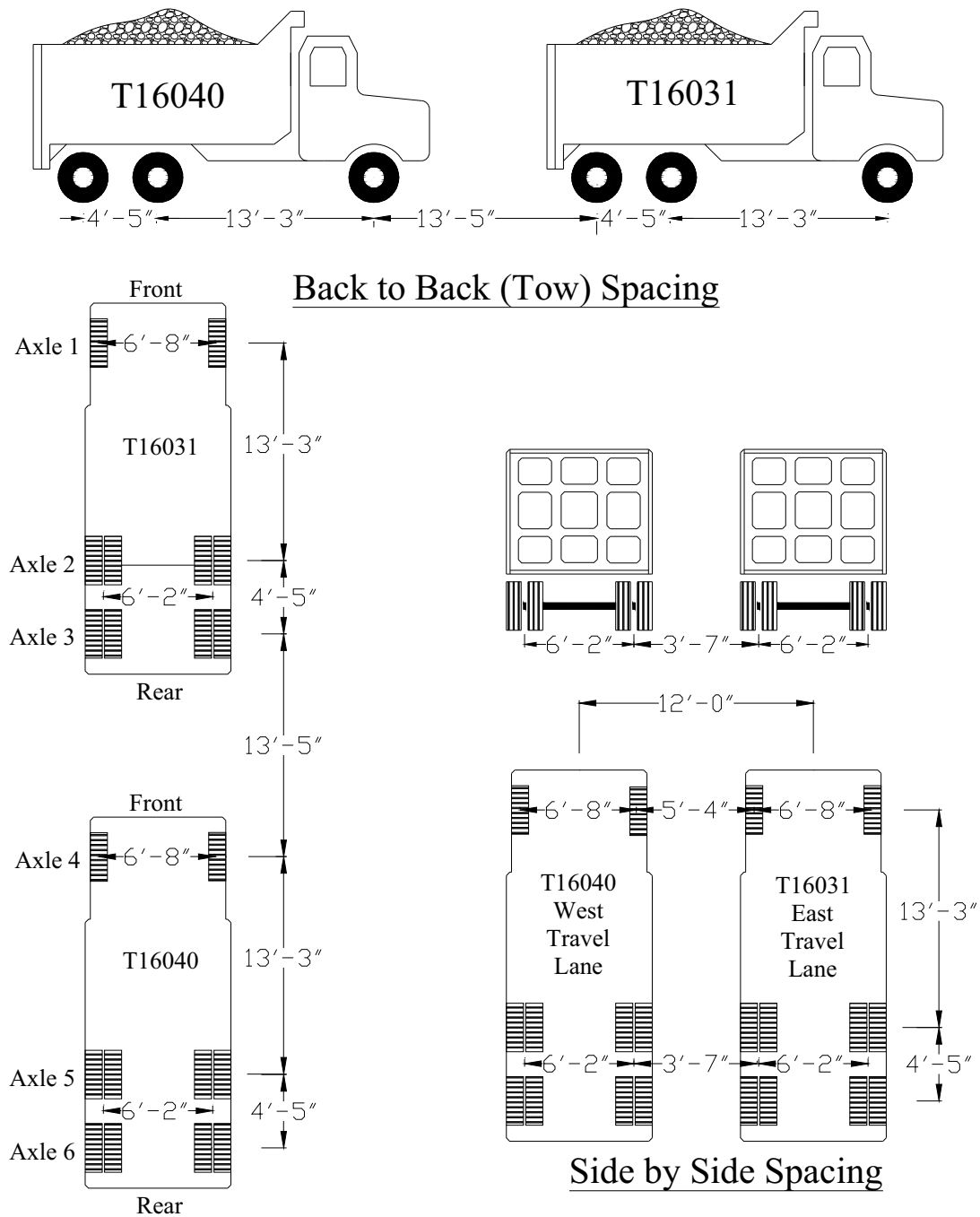


Figure 4.12: Dimensions of Weathersfield Load Vehicles

4.3.5.1 Transverse Position and Lanes

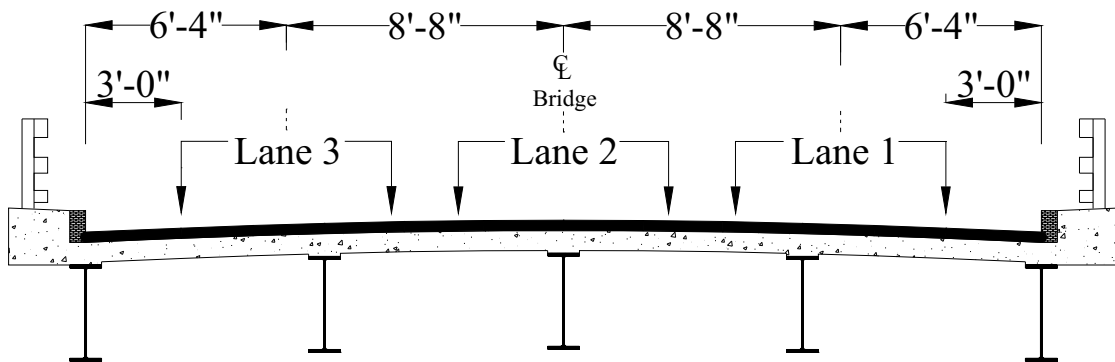
Lanes were established to align the load trucks on the bridge as shown in Figure 4.13. During the high-speed test runs, the load trucks were positioned side-by-side

using the travel lanes painted on the interstate as a guide. Additional lanes were established for load trucks traveling southbound with the back-to-back configuration.

Lane 1 was established by positioning the right tires of the load truck on the solid painted line marking the edge of the interstate travel lane on the west side of the bridge. During northbound travel in this lane, the left tires of the load truck were positioned on this solid line.

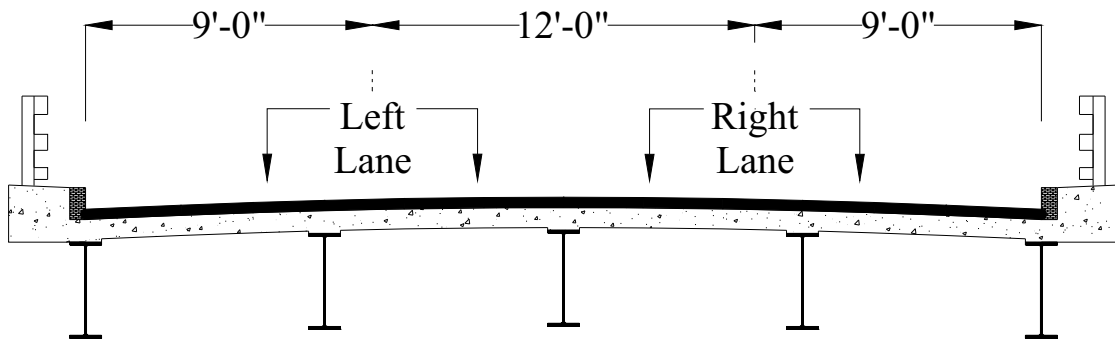
Lane 2 was established by positioning the load truck in the center of the bridge. The middle of the truck was centered by drivers above a painted dashed line dividing the two lanes of the interstate.

Lane 3 was established by positioning the left tires of the load truck on the solid painted line marking the edge of the interstate travel lane on the east side of the bridge. During northbound travel in this lane, the right tires of the load truck were positioned on this solid line.



Cross Section View: North to South

Back to Back (Tow)
Lane Dimensions



Cross Section View: North to South

Side by Side (Travel)
Lane Dimensions

Figure 4.13: Weathersfield Lane Positions

4.3.5.2 Longitudinal Position

The longitudinal position of the trucks was recorded using the AutoClicker, which was attached to the rear axle of the front truck. A distance of 10.92 feet (3.33 m) was measured per revolution of the tire with the attached AutoClicker.

A mark was painted on the roadway 50 feet (15.24 m) from the skewed abutment before the bridge in each lane to ensure a uniform start distance for each run. Before each test, the front tire of the truck was aligned on this paint mark. However, in some cases because of the skew angle and measurement to outside of the truck, the actual distance to the bridge abutment was 43.13 feet (13.15 m). While this distance does not effect the load applied or strain measured in the bridge, this difference was taken into account during data reduction to standardize analysis.

During the high-speed runs, the trucks started approximately $\frac{1}{4}$ mile (400 m) before the bridge and accelerated to approximately 20 miles per hour (32 km/hr). Drivers were asked to maintain a constant speed across the bridge. The AutoClicker could not be used as recommended by the manufacturer. Instead, a portable radio was manually used as a clicker to record when the front of the trucks crossed the abutment and piers. However the side-by-side configuration was difficult for drivers to maintain during acceleration, and it was observed that one driver was consistently well ahead of the other truck when crossing the bridge.

4.3.6 Repetition of Loading

For each configuration of the strain gauges under the structure, two passes were made and recorded in each lane, as shown in Table 4.6. Some runs had to be aborted due to problems with the data recording system or with the truck positioning in the lane. Duplicating each pass of the truck ensured that repeatable data was collected and reduces the possibility of erroneous data.

Table 4.6: Test Record for Weathersfield Bridge

Setup	Run ID	Lane	Direction	Configuration	Distance From Front Axle of Truck to Bridge Abutment at Start	
					(feet)	(meters)
A	1	Aborted	-	-	-	-
	2	3	Southbound	Back to Back	50	(15.24)
	3	3	Southbound	Back to Back	50	(15.24)
	4	2	Southbound	Back to Back	50	(15.24)
	5	2	Southbound	Back to Back	50	(15.24)
	6	Aborted	-	-	-	-
	7	1	Southbound	Back to Back	43.13	(13.14)
	8	1	Southbound	Back to Back	43.13	(13.14)
	9	3	Northbound	Back to Back	43.13	(13.14)
	10	2	Northbound	Back to Back	50	(15.24)
	11	1	Northbound	Back to Back	50	(15.24)
	12	Travel	Southbound	Side by Side		N/A
	13	Travel	Northbound	Side by Side		N/A
	14	Travel	Southbound	Side by Side		N/A
	15	Travel	Northbound	Side by Side		N/A
B	1	Aborted	-	-	-	-
	2	3	Southbound	Back to Back	50	(15.24)
	3	3	Southbound	Back to Back	50	(15.24)
	4	2	Southbound	Back to Back	50	(15.24)
	5	2	Southbound	Back to Back	50	(15.24)
	6	1	Southbound	Back to Back	43.13	(13.14)
	7	1	Southbound	Back to Back	43.13	(13.14)
	8	Travel	Southbound	Side by Side		N/A
	9	Travel	Southbound	Side by Side		N/A
C	1	3	Southbound	Back to Back	50	(15.24)
	2	3	Southbound	Back to Back	50	(15.24)
	3	2	Southbound	Back to Back	50	(15.24)
	4	2	Southbound	Back to Back	50	(15.24)
	5	1	Southbound	Back to Back	43.13	(13.14)
	6	1	Southbound	Back to Back	43.13	(13.14)
	7	Travel	Southbound	Side by Side		N/A

CHAPTER 5 - DATA REDUCTION

5.1 Data Records

During each test run, a record of the strain history for each strain gauge was recorded to the laptop computer in the field with WinSTS software written by BDI. The system began to record data after receiving the first click from the AutoClicker attached to the rear axle of the loading truck, as the truck started moving forward. The amount of data in the strain history is a function of the recording frequency that is set by the computer operator and the test duration. The data recording is manually stopped by the computer operator after the truck has traversed the bridge. For both tests, data was recorded at 33.3 Hz (33 data points per second).

Due to the large volume of data created with each load test, a single method of data reduction was created to streamline analysis. WinGRF software, written by BDI and compatible with WinSTS, is used to format the raw data file. The formatted raw data file was then converted to Microsoft Excel format, and a visual basic macro was used to sort and organize the strain data. This process automates data organization to save time and eliminate errors from manual data manipulation. Appendix D provides more details on the procedure for raw data formatting.

5.1.1 Initial Steps of Data Reduction

The first step of the data analysis was to determine the time each data point was recorded in the strain history. This information was then used with the recorded time of each AutoClicker mark in the strain history using Equation [D.1] to correlate each data point to loading truck position.

Timestamps from the AutoClicker marks in the data record were used to determine the position of the loading truck. Assuming a constant speed between subsequent points recorded by the AutoClicker, the load position for each point in the strain history was determined using Equation [D.2]. Additional parameters that were used to organize the data and obtain useful results are presented separately below for both the Royalton and Weathersfield Bridges.

5.2 Royalton Bridge Data Reduction

A total of 31 files, each with 20 strain gauge histories, were recorded using four different test setups, as shown in Table 4.3 during the Royalton Bridge tests. Using a recording frequency of 33.33 Hz and a travel distance of 10.78 ft (3.29 m) for each AutoClicker mark, the loading truck position for each point in the strain history was determined. Although strain gauges were balanced before the start of each test, small initial strains were sometimes recorded in strain gauges. Therefore, an initial offset was applied to all data in the Royalton test so that the strain in each gauge at the start of the

test was equal to zero; subsequent strain data points were adjusted by subtracting the initial strain offset value.

When plotting strain histories, the distance from the start of the test to the truck first loading the bridge was not altered. Therefore, the front axle in each test crossed the first abutment after the loading truck had traveled 40 ft (12.19 m).

Although the rear axle of the load vehicle moved completely off the bridge after 162 feet (49.38 m) in each test, the strain history for all gauges was plotted to 175 feet (53.34 m) for analysis. Data recorded in each history after the truck had traveled past 175 feet (53.34 m) from the starting position was not considered in the analysis.

The location of abutments and piers were also indicated on the raw strain data plots using a small triangle symbol drawn relative to the starting position of the front axle of the loading truck (Figure 5.1). These marks are useful as a quick reference when comparing data because inflections on the strain and moment diagrams tend to occur after truck axles move on or off the bridge or between the simply supported bridge spans.

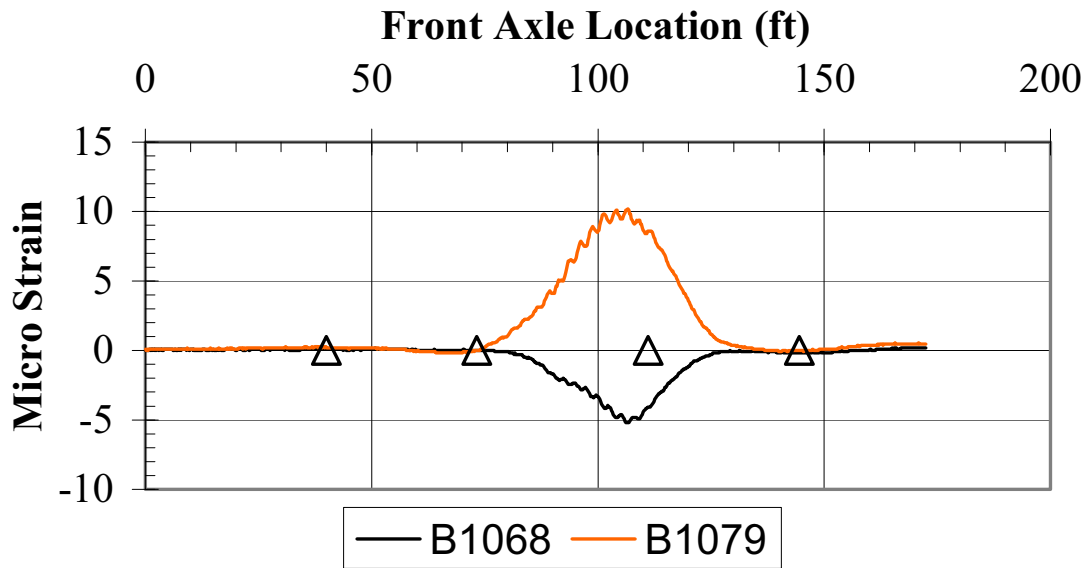
Strain gauge extensions were used for all gauges as recommended by the manufacturer of the test system. Strain gauge data recorded using extensions have to be corrected using a secondary gauge factor as described in Appendix B. All data recorded in the Royalton bridge were corrected to account for the extended effective strain length and the gauge factor. The effective gauge length for all strain data recorded in the Royalton tests was 18 in (457 mm). Therefore, the raw strain was divided by 6 to correct for the default strain gauge factor built into the system for standard 3 in (76 mm) strain gauges. The strain data adjusted for an 18 in (457 mm) gauge length were then multiplied by a correction factor of 1.11 that accounts for using gauge extensions. These manufacturer recommended adjustment factors were independently verified in the Structural Engineering Laboratory at the University of Massachusetts Amherst as described in Appendix B. The total correction factor used for all strain gauge channels in the Royalton bridge was equal to 0.185.

5.2.1 Assessment of Elastic Bridge Response from Raw Strain History Data

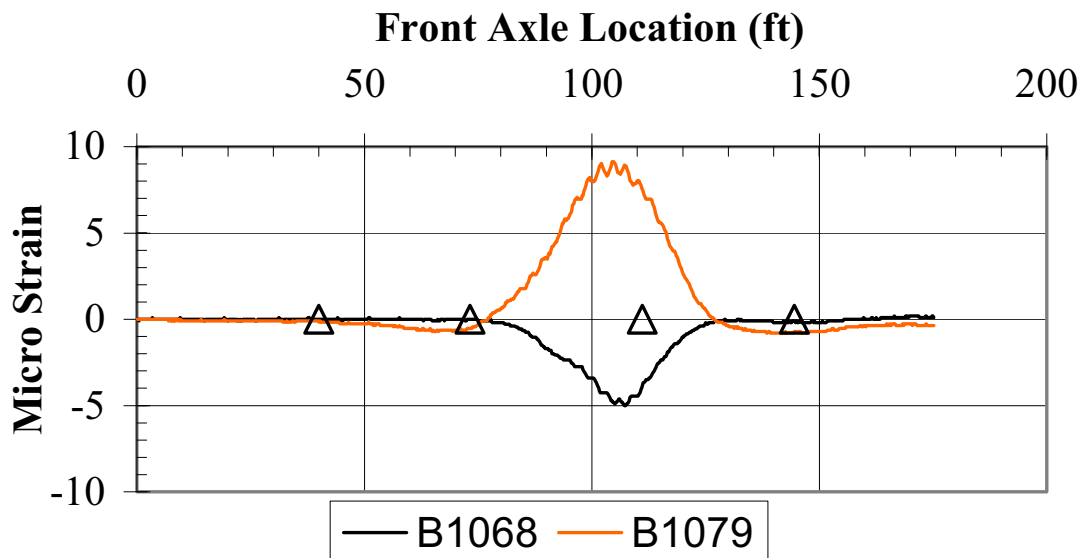
Plots of strain history versus truck position were created for each gauge pair in the bridge, similar to those in Figure 5.1. These figures show two strain histories for the same gauge pair, located at the center of span 2, for a repeated test run in the same lane. From visual inspection of the strain history data plots for each gauge pair, data reliability and linear response of the bridge was evaluated. Note that at approximately 162 feet (49.38 m), the loading truck was located completely off the bridge, and the strain values returned approximately to zero indicating that the bridge response remained within the linear elastic range.

The captions below plots in Figure 5.1 indicate the gauge serial numbers in the gauge pair used to record the strain data. The serial number to the left is the top gauge in the gauge pair and is always plotted with a darker shaded line (in these plots B1068). The serial number to the right is the bottom gauge in the gauge pair and is always plotted with a lighter shaded line (B1079). Positive strain values indicate compression and negative strain values are indicative of tension. All strain data recorded in the test

runs conducted for the Royalton bridge indicated that the bridge responded elastically; these data plots are contained in Appendix E.



(a) First Test Run



(b) Repeated Test Run

Figure 5.1: Strain History Gauge Pair #20 (Lane 2)

5.2.2 Repeatability of Data

Strain data from repeated test runs from different raw data files (such as Figure 5.1) were also compared for consistency by plotting the data together in the same plot (Figure 5.2). From a visual inspection of this plot, the data recorded in different runs showed similar trends and peak magnitudes so the average between two test runs was used for all subsequent engineering calculations.

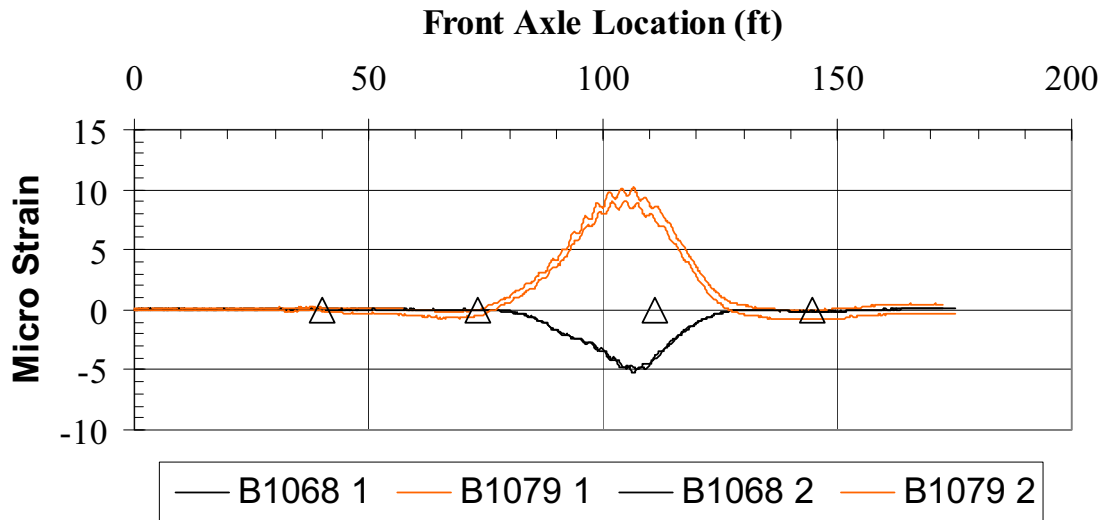


Figure 5.2: Strain Histories of Repeated Test Runs Plotted Together Gauge Pair #20 (Lane 2)

5.2.3 Neutral Axis Calculation

The neutral axis of sections corresponding to each gauge pair was calculated using the strain profile (Figure 5.3) and Equation [5.1] for each row of strain data, if the absolute value of measured strain in the lower gauge was above $5 \mu\epsilon$. Plots of neutral axis depth were then created (Figure 5.4) for instrumented sections. Neutral axis depth was determined using the gauge pair spacing listed in Table 5.1. Plots of neutral axis location for representative instrumented cross sections of the Royalton Bridge are discussed in Section 6.1.3.

The gauge pair spacing in the Royalton bridge tests varied depending on location of each pair. The distance between bottom and top gauges in instrumented sections (gauge pairs) were 2.583 ft (786 mm), 1.125 ft (343 mm), or 1.042 ft (318 mm) for the guard rail (Figure 4.7), T-Beam stem on the upstream side (Figure 4.6a), or T-beam stem on the downstream side (Figure 4.6b), respectively.

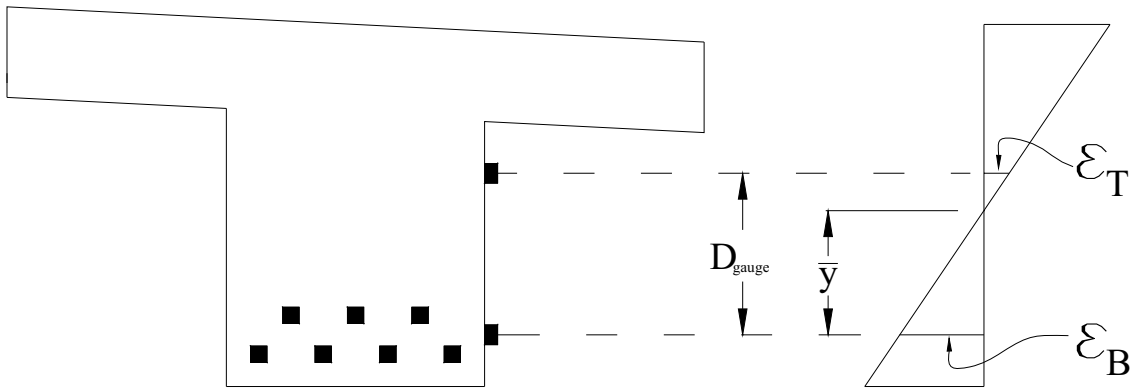


Figure 5.3: Royalton Strain Profile

$$\bar{y} = \frac{-\varepsilon_B \cdot D_{\text{Gauge}}}{\varepsilon_T - \varepsilon_B} \quad [5.1]$$

Where:

\bar{y} = Neutral axis depth above bottom gauge (ft)

D_{gauge} = Distance between top and bottom gauges attached at a cross section (ft)

ε_T = Strain in top gauge ($\mu\varepsilon$)

ε_B = Strain in bottom gauge ($\mu\varepsilon$)

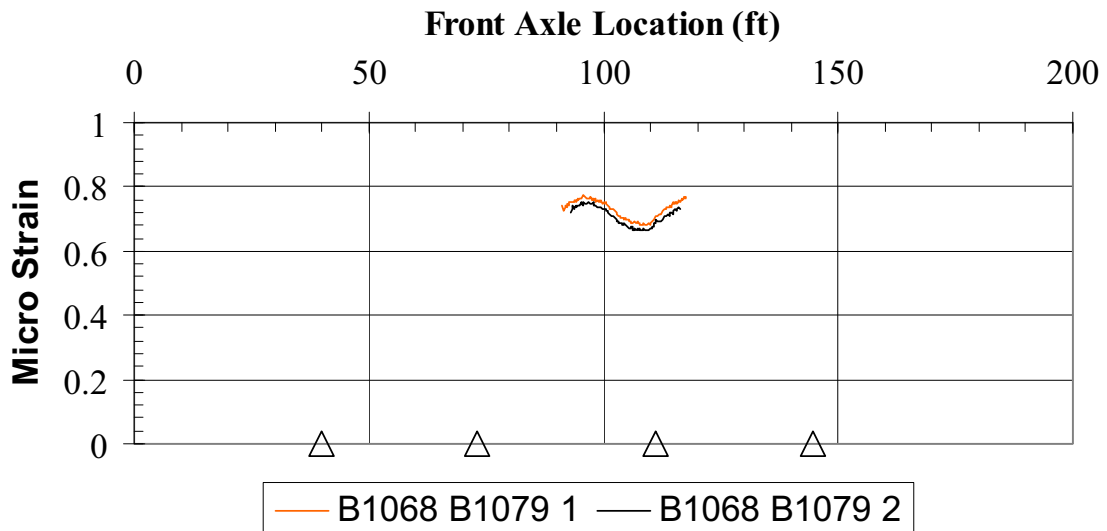


Figure 5.4: Neutral Axis Depths Calculated for Gauge Pair #20 (Lane 2)

Because strain data were not recorded when the loading truck was exactly at the same position along the bridge, strain data sets from different test runs were

interpolated at 1 ft (305 mm) increments to have values at common truck positions that could be averaged and used for engineering calculations.

5.2.4 Moment Calculation

The bending moment at each gauge pair location is calculated using the neutral axis depth and unique cross sectional properties of both the beam and deck where the gauges are attached. The moment at each gauge pair location is calculated from stresses in both steel and concrete that are determined using assumed material properties and measured strains.

Material properties assumed for moment calculation include the compressive strength of concrete to be 6,000 psi (41.4 MPa), concrete modulus of elasticity of 4,415 ksi (30.4 GPa), and a modulus elasticity of steel of 29,000 ksi (200 GPa). The area and centroid locations of steel reinforcing bars in each layer were taken from construction plans and are summarized in Table 5.2 for the deck slab and Table 5.3 for the T-beam stem (Figure 5.5), respectively. Assumptions about the cross sectional shape of the T-beam considering effective deck width in bending and guardrail sections is discussed in Section 5.2.6.3.

Moments were not calculated at all points measured in the strain history, as relatively small strain readings may introduce relatively large errors in moment calculations (Section A.4). Therefore, moments were only calculated at locations where the absolute value of the bottom gauge strain exceeded $6 \mu\epsilon$.

While the vast majority of moments calculated in both spans indicate positive bending, small negative moments were observed to occur near the bridge abutments and pier locations. Calculation of positive and negative bending is discussed in Sections 5.2.6.1 and 5.2.6.2.

5.2.4.1 Deck in Positive Bending

When calculating moments, a cross section is considered to be in positive bending when the top of the deck slab is in compression and the bottom of the T-beam is in tension. From the plots of neutral axis depth, the location of zero strain is often located below the deck slab in positive bending (Figure 5.5). Since the neutral axis sometimes shifts up or down in cross sections, it may sometimes be located in the deck slab (Figure 5.6).

Concrete areas in compression (above the neutral axis) as well as concrete areas in tension (below the neutral axis) were considered to contribute to the calculated moments. While tensile stresses in concrete are usually ignored in design of concrete structures, the tensile forces measured in these cross sections were found to be significant for the loading level imposed on the bridge during the field tests. Stresses in concrete were found by multiplying the measured strain by the assumed concrete modulus of elasticity indicated above. Forces in concrete were then determined by multiplying these stresses by the concrete area in compression or tension. The corresponding moment was calculated with Equation [5.2] for each concrete area, by

multiplying the force in each of the concrete component times their distance from the location of the stress resultant to the neutral axis location.

Similarly, stresses in each reinforcement layer were determined using the strain profile by multiplying the strain at the centroid of the layer times the steel modulus of elasticity. The force in each layer was calculated as the total area of steel in that layer multiplied by the calculated stress. Each steel force was then multiplied by the distance from the steel layer to the neutral axis location to calculate the moment contribution from steel. The area and centroid of each steel layer in the T-beam stem (Figure 5.5) are listed in Table 5.3.

While slight variations in the neutral axis depth measured during the load tests are of little concern, the differences in equations used to calculate positive moment if the neutral axis is located below the slab versus in the slab as are detailed in Section D.4.1 (Equation [D.14] and Equation [D.20]).

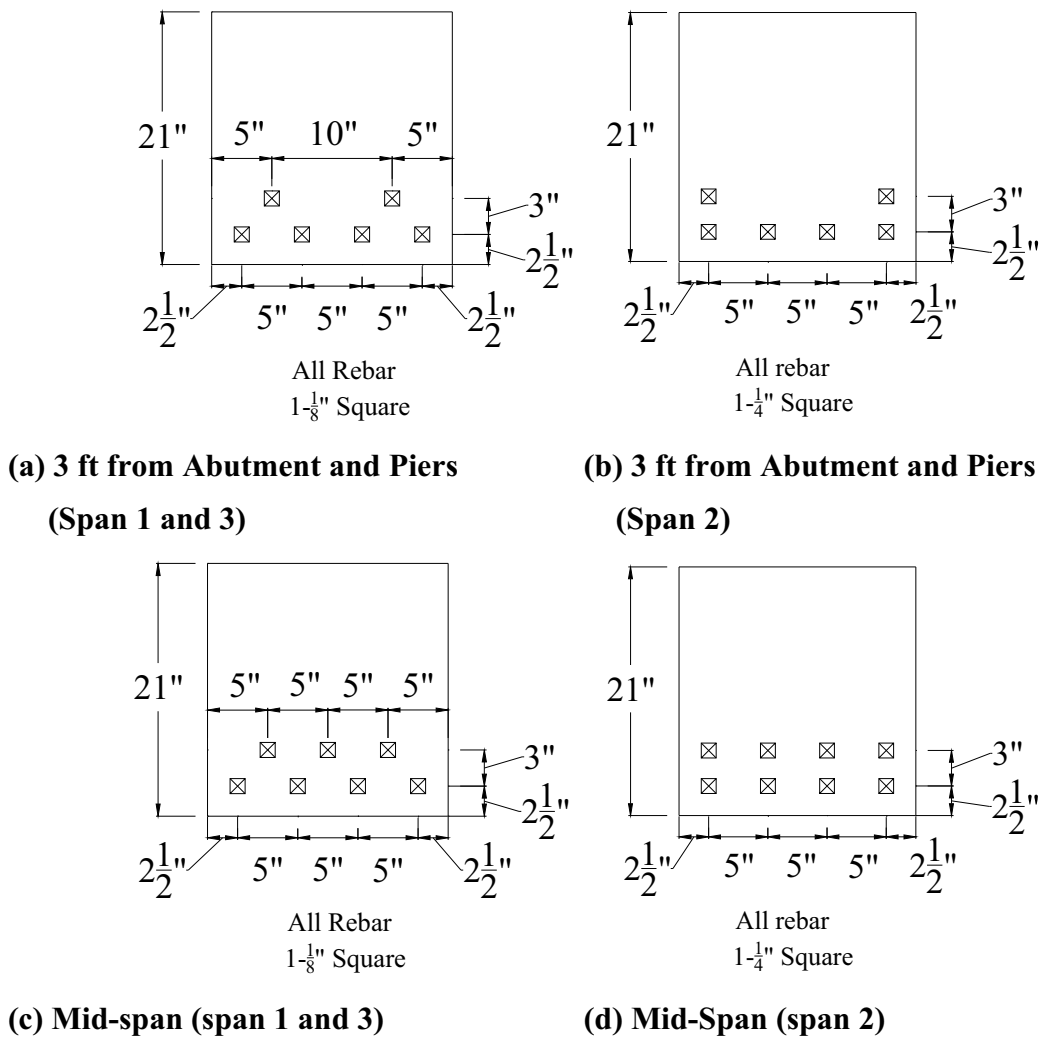
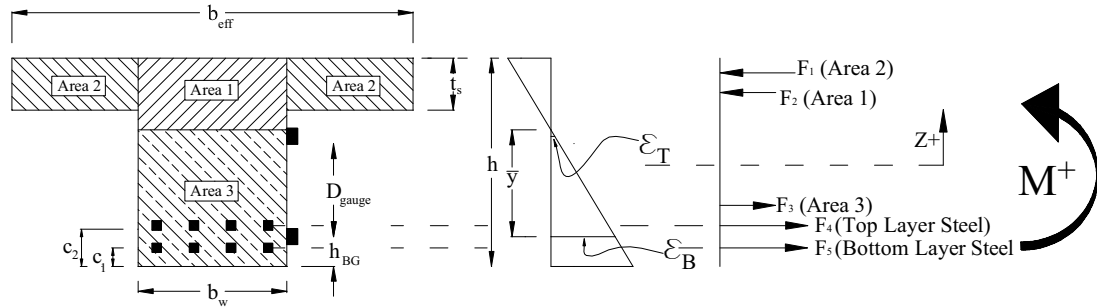
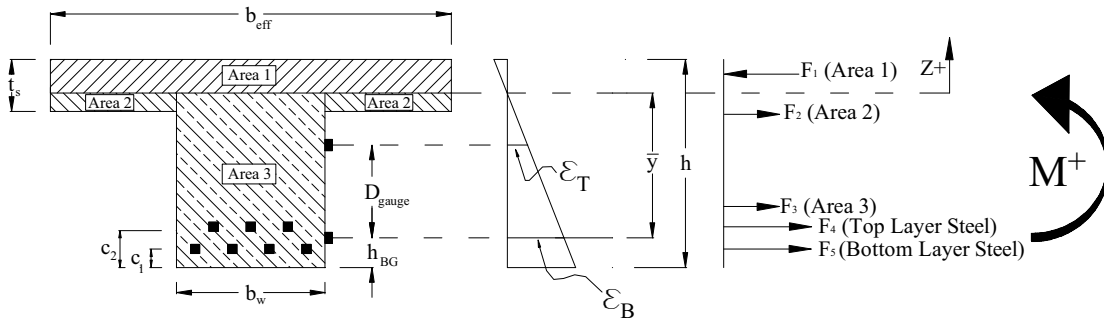


Figure 5.5: T-Beam Stem Dimensions and Rebar Configuration



(a) Neutral Axis below Deck Slab



(b) Neutral Axis in Deck Slab

Figure 5.6: Strain Profile and Force Diagram of Royalton Cross Section in Positive Bending

$$M = \sum_{i=1}^n |F_i \cdot z_i| \quad [5.2]$$

Where:

F = Force in concrete or steel (kip)

M = Moment (K-ft)

n = Number of concrete areas in compression and layers of steel in tension

Z = Distance from neutral axis of bending to centroid of stress (ft)

5.2.4.2 Deck in Negative Bending

A cross section is considered to be in negative bending when the top of slab is in tension, and the bottom of beam is in compression (Figure 5.7). Based upon observations of the test data, the neutral axis in negative bending was always determined to lie below the slab. The procedure for calculating the section moment in negative bending was similar to that used for positive bending, with the concrete areas

in compression and tension and the different steel reinforcing layers in tension considered in the calculations.

In negative bending, steel reinforcing bars in tension within the effective deck width (Section 5.2.6.3) were considered to contribute to the internal moment, while the reinforcing bars in compression near the bottom of the T-beam stem are ignored. Equation [5.3] is used to calculate negative bending moments. Additional detail and background for this equation are presented in Section D.4.1 (Equation [D.27]). The area and centroid of steel layers in the deck slab are listed in Table 5.2.

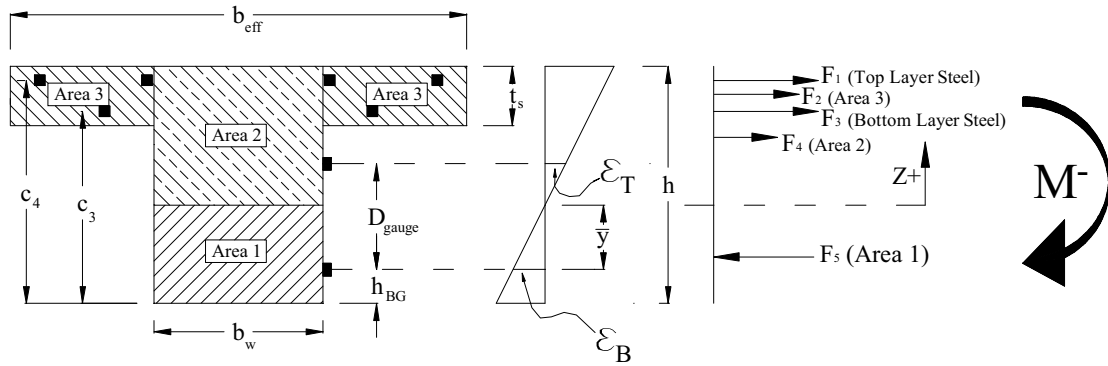


Figure 5.7: Stain Profile and Force Diagram of Royalton Cross Section in Negative Bending

$$M = \sum_{i=1}^n -|F_i \cdot z_i| \quad [5.3]$$

5.2.4.3 Effective Deck Width

The effective deck width assuming composite behavior was determined using American Association of State Highway Transportation Officials (AASHTO) guidelines 4.6.2.6.1. The effective deck width for interior beams was determined to be 54 inches (1,372 mm) taking the lesser of Equation [5.4] from AASHTO.

- One-quarter of the effective span length
 - 12.0 times the average depth of the slab, plus the greater of web thickness or one-half the width of the top flange of the girder; or
 - The average spacing of adjacent beams
- [5.4]

An effective deck width of 28 inches (711 mm) was calculated for exterior beams using the lesser of Equation [5.5] from AASHTO, considering 27 inches (686 mm) to be half the adjacent interior beam effective width plus a 1.5-inch (38 mm) overhang. Note that in this calculation the guardrail is not assumed to act compositely with the exterior beam.

If the concrete guardrail is assumed to be structurally continuous AASHTO commentary 4.6.2.6.1-1 allows an increase in the overhang width using Equation [5.6].

With a concrete guardrail area of 400-in² (2,580 cm²) and slab thickness of 7 inches (178 mm), this provision increases the effective flange width found with Equation [5.5] to be 57 inches (1,448 mm).

The effective deck width used to determine concrete and steel reinforcement areas for positive and negative bending at each gauge pair is listed in Table 5.2.

The effective flange width may be taken as one-half the web thickness or one-quarter of the width of the top flange of the basic girder, plus the least of:

- One-eighth of the effective span length [5.5]
- 6.0 times the average depth of the slab, plus the greater of one-half the web thickness or one-quarter the width of the top flange of the girder; or
- The width of the overhang

$$\Delta w = \frac{A_b}{2t_s} \quad [5.6]$$

Where:

A_b = cross sectional area of the barrier (in²)

t_s = depth of deck slab (in)

Table 5.1: Gauge Pair Properties Used in Royalton Calculations

Test Setup	Gauge Pair	Girder	Spacing	Top Gauge Height	Bottom Gauge Height
			(ft)	(in)	(in)
A	1	I-1	1.042	16.5	4
	2	I-2	1.042	16.5	4
	3	I-3	1.042	16.5	4
	4	II-1	1.042	16.5	4
	5	II-2	1.042	16.5	4
	6	II-3	1.042	16.5	4
	7	III-1	1.042	16.5	4
	8	III-2	1.042	16.5	4
	9	III-3	1.042	16.5	4
	31	GR I-2	2.583	0	0
B	10	V-1	1.125	17.5	4
	11	V-2	1.125	17.5	4
	12	V-3	1.125	17.5	4
	13	VI-1	1.125	17.5	4
	14	VI-2	1.125	17.5	4
	15	VI-3	1.125	17.5	4
	25	V-4	1.042	16.5	4
	26	V-5	1.042	16.5	4
	28	VI-4	1.125	17.5	4
	29	VI-5	1.125	17.5	4
C	22	III-4	1.125	17.5	4
	23	III-5	1.125	17.5	4
	24	III-6	1.125	17.5	4
	25	V-4	1.042	16.5	4
	26	V-5	1.042	16.5	4
	27	V-6	1.042	16.5	4
	28	VI-4	1.125	17.5	4
	29	VI-5	1.125	17.5	4
	30	VI-6	1.125	17.5	4
	33	GR V-5	2.583	0	0
D	16	I-4	1.042	16.5	4
	17	I-5	1.042	16.5	4
	18	I-6	1.042	16.5	4
	19	II-4	1.042	16.5	4
	20	II-5	1.042	16.5	4
	21	II-6	1.042	16.5	4
	22	III-4	1.125	17.5	4
	23	III-5	1.125	17.5	4
	24	III-6	1.125	17.5	4
	32	GR I-5	2.583	0	0

Table 5.2: Deck Slab Properties Used in Royalton Calculations

Test Setup	Gauge Pair	Girder	Depth of Slab (in)	Effective Slab Width (in)	Top Layer Steel Area (in2)	Top Layer Steel Centroid (in)	Bottom Layer Steel Area (in2)	Bottom Layer Steel Centroid (in)
A	1	I-1	7	71	0.625	25.9	0.375	23.2
	2	I-2	7	71	0.625	25.9	0.375	23.2
	3	I-3	7	71	0.625	25.9	0.375	23.2
	4	II-1	7	54	0.75	25.9	0.75	23.2
	5	II-2	7	54	0.75	25.9	0.75	23.2
	6	II-3	7	54	0.75	25.9	0.75	23.2
	7	III-1	7	54	0.75	25.9	0.75	23.2
	8	III-2	7	54	0.75	25.9	0.75	23.2
	9	III-3	7	54	0.75	25.9	0.75	23.2
	31	GR I-2	0	0	0	0	0	0
B	10	V-1	7	54	0.75	25.9	0.75	23.2
	11	V-2	7	54	0.75	25.9	0.75	23.2
	12	V-3	7	54	0.75	25.9	0.75	23.2
	13	VI-1	7	71	0.625	25.9	0.375	23.2
	14	VI-2	7	71	0.625	25.9	0.375	23.2
	15	VI-3	7	71	0.625	25.9	0.375	23.2
	25	V-4	7	54	0.75	25.9	0.75	23.2
	26	V-5	7	54	0.75	25.9	0.75	23.2
	28	VI-4	7	71	0.625	25.9	0.375	23.2
	29	VI-5	7	71	0.625	25.9	0.375	23.2
C	22	III-4	7	54	0.75	25.9	0.75	23.2
	23	III-5	7	54	0.75	25.9	0.75	23.2
	24	III-6	7	54	0.75	25.9	0.75	23.2
	25	V-4	7	54	0.75	25.9	0.75	23.2
	26	V-5	7	54	0.75	25.9	0.75	23.2
	27	V-6	7	54	0.75	25.9	0.75	23.2
	28	VI-4	7	71	0.625	25.9	0.375	23.2
	29	VI-5	7	71	0.625	25.9	0.375	23.2
	30	VI-6	7	71	0.625	25.9	0.375	23.2
	33	GR V-5	0	0	0	0	0	0
D	16	I-4	7	71	0.625	25.9	0.375	23.2
	17	I-5	7	71	0.625	25.9	0.375	23.2
	18	I-6	7	71	0.625	25.9	0.375	23.2
	19	II-4	7	54	0.75	25.9	0.75	23.2
	20	II-5	7	54	0.75	25.9	0.75	23.2
	21	II-6	7	54	0.75	25.9	0.75	23.2
	22	III-4	7	54	0.75	25.9	0.75	23.2
	23	III-5	7	54	0.75	25.9	0.75	23.2
	24	III-6	7	54	0.75	25.9	0.75	23.2
	32	GR I-5	0	0	0	0	0	0

Table 5.3: Beam Properties Used in Royalton Calculations

Test Setup	Gauge Pair	Girder	Total Beam Height (in)	Top Steel Layer Area (in ²)	Top Steel Layer Centroid (in)	Bottom Steel Layer Area (in ²)	Bottom Steel Layer Centroid (in)	Beam Width (in)
A	1	I-1	28	2.53	5.5	5.1	2.5	20
	2	I-2	28	3.8	5.5	5.1	2.5	20
	3	I-3	28	2.53	5.5	5.1	2.5	20
	4	II-1	28	2.53	5.5	5.1	2.5	20
	5	II-2	28	3.8	5.5	5.1	2.5	20
	6	II-3	28	2.53	5.5	5.1	2.5	20
	7	III-1	28	2.53	5.5	5.1	2.5	20
	8	III-2	28	3.8	5.5	5.1	2.5	20
	9	III-3	28	2.53	5.5	5.1	2.5	20
	31	GR I-2	0	0	0	0	0	0
B	10	V-1	28	2.53	5.5	5.1	2.5	20
	11	V-2	28	3.8	5.5	5.1	2.5	20
	12	V-3	28	2.53	5.5	5.1	2.5	20
	13	VI-1	28	2.53	5.5	5.1	2.5	20
	14	VI-2	28	3.8	5.5	5.1	2.5	20
	15	VI-3	28	2.53	5.5	5.1	2.5	20
	25	V-4	28	3.1	5.5	6.3	2.5	20
	26	V-5	28	6.3	5.5	6.3	2.5	20
	28	VI-4	28	3.1	5.5	6.3	2.5	20
	29	VI-5	28	6.3	5.5	6.3	2.5	20
C	22	III-4	28	3.1	5.5	6.3	2.5	20
	23	III-5	28	6.3	5.5	6.3	2.5	20
	24	III-6	28	3.1	5.5	6.3	2.5	20
	25	V-4	28	3.1	5.5	6.3	2.5	20
	26	V-5	28	6.3	5.5	6.3	2.5	20
	27	V-6	28	3.1	5.5	6.3	2.5	20
	28	VI-4	28	3.1	5.5	6.3	2.5	20
	29	VI-5	28	6.3	5.5	6.3	2.5	20
	30	VI-6	28	3.1	5.5	6.3	2.5	20
	33	GR V-5	0	0	0	0	0	0
D	16	I-4	28	3.1	5.5	6.3	2.5	20
	17	I-5	28	6.3	5.5	6.3	2.5	20
	18	I-6	28	3.1	5.5	6.3	2.5	20
	19	II-4	28	3.1	5.5	6.3	2.5	20
	20	II-5	28	6.3	5.5	6.3	2.5	20
	21	II-6	28	3.1	5.5	6.3	2.5	20
	22	III-4	28	3.1	5.5	6.3	2.5	20
	23	III-5	28	6.3	5.5	6.3	2.5	20
	24	III-6	28	3.1	5.5	6.3	2.5	20
	32	GR I-5	0	0	0	0	0	0

5.3 Weathersfield Bridge Data Reduction

A total of 28 files, each with 20 strain gauge histories, were recorded in 3 setups, as listed in Table 4.6 during the Weathersfield Bridge tests. Using a recording frequency of 33.33 Hz and a travel distance of 10.92 ft (277 mm) for each AutoClicker mark, the position of both loading trucks was determined for each point in the strain history. As for the Royalton bridge, initial strain readings were used to correct non-zero values from the initial recorded data points. This initial offset was applied to all strain data in each test run of the Weathersfield bridge tests.

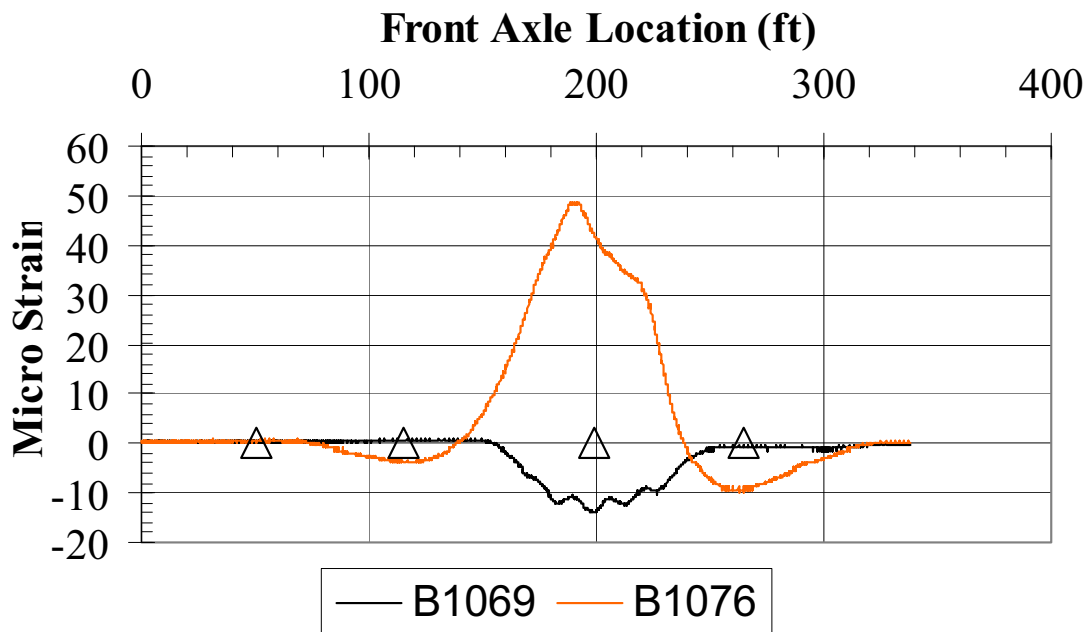
During test runs with the back-to-back spacing of load vehicles, the distance from the start of the test to the first bridge abutment was sometimes less than 50 feet (15.24 m) as listed in Table 4.6 because of the skew angle present in this bridge. Differences in the starting position of the truck were taken into account when plotting and analyzing data. The start distance, measured from the left front tire of the lead loading truck to the bridge abutment, was always 50 feet (15.24 m) when plotted and analyzed.

The strain history for all gauges is plotted until the last clicker time was recorded. Although the rear axle of the load vehicle moved completely off the bridge after 318 feet (96.93 m) in each test, some strain histories are plotted beyond this distance.

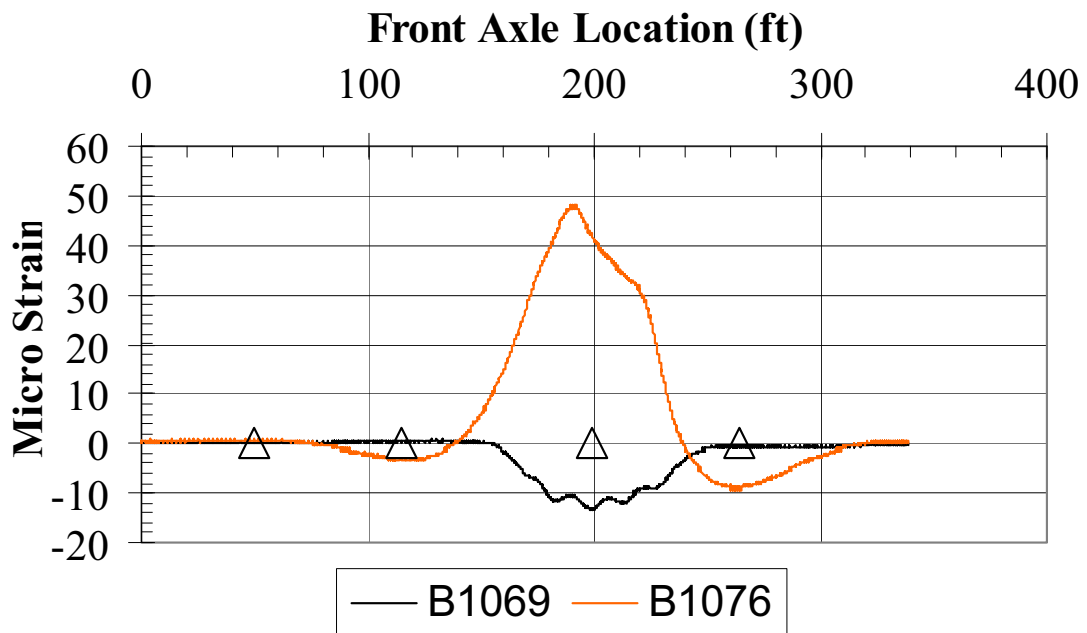
The location of abutments and piers, relative to the front axle of the truck, is plotted in figures of strain histories, neutral axis depths, and moments as a small triangles. These marks are useful as a quick reference when comparing data because inflections in strain and moment diagrams tend to occur after truck axles move on or off the bridge or between spans. Strain gauges were attached to girder flanges without using strain gauge extensions, so correction factors accounting for differences in gauge length or extension elongation were not necessary for Weathersfield bridge data.

5.3.1 Linear Bridge Response Determined from Raw Strain History Data

Plots of strain history versus truck position were created for each gauge pair, similar to those in Figure 5.8. These figures show the strain history of the same gauge pair, located at the center of span 2, for a repeated test run in lane 2 southbound. A visual inspection of these data revealed linear elastic response of the bridge during testing. Note that at approximately 318 feet (96.93 m), the load truck has moved completely off the bridge, and the strain has returned to zero, which indicates linear elastic behavior.



(a) First Test Run



(b) Repeated Test Run

Figure 5.8: Strain History of Gauge Pair #4 (Lane 2)

5.3.2 Repeatability of Data

Strain data from repeated test runs from different raw data files (such as Figure 5.8) were compared for consistency by plotting the data in the same figure (Figure 5.9). From a visual inspection of this plot, the data was consistent between test runs by comparing the general shape and magnitude of peak values. Subsequent engineering calculations used averaged strain data as indicated in the section below.

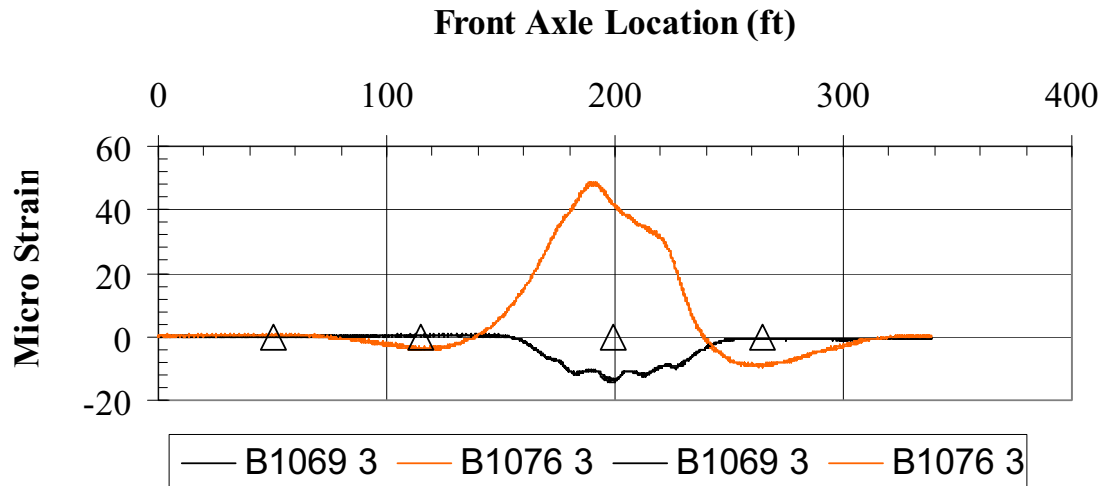


Figure 5.9: Combined Plot of Strain History of Gauge Pair #4 (Lane 2)

5.3.3 Averaging Data Runs

To compare data sets from different test runs, the strain data for each gauge was first interpolated at 1-foot increments (305 mm). These increments were used to create points in both raw data files that corresponded to the same location of the loading trucks along the bridge and for which data could be averaged. At each increment point, the neutral axis depth was calculated using Equation [5.1]. The calculated neutral axis depth was then used to calculate the moment versus loading truck position along the bridge.

5.3.4 Neutral Axis Calculation

The neutral axis depth of each gauge pair was calculated using the strain profile (Figure 5.10) and Equation [5.1] for each row of strain data, if the absolute value of measured strain in the lower gauge was greater than $20 \mu\epsilon$ unless otherwise noted. Plots of neutral axis depth were then created (Figure 5.11). The distance between top and bottom gauges listed in Table 5.3 was used to determine neutral axis location.

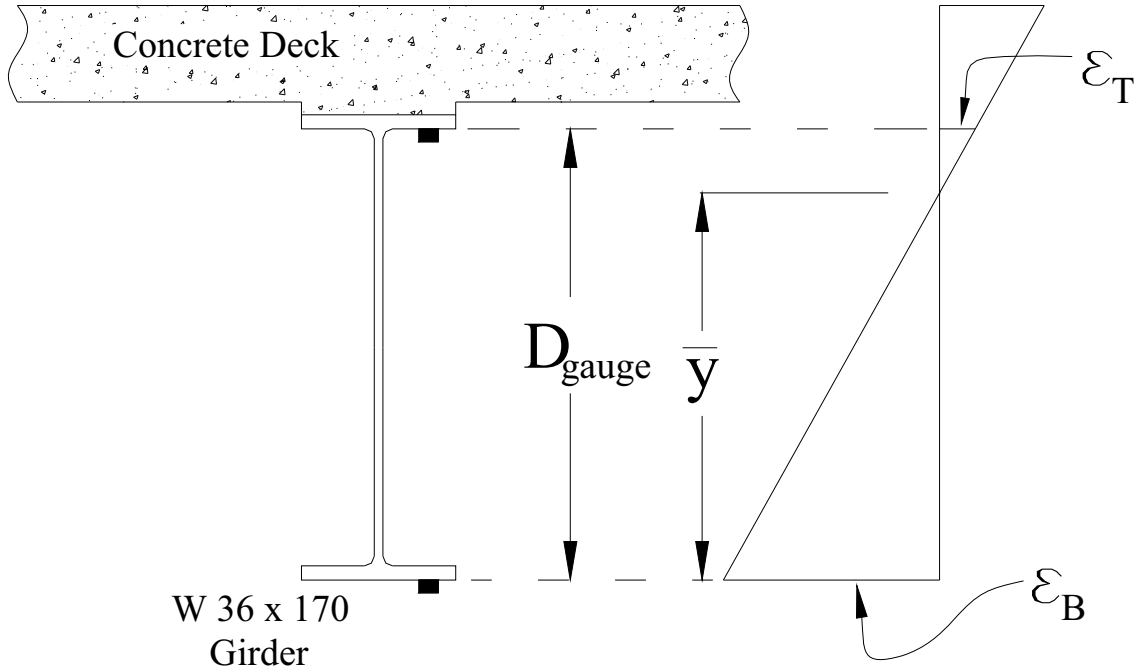


Figure 5.10: Weathersfield Strain Profile

The gauge pair spacing input for calculating neutral axis depth was 2.97 ft (905 mm) for gauges near the bearings at pier supports (sections 1 and 7) and 2.93 ft (893 mm) for all other gauge pairs (sections 2 through 6). The difference in spacing between gauges resulted from the use of cover plates near interior piers which added an additional 0.5 in. (13 mm) to the bottom flange of the girder.

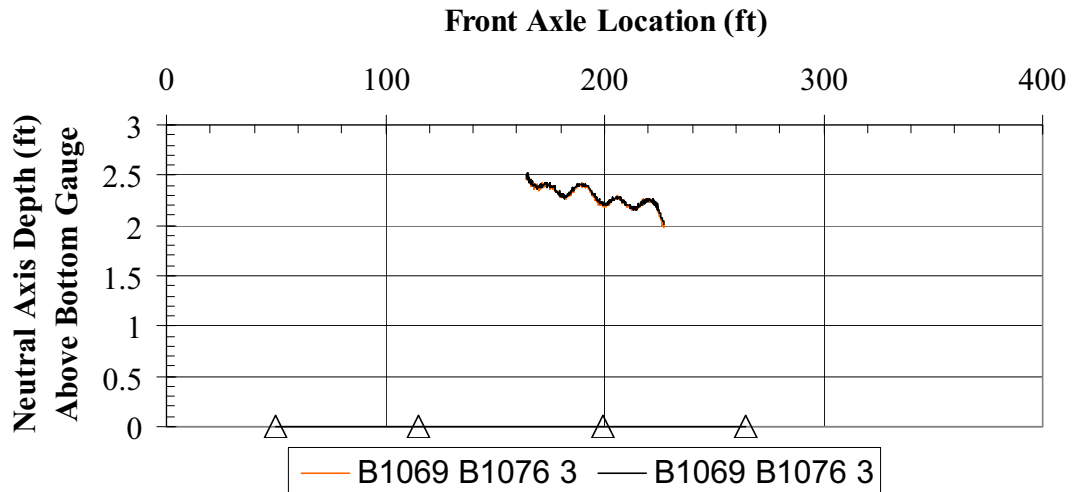


Figure 5.11: Calculated Neutral Axis Depth Gauge Pair #4 (Lane 2)

5.3.5 Moment Calculation

The moment at each gauge pair location was determined using the neutral depth and input parameters for the beam and deck with composite properties using Equation [5.7]. It was assumed that the deck concrete compressive strength is 4,000 psi (34.5 MPa) to account for an increase of concrete strength with age, and that the modulus of elasticity of the girder is 29,000 ksi (200 GPa).

The composite properties used to calculate moment were based upon usual assumptions of bending theory, considering girders subjected to either positive or negative bending, and was only calculated if the absolute value of measured strain in the lower gauge exceeded $21 \mu\epsilon$ unless otherwise noted. Positive bending was defined when the bottom strain gauge was positive (bottom flange in tension), and negative bending was defined when the bottom gauge readings were negative (bottom flange in compression).

$$M = \frac{\epsilon_b \cdot E_g \cdot I_{Comp}}{\bar{y} \cdot (1.44 \times 10^8)} \quad [5.7]$$

Where:

M = Moment (k-ft)

ϵ_b = Strain in bottom gauge ($\mu\epsilon$)

I_{Comp} = Effective moment of inertia of composite section (in^4)

E_g = Modulus of elasticity of girder material (ksi)

\bar{y} = Neutral Axis Depth (ft)

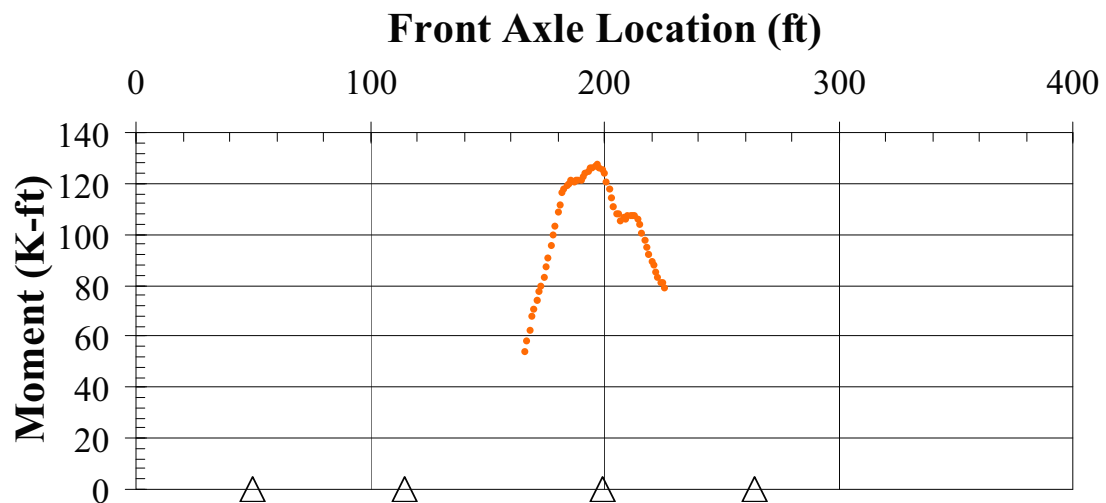


Figure 5.12: Calculated Moment of Gauge Pair #4 (Lane 2)

5.3.5.1 Moment of Inertia and Centroid of Steel Girder

The moment of inertia of the W36 x 170 steel girders is $10,500 \text{ in}^4$ ($4.37 \times 10^{-3} \text{ m}^4$) (AISC Manual of Steel Construction). The moment of inertia of the girder with welded cover plates near pier supports is calculated to be $13,867 \text{ in}^4$ ($5.77 \times 10^{-3} \text{ m}^4$).

The centroid of the girder sections is located at mid-depth due to symmetry. Measured from the bottom gauge, the centroid is 18.1 in (459 mm) for the girder with no cover plates and 18.6 in (472 mm) on the girder with cover plates.

5.3.5.2 Effective Deck Width

The effective deck width assuming composite behavior was found using AASHTO guidelines 4.6.2.6.1. The effective deck width for interior beams was determined to be 90 in. (2,286 mm) taking the lesser of Equation [5.4] from the *AASHTO LRFD Bridge Design Specifications*. An effective deck width of 29 in. (737 mm) was calculated for exterior beams using the lesser of Equation [5.5].

5.3.5.3 Deck in Positive Bending

When the lower strain was positive (flange in tension), the girder-deck cross section was considered to be in positive bending. The concrete area of the deck in positive bending was considered to act compositely with the girder and the moment of inertia for the composite steel girder and concrete deck was used in calculations. The assumption of composite action between deck and girder was used because the measured strains generated during the tests were not large. Steel reinforcement in the concrete deck when considered to be in compression was neglected in the calculations.

The resulting area of concrete in compression within the effective deck width was 675 in^2 ($4,355 \text{ cm}^2$) for interior girders and 218 in^2 (406 cm^2) for exterior girders. The area was simply determined by multiplying the deck height of 7.5 in (191 mm) times the effective width calculated in Section 5.3.6.2. The moment of inertia of the concrete deck slab about the deck centroid was calculated using Equation [5.8]. The composite moment of inertia of sections in positive bending used with Equation [5.7] is calculated with Equation [5.9]. In this equation, the concrete deck is transformed to steel by using the modular ratio between concrete and steel (E_d/E_s). Additional background for these equations is detailed Appendix D.4.2.

The centroid of the deck area in positive bending is located 41 in. (1,042 mm) above the bottom strain gauge in girder sections without a cover plate and 41.5 in. (1,054 mm) in sections with a cover plate, measured to slab mid-depth. Centroid locations used in calculations are listed in Table 5.5.

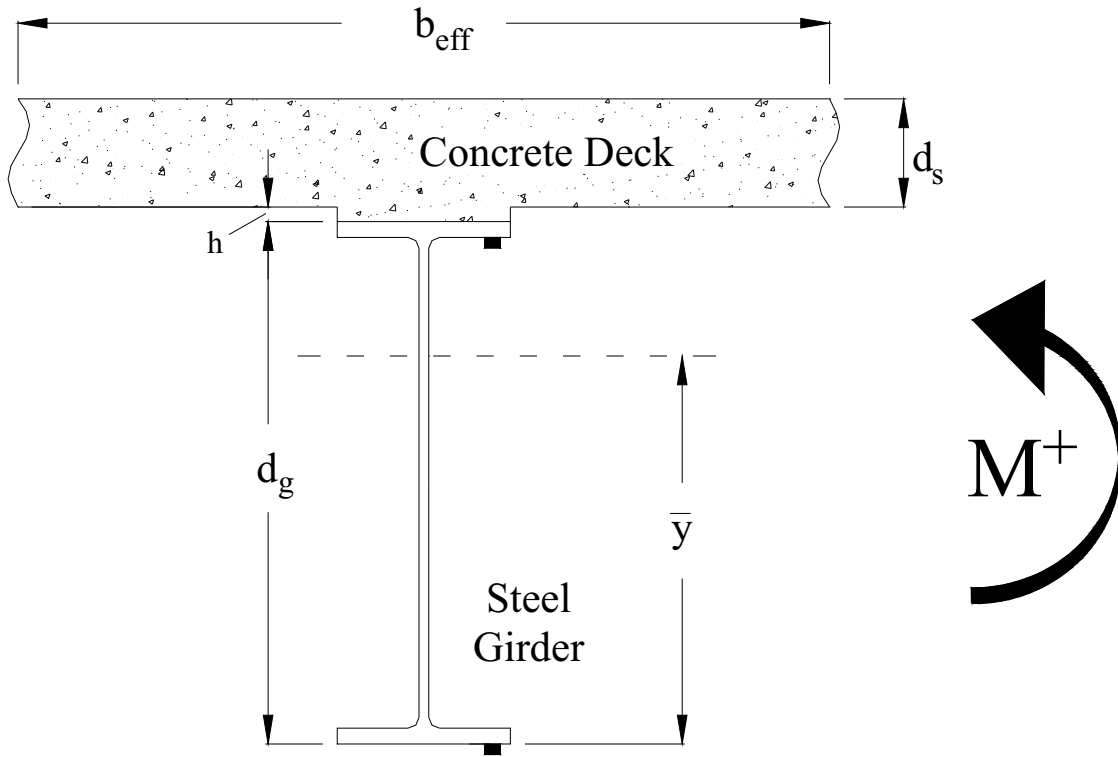


Figure 5.13: Weathersfield Cross Section in Positive Bending

$$I_d = \frac{b_{\text{eff}} \cdot (d_s)^3}{12} \quad [5.8]$$

$$I_{\text{Comp}} = \left[I_g + \left(A_g \cdot \left(\bar{y} - \frac{d_g}{2} \right)^2 \right) \right] + \frac{E_d}{E_g} \cdot \left[I_d + (b_{\text{eff}} \cdot d_s) \cdot \left(\left(d_g + h + \frac{d_s}{2} \right) - \bar{y} \right)^2 \right] \quad [5.9]$$

Where:

- A_g = Area of steel girder cross section (in²)
- b_{eff} = Effective width of concrete deck (in)
- d_g = Depth of steel girder (in)
- d_s = Depth of slab (in)
- E_d = Modulus of elasticity of concrete deck (ksi)
- E_g = Modulus of elasticity of steel girder (ksi)
- h = Depth of haunch (in)
- I_d = Moment of inertia of deck (in⁴)

I_g = Moment of inertia of girder (in⁴)

y = Neutral Axis depth above bottom gauge (in)

5.3.5.4 Deck in Negative Bending

When the lower strain was negative (flange in compression), the beam is considered to be in negative bending. The moment of inertia in negative bending is based on the reinforcing bars running parallel to the beam axis within the deck effective width determined in Section 5.3.6.2. Concrete in tension was assumed to be cracked and was ignored when calculating the moment of inertia of the section in negative bending.

The centroid and area of steel in each reinforcing bar layer within the effective deck width was used to determine the moment of inertia of the deck slab in negative bending with Equation [5.10]. The distance to the centroid of each bar layer is listed in Table 5.6, measured from the bottom strain gauge. The composite moment of inertia used in negative bending with Equation [5.7] is calculated with Equation [5.11]. The modular ratio between deck reinforcement and steel girder was taken as 1.0. Additional background for these equations is detailed Appendix D.4.2.

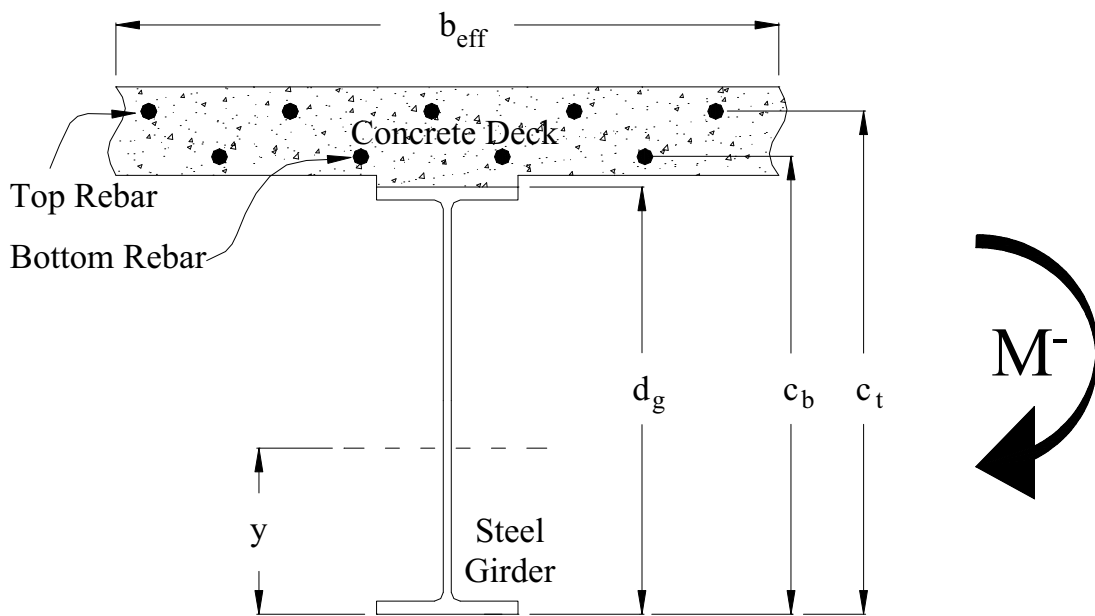


Figure 5.14 Weathersfield Cross Section in Negative Bending

$$I_{\text{Deck}} = A_{\text{st}} \cdot (\bar{y} - c_t)^2 + A_{\text{sb}} \cdot (\bar{y} - c_b)^2 \quad [5.10]$$

$$I_{\text{Comp}} = \left[I_g + \left(A_g \cdot \left(\bar{y} - \frac{d_g}{2} \right)^2 \right) \right] + \frac{E_s}{E_g} \cdot I_{\text{Deck}} \quad [5.11]$$

Where:

A_g = Area of steel girder cross section (in²)

A_{sb} = Area of bottom layer reinforcement (in²)

A_{st} = Area of top layer reinforcement (in²)

C_b = Centroid of bottom layer reinforcement above lower strain gauge (in)

C_t = Centroid of top layer reinforcement above lower strain gauge (in)

d_g = Depth of steel girder (in)

E_s = Modulus of elasticity of deck reinforcement (ksi)

E_g = Modulus of elasticity of girder material (ksi)

I_g = Moment of inertia of girder (in⁴)

\bar{y} = Neutral Axis depth above bottom gauge (in)

Table 5.4: Properties of Weathersfield Girder Used to Calculate Moment

Test Setup	Gauge Pair	Girder	Spacing (ft)	Moment of Inertia (in ⁴)	Modulus of Elasticity (ksi)	Centroid (in)	Area (in ²)
A	1	I-3	2.93	10500	29000	18.1	50.1
	2	I-5	2.93	10500	29000	18.1	50.1
	3	II-3	2.93	10500	29000	18.1	50.1
	4	II-4	2.93	10500	29000	18.1	50.1
	5	II-5	2.93	10500	29000	18.1	50.1
	6	III-4	2.93	10500	29000	18.1	50.1
	7	IV-3	2.93	10500	29000	18.1	50.1
	8	IV-4	2.93	10500	29000	18.1	50.1
	9	IV-5	2.93	10500	29000	18.1	50.1
	10	V-4	2.93	10500	29000	18.1	50.1
B	11	I-6	2.93	10500	29000	18.1	50.1
	12	I-7	2.97	13867	29000	18.6	60.1
	13	II-6	2.93	10500	29000	18.1	50.1
	14	II-7	2.97	13867	29000	18.6	60.1
	15	III-6	2.93	10500	29000	18.1	50.1
	16	III-7	2.97	13867	29000	18.6	60.1
	17	IV-6	2.93	10500	29000	18.1	50.1
	18	IV-7	2.97	13867	29000	18.6	60.1
	19	V-6	2.93	10500	29000	18.1	50.1
	20	V-7	2.97	13867	29000	18.6	60.1
C	21	I-1	2.97	13867	29000	18.6	60.1
	22	I-2	2.93	10500	29000	18.1	50.1
	23	II-2	2.97	13867	29000	18.6	60.1
	24	II-3	2.93	10500	29000	18.1	50.1
	25	III-1	2.97	13867	29000	18.6	60.1
	26	III-2	2.93	10500	29000	18.1	50.1
	27	IV-1	2.97	13867	29000	18.6	60.1
	28	IV-2	2.93	10500	29000	18.1	50.1
	29	V-1	2.97	13867	29000	18.6	60.1
	30	V-2	2.93	10500	29000	18.1	50.1

Table 5.5: Properties of Weathersfield Deck in Positive Bending

Test Setup	Gauge Pair	Girder	Moment of Inertia (in ⁴)	Modulus of Elasticity (ksi)	Centroid (in)	Area (in ²)
A	1	I-3	1020	3605	41	218
	1	I-5	1020	3605	41	218
	2.3	II-3	3164	3605	41	675
	2.3	II-4	3164	3605	41	675
	2.3	II-5	3164	3605	41	675
	2.3	III-4	3164	3605	41	675
	2.3	IV-3	3164	3605	41	675
	2.3	IV-4	3164	3605	41	675
	2.3	IV-5	3164	3605	41	675
	1	V-4	1020	3605	41	218
B	1	I-6	1020	3605	41	218
	1	I-7	1020	3605	42	218
	2.3	II-6	3164	3605	41	675
	2.3	II-7	3164	3605	42	675
	2.3	III-6	3164	3605	41	675
	2.3	III-7	3164	3605	42	675
	2.3	IV-6	3164	3605	41	675
	2.3	IV-7	3164	3605	42	675
	1	V-6	1020	3605	41	218
	1	V-7	1020	3605	42	218
C	1	I-1	1020	3605	42	218
	1	I-2	1020	3605	41	218
	2.3	II-2	3164	3605	42	675
	2.3	II-3	3164	3605	41	675
	2.3	III-1	3164	3605	42	675
	2.3	III-2	3164	3605	41	675
	2.3	IV-1	3164	3605	42	675
	2.3	IV-2	3164	3605	41	675
	1	V-1	1020	3605	42	218
	1	V-2	1020	3605	41	218

Table 5.6: Properties of Weathersfield Deck in Negative Bending

Test Setup	Gauge Pair	Girder	Modulus of Rebar (ksi)	Top Layer Rebar Area (in ²)	Top Layer Rebar Centroid (in)	Bottom Layer Rebar Area (in ²)	Bottom Layer Rebar Centroid (in)
A	1	I-3	29000	1	43	1	38
	2	I-5	29000	1	43	1	38
	3	II-3	29000	2	43	2	38
	4	II-4	29000	2	43	2	38
	5	II-5	29000	2	43	2	38
	6	III-4	29000	2	43	2	38
	7	IV-3	29000	2	43	2	38
	8	IV-4	29000	2	43	2	38
	9	IV-5	29000	2	43	2	38
	10	V-4	29000	1	43	1	38
B	11	I-6	29000	1	43	1	38
	12	I-7	29000	1	44	1	39
	13	II-6	29000	2	43	2	38
	14	II-7	29000	2	44	2	39
	15	III-6	29000	2	43	2	38
	16	III-7	29000	2	44	2	39
	17	IV-6	29000	2	43	2	38
	18	IV-7	29000	2	44	2	39
	19	V-6	29000	1	43	1	38
	20	V-7	29000	1	44	1	39
C	21	I-1	29000	1	44	1	39
	22	I-2	29000	1	43	1	38
	23	II-2	29000	2	44	2	39
	24	II-3	29000	2	43	2	38
	25	III-1	29000	2	44	2	39
	26	III-2	29000	2	43	2	38
	27	IV-1	29000	2	44	2	39
	28	IV-2	29000	2	43	2	38
	29	V-1	29000	1	44	1	39
	30	V-2	29000	1	43	1	38

CHAPTER 6 - DATA ANALYSIS

6.1 Royalton Bridge

6.1.1 Transverse Distribution of Strain

The response of the bridge was inferred from the strain history measured at each of the cross sections shown in Figure 6.1. The transverse strain distribution at individual girders was plotted and compared using readings from the lower strain gauges when the load truck was at a specific position along the bridge.

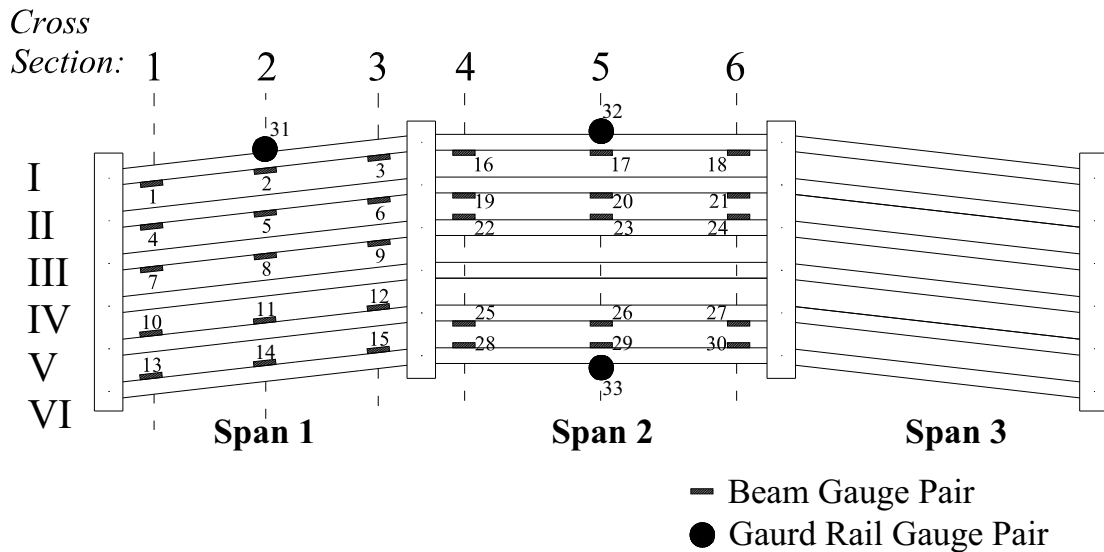


Figure 6.1: Royalton Bridge (Plan View) Cross-Sections and Gauge Numbering
6.1.1.1 Transverse Strain Distribution at Mid-Span

This section describes the strain readings taken at mid-span in spans 1 and 2 (sections 2 and 5, respectively). Figure 6.3 and Figure 6.4 illustrate the strain measured in the lower strain gauge in girders at each of the two mid-span cross sections that approximately corresponded to the peak response measured during the load test for positive bending.

These plots were created by first determining the peak strain for each test run in the lower gauge. The load truck location that produced the maximum strain for the majority of the gauges within a cross section was chosen as the truck position to compare all of the transverse strain readings with the load truck at the same location.

The procedure used to create plots corresponding to transverse distribution of strains is described based on the steps taken for cross section 2 as follows. The strain in each gauge pair for instrumented girders in cross section 2 is plotted in Figure 6.2. These plots represent the average strain data from two repeated test runs with the load truck in the same lane. The maximum strain in the history was determined along with

the corresponding location of the load truck front axle as listed in Table 6.1. The values used in this table are also marked on the lower strain gauge history plot using a diamond symbol in Figure 6.2.

Table 6.1: Maximum Strain Peaks and Truck Location Cross Section 2 (Lane 1)

Gauge Pair	2	5	8	11	14
Maximum Strain ($\mu\epsilon$)	7.1	7.7	49.4	9.2	*
Front Axle Location (ft)	74	72	72	71	*

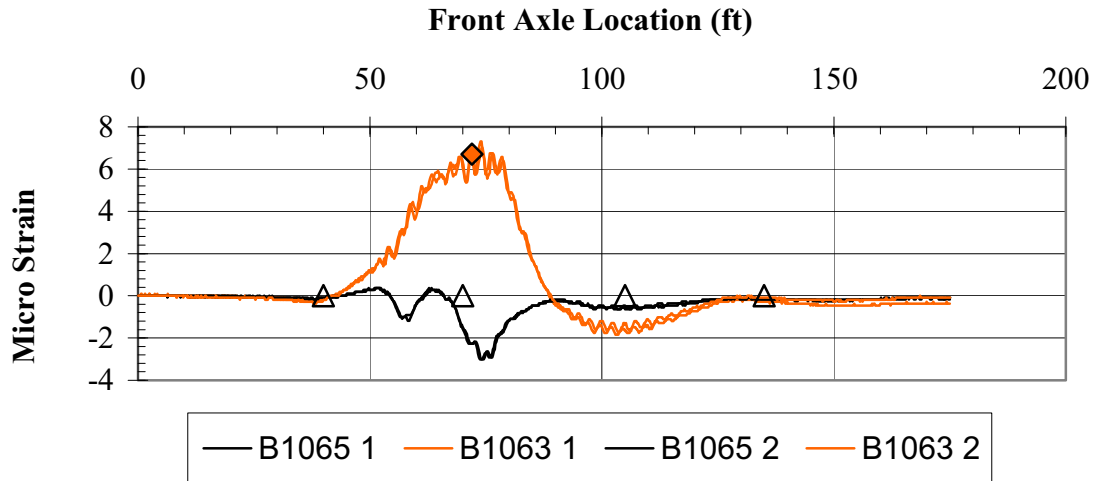
*Negligible strain data

Once the measured strain peaks and their location were determined for each gauge pair in the cross section, a single load truck position is selected for analysis. As shown in Figure 6.2e, the strain in the lower gauge of gauge pair #14 is negligible and may represent noise, so a peak strain could not be readily determined.

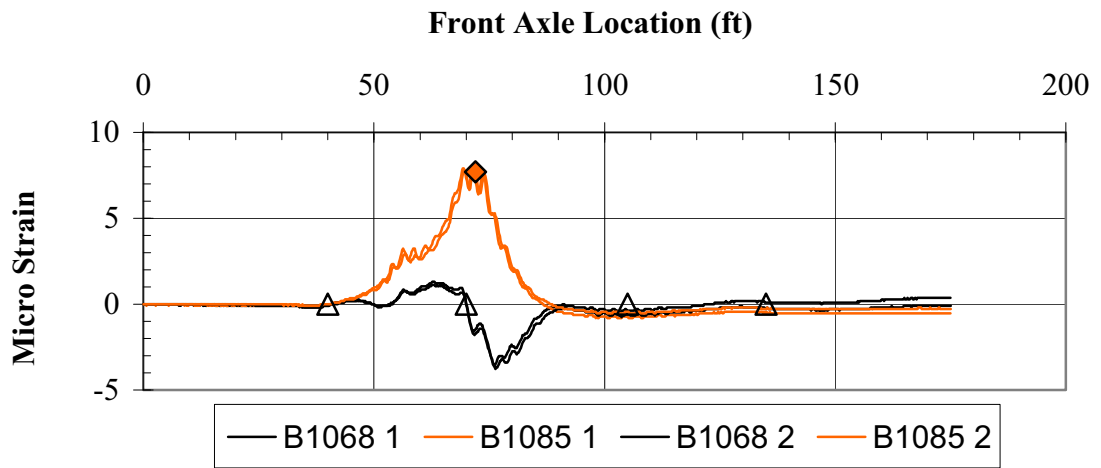
From the truck location values identified in Table 6.1 a front axle location of 72 ft (21.95 m) was selected to investigate the transverse distribution of mid-span strains for section 2 (see Table 6.2). A similar approach was used to determine the truck position in each lane that generated the maximum strain response in the six sections marked in Figure 6.1.

Table 6.2 lists the position of the loading truck front axle and the corresponding value of bottom gauge strain measured in the instrumented bridge girders for each travel lane used during the load test of the Royaltan Bridge. As before, the loading truck position is referenced relative to the starting point that was located 40 ft (12.2 m) from the bridge abutment. As anticipated, measured strains in sections close to the supports (sections 1 and 3 for span 1, and sections 4 and 6 for span 2) are much smaller than those measured near mid-span. Furthermore, the vast majority of strain values are positive indicating no evidence of rotational restraint at bridge supports as assumed during design. The only negative values in the table are negligible and are not believed to be an evidence of support restraint.

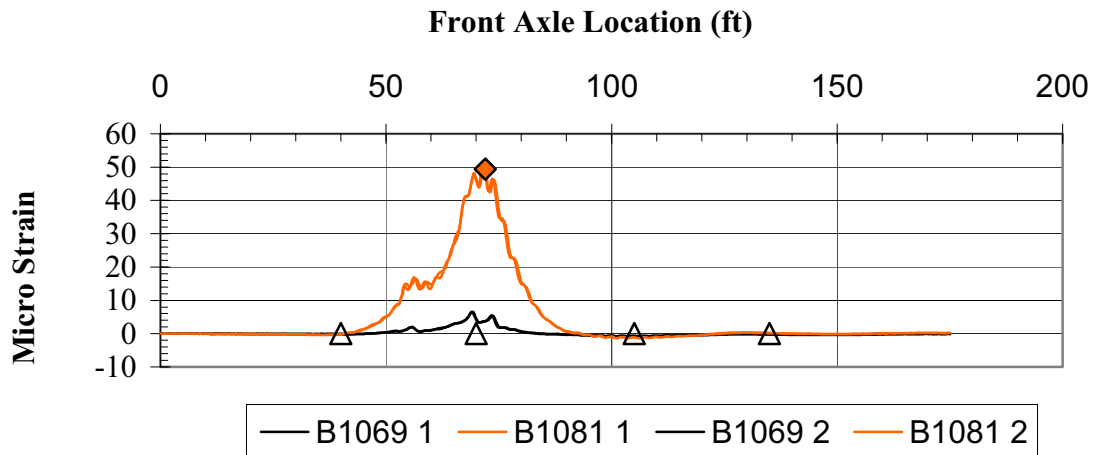
Values from Table 6.2 are plotted in Figure 6.3 and Figure 6.4 to illustrate the transverse distribution of strains at mid-span, and in Figure 6.7 to Figure 6.10 to illustrate the transverse distribution of strain at sections close to supports. The points between measured strains in adjacent girders are connected using straight lines on these graphs. Although the strain variation between girders may not be linear, the line is useful as a general aid to understand transverse strain distribution. In particular, because beam IV was not instrumented the line drawn from beam III to V represents an approximation to the true transverse distribution of strains.



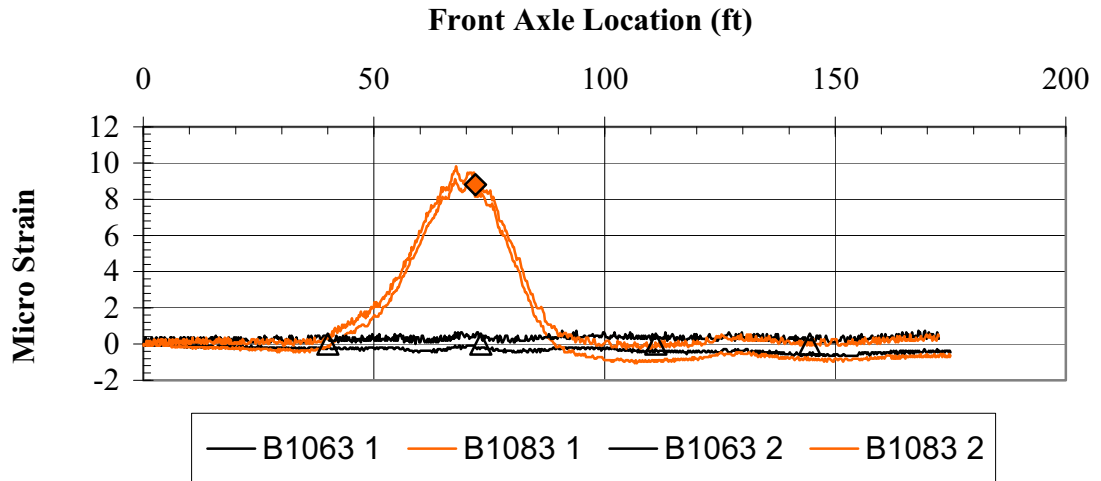
(a) Gauge Pair #2



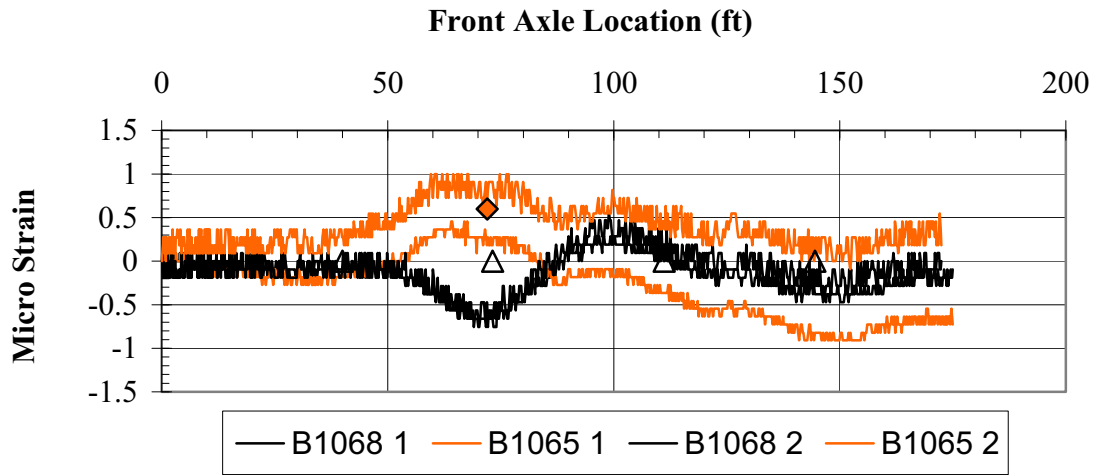
(b) Gauge Pair #5



(c) Gauge Pair #8 (Girder III)



(d) Gauge Pair #11 (Girder V)

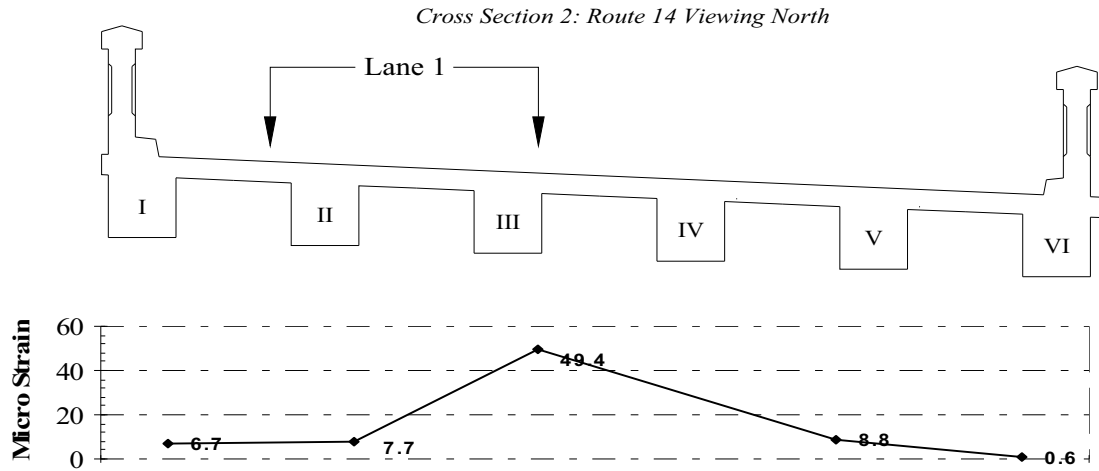


(e) Gauge Pair #14 (Girder VI)

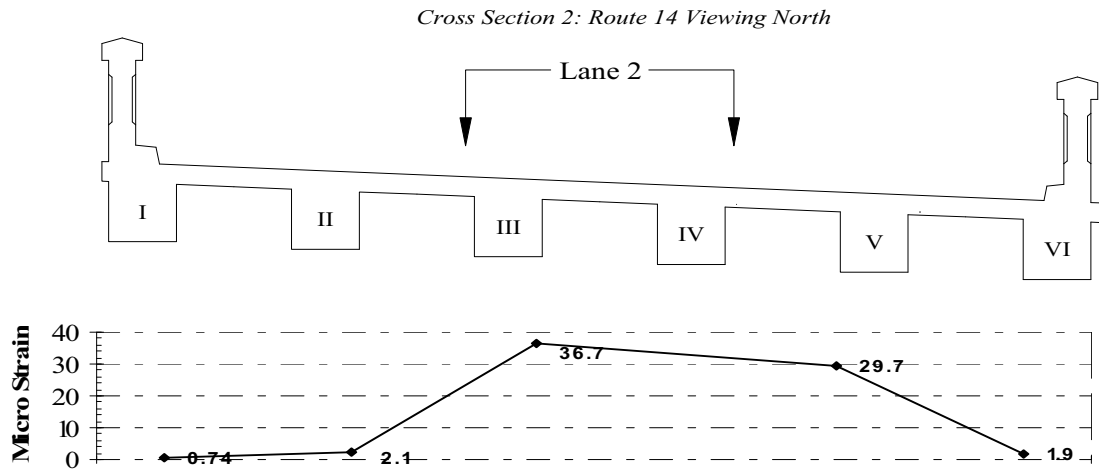
Figure 6.2: Strain Histories Measured at Cross-Section 2 (Truck on Lane 1)

Table 6.2: Bottom Gauge Strain for Transverse Distribution Evaluation

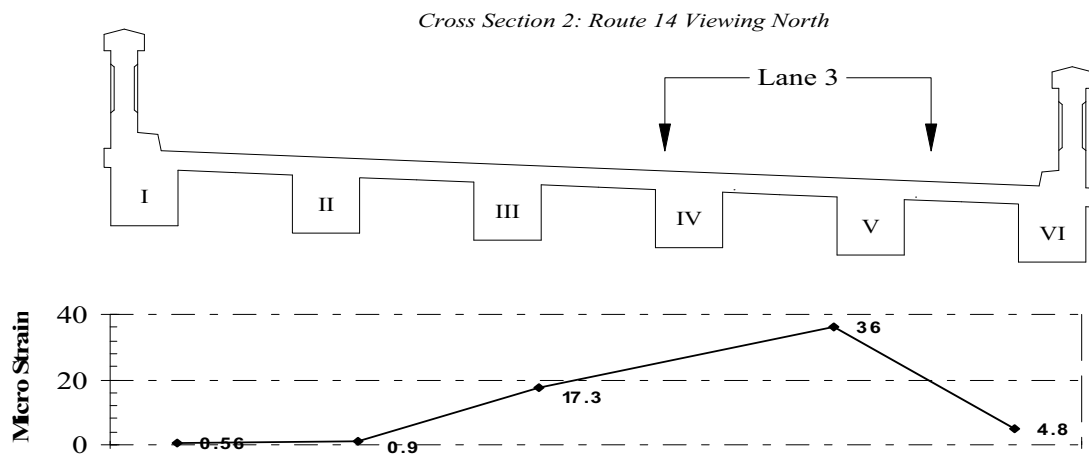
Cross Section	Lane	Distance (ft)	Strain				
			Beam I ($\mu\epsilon$)	Beam II ($\mu\epsilon$)	Beam III ($\mu\epsilon$)	Beam V ($\mu\epsilon$)	Beam VI ($\mu\epsilon$)
1	1	61	2.9	1.9	12.8	2.5	2.0
	2	61	0.7	-1.5	9.2	10.8	3.8
	3	65	0.5	-0.9	1.1	9.7	6.0
2	1	72	6.7	7.7	49.4	8.8	0.6
	2	73	0.74	2.1	36.7	29.7	1.9
	3	72	0.56	0.9	17.3	36	4.8
3	1	86	0.32	6.6	3.1	1.1	0.36
	2	81	0.96	-1.1	-2.2	-2.6	2.9
	3	83	0.14	0.36	0.14	10	4.9
4	1	94	5.6	2	7.6	1.6	1.2
	2	94	2.5	0.13	5.4	8.2	1.7
	3	95	1	0.1	0.4	7	1.6
5	1	106	6.5	25	44.3	10.6	0.77
	2	105	1.4	9.4	35.8	33.5	2.6
	3	109	0.32	3.8	18.5	37.6	8.4
6	1	120	0.41	9.9	12.8	1.35	0.68
	2	119	0.69	0.85	9.8	9.5	-0.17
	3	121	0.23	0.27	2.2	8.5	2.4



(a) Lane 1 – Truck at 72 ft

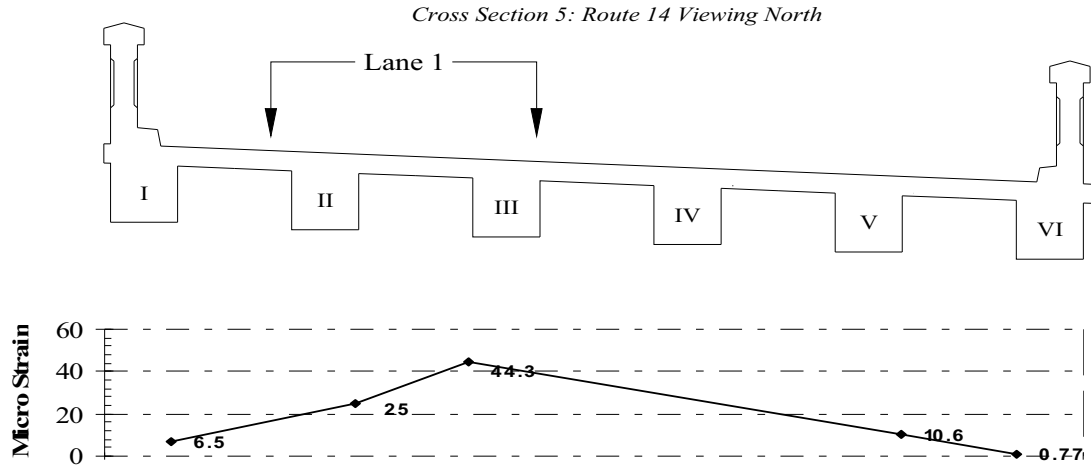


(b) Lane 2 – Truck at 73 ft

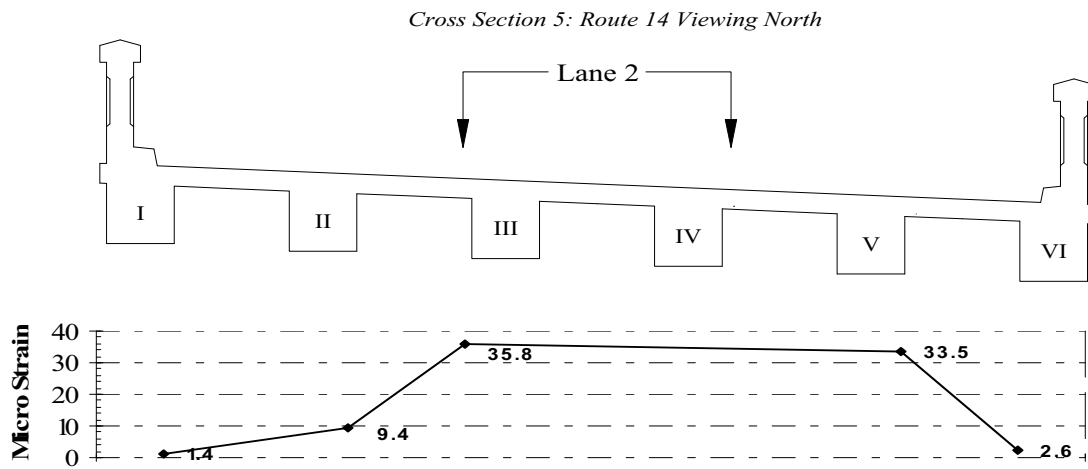


(c) Lane 3 – Truck at 72 ft

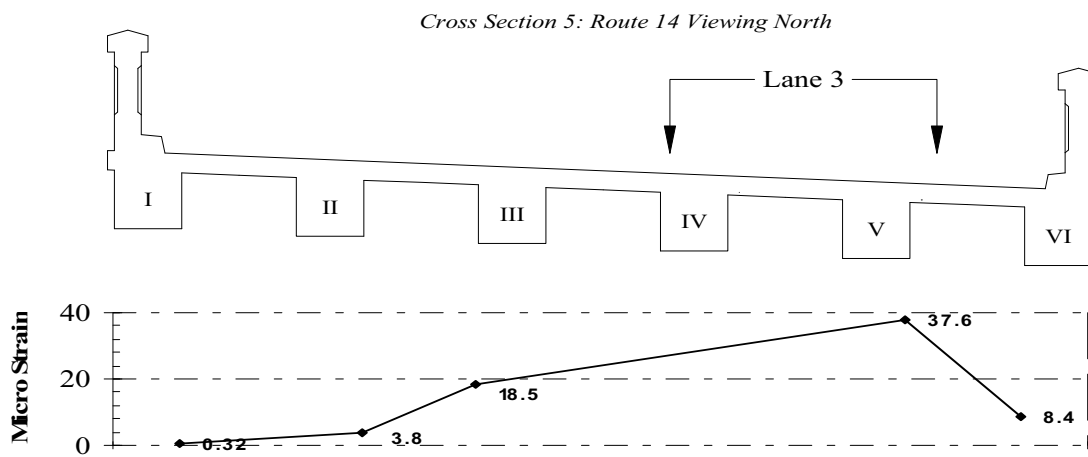
Figure 6.3: Measured Strain in Bottom Gauge in Cross Section 2



Lane 1 – Truck at 106 ft



Lane 2 – Truck at 105 ft



Lane 3 – Truck at 109 ft

Figure 6.4: Measured Strain in Bottom Gauge in Cross Section 5

From the distribution plots the strains in beams directly under the load vehicle are highest, as is expected. The strains in beams further from the load are lower. The strains in exterior beams next to guardrail sections are lower than would anticipated even in cases where the load truck was positioned next to the guardrail. This behavior may be an indication that the concrete guardrails contributed to the response of exterior bridge girders as will be discussed later.

The number of beams engaged by the load vehicle is also of interest to understand bridge response. A beam was considered to be engaged when measurable strain was observed in the strain profile of each cross section. As summarized in Table 6.3, the loading truck engaged at least four girders in all but one case for the two mid-span cross sections.

Table 6.3: Number of Engaged Beams in Bridge Response at Mid-Span

Lane	Cross Section	Figure	Number of Beams Engaged	Beams
1	2	Figure 6.3a	5	I, II, III, IV, V
2	2	Figure 6.3b	3	III, IV, V
3	2	Figure 6.3c	4	III, IV, V, VI
1	5	Figure 6.4a	5	I, II, III, IV, V
2	5	Figure 6.4b	4	II, III, IV, V
3	5	Figure 6.4c	4	III, IV, V, VI

The peak strain response in most of the plotted cross sections corresponded to a section almost directly below the load vehicle, with a reduction of away from the applied load (Figure 6.3c). In cross section 2 however with lane 1 loading (Figure 6.3a) the strain in beam II is lower than expected, when compared with a similar loading in cross section 5 (Figure 6.4a). The lower strain reading may be a result of damage to beam II (Figure 3.9a)

It is also observed that the maximum response at each cross section occurred when the load truck was positioned at approximately the same location even for different loaded lanes as listed in Table 6.2. The position of the weight resultant of the 63.7-kip (28,894 kg) load truck was determined to be 12.3 ft (3.75 m) behind the front axle as shown in Figure 6.5. Using the front axle positions listed in Table 6.2, the position of the loading truck resultant was plotted for each bridge cross section (Figure 6.6). It is interesting to note that the loading truck resultant is close to each cross section where the maximum response was measured. This indicates that the maximum response was primarily controlled by the weight and location of the two rear axles of the loading truck.

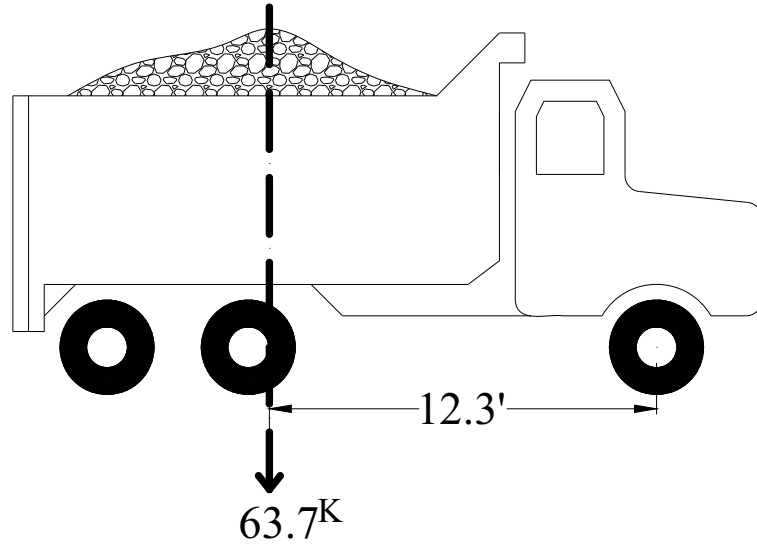


Figure 6.5: Centroid of Load in Vehicle

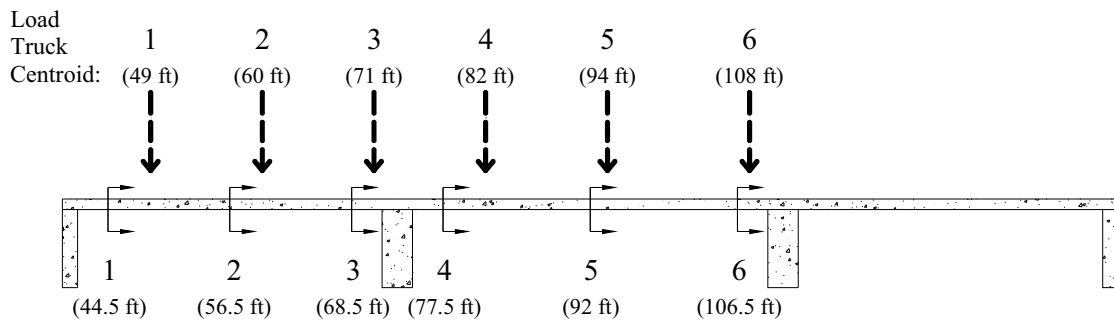
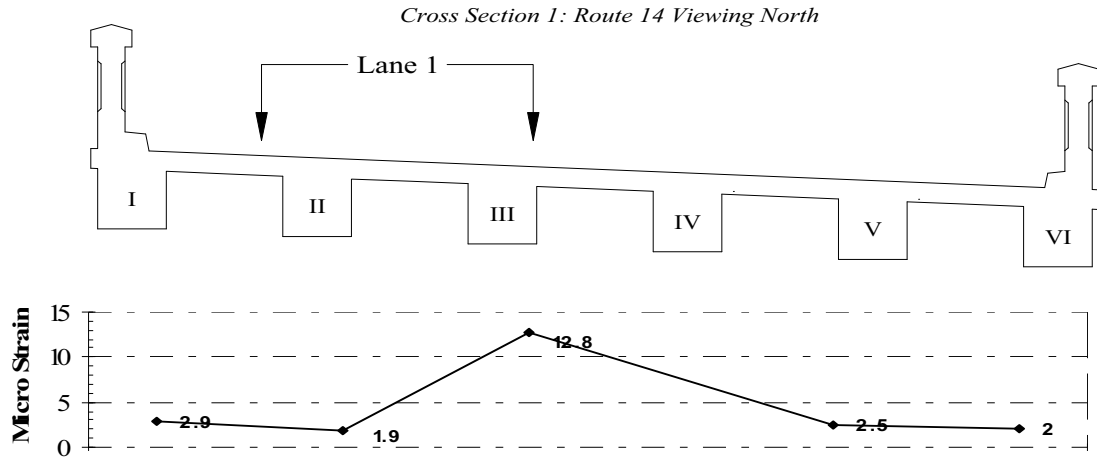
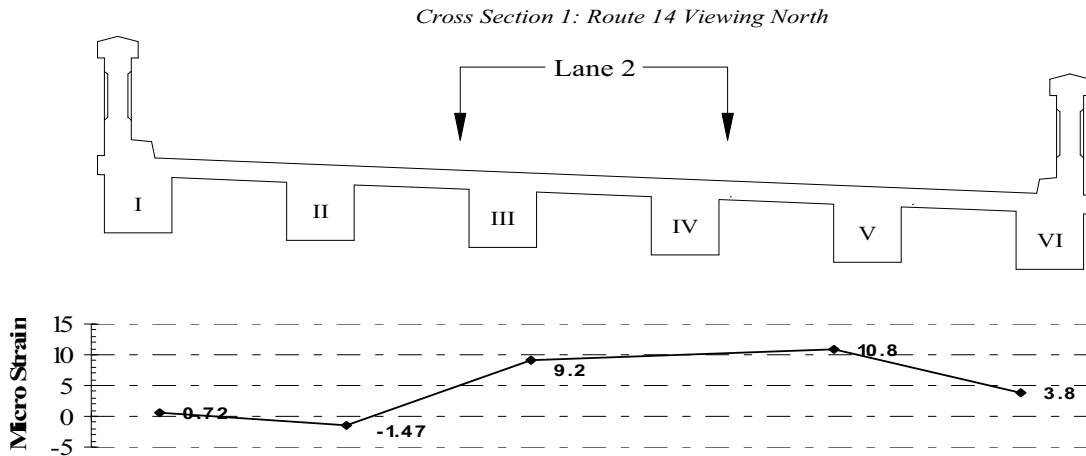


Figure 6.6: Centroid of Load Producing Maximum Response at Cross Sections
6.1.1.2 Transverse Strain Distribution Near Span Ends

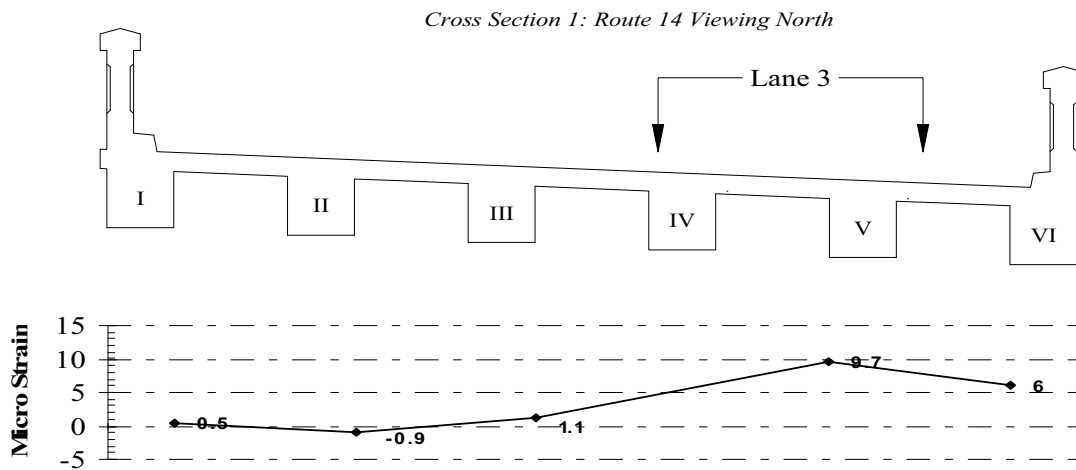
Strains measured at sections 1 and 3 in span 1 and sections 4 and 6 in span 2 are plotted in Figure 6.7 to Figure 6.10. Peak strain values at the loading truck positions used to create these plots are listed in Table 6.2.



Lane 1 – Truck at 61 ft

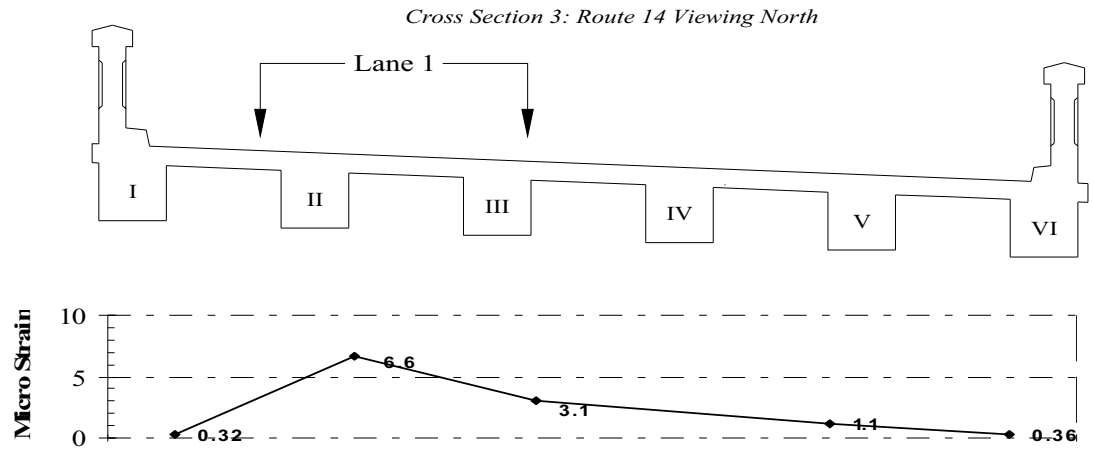


Lane 2 – Truck at 61 ft

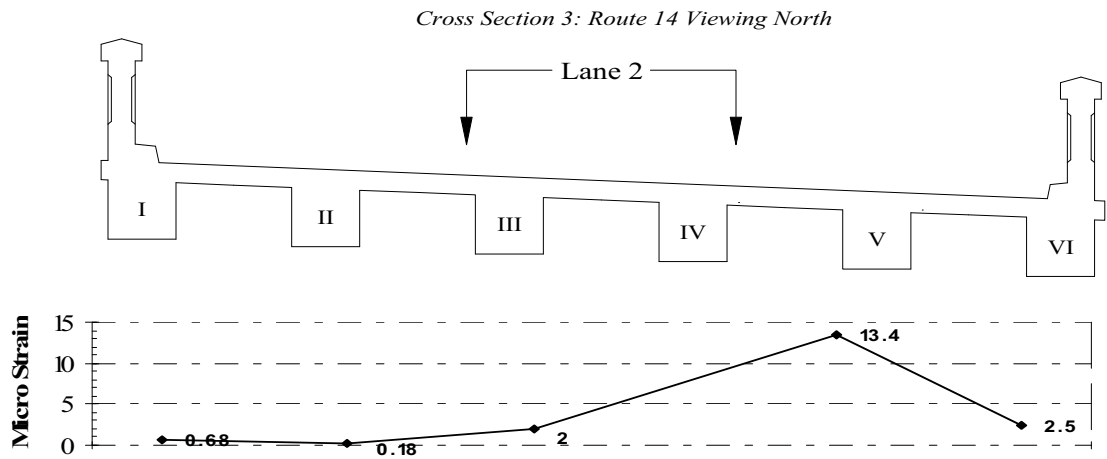


Lane 3 – Truck at 65 ft

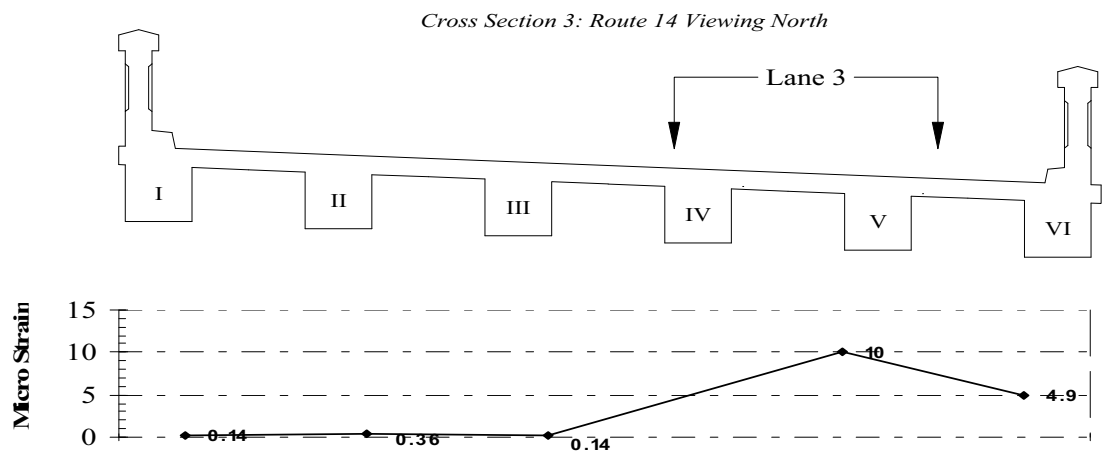
Figure 6.7: Measured Strain in Bottom Gauge in Cross Section 1



Lane 1 – Truck at 86 ft

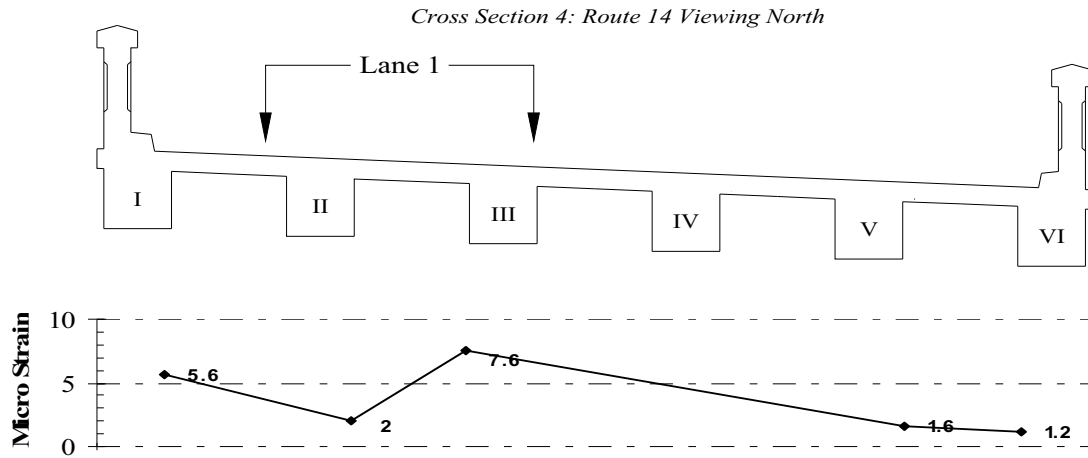


Lane 2 – Truck at 81 ft

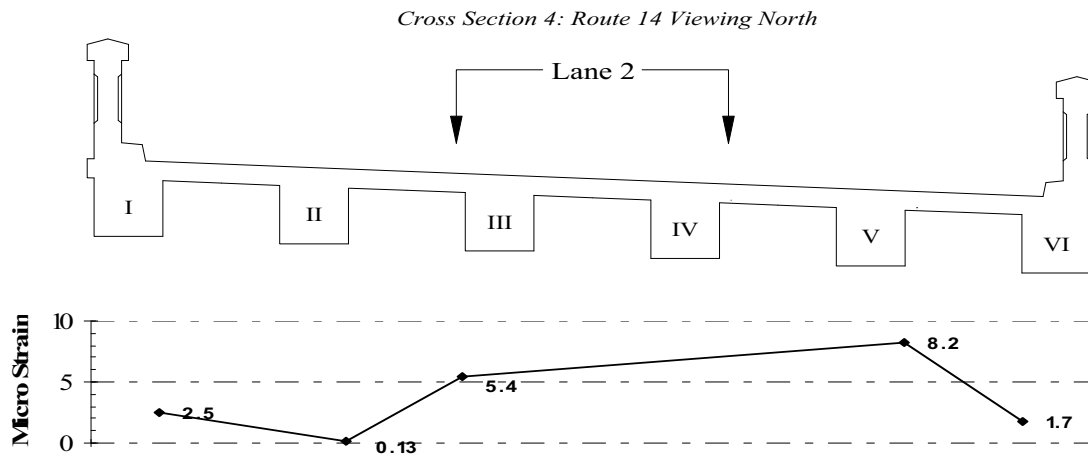


Lane 3 – Truck at 83 ft

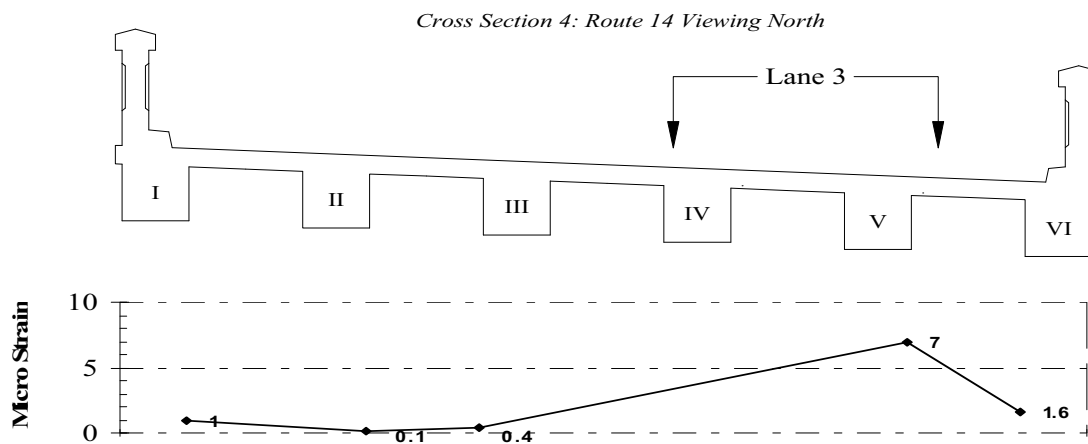
Figure 6.8: Measured Strain in Bottom Gauge in Cross Section 3



Lane 1 – Truck at 94 ft

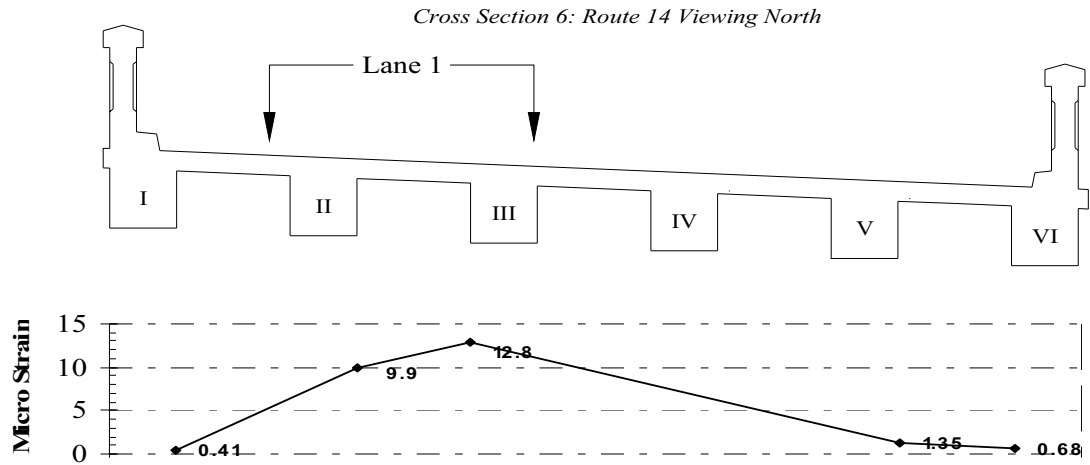


Lane 2 – Truck at 94 ft

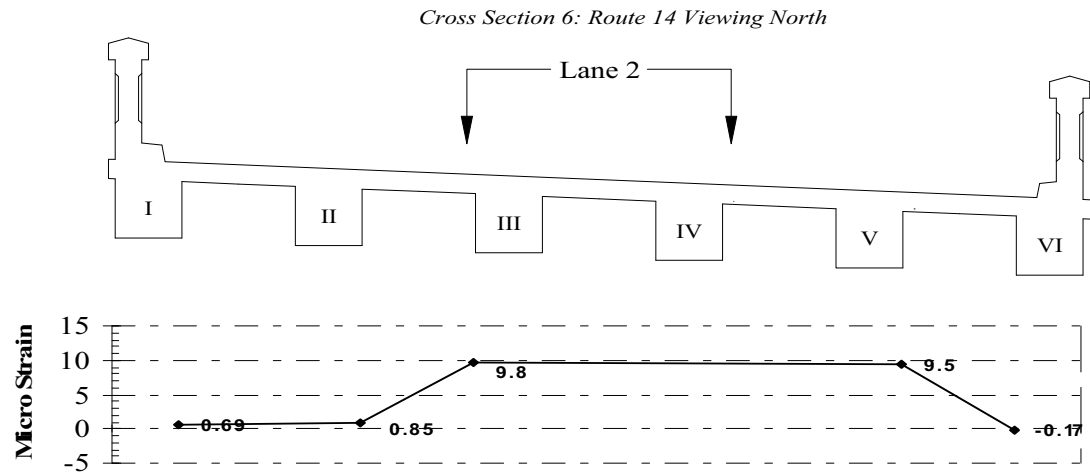


Lane 3 – Truck at 95 ft

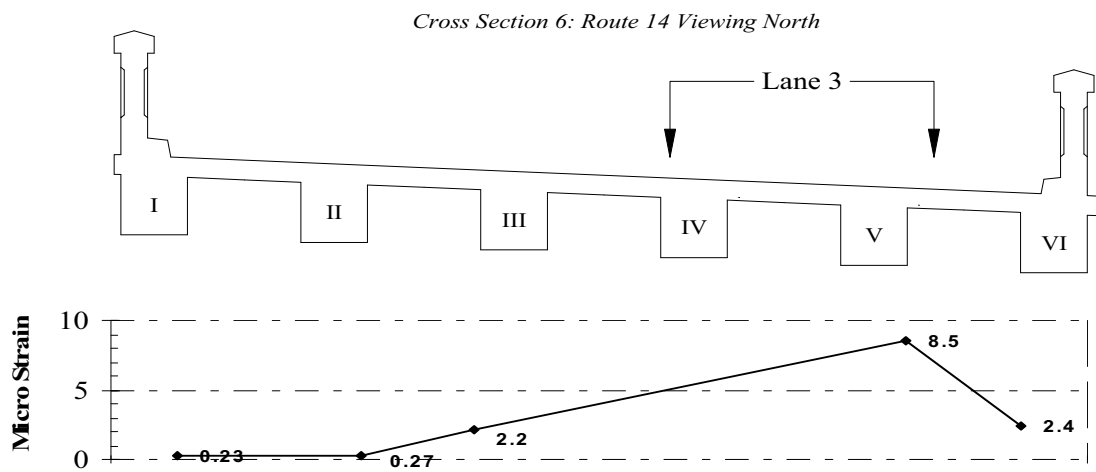
Figure 6.9: Measured Strain in Bottom Gauge in Cross Section 4



Lane 1 – Truck at 120 ft



Lane 2 – Truck at 119 ft



Lane 3 – Truck at 121 ft

Figure 6.10: Measured Strain in Bottom Gauge in Cross Section 6

The cross-sections used to generate plots in Figure 6.7 to Figure 6.10 were located approximately 3 feet (914 mm) from the end of each span. These strains were much lower than those measured at mid-span, as is expected. The general trend observed in comparison with mid-span plots that strain values are highest directly below the load truck and decrease away from applied load was also observed at sections near the end of beams. Exceptions were noticed however in girder II of cross sections 1 and 4 with the truck traveling in lanes 1 and 2.

As summarized in Table 6.4, between 2 and 3 girders were engaged in the bridge response when the loading truck was positioned to produce the maximum positive response. When compared with the transverse strain distribution at mid-span where 3 to 4 girders were typically engaged, the transverse strains decreased more rapidly near the ends of spans. This behavior may be attributable to the proximity of these sections to the supports. It is not unreasonable to expect that the support stiffness causes load to more easily be transferred directly into the support in the longitudinal direction than transversely into parallel girders.

Table 6.4: Number of Engaged Beams in Bridge Response at Beam Ends

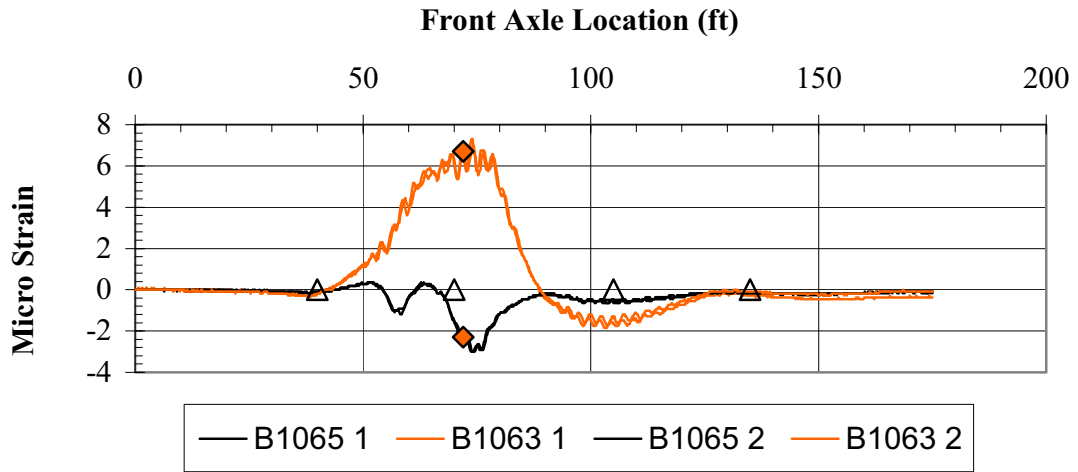
Lane	Cross Section	Figure	Number of Beams Engaged	Beams
1	1	Figure 6.7a	2	III, IV
2	1	Figure 6.7b	3	III, IV, V
3	1	Figure 6.7c	3	IV, V, VI
1	3	Figure 6.8a	2	II, III
2	3	Figure 6.8b	2	IV, V
3	3	Figure 6.8c	3	IV, V, VI
1	4	Figure 6.9a	2	I, III
2	4	Figure 6.9b	3	III, IV, V
3	4	Figure 6.9c	3	IV, V, VI
1	6	Figure 6.10a	3	II, III, IV
2	6	Figure 6.10b	3	III, IV, V
3	6	Figure 6.10c	2	IV, V

6.1.2 Contribution of Guard Rails

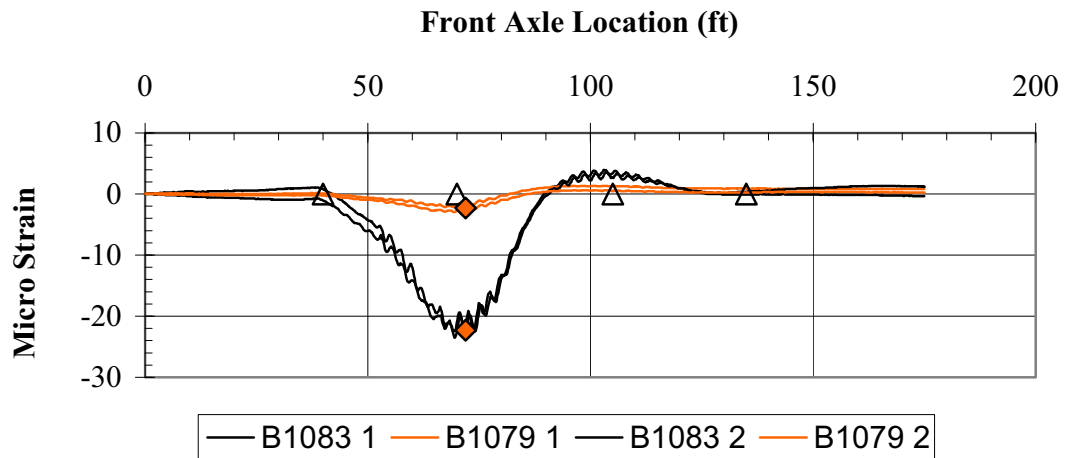
Although the guardrails are not usually designed to be structurally integral with the T-Beams, $\frac{1}{2}$ in. (13 mm) square reinforcing bars spaced 18 in. (457 mm) on center (Figure 3.12) connect the guardrail with the exterior girders. During the load tests, the guardrails were instrumented at mid-span in three locations to determine their contribution to the overall bridge response. Guardrail sections near the ends of each span were not instrumented because sections appeared to be separated from adjacent spans as observed in the field, with from noticeable gaps above pier locations.

6.1.2.1 Span 1 - Upstream Guard Rail

Span 1 was instrumented at mid-span with gauge pair #31 in the guardrail and #2 in the exterior girder. The strain histories of gauge pairs #31 and #2 with the load truck traveling along lane 1 are plotted in Figure 6.11. From these plots, the loading truck position (72 ft (21.95 m)) that produced the maximum strain response in the bridge was chosen to construct a strain profile for the composite guardrail-girder section. The resulting strain values are listed in Table 6.5 and plotted along the guardrail-girder cross section in Figure 6.12.



(a) Gauge Pair #2 (exterior girder)



(b) Gauge Pair #31 (upstream guardrail)

Figure 6.11: Strain Histories on Exterior Girder and Upstream Guardrail in Span 1 (Lane 1)

Table 6.5: Guardrail Strain Readings

Guardrail Gauge Pair	Lane	Distance (ft)	Strain			
			Beam Lower ($\mu\epsilon$)	Beam Upper ($\mu\epsilon$)	Guardrail Lower ($\mu\epsilon$)	Guardrail Upper ($\mu\epsilon$)
31	1	72	6.7	-2.3	-2.3	-22.3
32	1	106	6.5	-1.5	-1.0	-19.8
33	3	109	7.1	-2.0	-5.3	-19.1

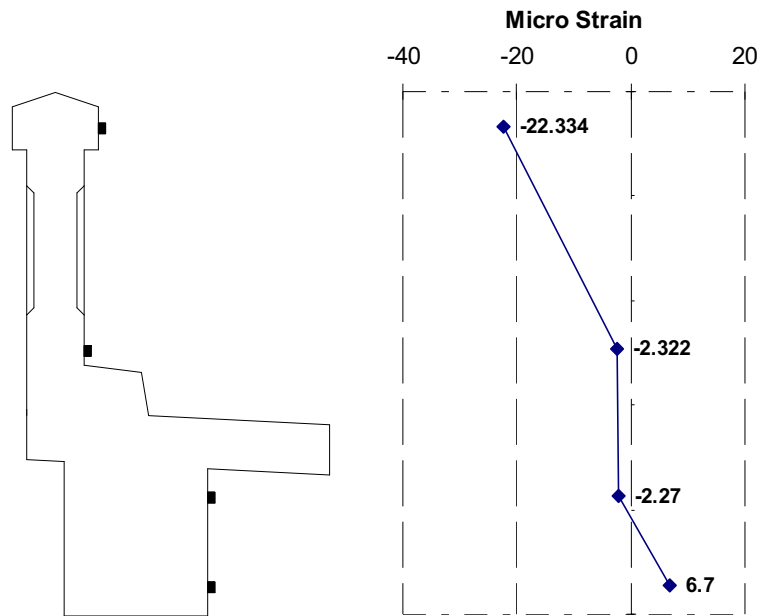


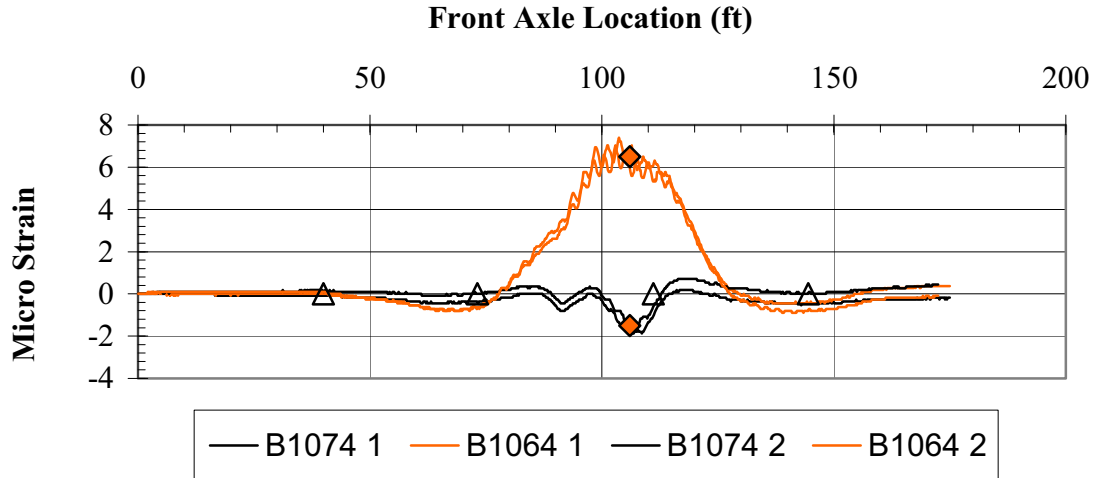
Figure 6.12: Strain in Guard Rail Gauge Pair #31 (Lane 1 – 72 ft)

Although the strains plotted over the composite cross section in Figure 6.12 do not follow exactly the common assumption of a linear variation of strain, a definite contribution from the guardrail to the response of the exterior girder can certainly be observed. This behavior partially explains the lower than anticipated strains measured near the bottom of the exterior girders as discussed earlier. With the limited number of points used to determine strains in this cross section, it is impossible to determine whether the guardrail could be considered to be acting fully compositely (without any slip) relative to the exterior girder.

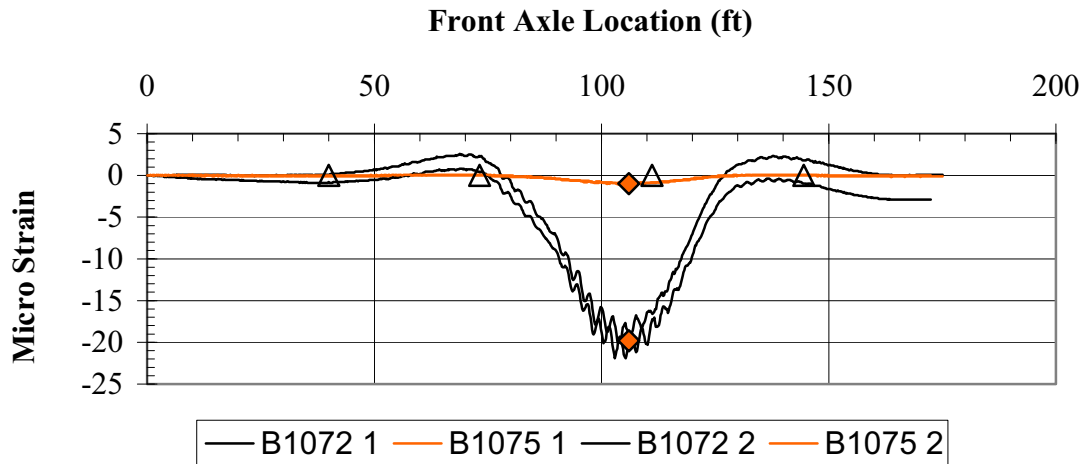
6.1.2.2 Span 2 - Upstream Guard Rail

Span 2 was instrumented at mid-span with gauge pair #32 in the guardrail and #17 in the exterior girder. The strain history of gauge pairs #17 and #32 with the load vehicle in lane 1 are plotted in Figure 6.13. From these plots, the strain producing the

maximum response was chosen, corresponding to a front axle of the loading truck positioned at 106 feet (32.31 m). The resulting strain values are listed in Table 6.5 and plotted in Figure 6.14. The observed strain distribution is similar to the one determined for span 1 in the upstream face of the bridge.



(a) Gauge pair #17 (exterior girder)



(b) Gauge pair #32 (guardrail)

Figure 6.13: Strain Histories on Exterior Girder and Upstream Guardrail in Span 2 (Lane 1)

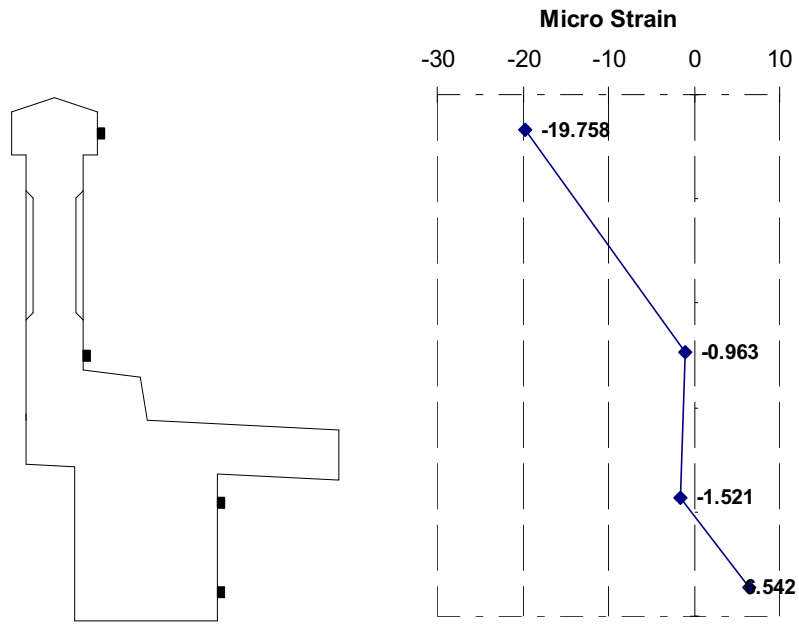
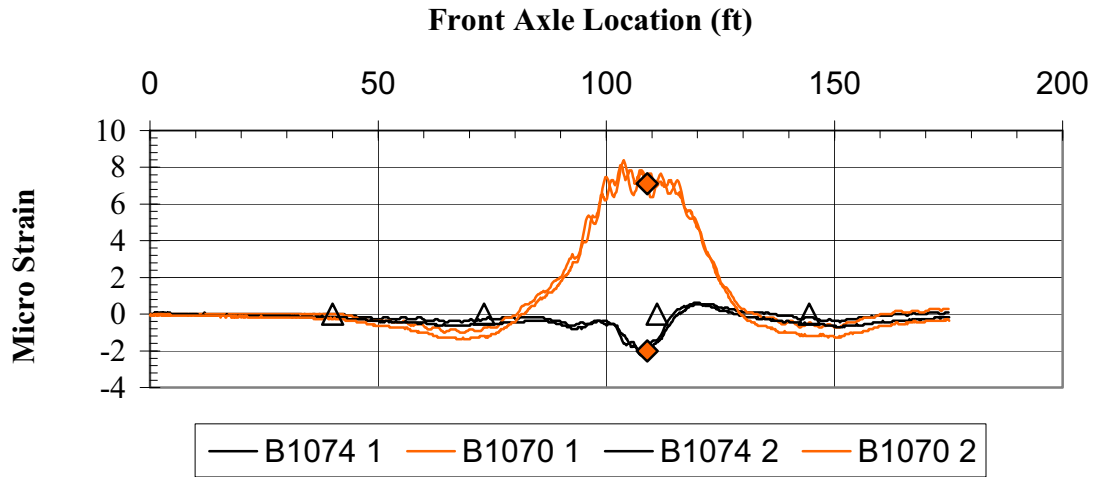
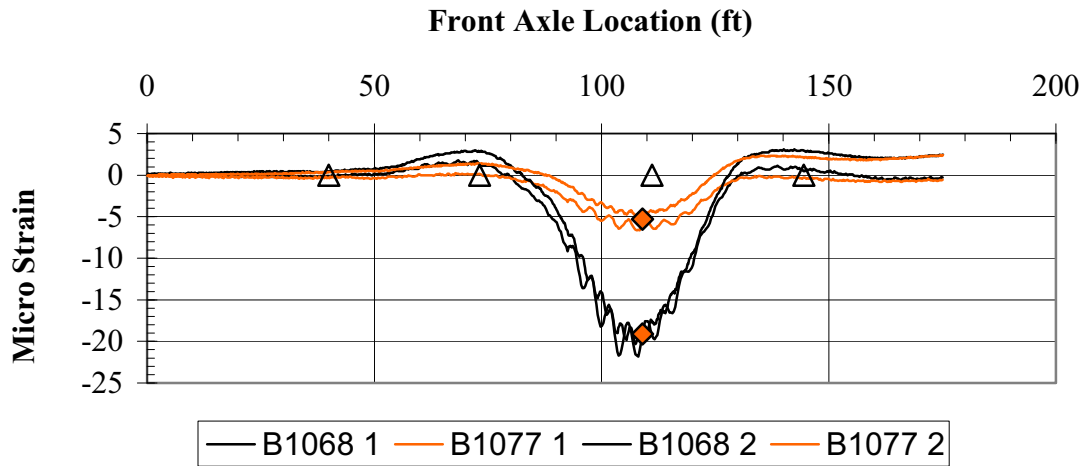


Figure 6.14: Strain in Guard Rail Gauge Pair #32 (Lane 1 – 106 ft)
6.1.2.3 Span 2 - Downstream Guard Rail

Span 2 was instrumented at mid-span with gauge pair #33 in the guardrail and #29 in the exterior girder. The strain histories for gauge pairs #29 and #33 with the loading vehicle traveling in lane 3 are plotted in Figure 6.15 and. Again, the maximum strain was chosen to determine the critical loading truck location, corresponding to a front axle position of the loading truck at 109 feet (33.22 m). The resulting strain values for this truck position are listed in Table 6.5 and plotted in Figure 6.16.



(a) Gauge pair #29 (exterior girder)



(b) Gauge pair #33 (downstream guardrail)

Figure 6.15: Strain Histories on Exterior Girder and Downstream Guardrail in Span 2 (Lane 3)

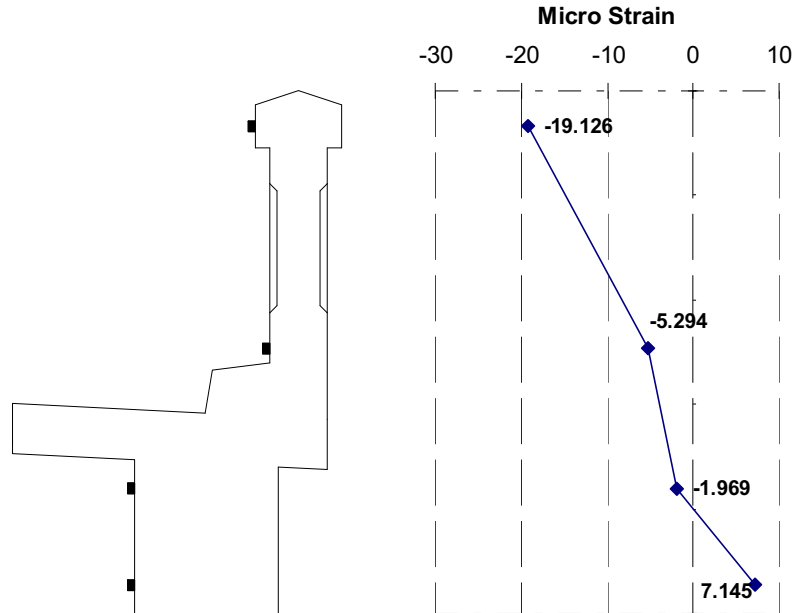


Figure 6.16: Strain in Guard Rail Gauge Pair #33 (Lane 1 -109 ft)

6.1.2.4 Analysis of Guardrail Contribution

The strain histories measured in instrumented guardrail sections indicate that the guardrail has a measured response to applied live loads on the bridge. Readings from gauges attached to the top of the guardrail recorded the highest strains observed during field testing.

The maximum strain in the upper gauges of the guardrail are all in compression and are in the range of -19.1 to -22.3 $\mu\epsilon$, a difference of only 3.2 $\mu\epsilon$. Peak tensile strains in the bottom gauge of the T-beam are in the range of 6.7 to 7.1 $\mu\epsilon$.

The neutral axis of bending for all instrumented guardrail sections (where the strain is approximately zero) occurs near the top gauges of the T-beam, which were attached 4 in (102 mm) below the deck slab. While the strain gauges used in this analysis are not aligned horizontally in the same plane, the results are useful to compare vertical differences in strain in the exterior girders and guardrail sections.

The linearity of the strain profile may also be indicative of the amount of composite behavior unintentionally created between the guardrail and exterior T-beam. Figure 6.16 illustrates a strain profile that is roughly linear through the guardrail and T-beam cross section which may indicate composite behavior. With the top of the guardrail in compression and the bottom strain gauge in tension, the neutral axis is located near the bottom of the deck slab.

Plots in Figure 6.12 and Figure 6.14 have a jump in strain between the guardrail and T-beam. These non-linear profiles have measured the strain in the upper T-beam that is the same or slightly less than the measured strain in the lower part of the

guardrail. This may indicate that there is partial composite action in the instrumented guardrail sections. The amount of composite action between guardrail and exterior girder is difficult to quantify given the relatively small number of gauges placed in the cross section as mentioned before.

6.1.3 Neutral Axis Depth

Neutral axis depths measured from the bottom strain gauge (4 in (102 mm) above beam bottom) are plotted for interior girders in Figure 6.18 to Figure 6.23. Neutral axis calculation for exterior girders was not performed because bottom gauge strains were not greater than the selected threshold of 5 microstrain (absolute value). Since neutral axis depth is plotted based on the geometry of the strain profile very small strain values can have a large amount of error when calculating neutral axis depth (Section A.4).

Each neutral axis plot has two lines: The darker line was calculated using data from the first test run, and the lighter line from a repeated test run with the loading truck traveling along the same lane. The neutral axis depth data show repeatability of different test runs even though the loading truck transverse position may have varied slightly in each test run. Therefore, moments generated in interior girders were calculated using the average of the calculated neutral axis depth at each load truck location.

The highest strains were measured when the truck was positioned on the span and lane directly above the corresponding gauge pair for which strain was being measured (Section 6.1.1.1). Therefore, when axles of the loading truck lied in adjacent spans or in lanes not directly above the monitored girder, the neutral axis was often not calculated for the entire test run because of strains below the threshold value in the bottom gauge.

The calculated neutral axis depths varied by less than 2 in (51 mm) in most plots, with a peak variation of 4.4 in (112 mm) (Table 6.6). This result gave confidence in the load tests and indicated that there was very little variation of neutral axis depth with loading truck position.

Neutral axis depths determined from the tests were compared with depths calculated from an elastic section analysis of the T-beam cross sections in spans 1 and 2. Neutral axis depths of 12.2 and 11.4 in (310 and 290 mm) measured from the bottom strain gauge for spans 1 and 2, respectively, were calculated using uncracked T-beam section properties, a concrete strength of 6,000 psi (41.4 MPa), and an effective deck width of 54 in (1.37 m). The calculated values using standard reinforced concrete elastic theory are slightly below or between the maximum and minimum neutral axis depths determined from field data listed in Table 6.6.

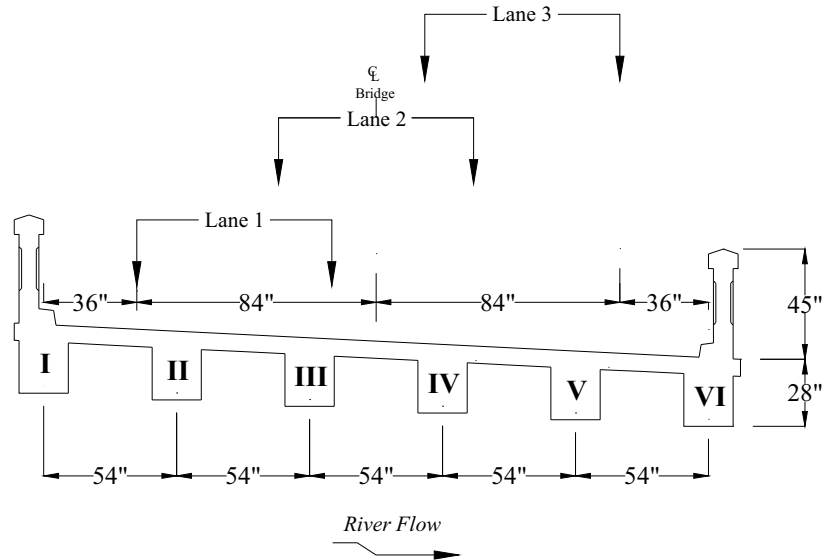
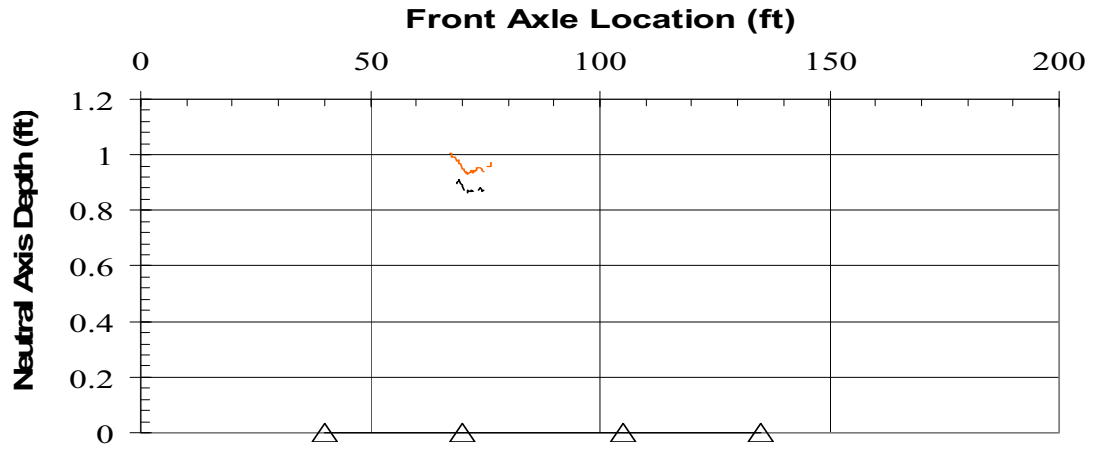


Figure 6.17: Cross Section of Royalton Bridge with Load Truck Lanes

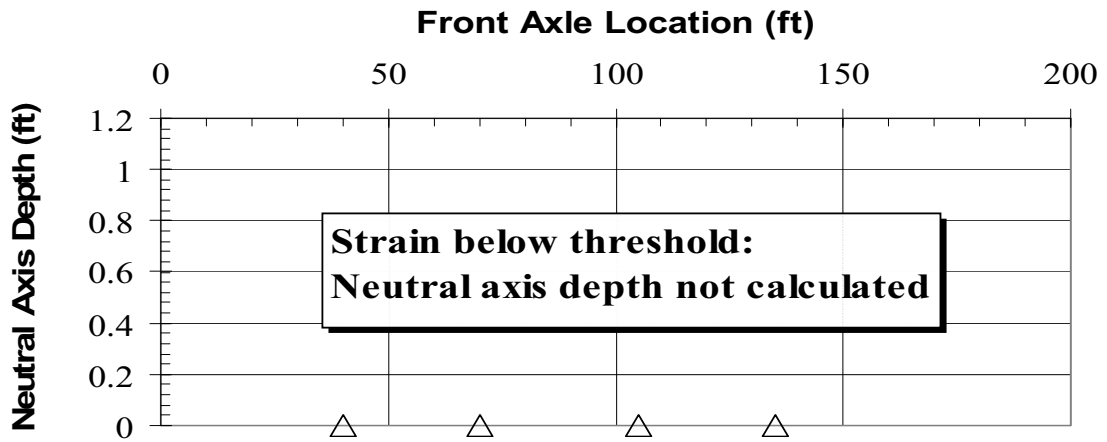
Table 6.6: Variation of Neutral Axis Depth at Mid-Span in Interior Beams

Span	Beam	Lane	Neutral Axis Depth [†]		
			Minimu m (in)	Maximu m (in)	Range (in)
1	II	1	10.2	14.6	4.4
	II	2	*	*	
	II	3	*	*	
	III	1	12.5	14.5	2
	III	2	10.7	13.9	3.2
	III	3	10.2	13	2.8
	V	1	13	13.8	0.8
	V	2	13.2	14.4	1.2
2	V	3	12.6	14	1.4
	II	1	10.1	12.3	2.2
	II	2	8	9	1
	II	3	*	*	
	III	1	13.6	14.7	1.1
	III	2	13.3	14.1	0.8
	III	3	12.9	14.1	1.2
	V	1	14.3	14.7	0.4
V	2	14.1	15.6	1.5	
V	3	14.1	16.7	2.6	

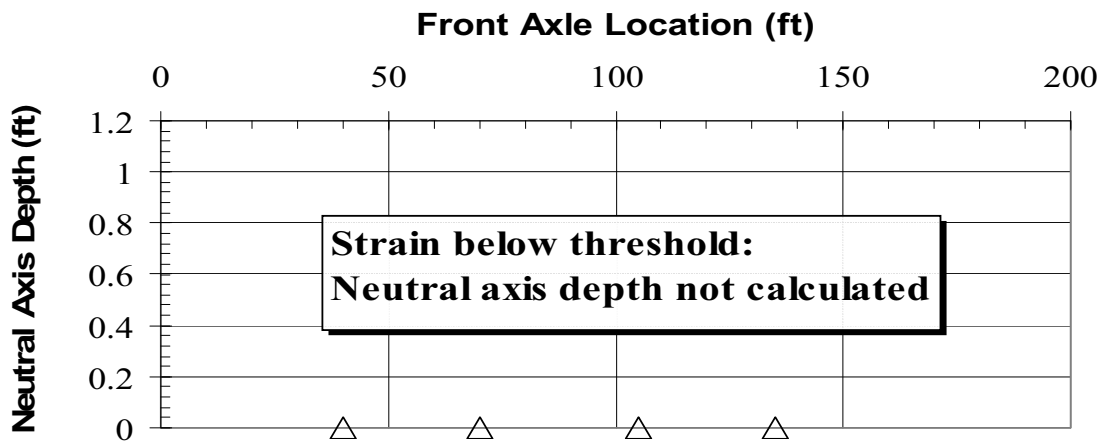
[†] The neutral axis depth is measured from bottom strain gauge (4 in above beam bottom). * Neutral axis depth was not calculated when bottom gauge recorded less than 5 micro strain



(a) Truck in Lane 1

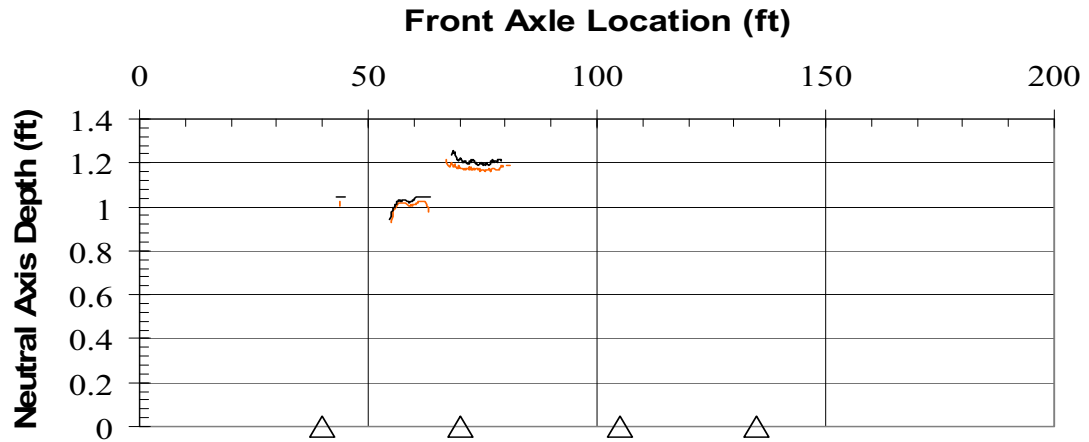


(b) Truck in Lane 2

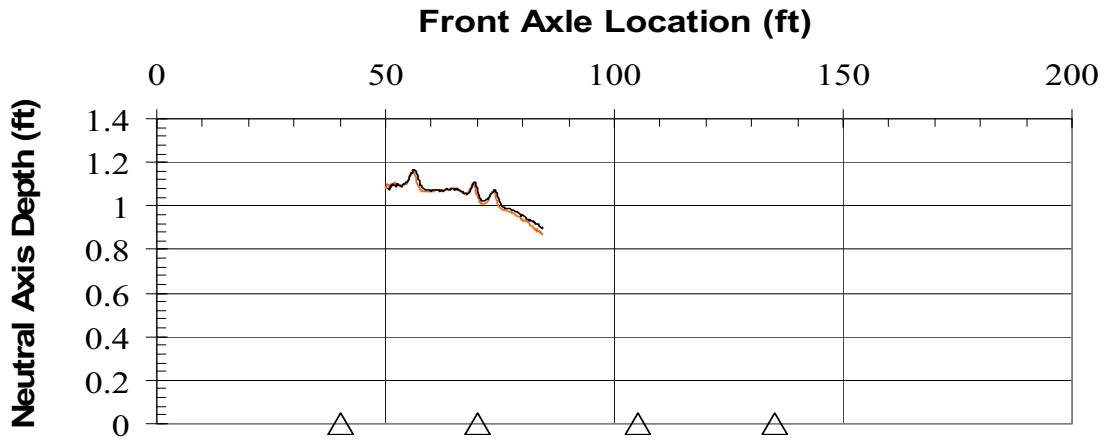


(c) Truck in Lane 3

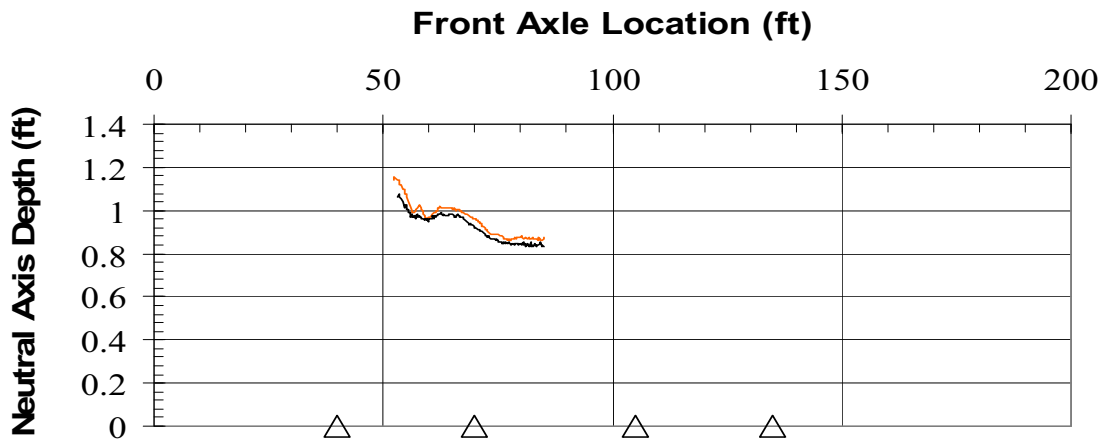
Figure 6.18: Beam II Span 1



(a) Truck in Lane 1

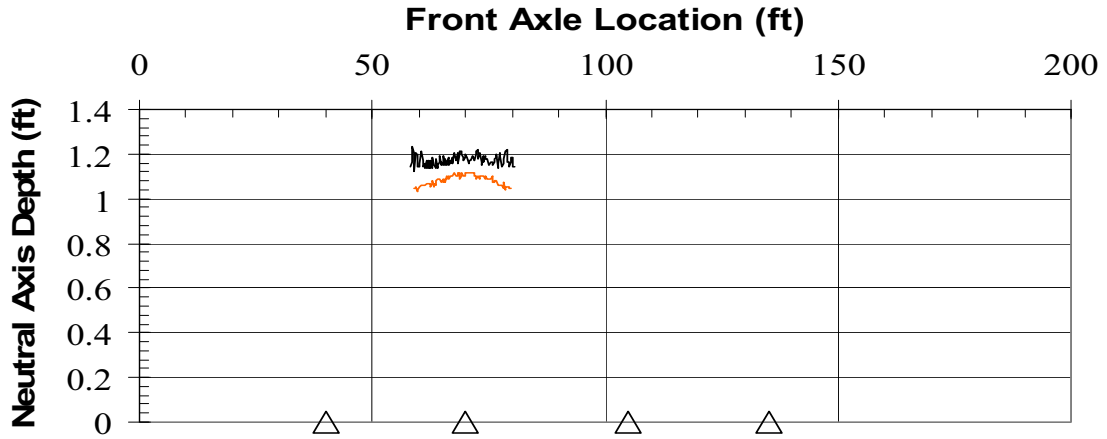


(b) Truck in Lane 2

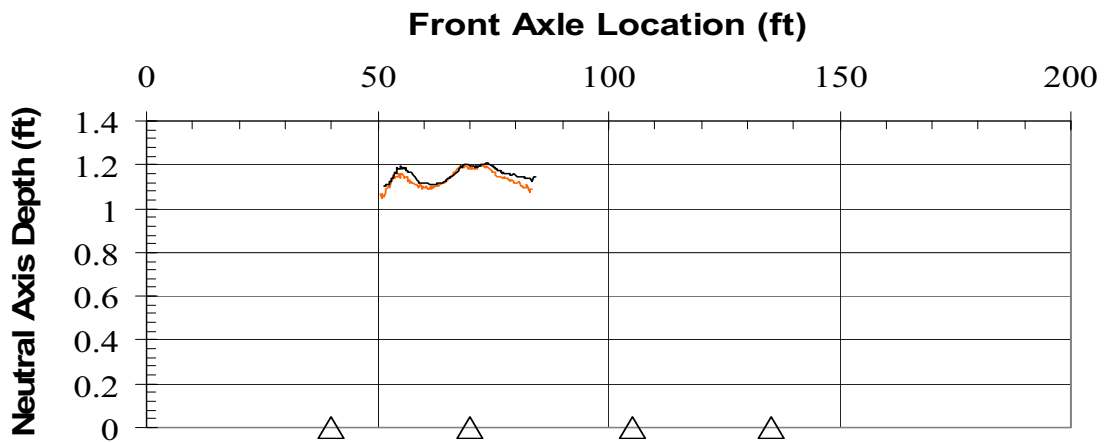


(c) Truck in Lane 3

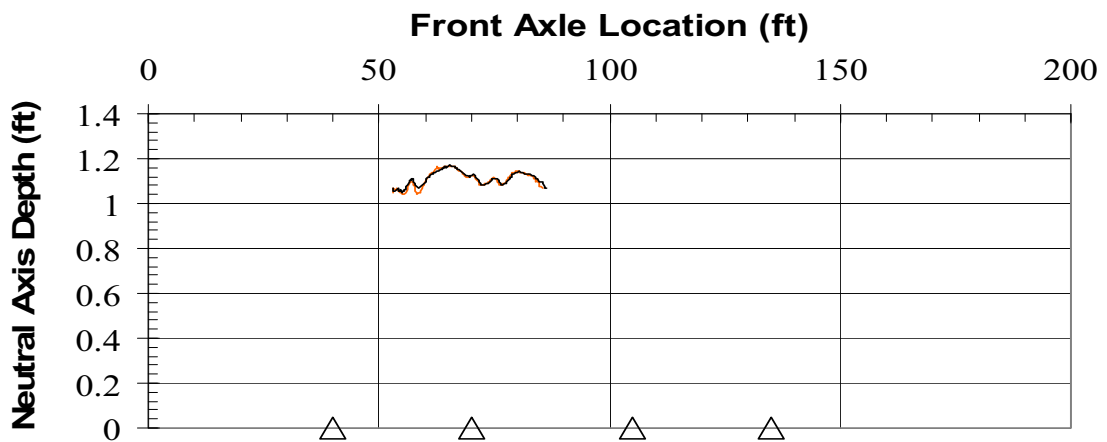
Figure 6.19: Beam III Span 1



(a) Truck in Lane 1

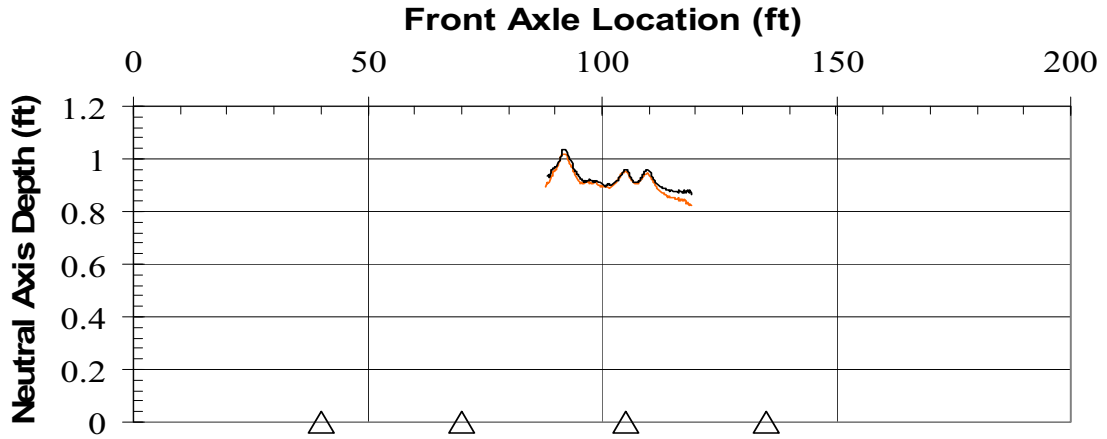


(b) Truck in Lane 2

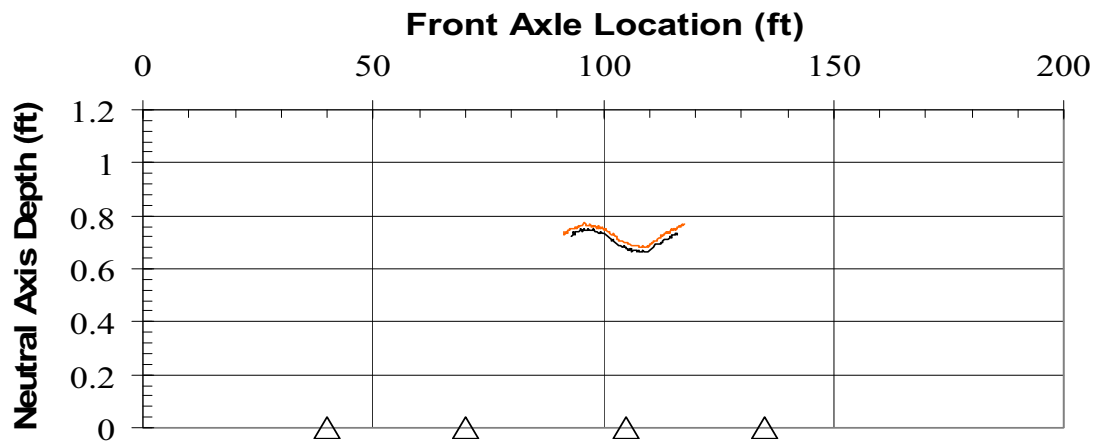


(c) Truck in Lane 3

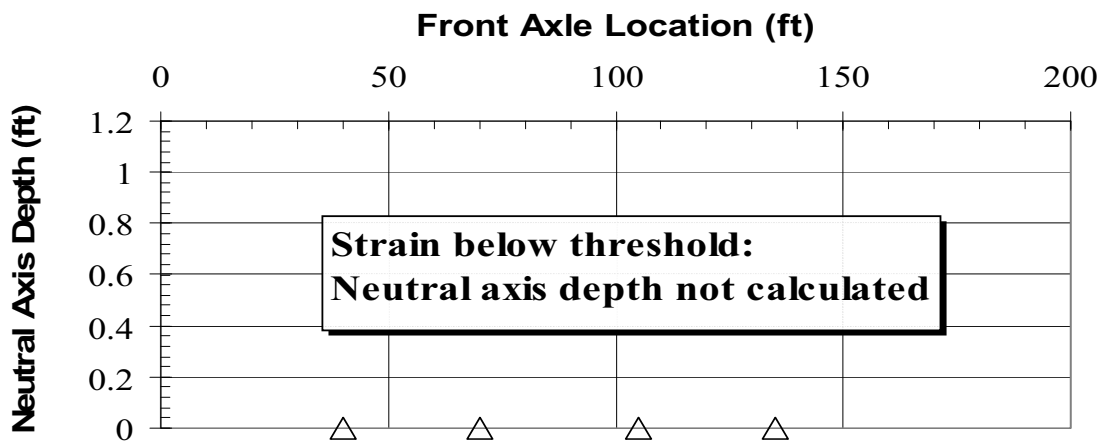
Figure 6.20: Beam V Span 1



(a) Truck in Lane 1

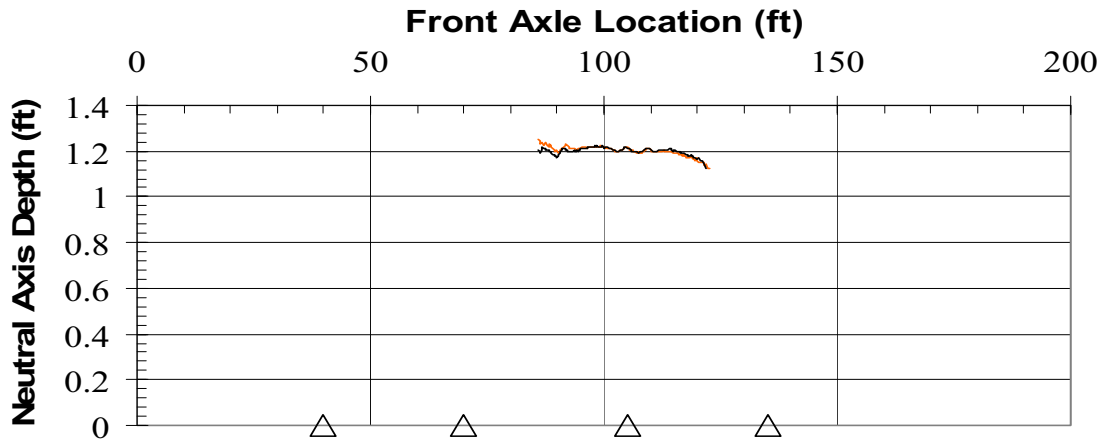


(b) Truck in Lane 2

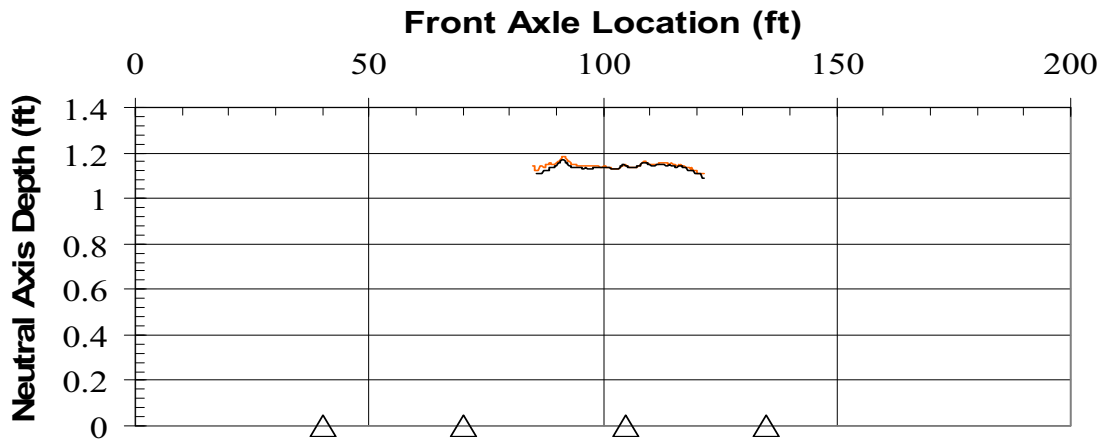


(c) Truck in Lane 3

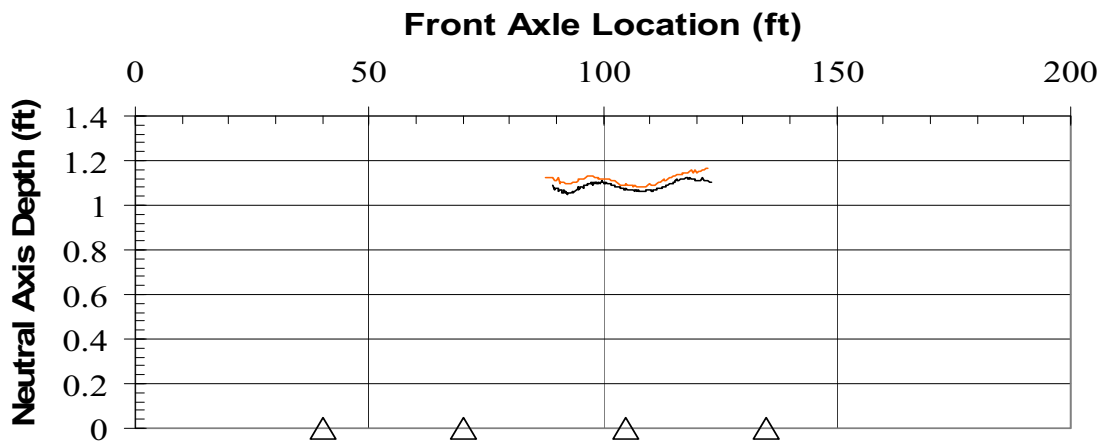
Figure 6.21: Beam II Span 2



(a) Truck in Lane 1

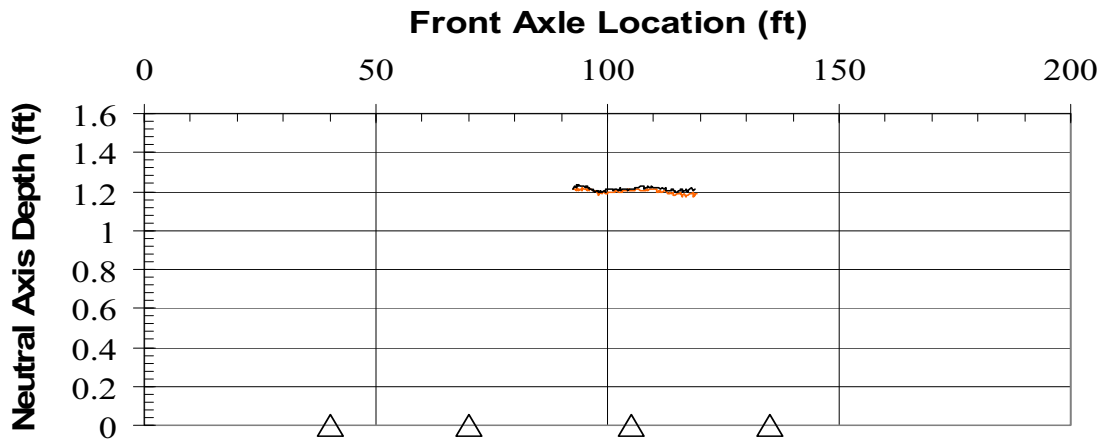


(b) Truck in Lane 2

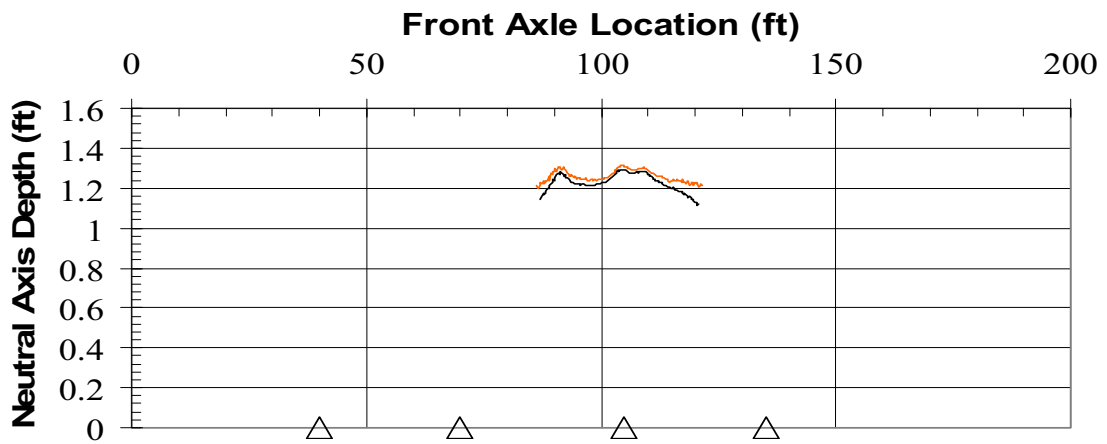


(c) Truck in Lane 3

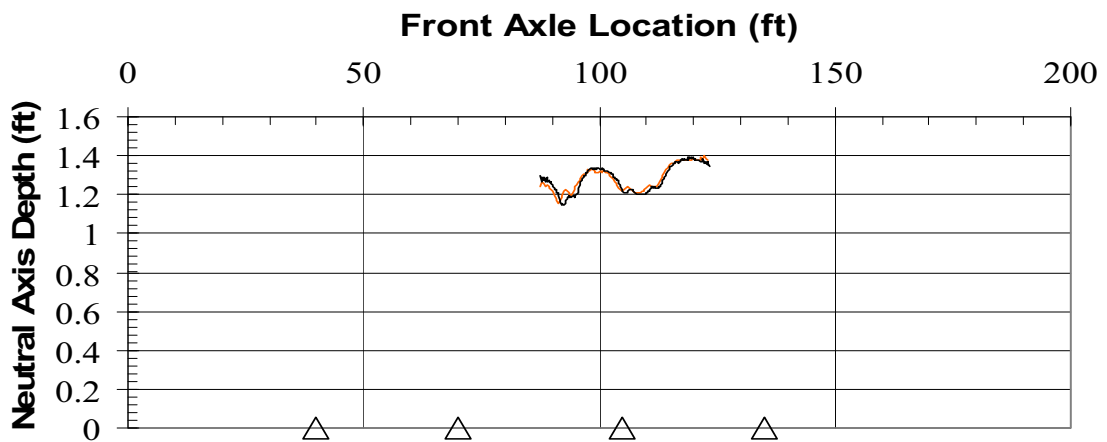
Figure 6.22: Beam III Span 2



(a) Truck in Lane 1



(b) Truck in Lane 2



(c) Truck in Lane 3

Figure 6.23: Beam V Span 2

6.1.4 Modulus of Concrete in Moment Calculation

The modulus of elasticity of the material in a cross-section is an important factor in the calculation of moment. The exact modulus of concrete in the Royalton Bridge however, was unknown and had to be estimated. Design concrete strength was not available through the original construction documents dating to the late 1920s for the Royalton bridge. The concrete strength may also have some variability throughout the structure in beams, deck, and guardrail sections. In past load ratings of the Royalton Bridge, state engineers estimated the concrete strength to be 3,000 psi (20.7 MPa).

Past research suggests that concrete strength increases over time for the first 50 years after casting when stored outdoors, with ultimate strength approximately 2.4 times the 28-day strength (Neville, 1996). A design concrete strength of 3,000 psi (20.7 MPa) in the Royalton Bridge could potentially have increased to 6,000 psi (41.4 MPa) or higher over 80 years that the bridge has been in service. Therefore, concrete strength of 6,000 psi (41.4 MPa) was assumed in calculations involving neutral axis depth and moment in girders for the Royalton Bridge.

The modulus of elasticity of concrete can be estimated from concrete strengths using Equation [6.1]. For a concrete strength of 3,000 psi (20.7 MPa) the modulus is 3,122 ksi (21.5 GPa). Similarly, 6,000 psi (41.4 MPa) concrete has an estimated modulus of 4,415 ksi (21.5 GPa).

$$E_c = 57\sqrt{f'_c} \quad [6.1]$$

Where:

E_c = Elastic modulus of concrete (ksi)

f'_c = Concrete compressive strength (psi)

6.1.5 Concrete Areas in Tension in Moment Calculation

The first step in analyzing moment at each cross section was to determine the stresses in concrete and steel reinforcing bars using the estimated strain profile created from the measured strains at the two gauge locations. It was initially assumed that the tensile forces in concrete should not be considered, since most concrete structures have cracked in service properties and tensile forces contributed from the concrete are insignificant. However, small service loads induce low concrete tensile stresses in a cross section, so the tensile forces contributed by uncracked concrete become significant when calculating moments.

The following example illustrates the importance of including tension forces developed in the concrete in moment calculations. The strain in gauge pair 23, at the mid-span of span 2 with the loading truck at 108 ft (108 m) in lane 1 was measured to be 2.56×10^{-6} in the top gauge and 44.32×10^{-6} in the bottom gauge (Figure 6.24). This cross section and load truck location is selected because it created the maximum positive bending of the instrumented cross sections during the load tests.

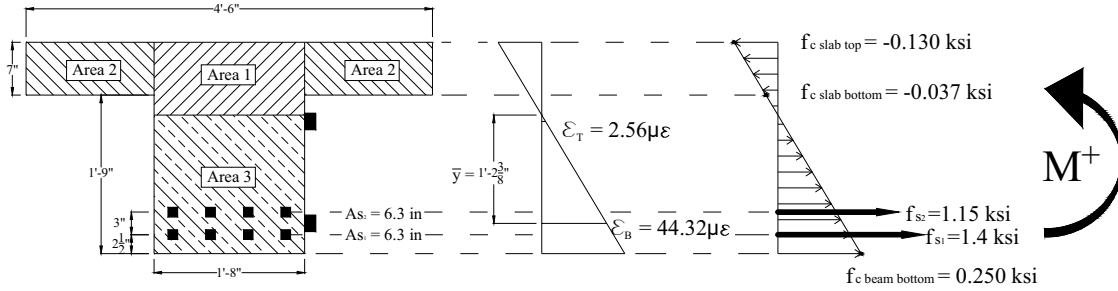


Figure 6.24: Strain and Stress Profile (Gauge Pair #23 – Truck at 108 ft)

From the strain profile a neutral axis depth (measured from the bottom strain gauge) of 14.3 in (363 mm). was first determined using Equation [6.2]. The strain and neutral axis depth was used to calculate the stresses and strains listed in Table 6.7 with Equation [6.3] through Equation [6.7]. Background for this calculation is presented in Section D4.1. These calculations were performed twice, first with a concrete modulus of 4,414 ksi (30.4 MPa) (shown below, corresponding to a concrete compressive strength of 6,000 psi (41.4 MPa)), and second with a modulus of 3,122 ksi (21.5 MPa) (not shown, corresponding to a concrete compressive strength of 6,000 psi (41.4 MPa)). The modulus of steel rebar was assumed to be 29,000 ksi (200 MPa). Results from both calculations are listed in Table 6.7.

$$\bar{y} = \frac{-44.32 \cdot 13.5 \text{ in}}{2.56 - 44.32} = 14.3 \text{ in} \quad [6.2]$$

$$f_{s1} = 29,000 \text{ ksi} \cdot \left[\frac{5.5 \text{ in} - (14.3 \text{ in} + 4 \text{ in})}{\frac{13.5 \text{ in}}{2.56 \times 10^{-6} - 44.32 \times 10^{-6}}} \right] = 1.150 \text{ ksi} \quad [6.3]$$

$$f_{s2} = 29,000 \text{ ksi} \cdot \left[\frac{2.5 \text{ in} - (14.3 \text{ in} + 4 \text{ in})}{\frac{13.5 \text{ in}}{2.56 \times 10^{-6} - 44.32 \times 10^{-6}}} \right] = 1.41 \text{ ksi} \quad [6.4]$$

$$f_{c \text{ slab top}} = 4,414 \text{ ksi} \cdot \left[\frac{28 \text{ in} - (14.3 \text{ in} + 4 \text{ in})}{\frac{13.5 \text{ in}}{2.56 \times 10^{-6} - 44.32 \times 10^{-6}}} \right] = -0.130 \text{ ksi} \quad [6.5]$$

$$f_{c \text{ slab bottom}} = 4,414 \text{ ksi} \cdot \left[\frac{21 \text{ in} - (14.3 \text{ in} + 4 \text{ in})}{\frac{13.5 \text{ in}}{2.56 \times 10^{-6} - 44.32 \times 10^{-6}}} \right] = -0.037 \text{ ksi} \quad [6.6]$$

$$f_{C \text{ beam bottom}} = 4,414 \text{ ksi} \cdot \left[\frac{-(14.3 \text{ in} + 4 \text{ in})}{\left[\frac{13.5 \text{ in}}{2.56 \times 10^{-6}} - 44.32 \times 10^{-6} \right]} \right] = 0.250 \text{ ksi} \quad [6.7]$$

The concrete modulus linearly relates stress and strain, doubling the assumed concrete compressive strength increases calculated stresses by 41%. As listed in Table 6.7 the stresses calculated in the cross section are very small using strength assumptions of either 3,000 or 6,000 psi (20.7 or 41.4 MPa) concrete. These maximum stresses in concrete and steel are well below what one would typically use in reinforced concrete strength design.

The typical range of accepted concrete tensile stress is determined using Equation [6.8] to be (164-273 psi, 1.13-1.88 MPa) at 3,000 psi (20.7 MPa) and (232-387 psi, 1.60-2.67 MPa) at 6,000 psi (41.4 MPa). As the tensile stresses in bending (187 and 250 psi, 2.67 and 1.72 MPa) are in the lower end each range and the cross section in this example measured the greatest bending stress during test, it is assumed that the concrete remained uncracked and contributed to tensile forces for use in overall moment generated in the cross section.

$$\text{concrete tensile strength} = 3 \text{ to } 5 \sqrt{f'_c} \quad [6.8]$$

With stresses determined, the moment at each cross-section was calculated using the concrete areas and layers of steel illustrated in Figure 6.24. Moment contribution from concrete in compression (areas 1 and 2) are found with Equation [6.9] and Equation [6.10]. Moment contribution from steel layers 1 and 2 are calculated using Equation [6.11] and Equation [6.12]. The total moment, excluding any contribution from tensile stresses in the concrete, is found using Equation [6.14].

The moment contribution from concrete in tension (area 3) was calculated using Equation [6.13]. The total moment including concrete tensile stresses can then determined using Equation [6.15].

$$M_{\text{Area 1}} = (28 - 14.3 - 4) \cdot 20 \cdot \frac{0.130}{2} \cdot \frac{2}{3} \cdot (28 - 14.3 - 4) = -82 \text{ K-in} \quad [6.9]$$

$$M_{\text{Area 2}} = 7 \cdot (54 - 20) \cdot \left(\frac{0.130 - 0.037}{2} \right) \cdot \left(28 - 14.3 - 4 - \frac{7}{3} \right) + 7 \cdot (54 - 20) \cdot 0.130 \cdot \left(28 - 14.3 - 4 - \frac{7}{2} \right) = -137 \text{ K-in} \quad [6.10]$$

$$M_{\text{Steel Layer 2}} = 9 \cdot 1.15 \cdot (28 - 5.5 + 4) = 132 \text{ K-in} \quad [6.11]$$

$$M_{\text{Steel Layer 1}} = 9 \cdot 1.41 \cdot (28 - 2.5 + 4) = 202^{\text{K-in}} \quad [6.12]$$

$$M_{\text{Area 3}} = (14.3 + 4) \cdot 20 \cdot \frac{0.250}{2} \cdot \frac{2}{3} \cdot (14.3 + 4) = 561^{\text{K-in}} \quad [6.13]$$

$$M_{\text{without tension concrete}} = \frac{1}{12} [|-82| + |-137| + |132| + |202|] = 46.2^{\text{K-ft}} \quad [6.14]$$

$$M_{\text{with tension concrete}} = \frac{1}{12} [|-82| + |-137| + |132| + |202| + |561|] = 93^{\text{K-ft}} \quad [6.15]$$

The assumption that tensile forces in concrete contribute to the bending moment in this cross section increases the calculated moment by 85-123% which is significant. In comparison, the calculated difference in moment assuming 3,000 and 6,000 psi (20.7 and 41.4 MPa) concrete is between 15-25% for this cross section.

Table 6.7: Stress and Moment in Cross Section (Gauge Pair #23 – Truck at 108 ft)

Calculated Property	Concrete Modulus	
	3,122 ksi	4,414 ksi
Stress in top steel layer	1.15	1.15
Stress in bottom steel layer	1.41	1.41
Stress at slab top	-0.093	-0.130
Stress at slab bottom	-0.026	-0.037
Stress at beam bottom	0.178	0.250
Moment without tension concrete	40 (K-ft)	38 (K-ft)
Moment including tension concrete	74 (K-ft)	84 (K-ft)

6.1.6 Beam Line Analysis of Span Moments

To examine the positive moment at the center of spans 1 and 2, a beam line analysis was performed for both simply supported and fixed-fixed support conditions (Figure 6.26 and Figure 6.25). This analysis estimates the total moment in each cross section at mid-span. Although the Royalton Bridge was designed to be simply supported, unintended end restraint may generate moments at the end of each span. The simply supported analysis therefore provides an upper bound of expected moment at mid-span, while the fixed-fixed analysis provides a lower bound. Results from these analyses are listed in Table 6.8. Note the beam line analysis calculation assumes that axle loads act as point loads on the beam, and does not account for distribution of loads over a finite length along the girders, which would decrease the moment magnitude determined from the analyses. Additionally, these calculated moments correspond to the total moment generated on the entire bridge width by the loading truck. These

values are compared with moments measured in all bridge girders in the corresponding cross section when the truck was positioned at 108 ft (33 m) from the starting point as discussed in the following section.

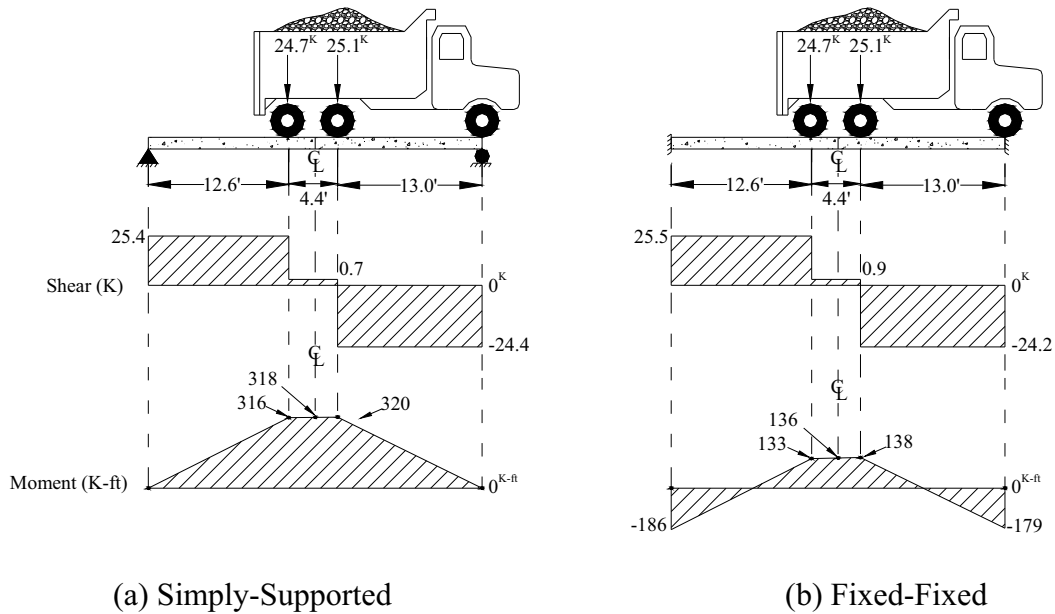


Figure 6.25: Beam Line Analysis of Span 1 (Load Vehicle at 70 ft)

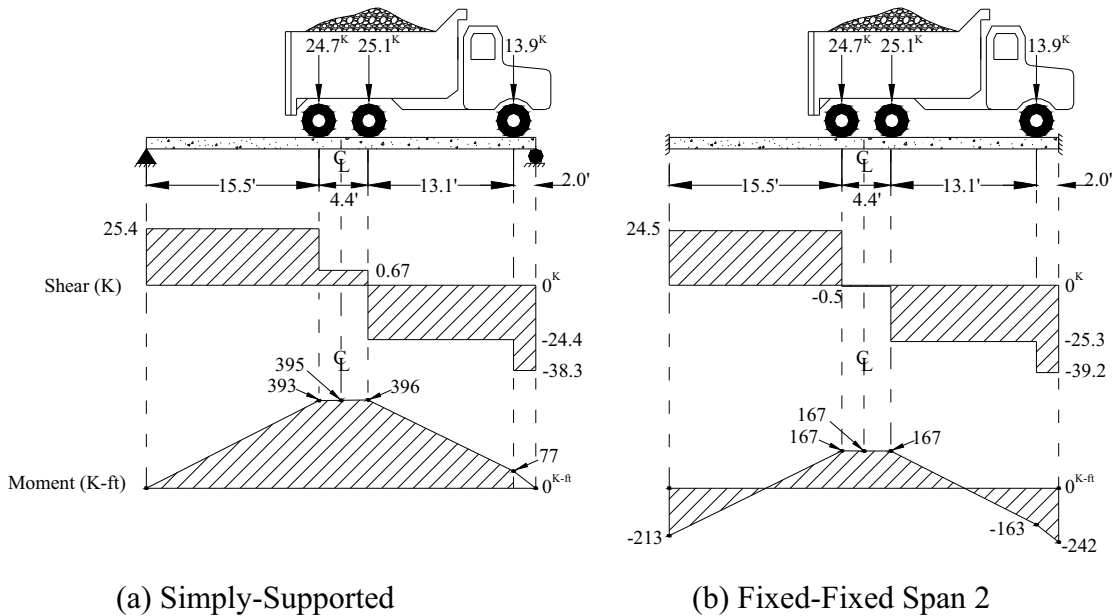


Figure 6.26: Beam Line Analysis of Span 2 (Load Vehicle at 108 ft)

Table 6.8: Moments from Beam Line Analysis in Cross-Sections at Mid-Span

Cross Section	Truck Position (ft)	Fixed-Fixed (K-ft)	Simply Supported (K-ft)
2	70	136	318
5	108	167	395

6.1.7 Measured Positive Moment Transverse Distribution

The moments from the beam line analysis were compared with calculated moments in all girders across the bridge from measured strains during testing. The distributed moments are plotted at mid-span cross sections 2 (span 1) and 5 (span 2), (Figure 6.1), with separate plots assuming a modulus of concrete of 3,122 and 4,415 ksi (21.5 and 30.4 GPa) in calculations.

Moments at mid-span of span 1 (section 2) with the loading truck in each lane at 70 ft (21 m) are plotted in Figure 6.27 and Figure 6.29 assuming a concrete modulus of elasticity of 3,122 and 4,415 ksi (21.5 and 30.4 GPa), respectively. Moments in girder I with the load vehicle in lane 1 and 2 are calculated using measured strains in both the girder and guardrail sections, assuming full composite behavior. With the load truck in lane 3, a jump in the strain profile was observed between the measured strain at the bottom of the guardrail and the top of girder, indicating that the guardrail and girder were bending separately. To determine the moment in this cross section, moments in the guardrail and girder were calculated separately about their neutral axis and added together.

Moments in girder VI of span 1 (section 2) are calculated only from the strain measured in the girder section, without considering any contribution from the guardrail, which was not instrumented. It is likely that if the guardrail was considered the calculated moment in this section would be greater, however this behavior cannot be verified. Guardrail contribution to the total moment was not assumed when plotting moments in Figure 6.29.

The moments at mid-span of span 2 (section 5) with the loading truck at 108 ft (33 m) in each lane are plotted in Figure 6.28 and Figure 6.30 assuming a concrete modulus of elasticity of 3,122 and 4,415 ksi (21.5 and 30.4 GPa), respectively. The moments in girders I and VI were calculated using measured strains in both the girder and guard rail section, assuming fully composite behavior.

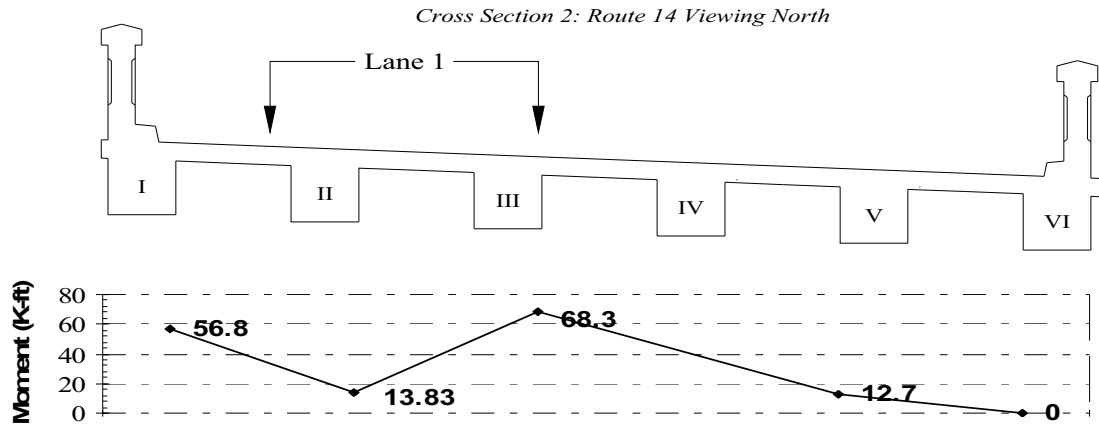
Girder IV was not instrumented during the field test in either span, so strains in this girder were assumed to vary linearly between girders III and V as an approximation. It is recognized that the actual moment in this girder may be slightly higher when the loading truck traveled in lanes 2 and 3, and lower with the truck in lane 1.

The percent difference in moment as a result of different concrete modulli is listed Table 6.9 for each cross section. On average, the global bridge moment calculated with a modulus of 3,122 ksi (21.5 GPa) is only 75% of the moment when calculated using 4,415 ksi (30.4 GPa). It is worthwhile noting that the global bridge

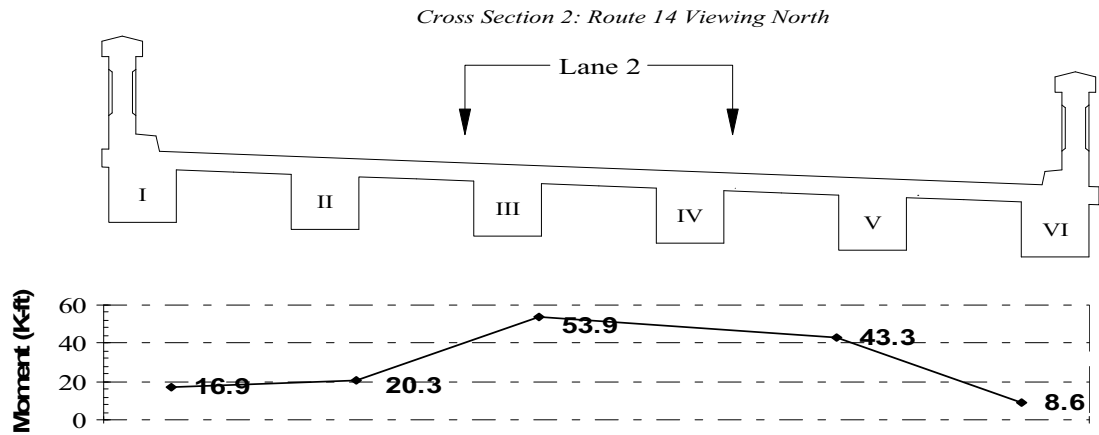
moment calculated from individual girder contributions at a given cross section when the loading truck traveled in either lane 1 or lane 2 was almost identical, as would be expected if the applied load remained constant for different travel lanes. On the other hand, when the loading truck traveled in lane 3, the global bridge moment was smaller than calculated for lanes 1 and 2. This difference may be attributed to different assumptions used when calculating the moment from the guard rails in the upstream and downstream bridge sides. From this result, it appears that the guardrail on the downstream side of the bridge also contributed to the global bridge moment.

Table 6.9: Comparison of Modulus and Cross Sectional Moment

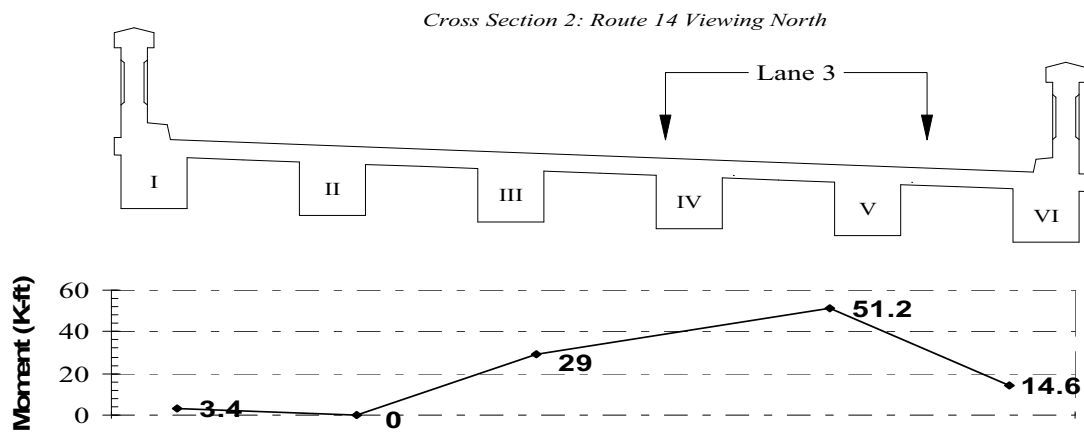
Cross Section	Lane	Truck Position (ft)	Calculated Moment with $E_c=3,122$ ksi (M_1) (K-ft)	Calculated Moment with $E_c = 4,415$ ksi (M_2) (K-ft)	Moment Ratio (M_1/M_2) (%)
2	1	70	192	259	74
	2	70	192	253	76
	3	70	138	187	74
5	1	108	221	293	75
	2	108	220	289	76
	3	108	201	276	73



(a) Load Truck in Lane 1 (70 ft)

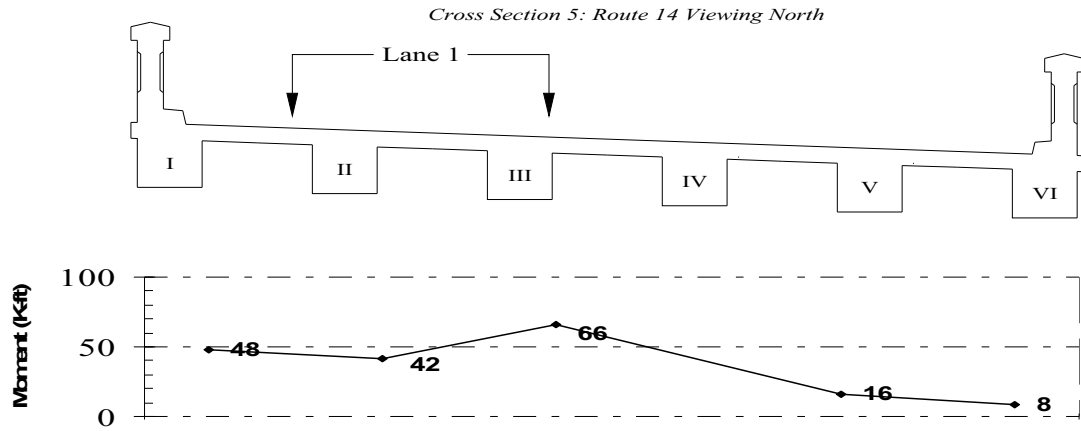


(b) Load Truck in Lane 2 (70 ft)

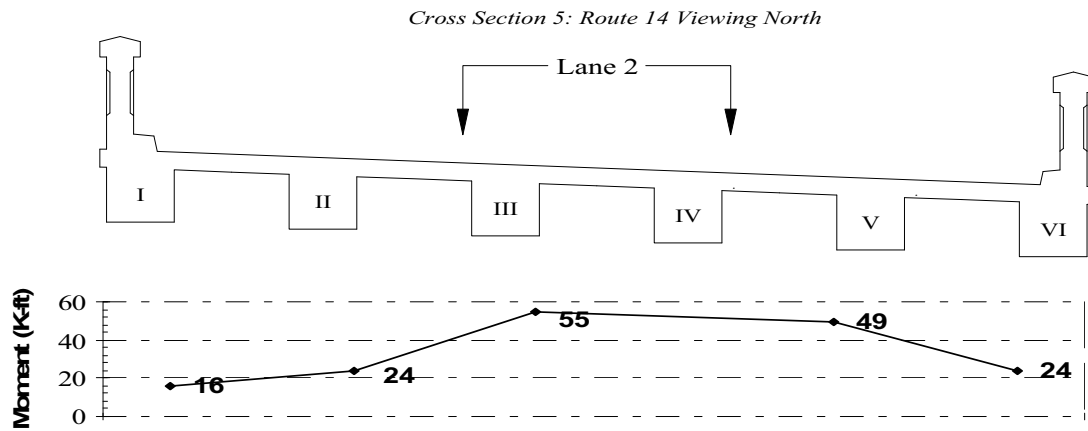


(c) Load Truck in Lane 3 (70 ft)

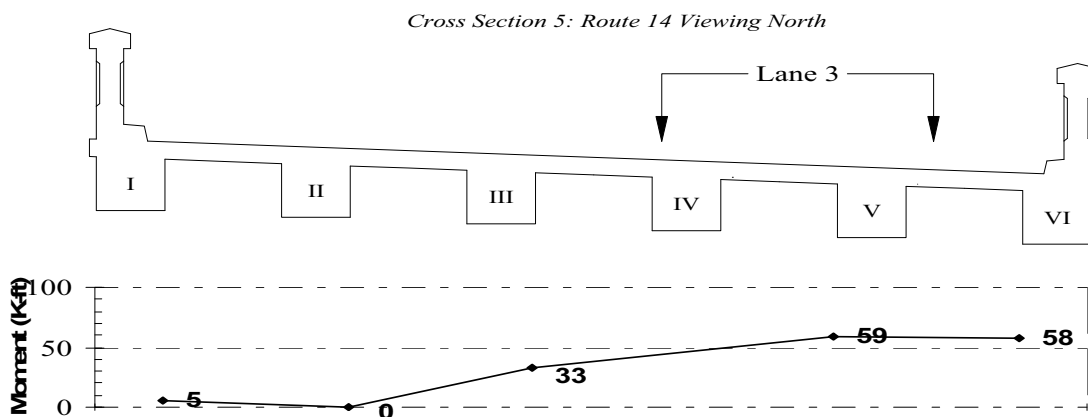
Figure 6.27: Calculated Moment in Cross Section 2 with $E_c=3,122$ ksi



(a) Load Truck in Lane 1 (108 ft)

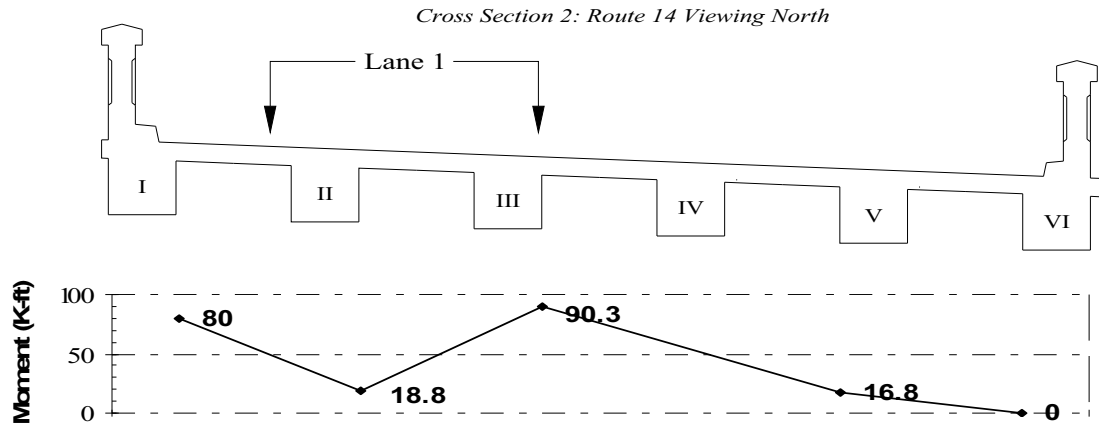


(b) Load Truck in Lane 2 (108 ft)

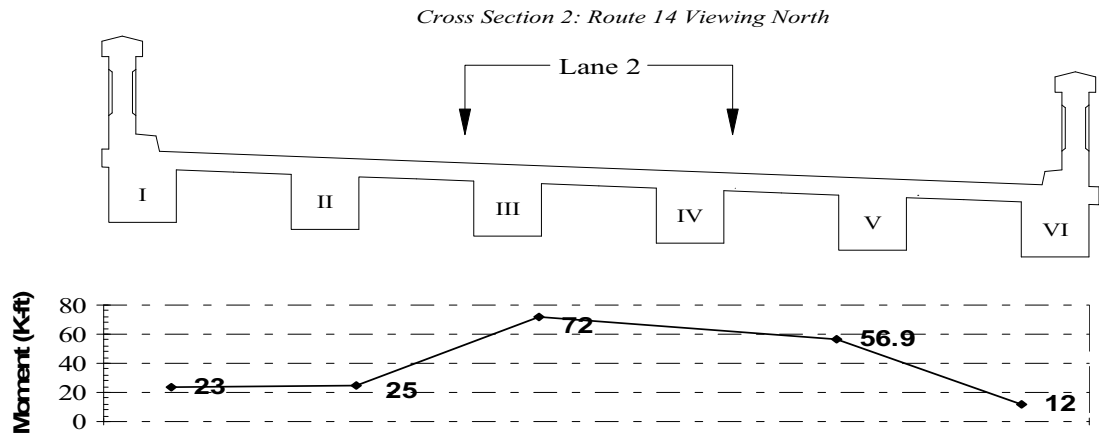


(c) Load Truck in Lane 3 (108 ft)

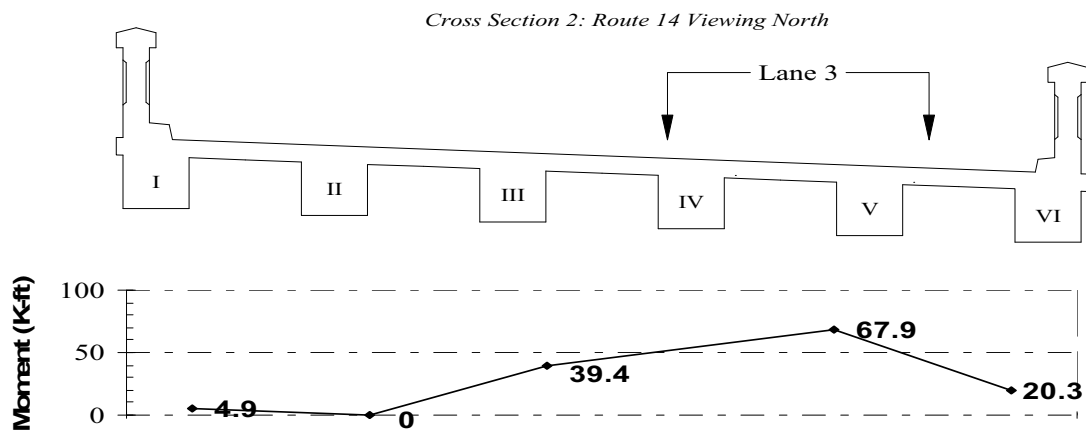
Figure 6.28: Calculated Moment in Cross Section 5 with $E_c=3,122$ ksi



(a) Load Truck in Lane 1 (70 ft)

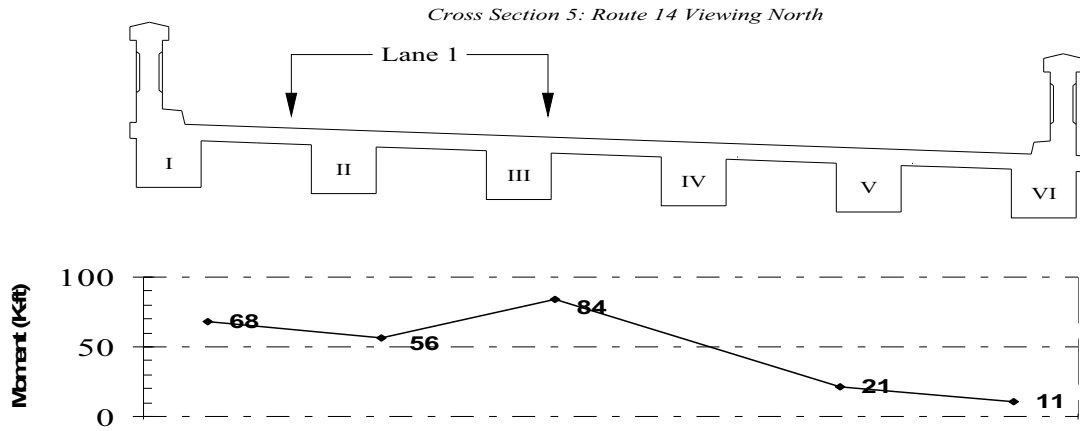


(b) Load Truck in Lane 2 (70 ft)

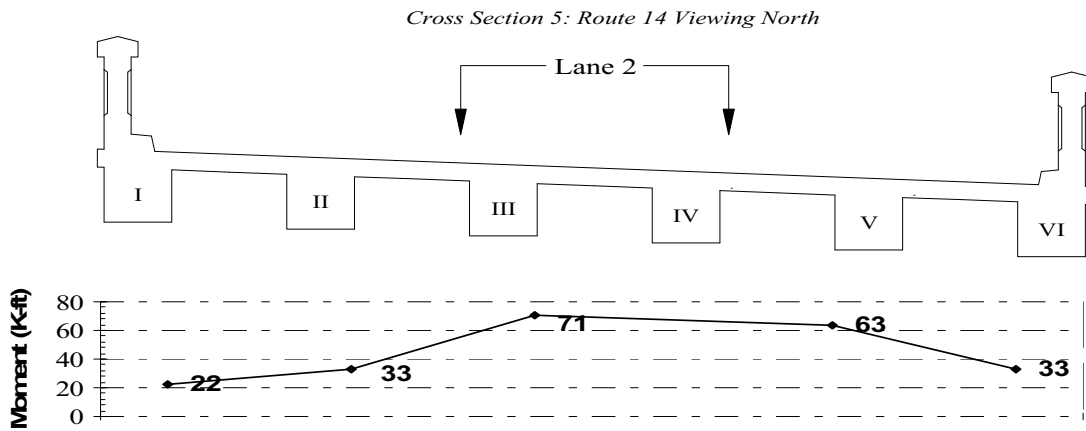


(c) Load Truck in Lane 3 (70 ft)

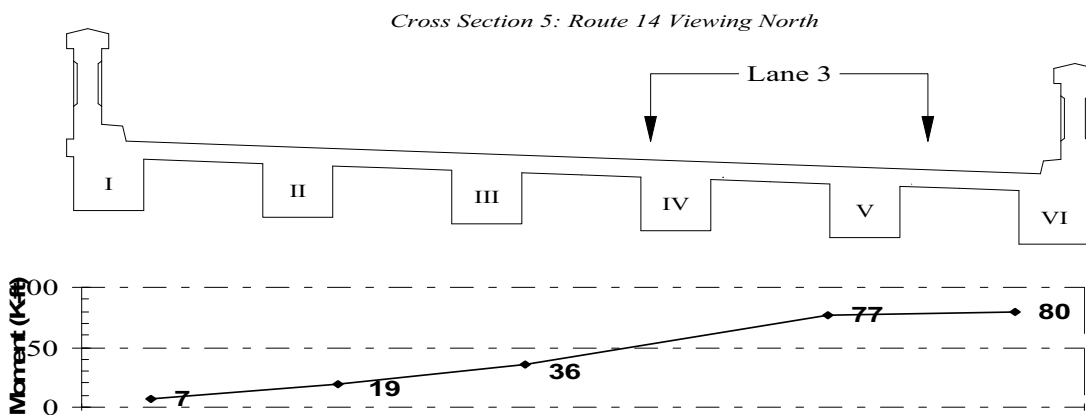
Figure 6.29: Calculated Moment in Cross Section 2 with $E_c=4,415$ ksi



(a) Load Truck in Lane 1 (108 ft)



(b) Load Truck in Lane 2 (108 ft)



(c) Load Truck in Lane 3 (108 ft)

Figure 6.30: Calculated Moment in Cross Section 5 with $E_c=4,415$ ksi

6.1.7.1 Global Moment Comparison with Beam Line Analysis

Moments calculated in each girder from measured strains are compared with the beam line analysis results in Table 6.11. In all cross sections the total cross sectional moment falls between the upper and lower bounds defined by fixed-fixed and simply supported assumptions regardless of the assumed modulus of elasticity for the concrete.

The moments in cross sections calculated with a modulus of 3,122 ksi (21.5 GPa) are approximately 60% of the predicted moment for a simply supported beam line analysis. Moments calculated with a modulus of 4,415 ksi (30.4 GPa) are approximately 79% of the predicted analytical moment. The positive moments across the bridge determined from the load tests are approximately 142% and 186% greater than those from a beam line analysis with fixed supports assuming a modulus of 3,122 and 4,415 ksi (21.5 and 30.4 GPa), respectively. Therefore, the assumption of 6,000 psi (41.4 MPa) concrete and corresponding modulus of elasticity of 4,415 ksi (30.4 GPa) appears to more closely represent measured bridge behavior.

There are two likely reasons that the field moments are lower than those calculated for simply supported spans. The first is that the in situ bridge behavior is not simply supported as designed and end restraint creates partial fixity. This would reduce the total positive moment at mid-span. A second reduction in the moments would occur with the beam line analysis if the truck loads are considered to be distributed by the deck, and not as point loads on the beam. Either of these two effects is difficult to quantify using the field data but at least provide insight into qualitative bridge behavior.

It is also noted that the highest moments occur in girders located directly under or adjacent to loaded lanes. Girders farther from the loading truck contribute less to the overall moment in the bridge cross section. These results are consistent with similar observations made from measured raw strain data in Section 6.1.1.1.

Table 6.10: Calculated Moments from Field Measurements

Modulus of Elasticity (ksi)	Cross Section	Lane	Figure	Calculated Moment (K-ft)	Percent of Analytical Fixed-Fixed Calculation (%)	Percent of Analytical Simply Supported Prediction (%)
3,122	2	1	Figure 6.27a	192	141	60
		2	Figure 6.27b	192	141	60
		3	Figure 6.27c	138	102	43
	5	1	Figure 6.28a	221	132	56
		2	Figure 6.28b	220	132	56
		3	Figure 6.28c	201	120	51
4,415	2	1	Figure 6.29a	259	191	82
		2	Figure 6.29b	253	186	80
		3	Figure 6.29c	186	137	59
	5	1	Figure 6.30a	293	175	74
		2	Figure 6.30b	289	173	73
		3	Figure 6.30c	276	165	70

6.1.7.2 Guardrail Contribution to Moment

Calculated moments in instrumented cross sections indicate that the guardrails effectively contribute to the strength and stiffness of exterior T-beams. Table 6.11 lists the relative contribution to the total moment across the bridge in each guardrail cross section plotted in Figure 6.29 and Figure 6.30. In all cases where composite behavior was observed in the strain profile, the guardrail contributes between 77-91% of the total moment in the girder cross section. The T-beam and slab in exterior sections contribute between 9 to 23% of the total moment generated in the bridge cross section.

Since guard rails at cross sections other than mid-span were not instrumented, it is uncertain if composite behavior or if similar contribution to the moment also occurs at the end of each span. Due to smaller moments occurring at span ends, however, guardrail contribution at span ends is not expected to affect bridge response as significantly as it does at mid-span.

Table 6.11: Calculated Moment in Instrumented Guard Rail Sections

Span	Lane	Beam	Guard Rail Moment		Beam and Slab Moment	
			(K-ft)	%	(K-ft)	%
1	1	I	73	91	7.3	9
	2	I	21	87	3.0	13
	3	I	4.5*	54	3.8*	46
2	1	I	64	93	4.8	7
	2	I	20	92	1.8	8
	3	I	5.5	77	1.6	23
	1	VI	10	81	2.2	19
	2	VI	26	79	7.2	21
	3	VI	74	90	7.8	10

*Moment calculated assuming non-composite cross section

6.1.7.3 AASHTO Distribution Factors Comparison

The live load distribution factors (g) used by AASHTO in bridge design for one or two lanes loaded can be compared with the distributed moments measured at mid-span during the load tests. The distribution factor for interior girders of T-beam construction can be calculated using Equation [6.16a] from AASHTO LRFD Table 4.6.2.2.2b-1, which includes multiple presence factors (*AASHTO LRFD Bridge Design Specifications*). The distribution factor for exterior girders (AASHTO LRFD Table 4.6.2.2.2.1-1) was calculated using the lever rule, and multiplied by a multiple presence factor of 1.2 for one lane loaded. For comparison purposes, wheel load distribution factors were also determined according to the *AASHTO Standard Specification* (2002). For the Royalton Bridge, the wheel load distribution factors according the AASHTO Standard Specification are equal to $S/6.5$ or $S/6.0$ for one or two loaded lanes, respectively. Calculated distribution factors for the Royalton Bridge using AASHTO specifications are listed in Table 6.12.

$$g_{\text{int-1}} = 0.06 + \left(\frac{S}{14}\right)^{0.4} \left(\frac{S}{L}\right)^{0.3} \left(\frac{K_g}{12.0 \cdot L \cdot t_s^3}\right)^{0.1} \quad [6.16a]$$

$$g_{\text{int-2}} = 0.075 + \left(\frac{S}{9.5}\right)^{0.6} \left(\frac{S}{L}\right)^{0.2} \left(\frac{K_g}{12.0 \cdot L \cdot t_s^3}\right)^{0.1} \quad [6.17b]$$

$$K_g = \frac{E_B}{E_D} (I_g + A \cdot e_g^2) \quad [6.18]$$

Where:

A = Area of beam (in^2)

E_B = Modulus of elasticity of beam material (ksi)

E_D = Modulus of elasticity of deck material (ksi)

e_g = Distance between centers of gravity of the basic beam and deck (in)

$g_{\text{int-1}}$ = Distribution factor for interior girders, one lane loaded

g_{int-2} = Distribution factor for interior girders, two lanes loaded
 I_g = Moment of inertia of the beam (in⁴)
 K_g = Longitudinal stiffness parameter (in⁴)
 L = Span length (ft)
 S = Beam spacing (ft)
 t_s = Depth of concrete slab (in)

From the beam line analysis (Section 6.1.6) moments at mid-span assuming simple supports were calculated to be 318 K-ft (431 kN-m) in span 1 and 395 K-ft (536 kN-m) in span 2 with the load vehicle at 70 and 108 ft (21.3 and 32.9 m), respectively. Moments calculated for interior and exterior beams based distribution factors in the *AASHTO LRFD Specifications* and the *AASHTO Standard Specifications* are listed in Table 6.12. These moments are based on the moments generated by the test truck but using the distribution factors included in these specifications. The distribution factors for the *AASHTO Standard Specification* are based on wheel loads, so the beam-line analysis moments were divided by two to obtain wheel load moments.

Table 6.12: AASHTO Distribution Factors and Design Moment for Royalton Bridge Girders

Span	Beam Line Analysis Moment (K-ft)	Girder Location	No. of Loaded Lanes	g AASHTO LRFD	AASHTO LRFD Moment (K-ft)	g AASHTO STD Spec	AASHTO STD Spec Moment (K-ft)
1	318	Interior	1 lane	0.40	127	0.69	110
			2 lanes	0.49	156	0.75	119
		Exterior	1 lane	0.36	114	0.36	114
2	395	Interior	1 lane	0.38	150	0.69	136
			2 lanes	0.48	190	0.75	148
		Exterior	1 lane	0.36	142	0.36	142

The maximum moment in interior girders was compared with moments calculated using *AASHTO LRFD* distribution factors for one or two lanes loaded. Assuming a concrete compressive strength of 6,000 psi (41.4 MPa) the maximum moment measured for an interior T-beam in the Royalton test is 90 K-ft (122 kN-m) in girder III in span 1 (Figure 6.29a) and 84 K-ft (114 kN-m) in girder III in span 2 (Figure 6.30a). Both of these mid-span moments occurred when the load truck was travelling in lane 1. To compare the test moments for two loaded lanes, values obtained in girder III when the test truck was travelling along lane 1 and lane 3 were added. These values are compared with moments calculated for 2 loaded lanes using AASHTO distribution factors.

The maximum moment measured in exterior T-beams, without including any contribution or properties of the guardrail is 7 K-ft (9.5 kN-m) in span 1 and 8 K-ft (10.8 kN-m) in span 2 (Table 6.11).

The AASHTO live load moments are greater than measured field moments (Table 6.13). In particular, the moments determined during the field tests in spans 1 or

2 are similar, but the AASHTO moments are larger in span 2 because of the longer span. This is may be due in large part to varying effects of guardrail contribution in internal moment distribution among girders, since the guardrails carry a significant portion of the moment along the exterior of the bridge at mid-span (Section 6.1.7.2). Accounting for the field performance of guardrails in spans 1 and 2 in the Royalton Bridge, calculated moments using AASHTO distribution factors for interior girders are conservative.

Table 6.13: Comparison of Measured Moment to AASHTO Design Moment

Span	No. of loaded lanes	Field Moment	AASHTO LRFD Moment	Field Moment/AASHTO LRFD Moment
		(K-ft)	(K-ft)	(%)
1	1 lane	90	127	71
	2 lanes	129	156	83
2	1 lane	84	150	56
	2 lanes	120	190	63

6.1.8 Transverse Negative Moment Distribution

Cross-sections 1, 3, 4, and 6 (Figure 6.1) of the bridge were instrumented 3 feet from the end of each span to determine moment transfer into piers or abutments, indicating partial restraint between bridge spans. Partial rotational restraint would explain why measured positive moments were lower than anticipated from a simple beam line analysis. As the spans were designed to be simply supported, little or no moment was expected at the end of the beams.

To compare end of span and mid-span moments, the cross sections were analyzed using the same truck locations as those generating maximum positive moment in each span (front axle at 70 and 108 ft (21.3 and 32.9 m) for spans 1 and 2, respectively). From beam-line models of the bridge (Figure 6.26a and Figure 6.25a), it is expected that moments in cross sections near abutments and piers will be positive, and relatively small. Moments in each cross section were calculated and plotted (Figure 6.31 to Figure 6.34), assuming a modulus of concrete of 4,415 ksi (30.4 GPa).

In most cases the strain used to calculate moment at these locations was very small (1.0-5.0 $\mu\epsilon$), which causes a higher degree of uncertainty in the calculations; however, the plots are useful to give a general idea of the magnitude and direction of bending of the girders. In locations with less than 1.0 micro strain in the bottom strain gauge, the cross section was considered to have zero moment. Additionally, moments in exterior beams were calculated without including guardrail properties since instruments were not placed on guardrails at these sections.

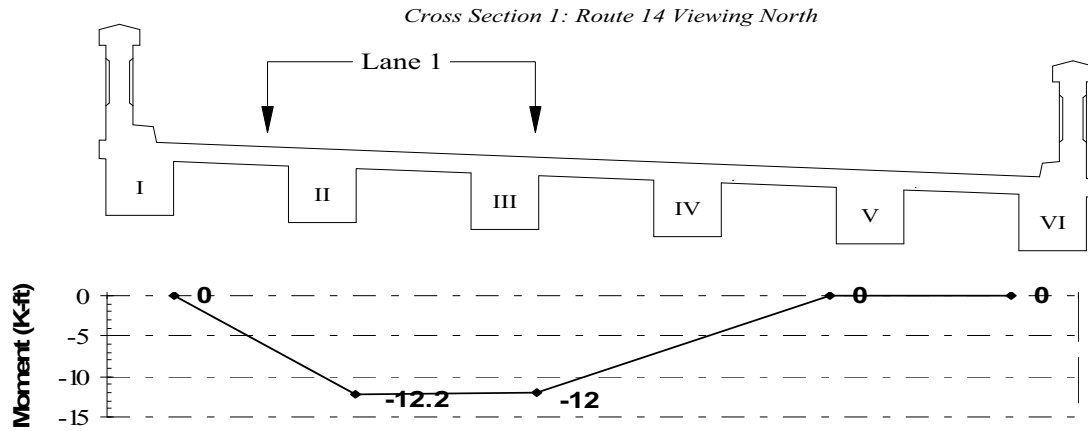
In contrast with moments predicted by a simply supported beam line analysis, negative moments were observed in cross sections 1, 3, and 4. Since these moments were calculated with gauges centered 3 ft (914 mm) from the end of the span, it is likely that higher negative moments occur at the abutment or pier face. However, not all of the moments in each cross section indicate negative bending. Some of the moments

were found to be positive (mostly in exterior girders). From these plots, no general trend could be established between cross sections to predict positive or negative bending.

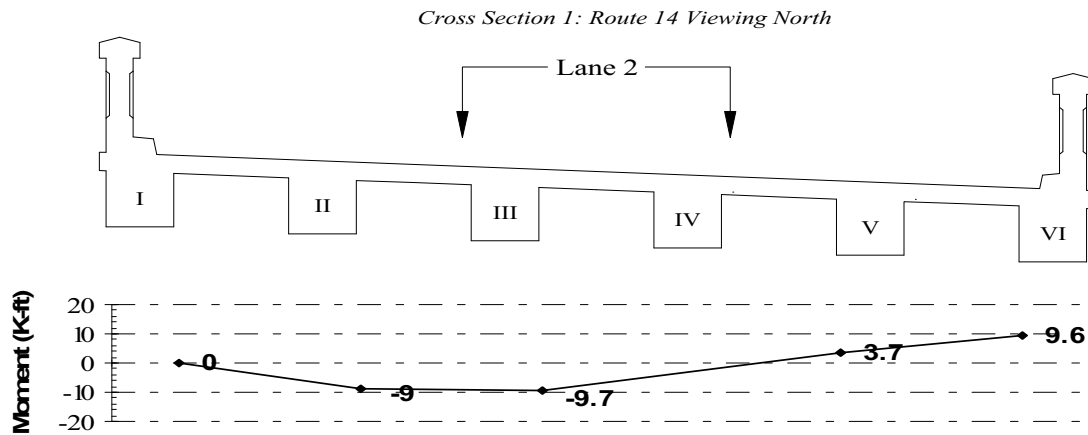
The overall effects of end moments appear to be insignificant when compared to the total positive moments in cross sections at mid-span (Table 6.14). The presence of some negative bending moments, however, are consistent with the lower moments that were observed at mid-span (Section 6.1.1.1), as they indicate that some partial fixity exists at beam supports. This fixity may be a result of pavement overlays on deck surface, debris accumulation in joints, or the connection of beams to supports. Since the negative moments appear to be negligible and highly variable, any bridge load rating should be done considering all spans to be simply supported as a conservative approach.

Table 6.14: Moment Comparison of End Span to Mid-Span

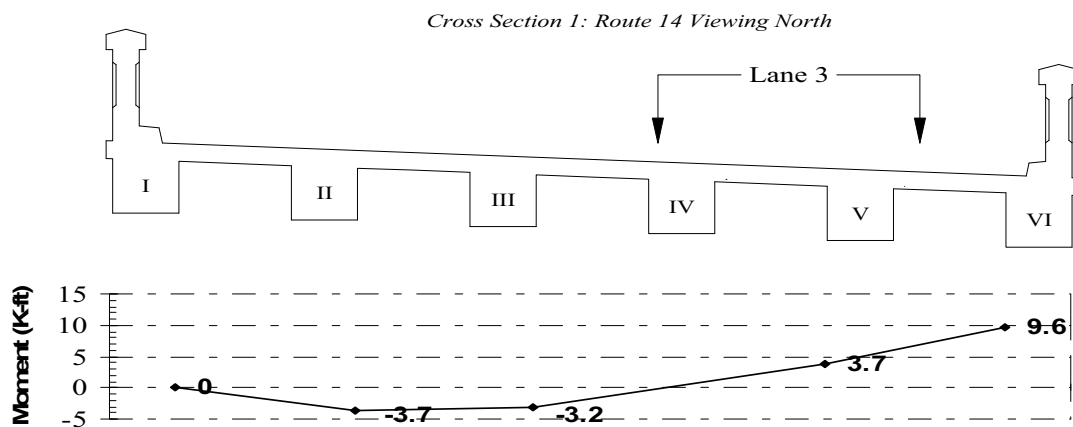
Span and Truck Position	Cross Section	Figure	Calculated Moment at End of Span (K-ft)	Positive Moment At Mid-Span (K-ft)	Percent of Mid-Span Moment (%)
1 - 70 feet	1	Figure 6.31a	-30	259	-12
	1	Figure 6.31b	-8	253	-3
	1	Figure 6.31c	7	186	4
	3	Figure 6.32a	2	259	1
	3	Figure 6.32b	5	253	2
	3	Figure 6.32c	-5	186	-2
2 - 108 ft	4	Figure 6.33a	-9	313	-3
	4	Figure 6.33b	-8	313	-3
	4	Figure 6.33c	-2	304	-1
	6	Figure 6.34a	0	313	0
	6	Figure 6.34b	8	313	3
	6	Figure 6.34c	11	304	4



(a) Load Truck in Lane 1

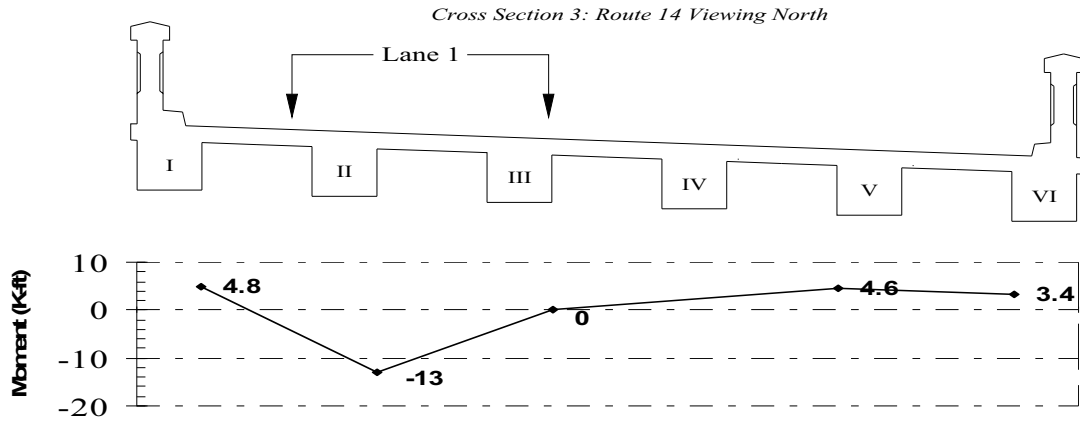


(b) Load Truck in Lane 2

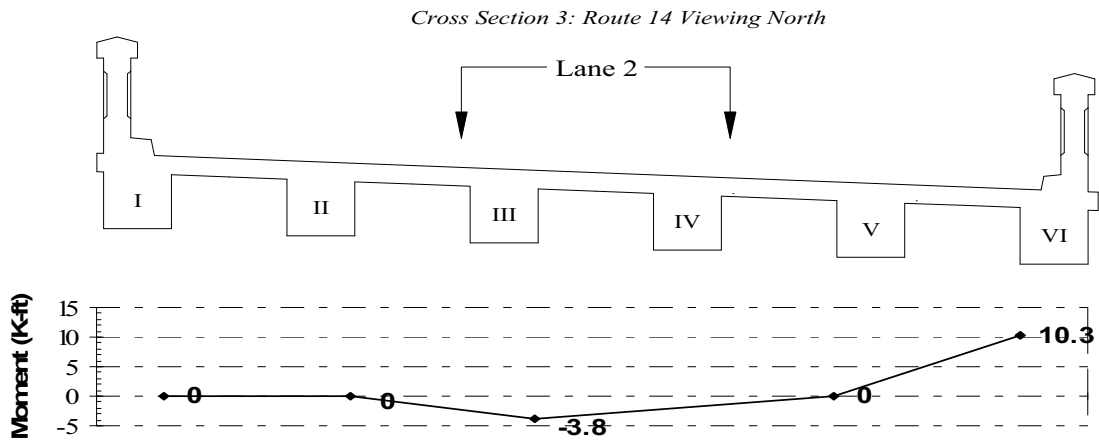


(c) Load Truck in Lane 3

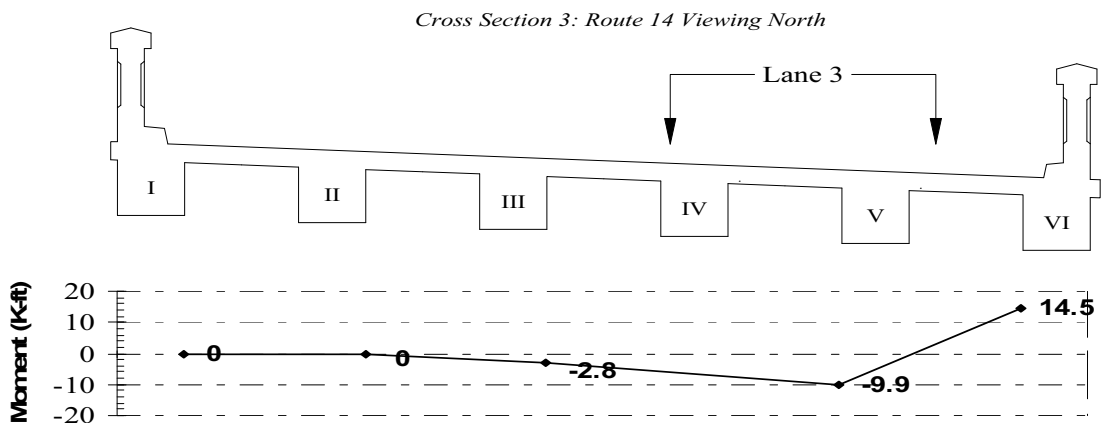
Figure 6.31: Moment in Cross Section 1 (Truck at 70 ft)



(a) Load Truck in Lane 1

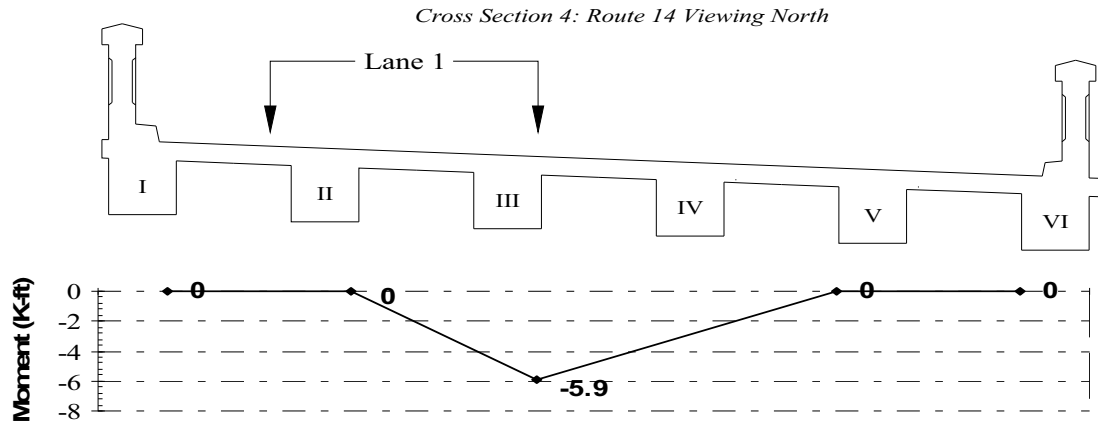


(b) Load Truck in Lane 2

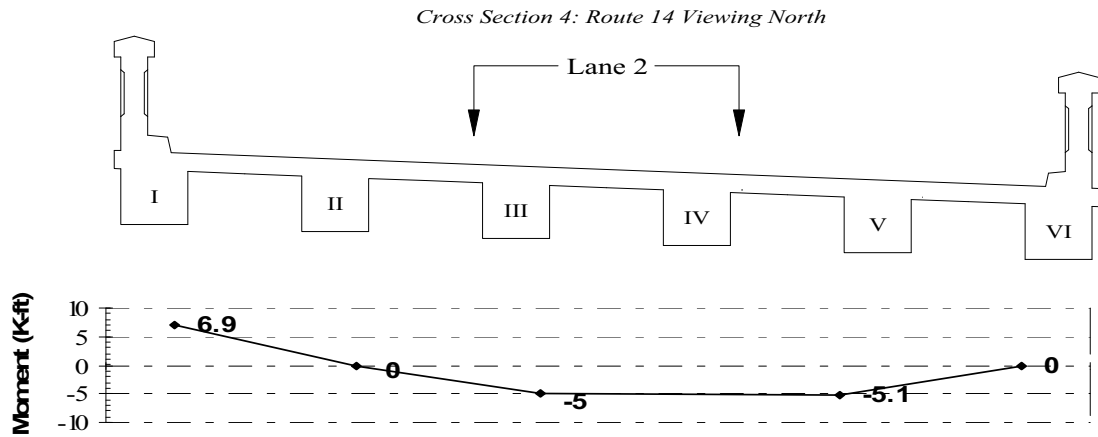


(c) Load Truck in Lane 3

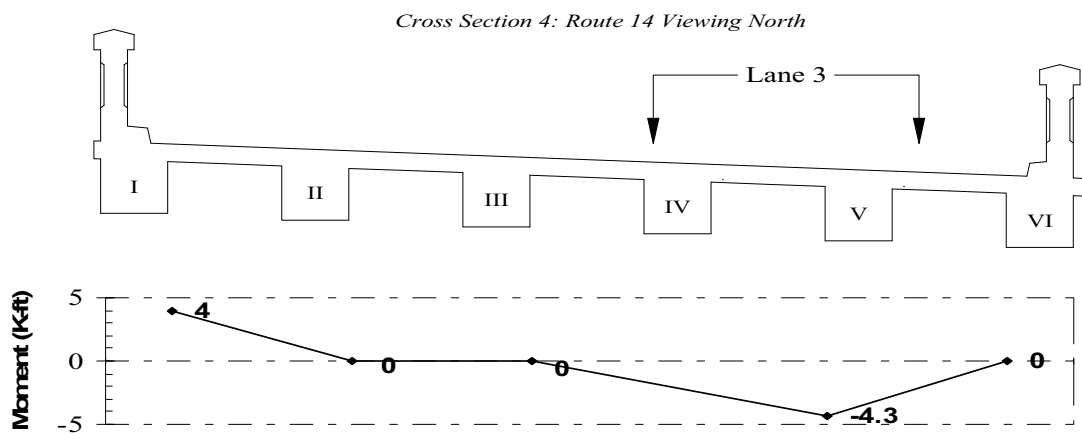
Figure 6.32: Moment at Cross Section 3 (Truck at 70 ft)



(a) Load Truck in Lane 1

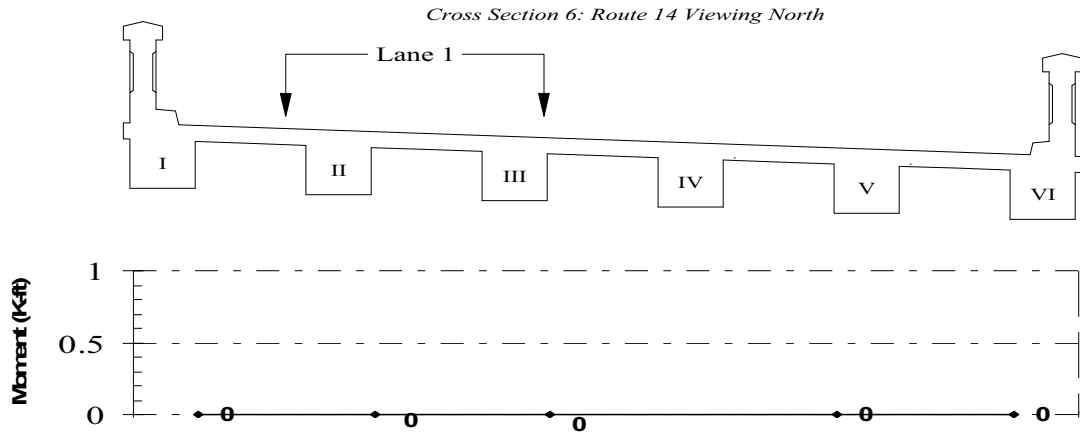


(b) Load Truck in Lane 2

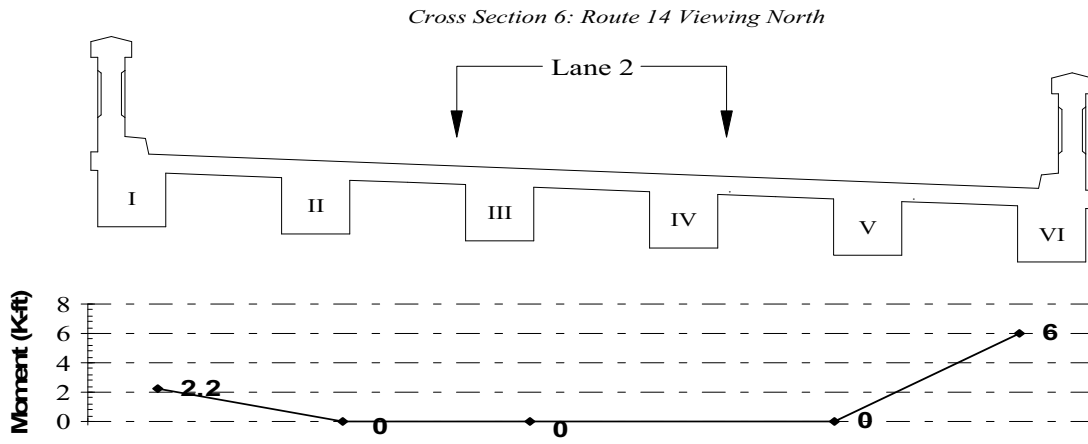


(c) Load Truck in Lane 3

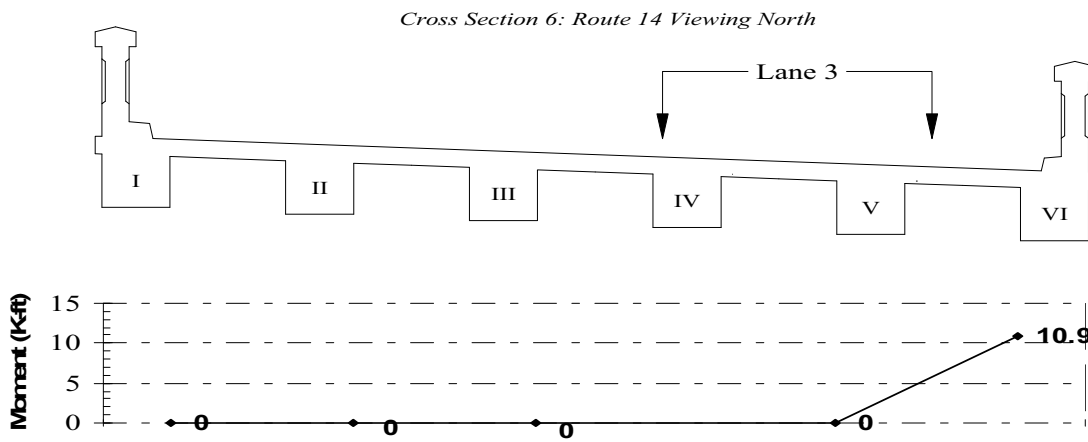
Figure 6.33: Moment at Cross Section 4 (Truck at 108 ft)



(a) Load Truck in Lane 1



(b) Load Truck in Lane 2



(c) Load Truck in Lane 3

Figure 6.34: Moment at Cross Section 6 (Truck at 108 ft)

6.2 Weathersfield Bridge

6.2.1 Negative Bending Strain Distribution at Pier Support Sections

The response of the bridge over pier supports was inferred from the strain history measured in cross sections 1 and 7 shown in Figure 6.35. The transverse strain distribution of individual girders was subsequently plotted and compared using readings from the bottom strain gauges when the loading trucks were at a specific position along the bridge.

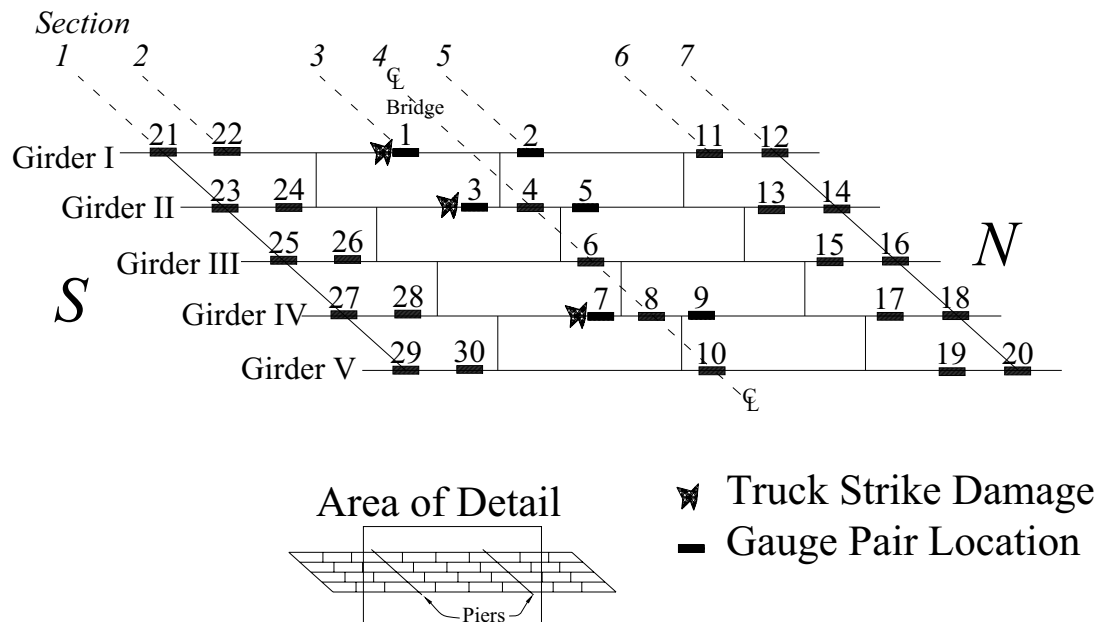
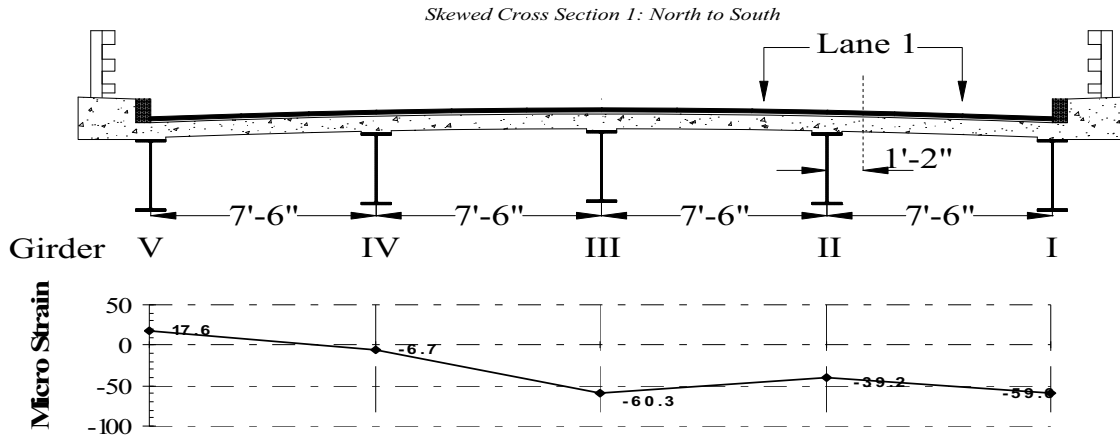


Figure 6.35: Weathersfield Bridge (Plan View) Cross-Sections and Gauge Numbering

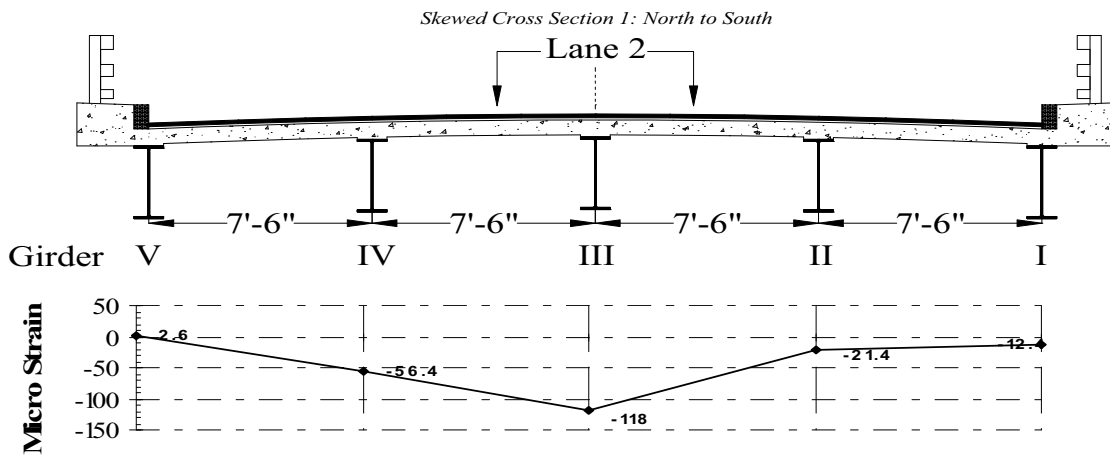
Strain in the negative bending region over pier supports is of particular interest in this bridge. The location of the front axle of the leading loading truck producing the maximum negative bottom strain for cross section 1 and 7 was 200 and 183 ft (61.0 and 55.8 m), respectively. These truck positions were determined graphically from the strain histories measured during the tests and correlated well with the locations of peak influence function ordinates determined analytically using a spline model. The truck positions relative to pier locations when the front axle of the leading truck is located at 200 ft (61.0 m) in lane 1 and 183 ft (55.8 m) in lane 3 are illustrated graphically in Figure 6.38 and Figure 6.40, respectively. Strain values in the bottom flange of all instrumented girders measured for each travel lane at these two locations are listed in Table 6.15 and plotted in Figure 6.36 and Figure 6.37.

Table 6.15: Weathersfield Transverse Strain at Pier Supports

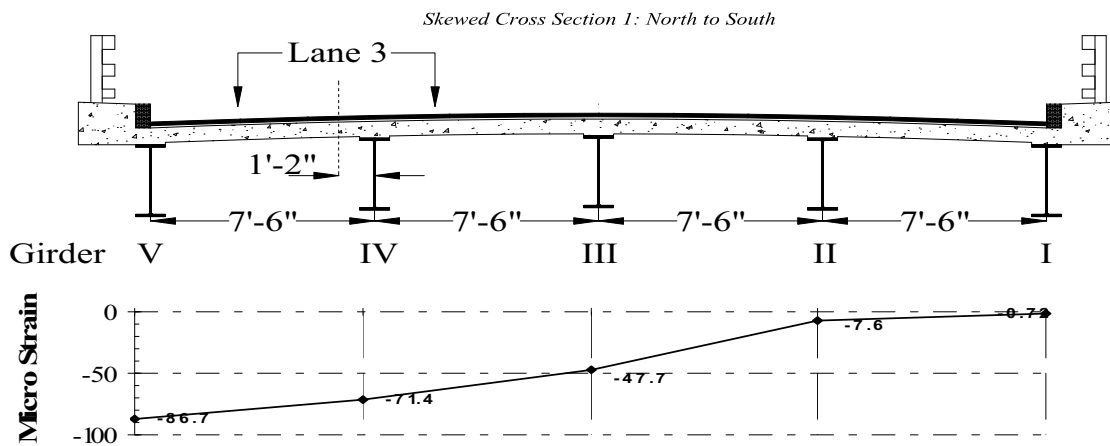
Cross Section	Lane	Front Axle Location (ft)	Strain				
			Girder I ($\mu\epsilon$)	Girder II ($\mu\epsilon$)	Girder III ($\mu\epsilon$)	Girder IV ($\mu\epsilon$)	Girder V ($\mu\epsilon$)
1	1	200	-59.6	-39.2	-60.3	-6.7	17.6
	2	200	-12.4	-21.4	-118	-56.4	2.6
	3	200	-0.72	-7.6	-47.7	-71.4	-86.7
7	1	183	-75	-92.4	-24.1	-14.3	-2.7
	2	183	21.7	-49.3	-46.7	-40.6	-19.4
	3	183	26.7	-4.8	-20.9	-59	-64.5



(a) Lane 1 – Truck at 200 ft

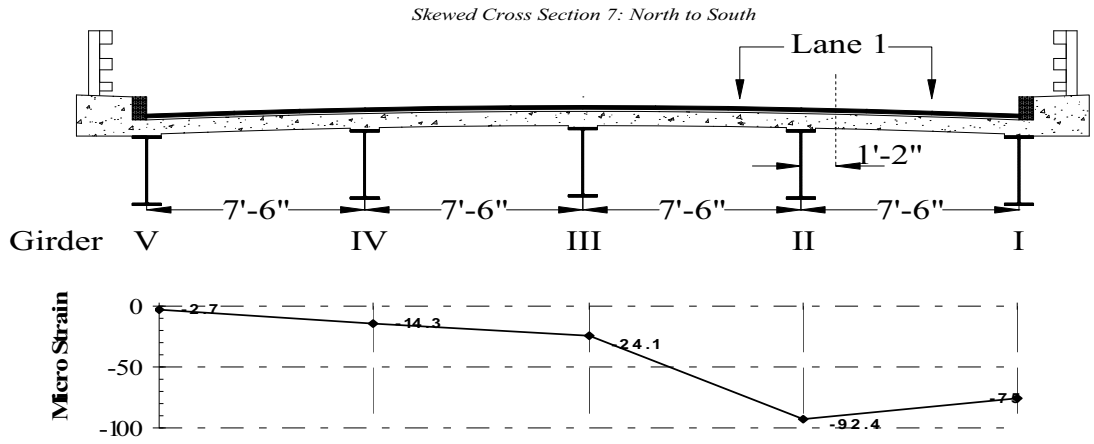


(b) Lane 2 – Truck at 200 ft

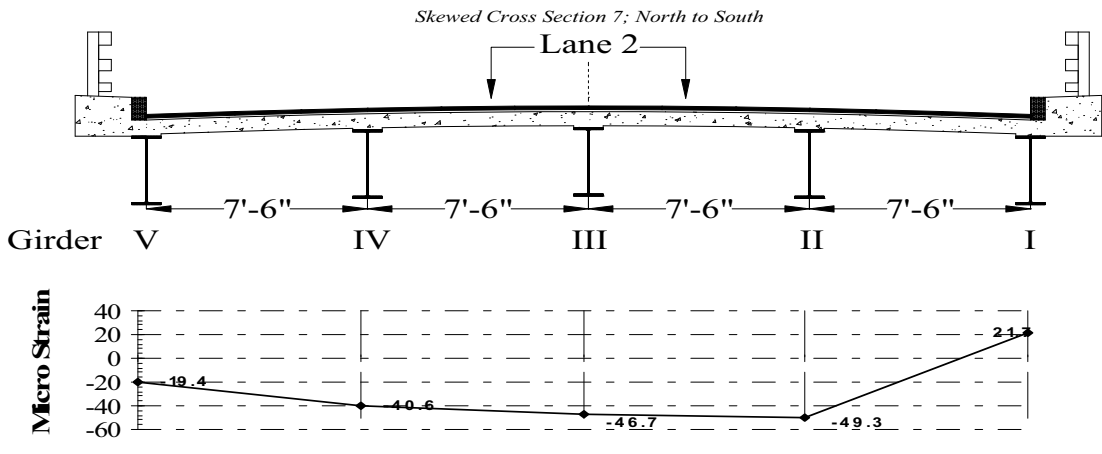


(c) Lane 3 – Truck at 200 ft

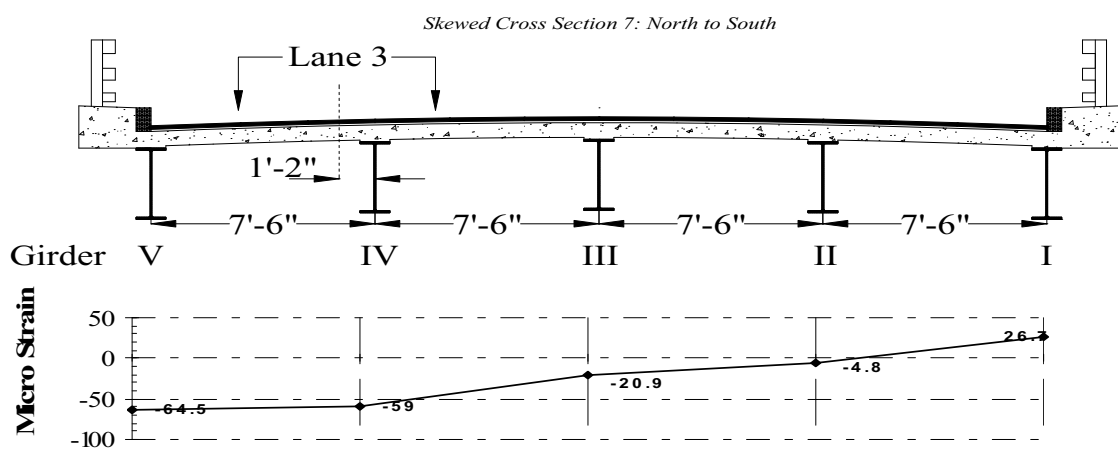
Figure 6.36: Measured Strain in Gauge Cross Section 1



(a) Lane 1 – Truck at 183 ft



(b) Lane 2 – Truck at 183 ft



(c) Lane 3 – Truck at 183 ft

Figure 6.37: Lower Gauge Strain in Cross Section 7 (Lane 3 – 183 ft)

The distribution of strain in each of the cross sections illustrated above appears to be approximately multi-linear, with higher strain values in girders near the location of wheel loads, and smaller strain in girders located farther from the loads. The magnitude of strains measured in skewed cross sections (approximately parallel to abutment skew) appear to be a function of two factors: (1) the transverse proximity of a wheel load to gauges on nearby girders, and (2) longitudinal position of the loading trucks in the span.

The effect of wheel load proximity on strains measured in girders transversely near to the loads can be evaluated qualitatively by relating the transverse strain distribution with the loading truck position along the bridge. For example, the influence of wheel load proximity on strain in a skewed cross section can be seen in Figure 6.36a when the bridge was being loaded along lane 1 at a front axle position of the leading truck of 200 ft (61.0 m). In this position the rear axle loads of the front truck, which account for 74% of the total truck weight, are longitudinally closer to the strain gauge attached to girder III than girder I or II (Figure 6.38). Consequently, the measured strain in girder III is greater than strain in both girders I and II. Due to the skew, gauges in each instrumented section are longitudinally spaced 8 ft 4 in (2.54 m) relative to a line drawn perpendicular to the girder axes (transverse spacing of girders is 7 feet 6 inches (2.29 m)). Without a skew one would expect the strain in girders I and II (directly under loaded lane) to be greater than girder III (further from loaded lane). This effect is more pronounced at pier supports because of the existence of bridge diaphragms that complement the transverse stiffness of the deck slab.

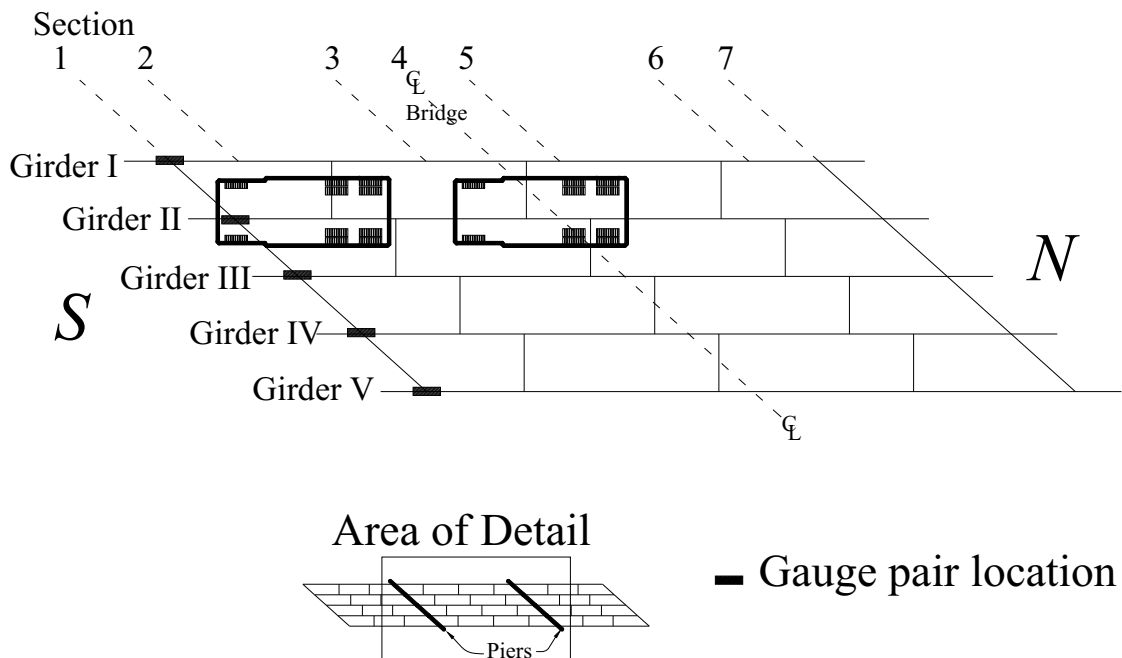


Figure 6.38: Plan View of Bridge with Load Trucks at 200 ft in Lane 1

Similarly, strains in girders transversely far from the proximity of heavy loads are lower than would be expected if the bridge was not skewed. At cross section 1 when loading was placed along lane 3 and the lead truck was positioned at 200 ft

(Figure 6.36c) the rear axles of the lead truck are now longitudinally farther from the gauge location in girder III but closer to girders IV and V (Figure 6.39). Consequently, the measured strains in girder III were lower than the strains in both girders IV and V.

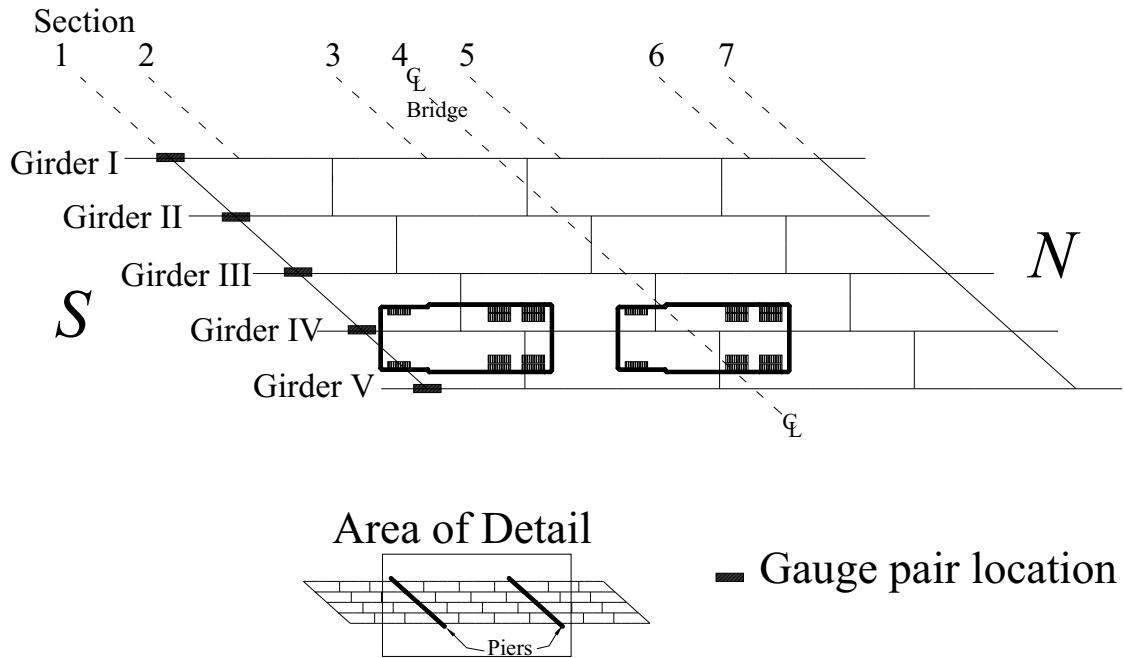


Figure 6.39: Plan View of Bridge with Load Trucks at 200 ft in Lane 3

The second factor influencing negative bending strain in the girders over piers is the longitudinal location of the loading trucks relative to the position that would generate the maximum negative bending moment in the bridge girders. The longitudinal truck position that generates the maximum moment response of individual girders can be determined by conducting an influence line analysis of a spline model of the bridge.

For cross section 7 with loading along lane 3 and a lead truck front axle position of 183 ft (55.8 m) (Figure 6.37c), the rear of the truck is closest to the gauge in girder III (Figure 6.40). However, the measured bottom strain in girders IV and V was greater than that in girder III. This effect appears to be a result of the axle loads being located at sections corresponding to higher influence function moment ordinates in girders IV and V than those in girder III. An influence function analysis for negative girder moment over pier locations reveals that the peak value would be achieved by placing a point load at 32 ft (9.8 m) into span 2, or approximately 38% of the middle span length. This location corresponds to the front axle of lead truck positioned at 147 ft (44.8 m) from the truck starting position.

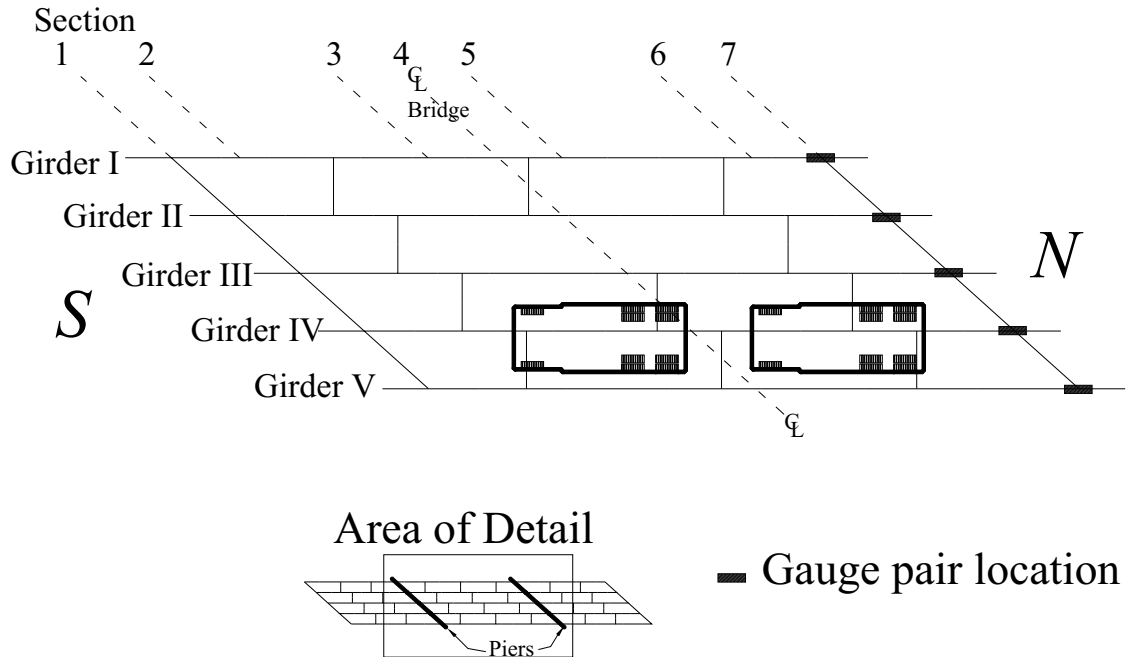


Figure 6.40: Plan View of Bridge with Load Trucks at 183 ft in Lane 3
6.2.2 Positive Bending Strain Distribution at Sections within Middle Span

The distribution of load in the deck was analyzed for a section at mid-span (section 4) and 9 feet (2.74 m) from piers (sections 2 and 6). The truck location for each cross-section that produced the maximum bottom flange strain in positive bending is listed in Table 6.16, with corresponding strain values plotted in Figure 6.41 to Figure 6.43.

It is worthwhile noting that maximum positive bending strain at cross section 6 occurs when both loading trucks were positioned in span 3 (front axle of lead truck at 265 ft (80.8 m)), and maximum bending strain in section 2 occurred when most of the loading axles were in span 1 (front axle of lead truck at 126 ft (38.4 m)).

The positive strains in cross sections 2 and 6 are relatively small when compared to those measured in cross section 4. This result is consistent with results from an analysis using influence functions for moment at these two cross sections (sections 2 and 6), since the loading trucks are positioned in adjacent spans and thereby generate a smaller moment at these locations. Since the strain readings are lower, there is also more inherent error in these measurements but a general trend of strain can be identified by viewing the plots.

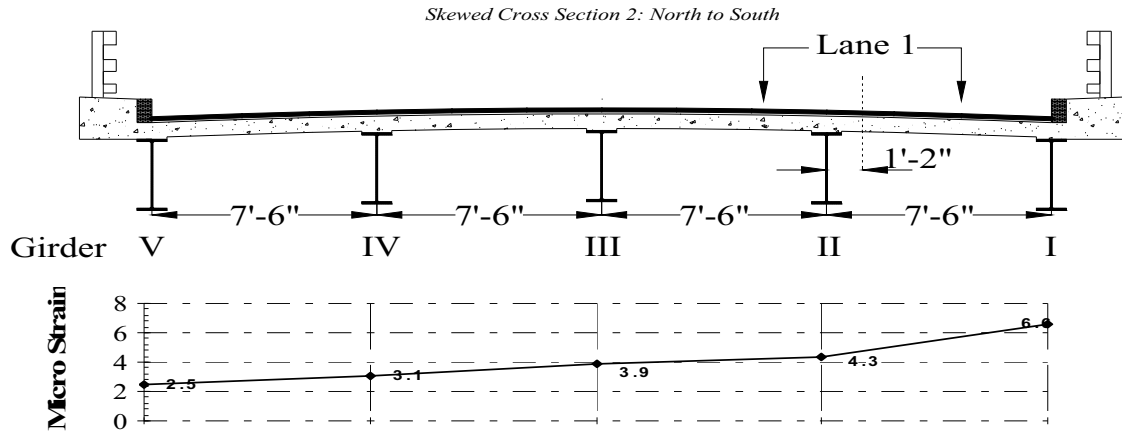
For sections close to supports (sections 2 and 6) when the loading trucks traveled along lane 1 or 3, the exterior girder under the load exhibited the highest strain, with a linear decrease across the deck. When lane 2 (center) is loaded, girder III usually has the higher strain with smaller strain in exterior girders. Strains measured in section 4 did not exhibit a linear decrease with transverse distance from the loaded lane. The highest strains were again measured in girders located close to the loaded lane with a non-uniform strain reduction observed in girders away from the loaded lane. This strain

reduction non-linearity is most likely caused by the skewed cross section and the proximity of the load truck to the mid-span section.

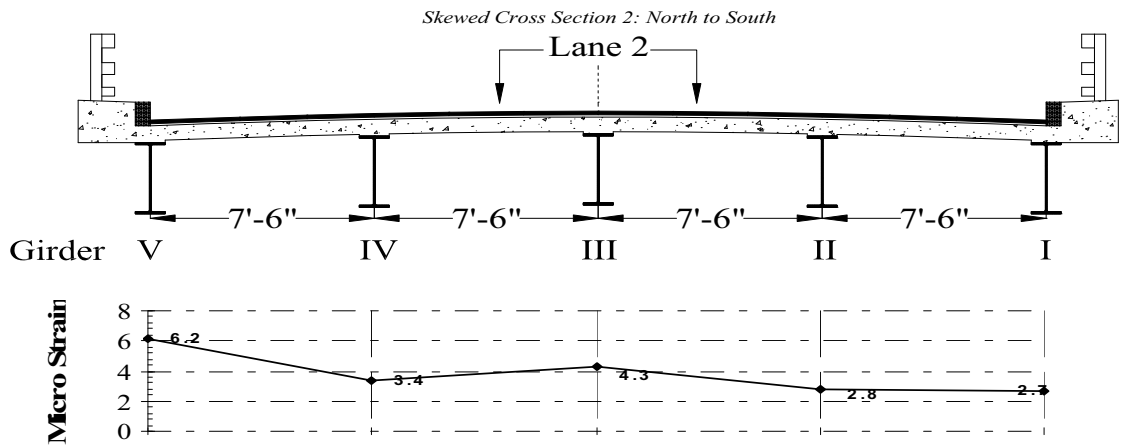
Table 6.16: Weathersfield Transverse Strain Measurement and Distance

Cross Section	Lane	Front Axle Location (ft)	Strain				
			Girder I ($\mu\epsilon$)	Girder II ($\mu\epsilon$)	Girder III ($\mu\epsilon$)	Girder IV ($\mu\epsilon$)	Girder V ($\mu\epsilon$)
2	1	126	6.6	4.3	3.9	3.1	2.5
	2	126	2.7	2.8	4.3	3.4	6.2
	3	126	2.5	2.0	3.4	5.6	12.3
4	1	181	*	44.3	65.6	14.5	8.5
	2	192	*	48.2	94.3	46.0	42.9
	3	189	*	23.3	80.9	64.6	109.9
6	1	263	11.0	7.5	4.8	1.0	0.8
	2	267	6.6	4.0	11.0	4.3	6.3
	3	265	3.2	3.4	7.5	5.8	8.5

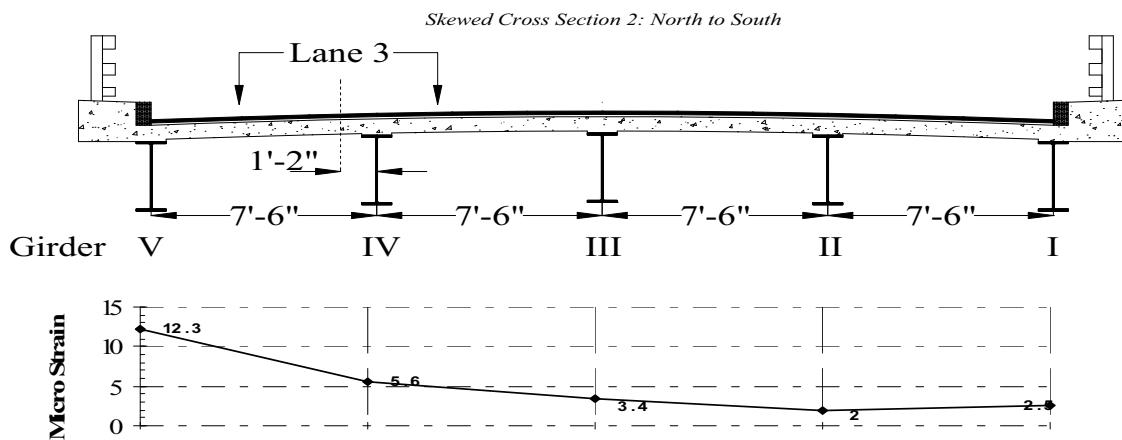
* Strain not recorded at mid-span of girder I



(a) Lane 1 – Truck at 126 ft

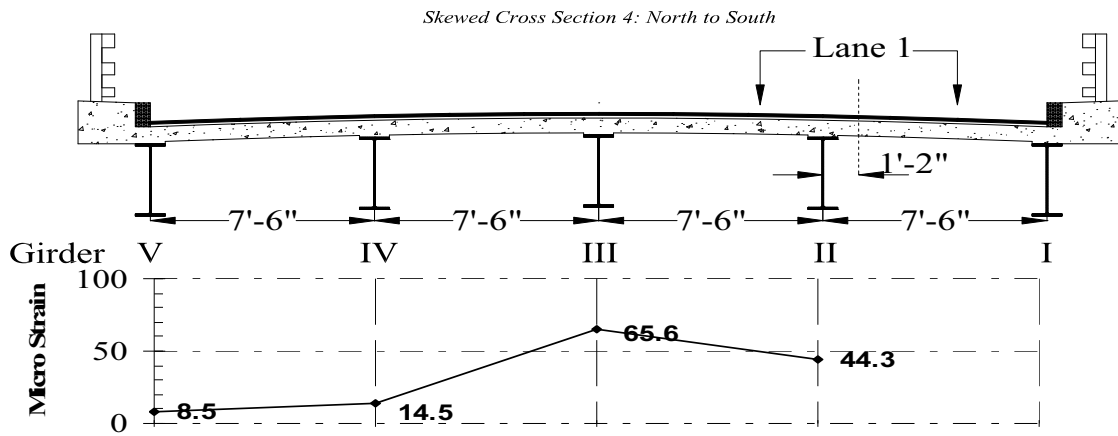


(b) Lane 2 – Truck at 126 ft

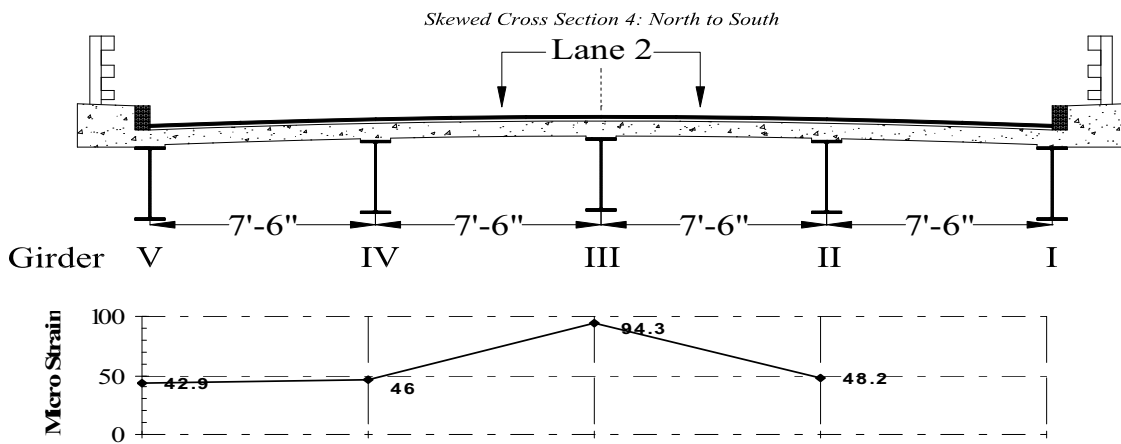


(c) Lane 3 – Truck at 126 ft

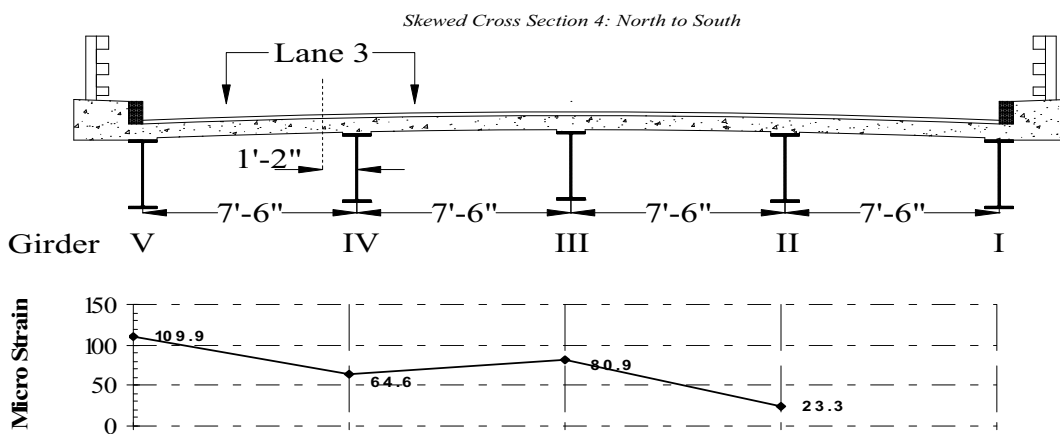
Figure 6.41: Measured Bottom Gauge Strain in Cross Section 2



(a) Lane 1 – Truck at 189 ft

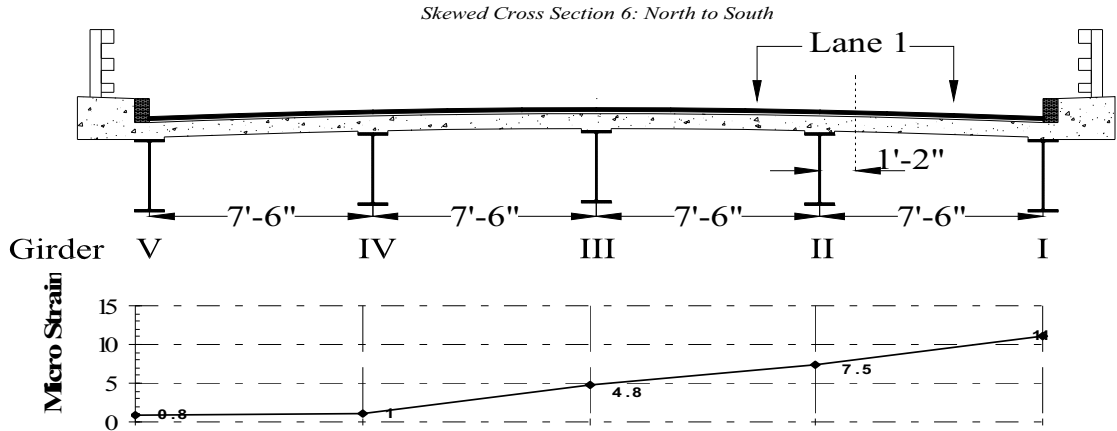


(b) Lane 2 – Truck at 189 ft

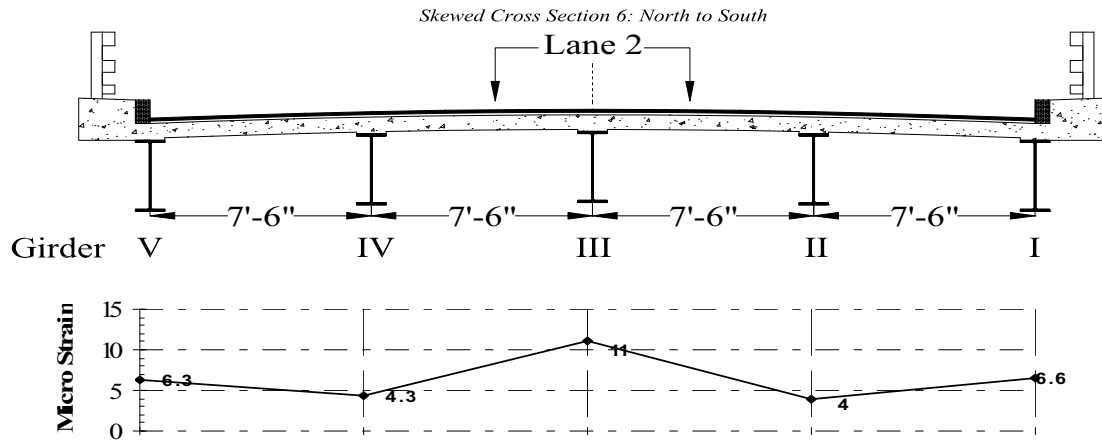


(c) Lane 3 – Truck at 189 ft

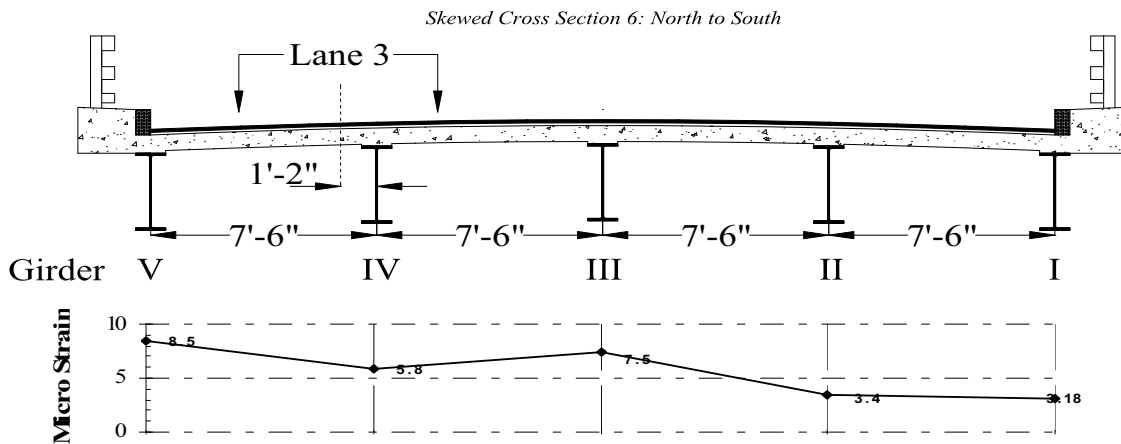
Figure 6.42: Measured Bottom Gauge Strain in Cross Section 4



(a) Lane 1 – Truck at 265 ft



(b) Lane 2 – Truck at 265 ft



(c) Lane 3 – Truck at 265 ft

Figure 6.43: Measured Bottom Gauge Strain in Cross Section 6

6.2.3 Effect of Truck Impact Damage on Strain Distribution

To evaluate the effects of truck impact damage to girders I, II, and IV (Figure 3.22) gauges were placed near the damaged region of these girders and at an undamaged section symmetrically opposite about the bridge centerline (Figure 6.35). The trucks were run northbound and southbound in the tow configuration in each lane during this setup to produce the same loading effects at the damaged and undamaged sections from the loading trucks for this comparison.

In theory, since the bridge has symmetrical span lengths, if trucks are stopped after moving an equal distance onto the bridge from opposite abutments, the strain profiles plotted together along a girder from both runs should create a mirror image about the bridge centerline. Resulting strain profiles that do not resemble a mirror image might be indicative of a detrimental effect from impact damage. In particular, if strains at damaged sections were lower than those measured in the undamaged sections for the symmetric loading configuration, then the tests would indicate that bending moments were distributed laterally to undamaged girders at that section.

Testing with setup A (sections 3 to 5) included runs in the northbound direction to compare strain data plots with the measured strain in damaged sections measured during southbound test runs. Strain was recorded for all gauge pairs with the trucks moving in the southbound direction with setups A, B, and C (see Section 4.3.2.1 for instrument setup identification).

Loading truck locations for each damaged girder that produced the maximum bottom gauge strains in different instrumented sections along a girder were determined and listed in Table 6.17. Using strain values measured in each of these locations allowed construction of a longitudinal strain profile in the middle span of the bridge. The front axle location of the lead truck was measured from the start of the load test as before, which was located 50 ft (15.2 m) before the abutment. The strains were then plotted in Figure 6.44 to Figure 6.46, with the circled 'X' drawn on the bridge symbolizing the location of damage in each girder. Strain data recorded with trucks moving southbound are labeled using a diamond symbols, while northbound strains are labeled using square symbols. The strain values measured during northbound loading are also enclosed in a rectangle in the figures for clarity. Strain data points are connected with straight lines to approximate the general shape of strain variation along the length of each girder.

It is observed that the strain profiles in positive bending strain (lower flange in tension) are as expected from theory with a mirror image of strain data from trucks moving in opposite directions (Figure 6.44b, Figure 6.45b, and Figure 6.46b). In these plots strain measured in cross section 3 from southbound runs and 5 from northbound runs are approximately equivalent. Additionally, strain measured in cross section 5 from northbound runs and 3 from southbound runs are approximately equivalent. The mid-span strain data (cross section 4) from girder II and IV also appear to be approximately equal for both north and southbound runs. Girder I was not instrumented at mid-span.

Plots (a) and (b) in Figure 6.44 to Figure 6.46 show bottom flange strains when the loading truck positions generate negative bending (lower flange in compression) in

sections 3 to 5. Unlike strains induced by positive bending moment, the longitudinal distribution of strains plots from northbound and southbound runs are not symmetrically opposite as one would expect from theory. The results seem to indicate that effects from girder damage are more noticeable when the bottom flange is subjected to compression than when it is in tension. Because over-height truck impact buckled the bottom flange of girders I, II, and IV near section 3, the compressive strains measured near damaged locations with loading in the northbound direction did not correlate well with those strain values measured in section 5 when loading in the southbound direction. In most cases strains in section 4 were largely insensitive to the direction of loading, which resulted in similar strains measured for northbound or southbound loading directions. This behavior is attributed to damage present in girders I, II, and IV (bottom flange). It should be noted, however, that although there is a measurable difference in bottom flange strain from the anticipated values, the magnitude of this difference is not considered to affect the overall safety of the bridge.

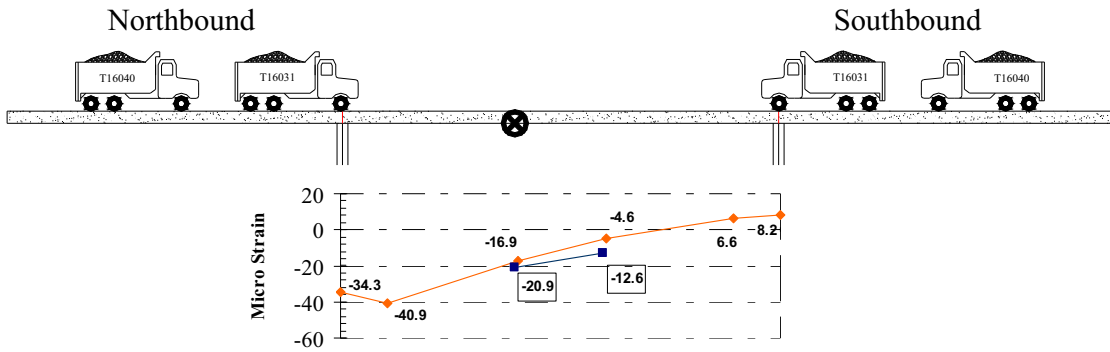
Table 6.17: Bottom Gauge Strain for Girder Damage Evaluation

Girder	Front Axle Location (ft)	Strain at Cross Section									
		1 (μ ϵ)	2 (μ ϵ)	3 (μ ϵ)	3 (μ ϵ)	4 (μ ϵ)	4 (μ ϵ)	5 (μ ϵ)	5 (μ ϵ)	6 (μ ϵ)	7 (μ ϵ)
I (Lane 1)	115	-34.3	-40.9	-16.9	-20.9	*	*	-4.6	-12.6	6.6	8.2
	185	78.7	2	88.6	63.6	*	*	55.4	85.9	-32.2	-50.9
	265	22.4	11	-17.6	-6.8	*	*	-23.3	-24.6	-44.2	-20.4
II (Lane 1)	117	-28.5	-38.5	-12.4	-12.6	-6.4	-5.9	-5.8	-4.9	5.6	4.6
	179	-92.7	14.6	45.2	75.6	66.9	71.5	71.5	41.8	-28.3	-29.2
	261	9	7.1	-6.3	-9.7	-8.6	-11.8	-15.5	-18	-45.4	-12.7
IV (Lane 3)	118	-38	-46.8	-15.7	-19	-10.6	-7.7	-9	-7.2	5.3	7.8
	193	-46.7	-22.3	54	113	62.2	59.5	114	52.6	-29	-65
	264	13.5	5.8	-4.3	-9.5	-10.2	-11.6	-21.8	-15.5	-39.9	-22.6

* Girder I not instrumented at cross-section 4.

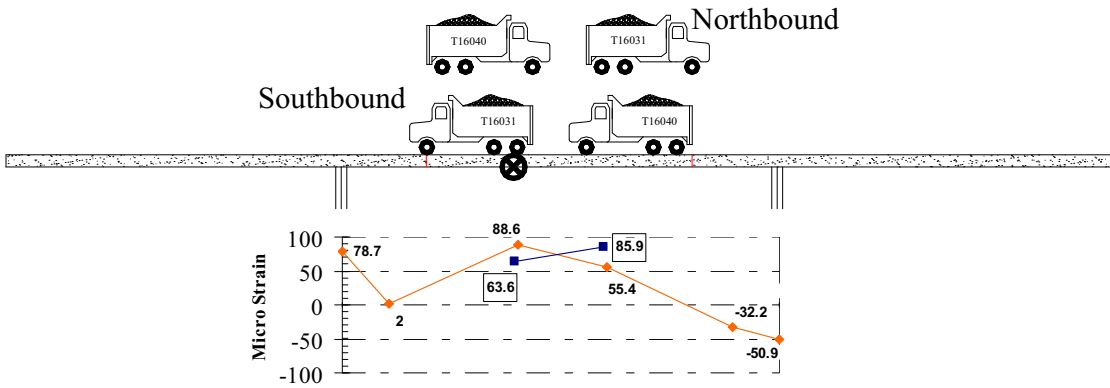
Note: Shaded columns are northbound load truck strain.

Girder I and Lane 1 Loaded



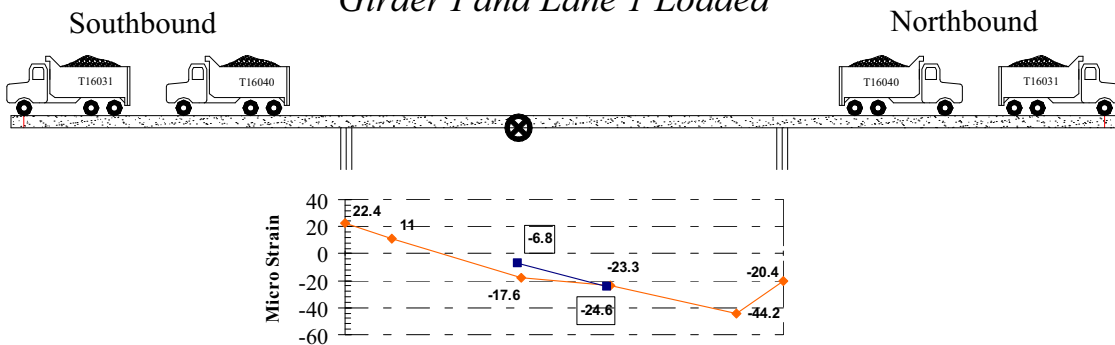
(a) Front Axle at 115 ft

Girder I and Lane 1 Loaded



(b) Front Axle at 185 ft

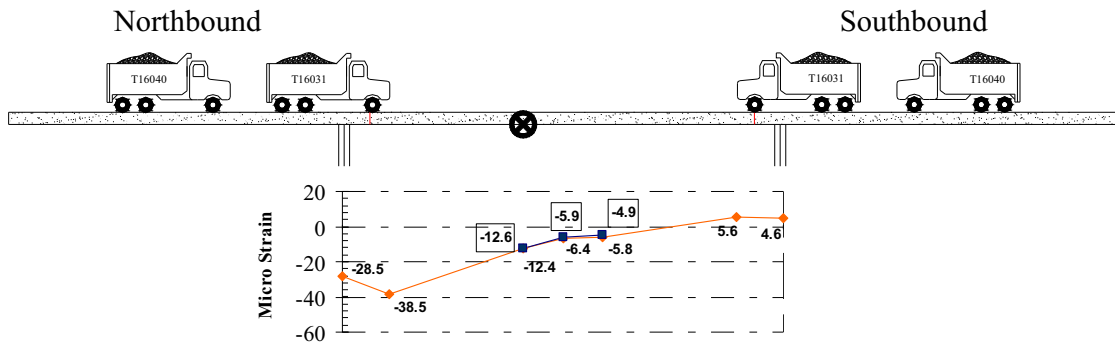
Girder I and Lane 1 Loaded



(c) Front Axle at 265 ft

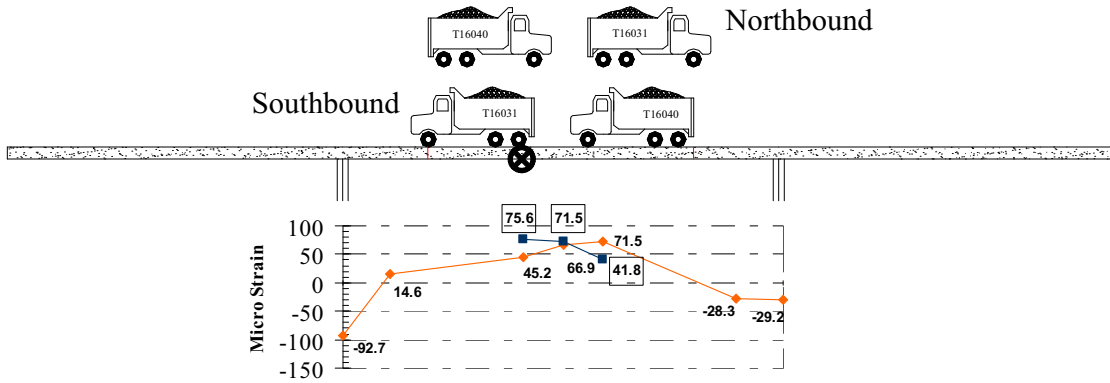
Figure 6.44: Measured Strain in Bottom Gauge of Girder I with Truck in Lane 1

Girder II and Lane 1 Loaded



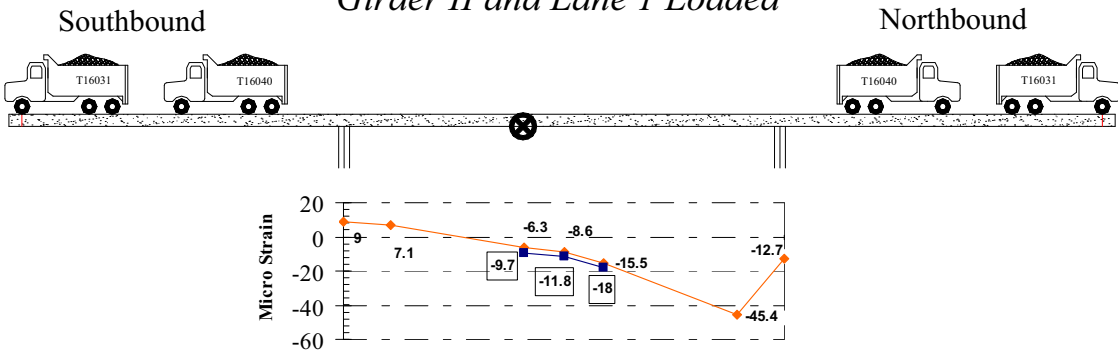
Front Axle at 117 ft

Girder II and Lane 1 Loaded



(b) Front Axle at 179 ft

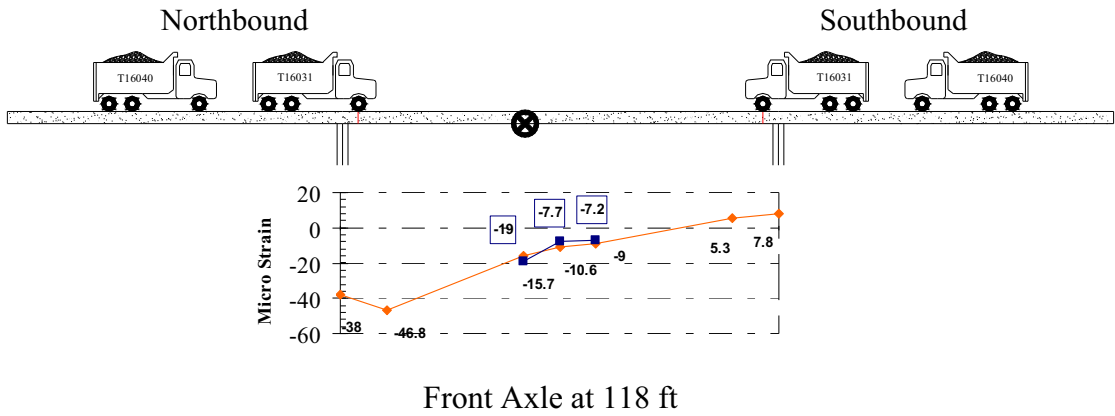
Girder II and Lane 1 Loaded



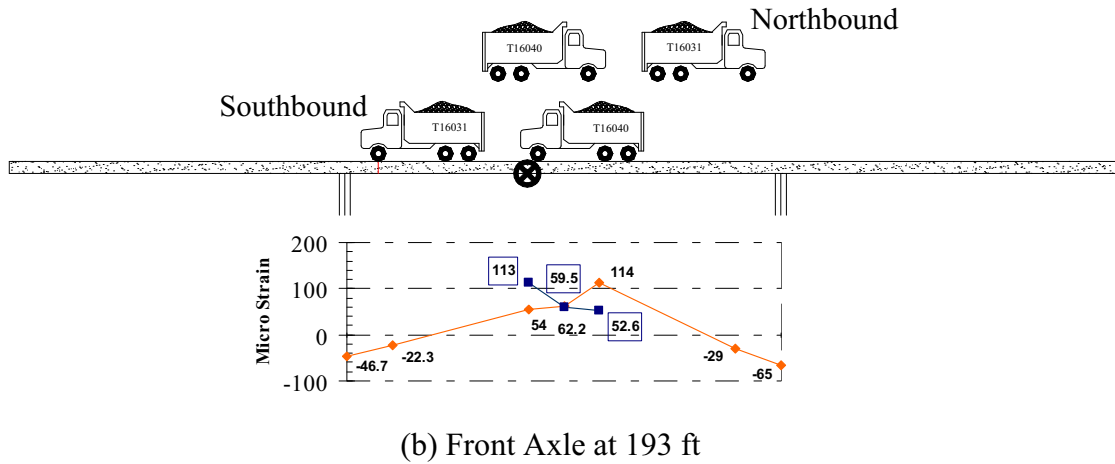
(c) Front Axle at 261 ft

Figure 6.45: Measured Strain in Bottom Gauge of Girder II with Truck in Lane 1

Girder IV and Lane 3 Loaded



Girder IV and Lane 3 Loaded



Girder IV and Lane 3 Loaded

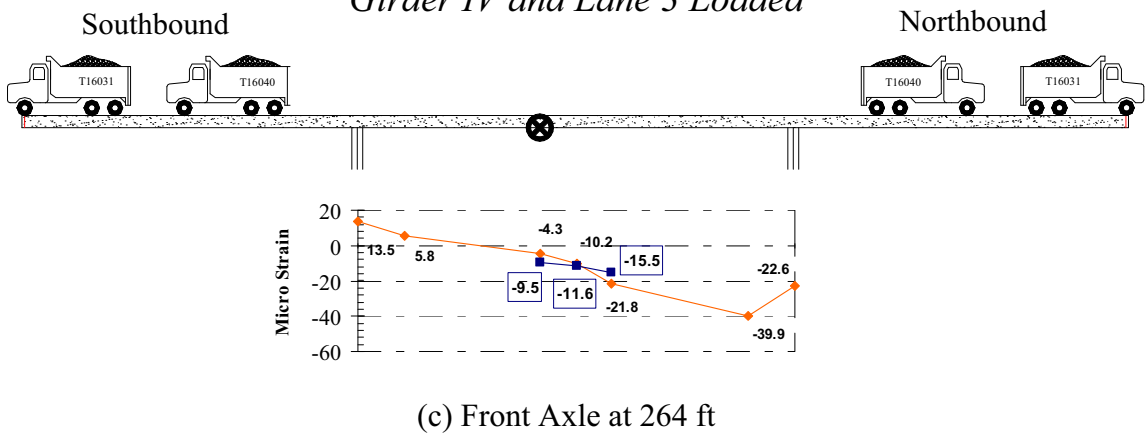


Figure 6.46: Measured Strain in Bottom Gauge of Girder IV with Truck in Lane 3

6.2.4 Neutral Axis Depth

The neutral axis position is of interest as an indication of the amount of composite action between the steel girders and concrete deck. From beam bending theory, a neutral axis location at mid-height of the steel girders would be indicative of non-composite behavior between steel girders and concrete deck. Higher positions of the neutral axis on the steel girder would indicate some level of composite action with the concrete deck. The test strain data were used to determine neutral axis location measured from the bottom gauge to assess whether the bridge behaved non-compositely as originally assumed in design.

6.2.4.1 Neutral Axis Depth at Mid-Span

Neutral axis depths at mid-span varied from approximately 22 in to 38 in (559 to 965 mm), with three recorded peaks over 40 in (1016 mm). These results indicate that the steel girder mid-span sections acted compositely with the deck slab during the field tests, since the measured neutral axis depths were greater than mid-height of the girder (18.1 in (460 mm)). Neutral axis depths are plotted in Figure 6.47 to Figure 6.50. Data from repeated test runs with loading trucks traveling along the same lane are plotted together, and are denoted by darker and lighter lines in these figures.

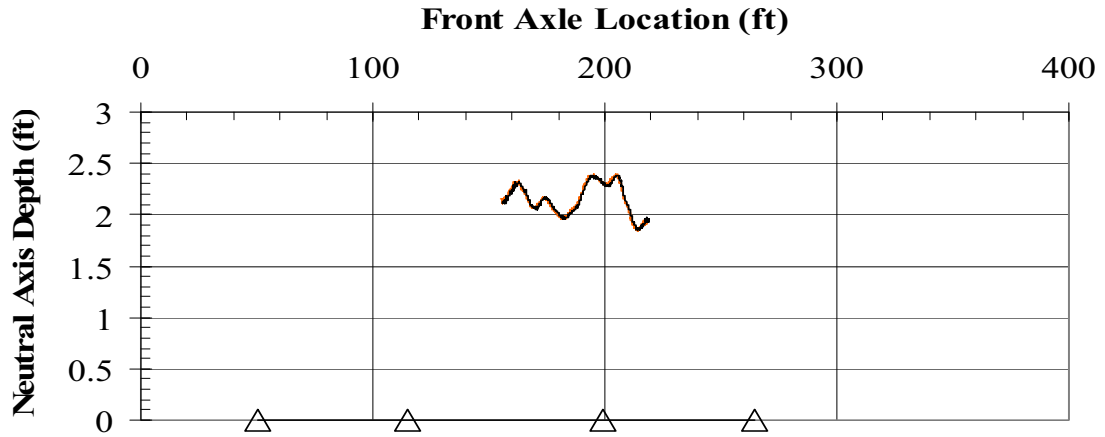
In most plots the top strain gauge is in compression, with the neutral axis depth well below the top flange of the girder. A larger variation in the measured neutral axis depth occurred when strain values measured in the bottom strain gauge approached $20 \mu\epsilon$, the value used as a cutoff for calculating neutral axis depth. Higher errors in calculation of neutral axis location are also introduced when the neutral axis is located near the top strain gauge. Small tensile strains were occasionally measured in the top strain gauge resulting in neutral axis depths above the top flange of the girder, within the concrete deck.

Higher variability in the neutral axis depth was observed in several of the plots, particularly when the gauge pair was located directly under a loaded lane. In Figure 6.47 (beam II of Table 6.18) there is more variability in neutral axis depth when trucks travel in lane 1 than lane 3. The neutral axis depths remain approximately constant for test runs in all three lanes. Similar behavior is observed in beam III at mid-span (Figure 6.48) where the neutral axis depth has more variability with trucks in lane 2 than in 1 or 3.

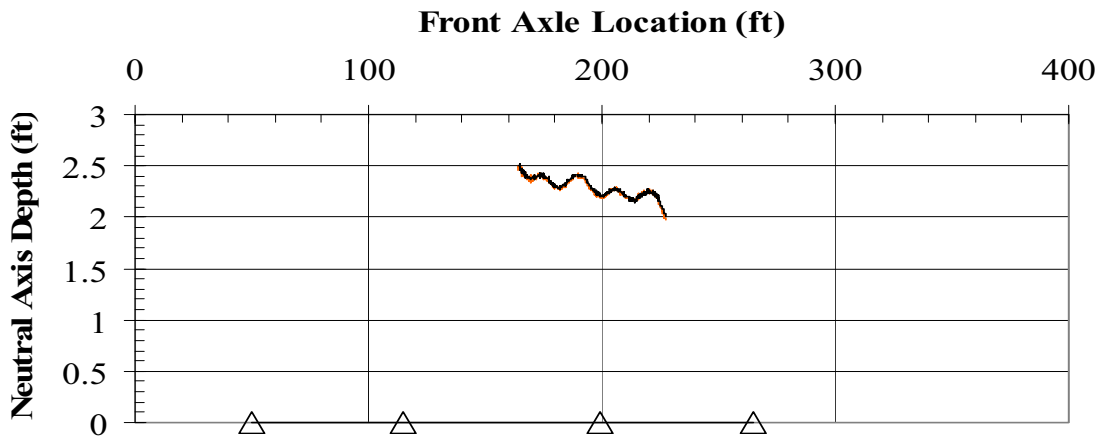
Some of the neutral axis depths were calculated to be above the deck slab (Figure 6.48b and Figure 6.49b and c). These values, however, were not used to calculate girder moments because of the likelihood of errors introduced by the small strain gauge readings associated with these neutral axis positions. The observed spikes in some of the plots occurred in gauge pairs located near a loaded lane. The spikes in Figure 6.49, for example, occurred approximately at the same spacing as the loading truck axle spacing. Therefore, these strain spikes are believed to be the result of local effects generated by passing of the loading truck axles directly over a gauge pair.

Table 6.18: Neutral Axis Depth at Mid-Span

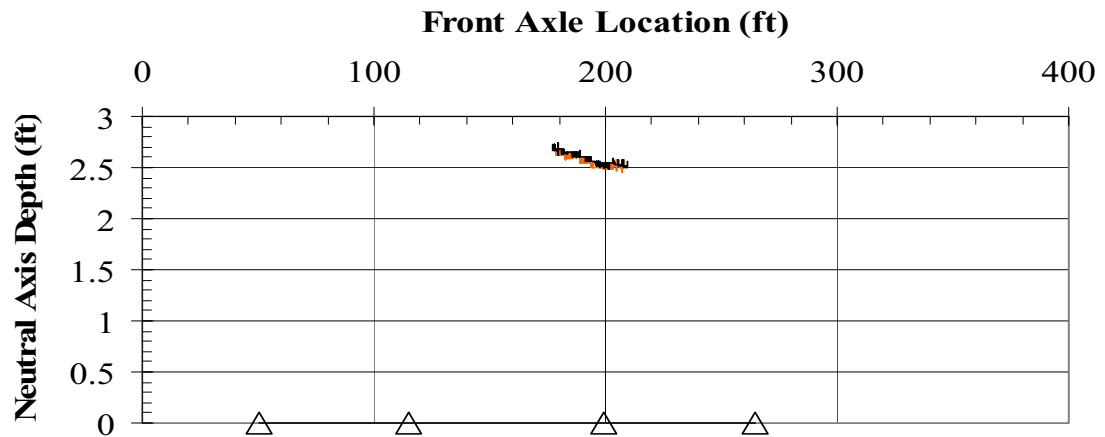
Cross Section	Beam	Lane	Minimum (in)	Maximum (in)	Range (in)
4	II	1	22.3	28.6	6.2
		2	24.1	29.6	5.5
		3	29.9	32.0	2.2
	III	1	29.8	32.9	3.1
		2	27.8	42.0	14.2
		3	30.2	34.8	4.6
	IV	1	*	*	
		2	29.6	46.1	16.4
		3	28.1	46.8	18.7
	V	1	*	*	
		2	34.8	37.0	2.2
		3	36.6	38.4	1.8



(a) Load Trucks in Lane 1

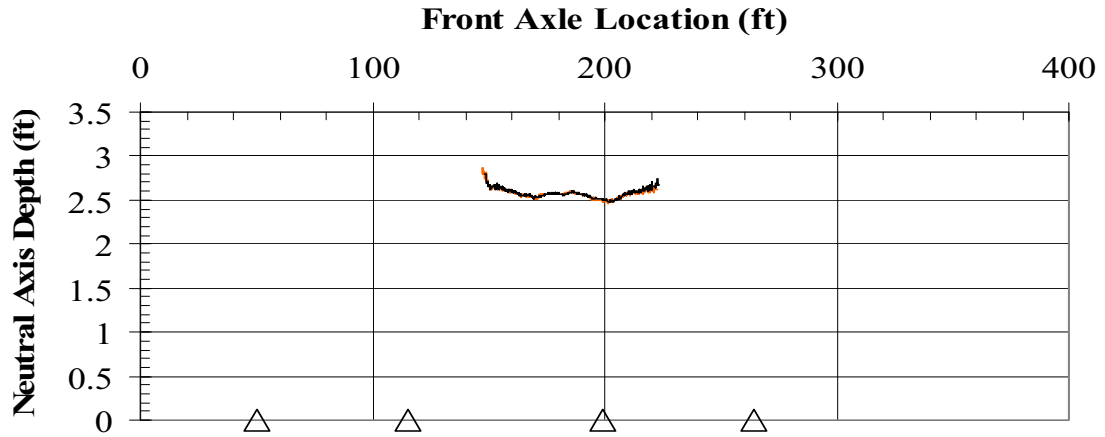


(b) Load Trucks in Lane 2

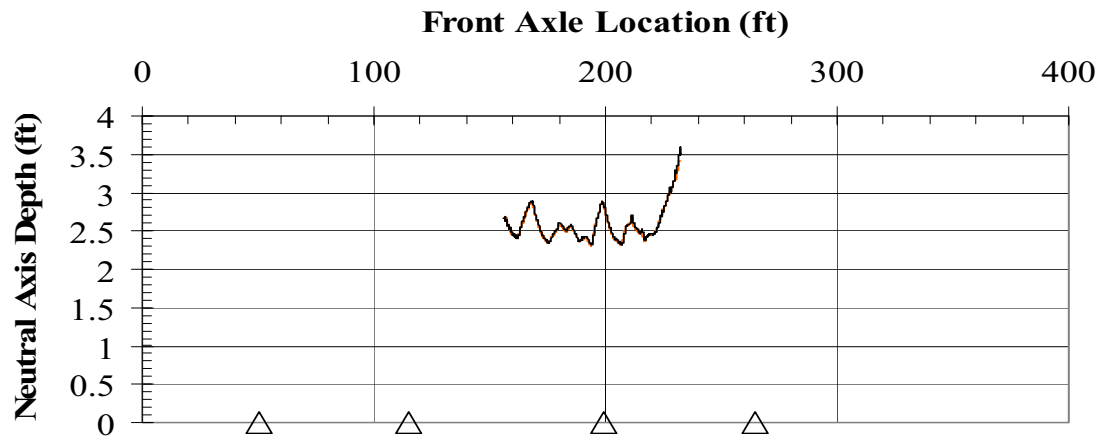


(c) Load Trucks in Lane 3

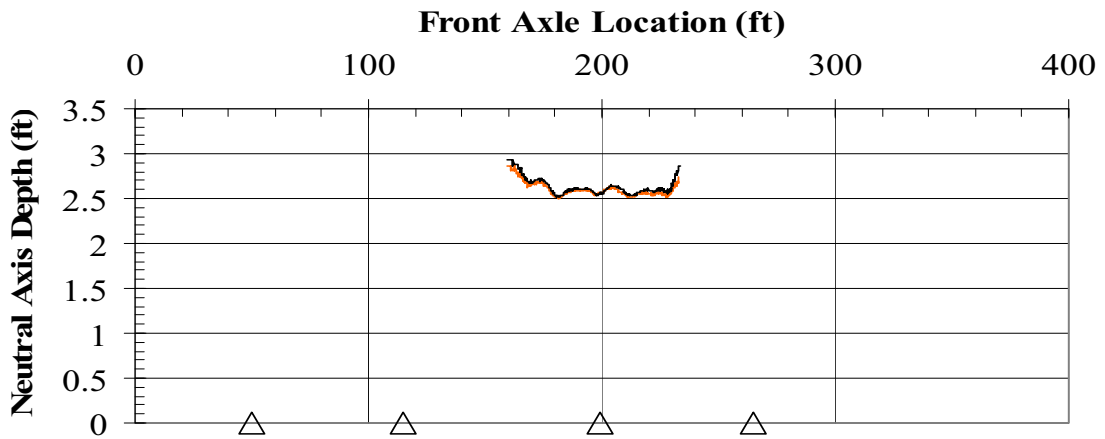
Figure 6.47: Neutral Axis Depth in Cross Section 4 Beam II



(a) Load Trucks in Lane 1

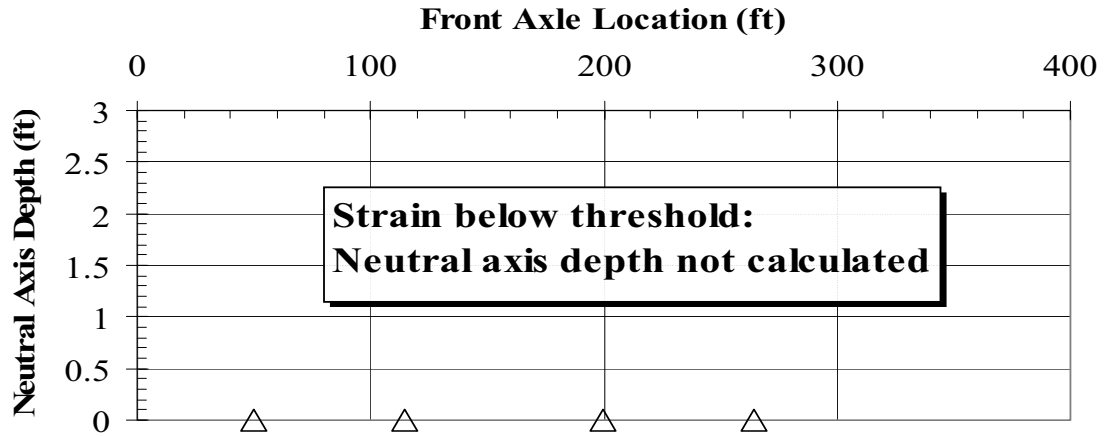


(b) Load Trucks in Lane 2

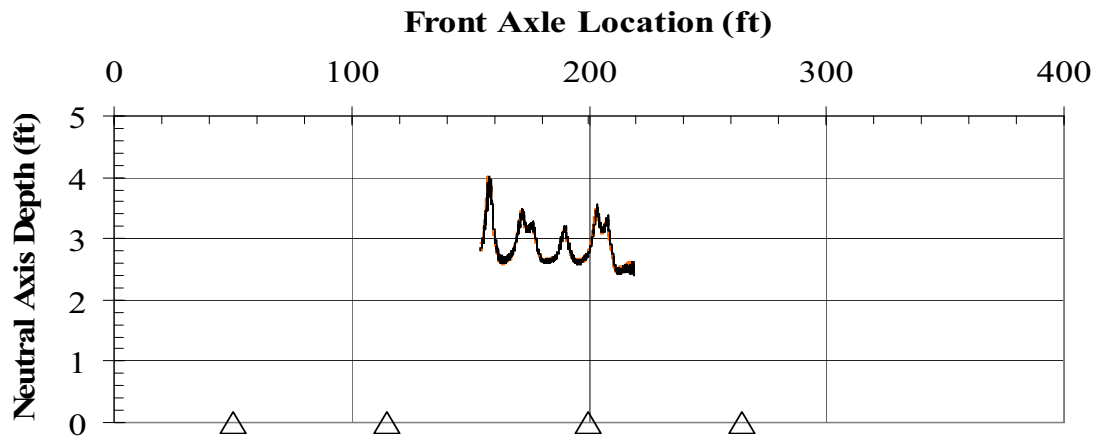


(c) Load Trucks in Lane 3

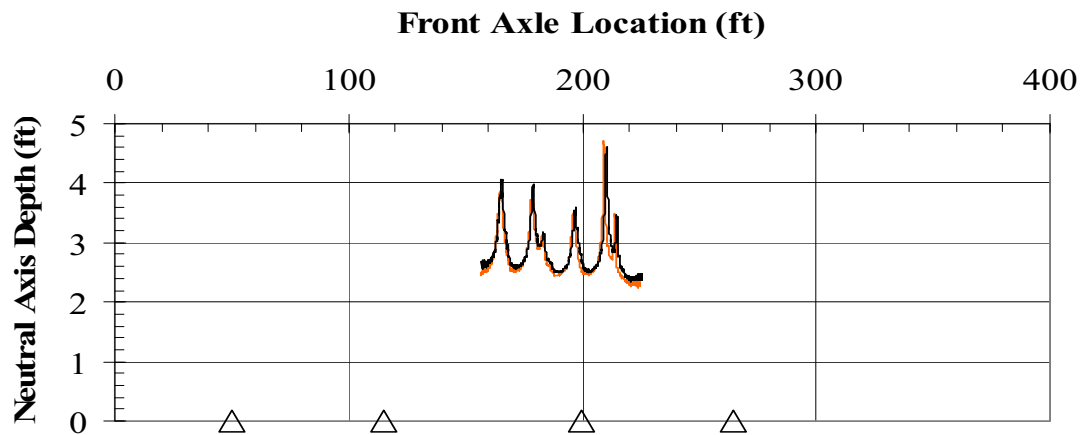
Figure 6.48: Neutral Axis Depth in Cross Section 4 Beam III



(a) Load Trucks in Lane 1

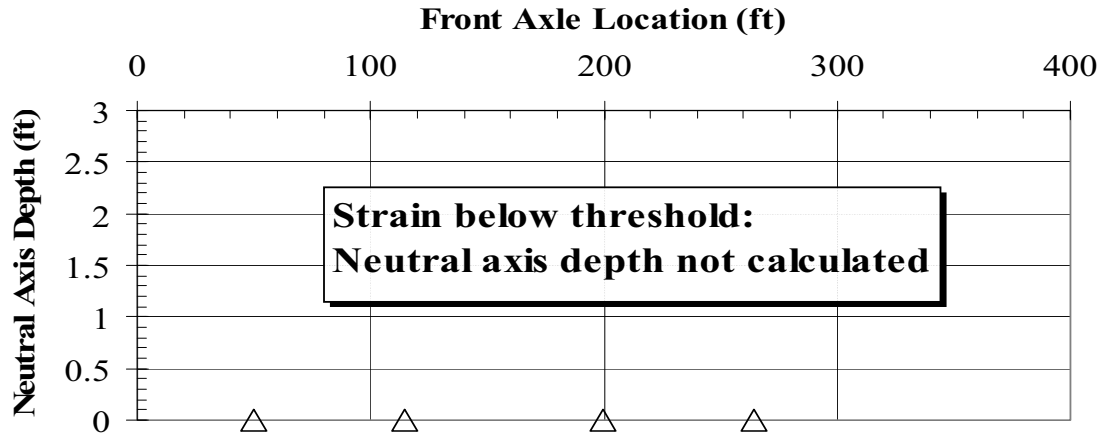


(b) Load Trucks in Lane 2

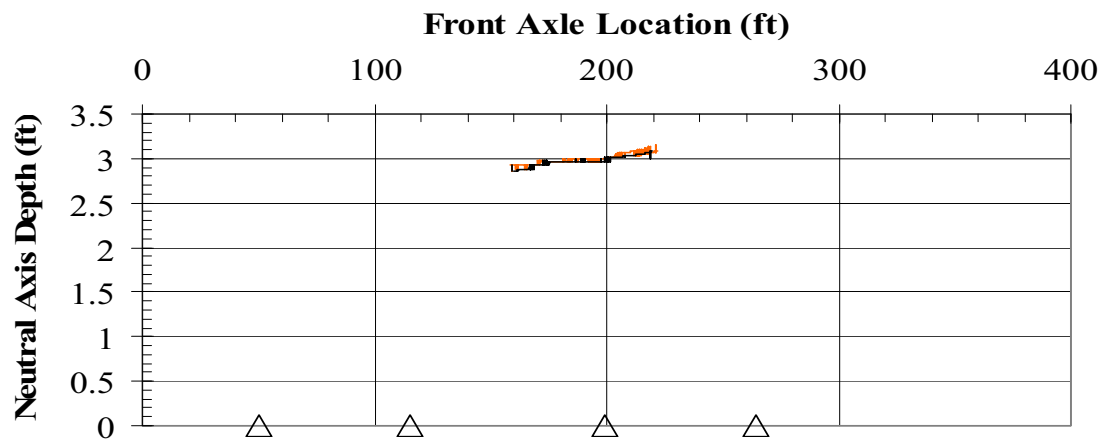


(c) Load Trucks in Lane 3

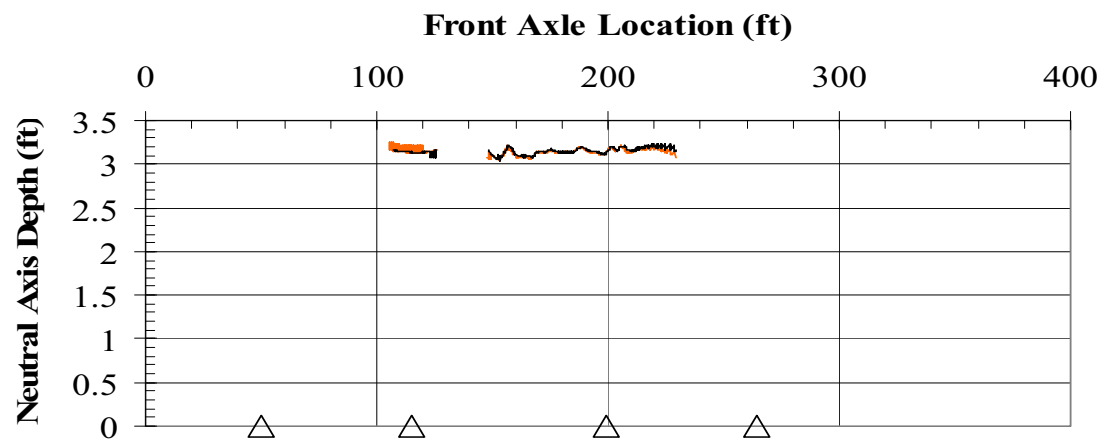
Figure 6.49: Neutral Axis Depth in Cross Section 4 Beam IV



(a) Load Trucks in Lane 1



(b) Load Trucks in Lane 2



(c) Load Trucks in Lane 3

Figure 6.50: Neutral Axis Depth in Cross Section 4 Beam V

6.2.4.2 Neutral Axis Depth Near Pier Support

Slightly lower neutral axis depths were observed at pier supports than at mid-span, with a range between 14 and 38 in (356 to 965 mm) (Table 6.19). In contrast to mid-span where large tensile strains occur in the bottom gauge (positive bending), the bottom gauge strain values measured near the piers indicated compression, consistent with negative bending of the girder section. Plots of neutral axis depths at pier supports are plotted in Figure 6.51 to Figure 6.59.

The compression strains in the bottom gauge have a smaller absolute value than the tension strains at mid-span. Smaller strains in the lower gauge create larger error in the neutral axis depth calculation, which explains the larger range of values observed at this section. Additionally, fewer neutral axis plots have been generated at these locations since many of the measured strains were below the $20 \mu\varepsilon$ threshold.

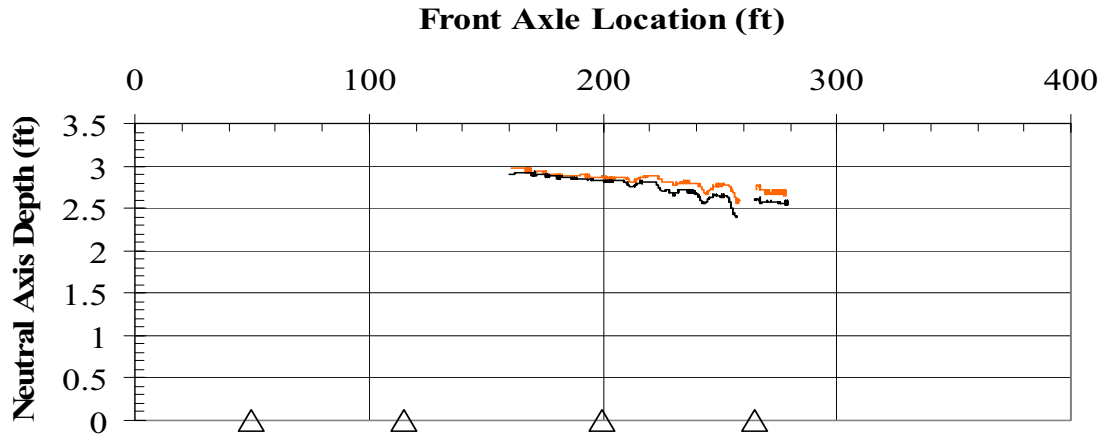
In some cases, positive moments were also observed to occur near pier supports in beam I in cross section 7, at the obtuse angle side of the skewed pier support. The neutral axis depth in this case falls within the range of depths in negative bending, with little variability.

The neutral axis depth plots at pier supports have fewer spikes when compared to the mid-span region. Because of girder proximity to a stiff support (pier), individual axle loads did not generate the spikes in strain data observed at mid-span (Section 6.2.4.1).

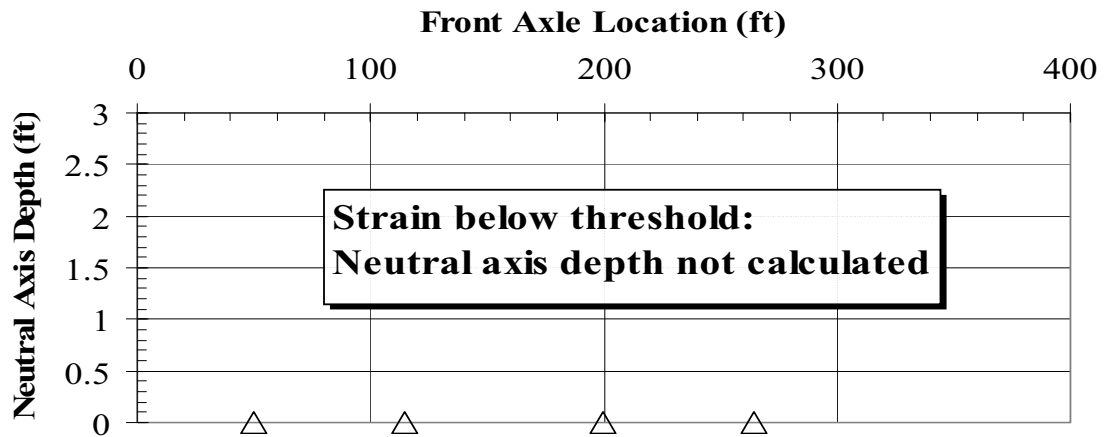
Table 6.19: Neutral Axis Depth at Pier Support Cross Sections

Cross Section	Beam	Lane	Minimum (in)	Maximum (in)	Range (in)
1	I	1	30.1	35.4	5.3
		2	*	*	
		3	*	*	
	II	1	17.9	25.7	7.8
		2	22.9	24.0	1.1
		3	*	*	
	III	1	23.8	32.5	8.8
		2	26.6	33.2	6.6
		3	25.2	32.5	7.3
	IV	1	*	*	
		2	20.5	33.8	13.3
		3	20.0	33.0	13.0
	V	1	*	*	
		2	*	*	
		3	30.7	37.6	6.8
7	I	1	29.3	36.5	7.2
		2	36.0	37.0	1.0
		3	36.0	37.3	1.3
	II	1	14.0	34.8	20.8
		2	13.9	27.4	13.4
		3	*	*	
	III	1	23.2	25.4	2.3
		2	18.1	26.5	8.4
		3	23.4	26.4	3.0
	IV	1	*	*	
		2	18.7	25.0	6.2
		3	15.1	25.0	9.8
	V	1	*	*	
		2	15.4	16.0	0.6
		3	32.9	38.5	5.6

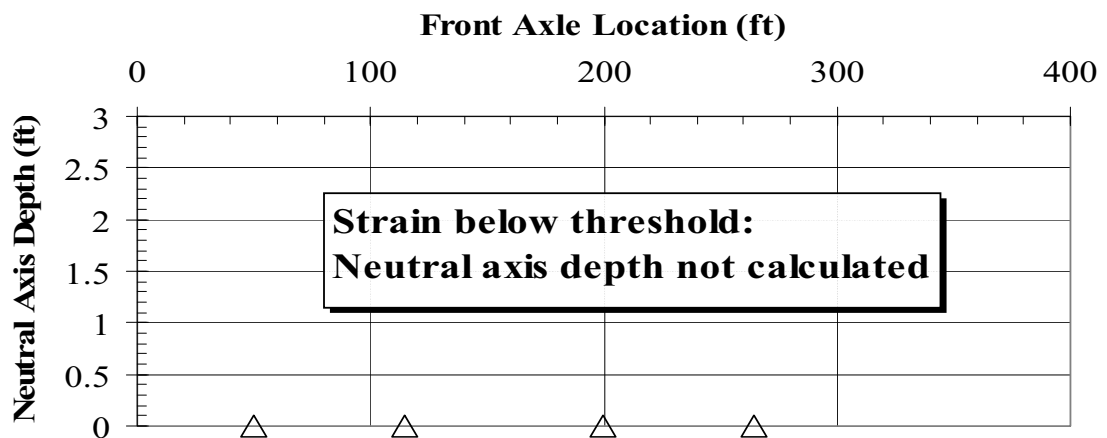
Note: Shaded areas are depths measured in positive bending



(a) Load Trucks in Lane 1

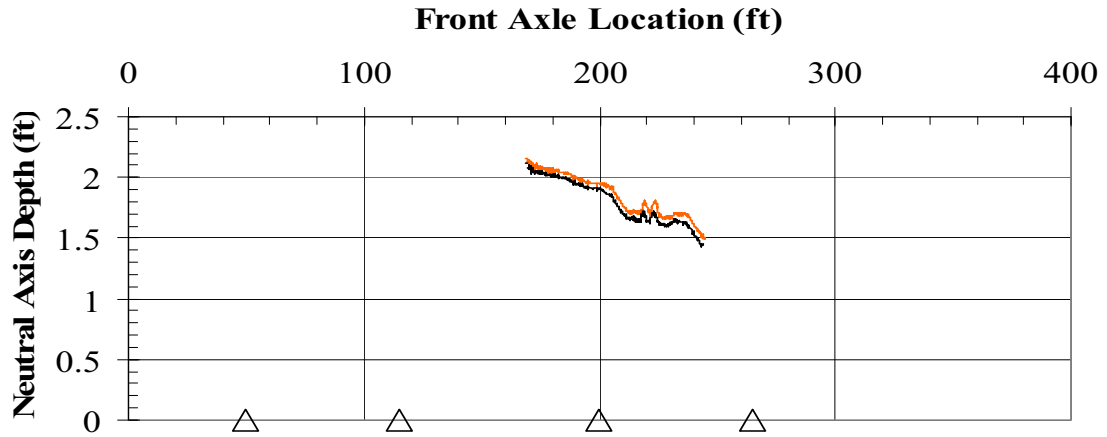


(b) Load Trucks in Lane 2

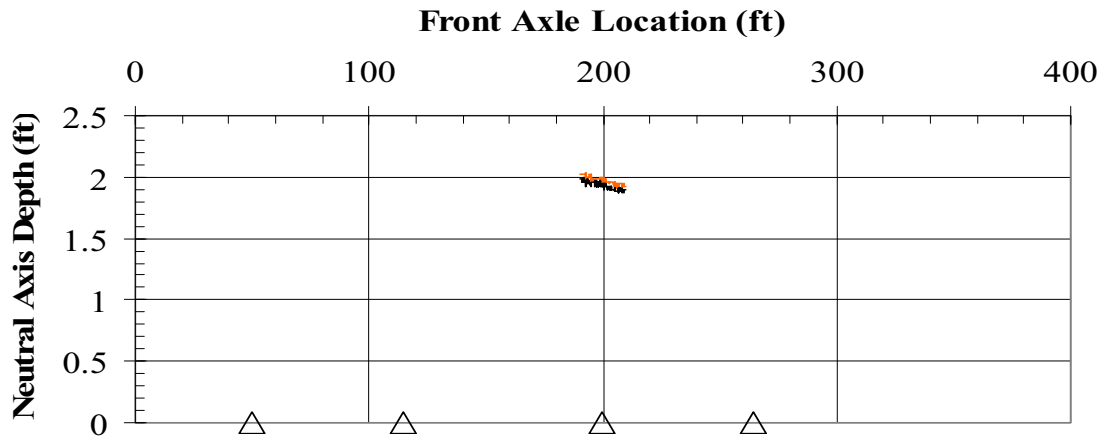


(c) Load Trucks in Lane 3

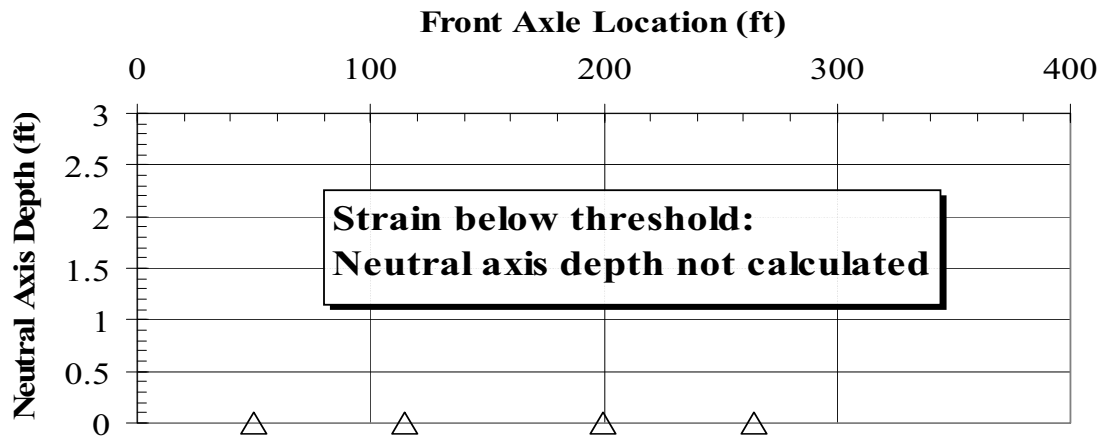
Figure 6.51: Neutral Axis Depth in Cross Section 1 Beam I



(a) Load Trucks in Lane 1

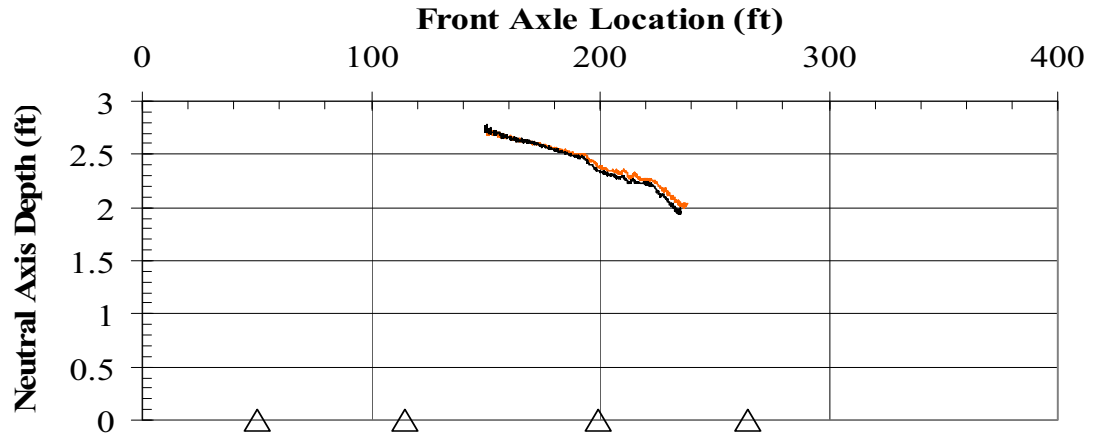


(b) Load Trucks in Lane 2

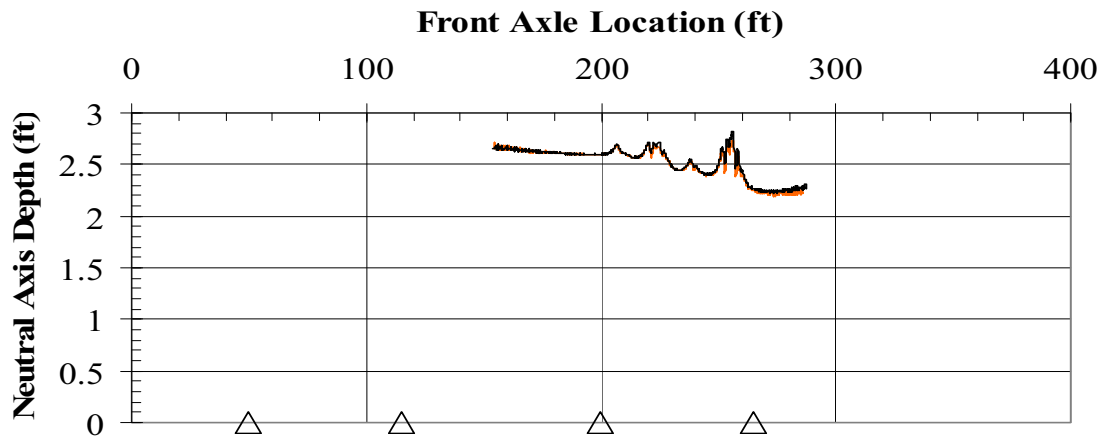


(c) Load Trucks in Lane 3

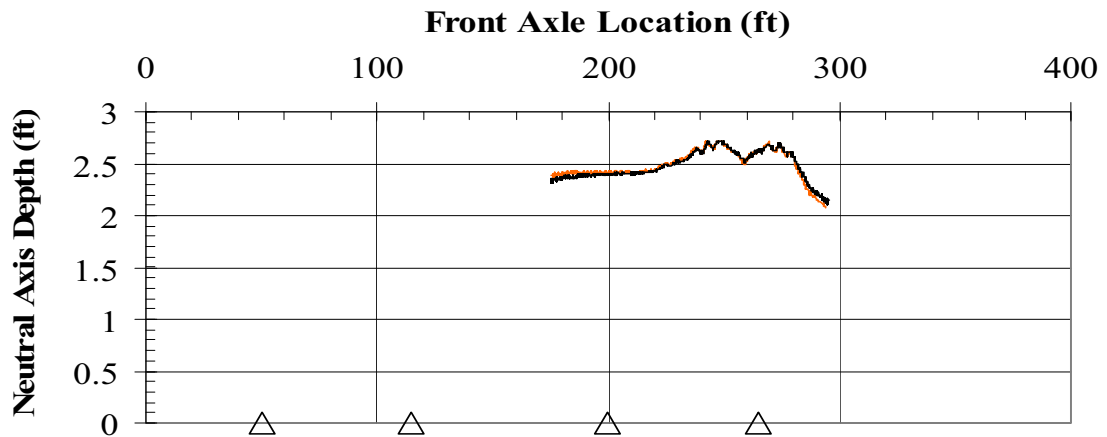
Figure 6.52: Neutral Axis Depth in Cross Section 1 Beam II



(a) Load Trucks in Lane 1

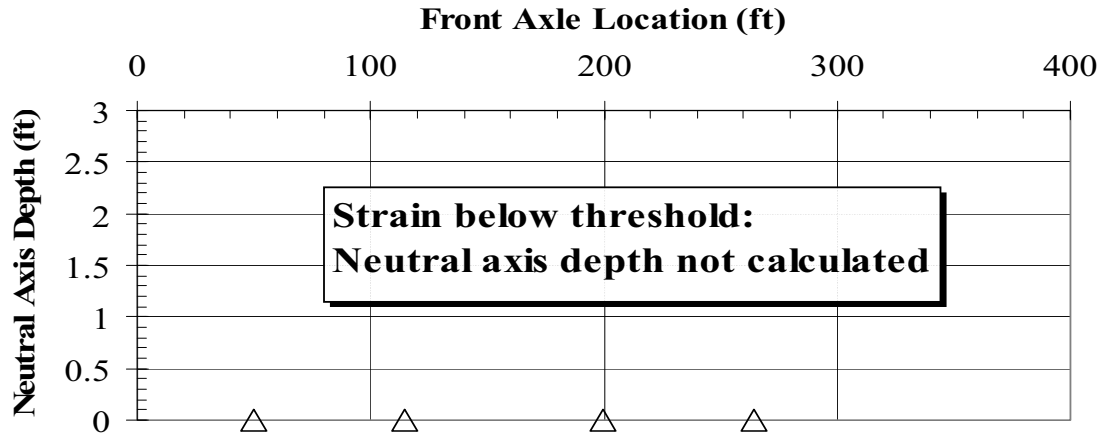


(b) Load Trucks in Lane 2

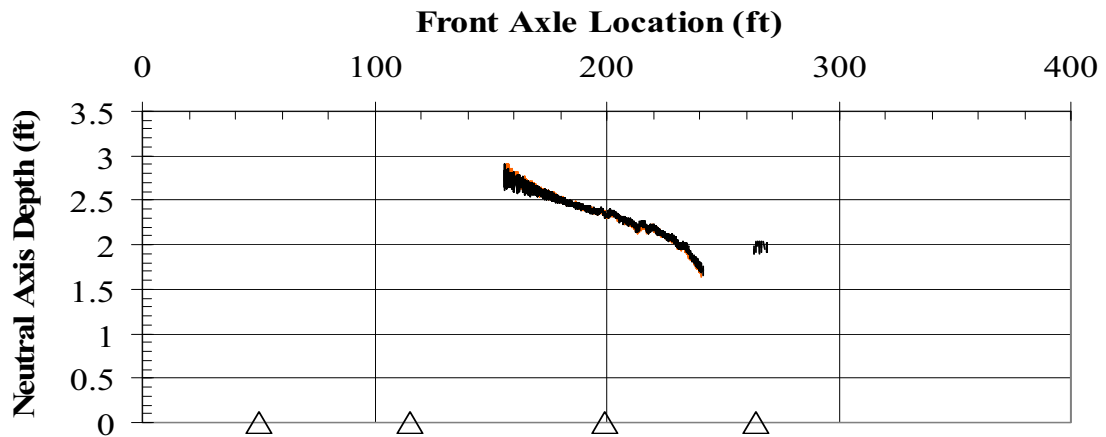


(c) Load Trucks in Lane 3

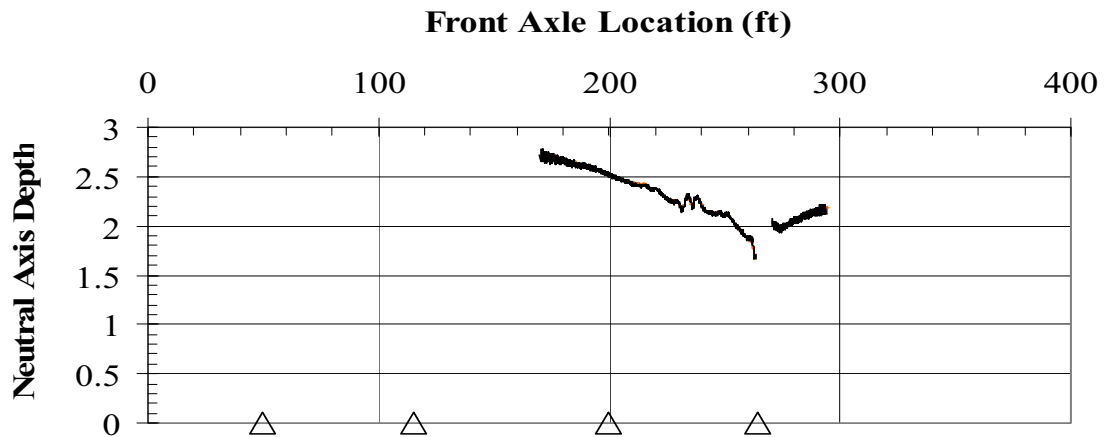
Figure 6.53: Neutral Axis Depth in Cross Section 1 Beam III



(a) Load Trucks in Lane 1

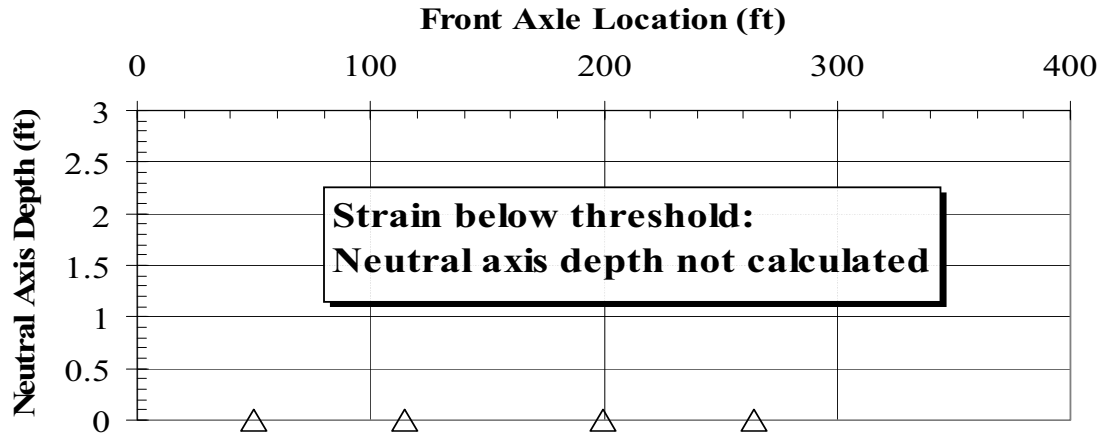


(b) Load Trucks in Lane 2

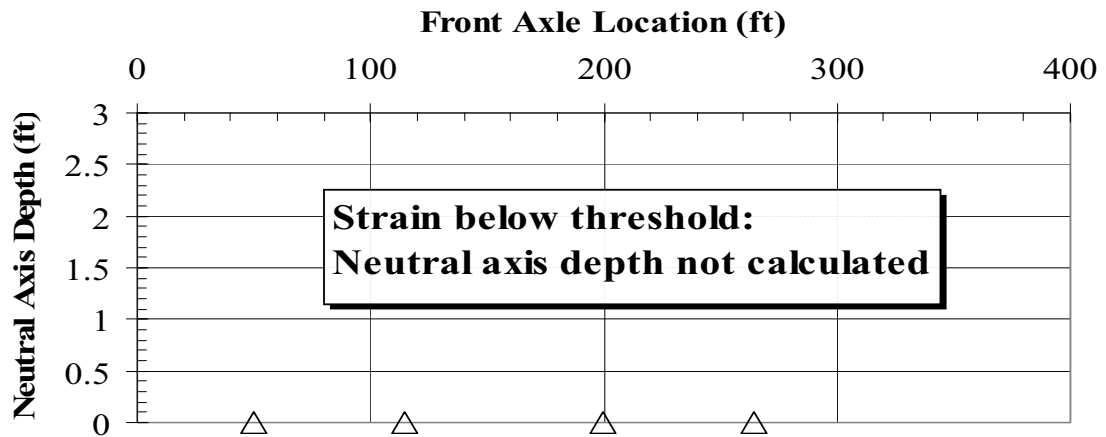


(c) Load Trucks in Lane 3

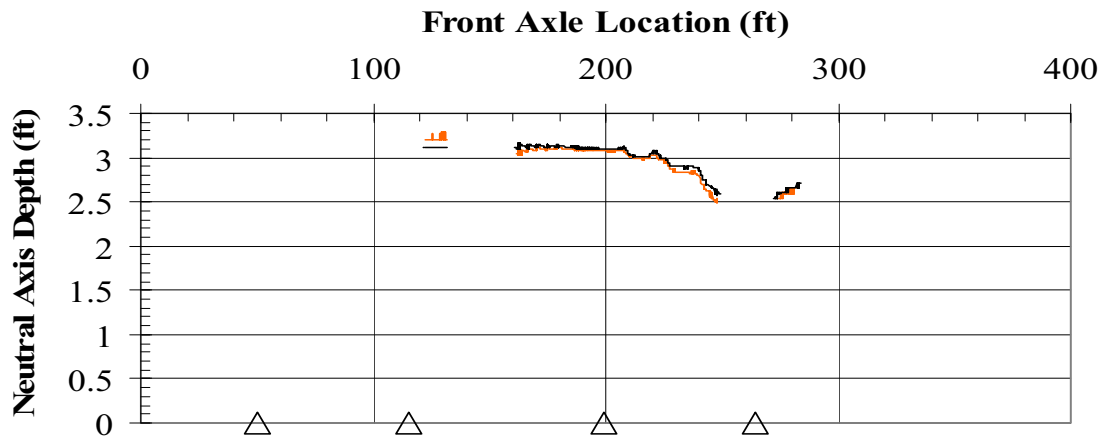
Figure 6.54: Neutral Axis Depth in Cross Section 1 Beam IV



(a) Load Trucks in Lane 1

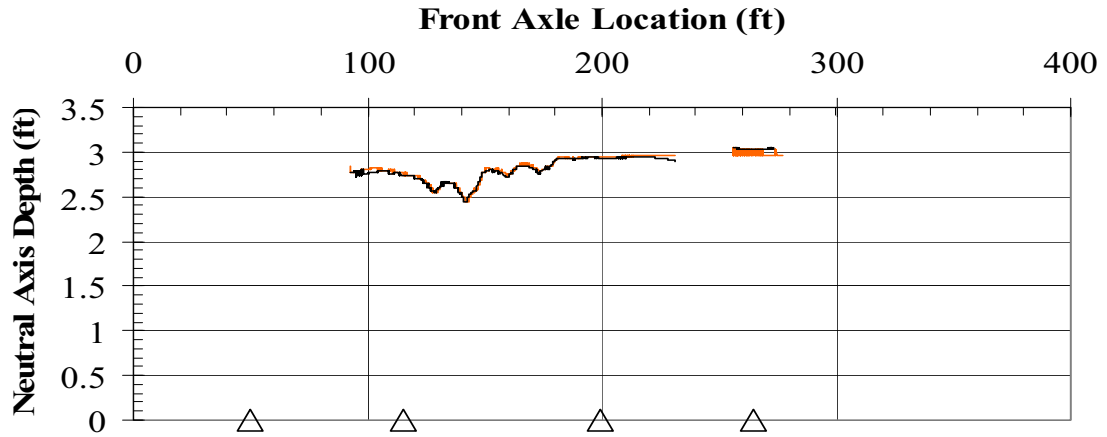


(b) Load Trucks in Lane 2

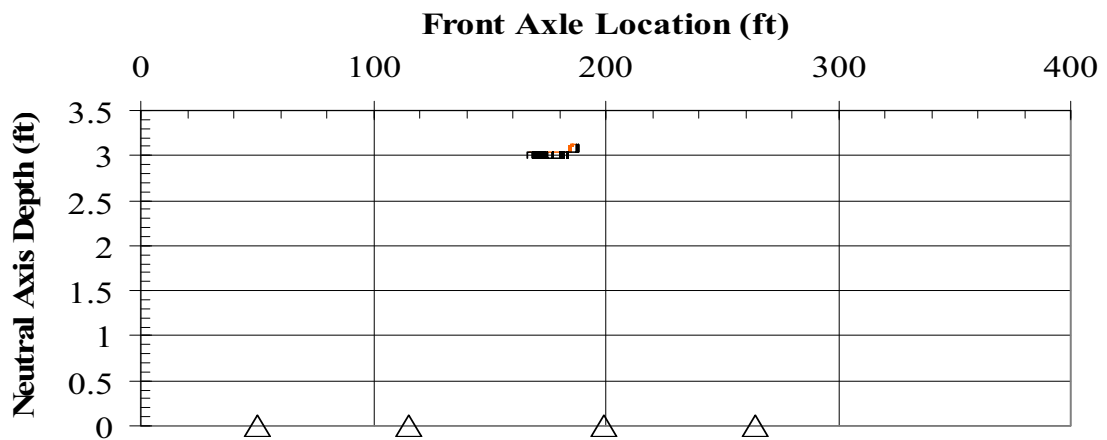


(c) Load Trucks in Lane 3

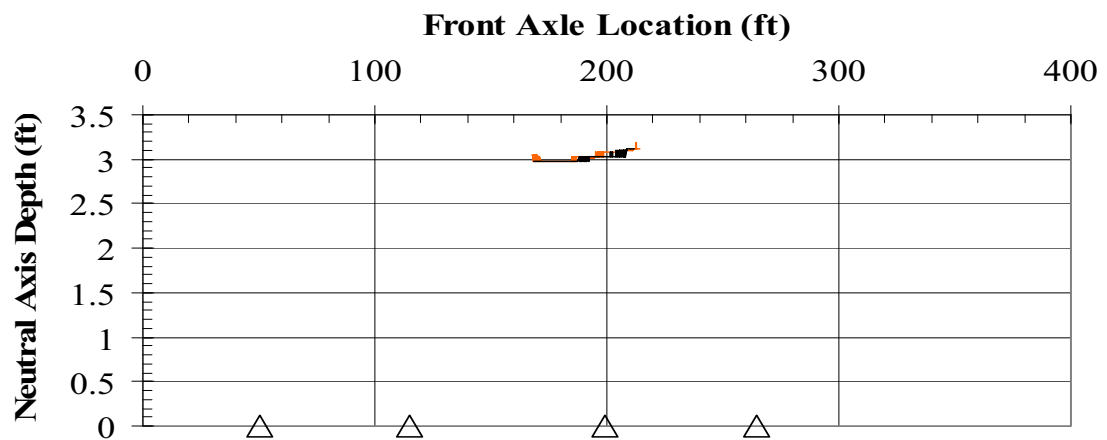
Figure 6.55: Neutral Axis Depth in Cross Section 1 Beam V



(a) Load Trucks in Lane 1

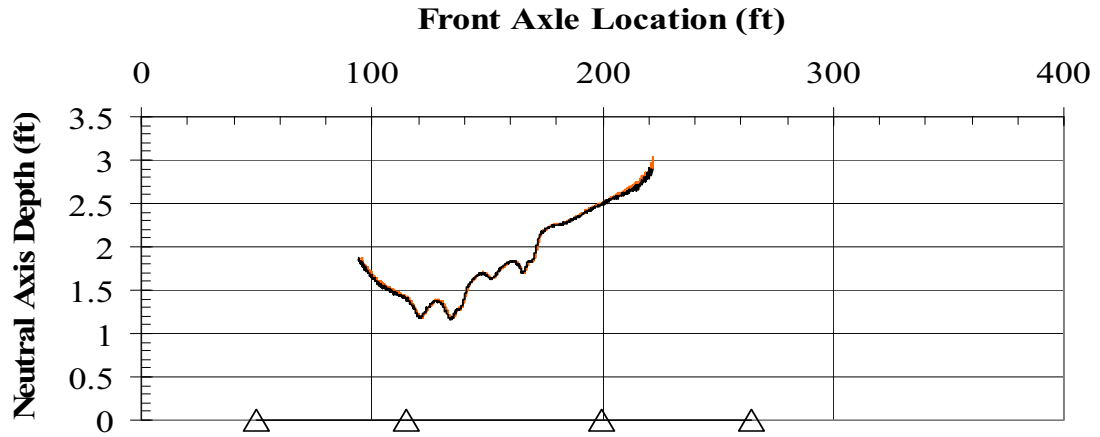


(b) Load Trucks in Lane 2

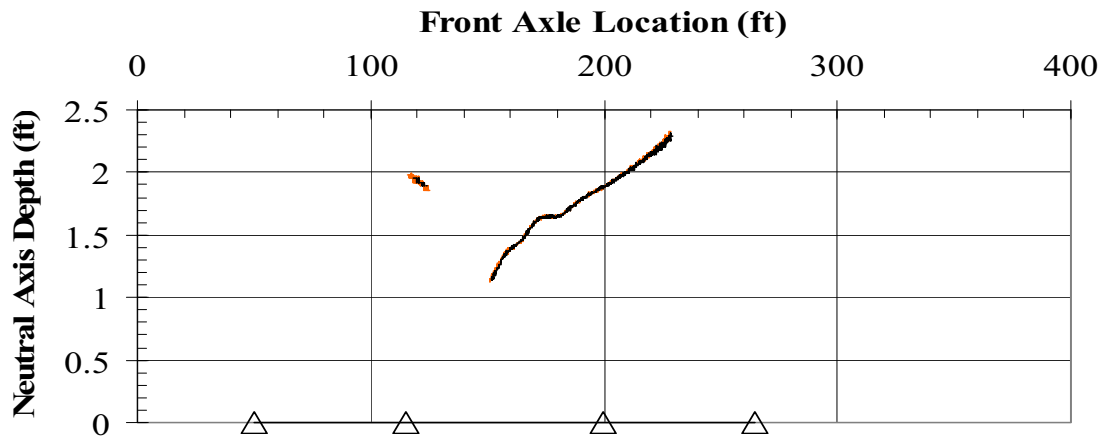


(c) Load Trucks in Lane 3

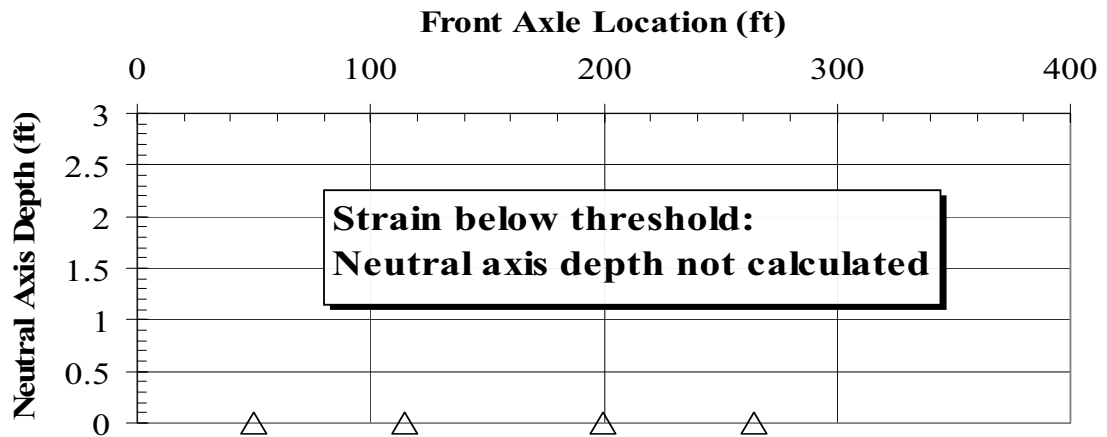
Figure 6.56: Neutral Axis Depth in Cross Section 7 Beam I



(a) Load Trucks in Lane 1

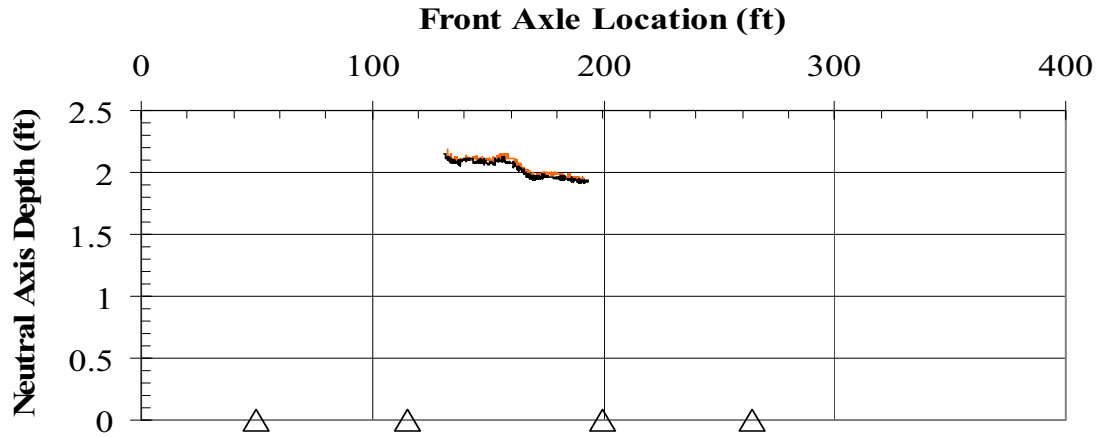


(b) Load Trucks in Lane 2

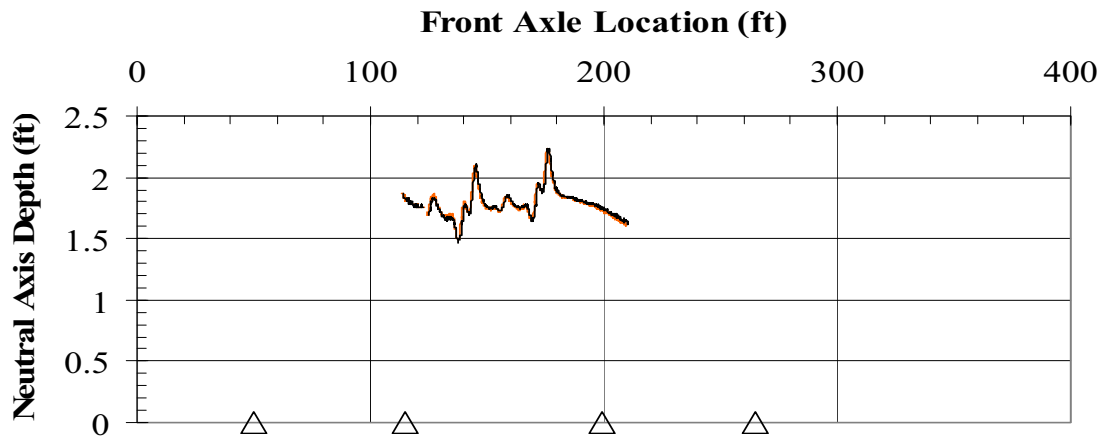


(c) Load Trucks in Lane 3

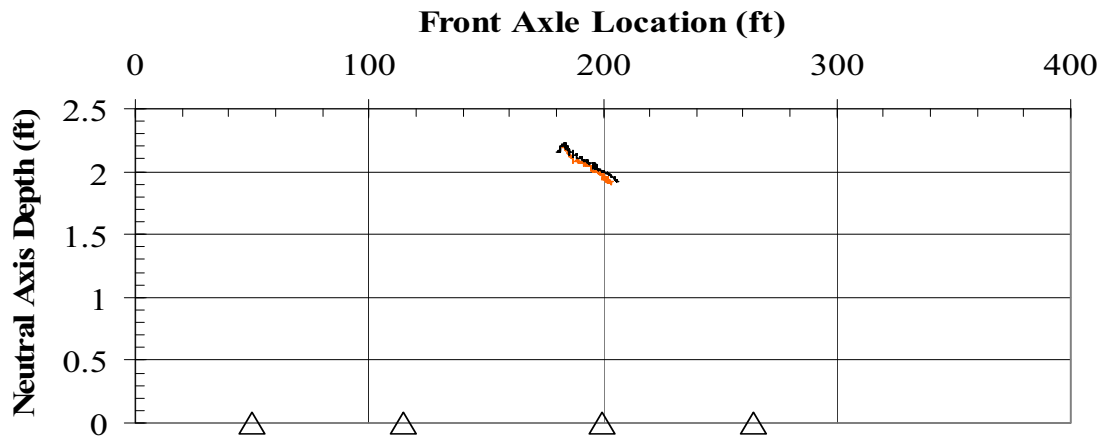
Figure 6.57: Neutral Axis Depth in Cross Section 7 Beam II



(a) Load Trucks in Lane 1

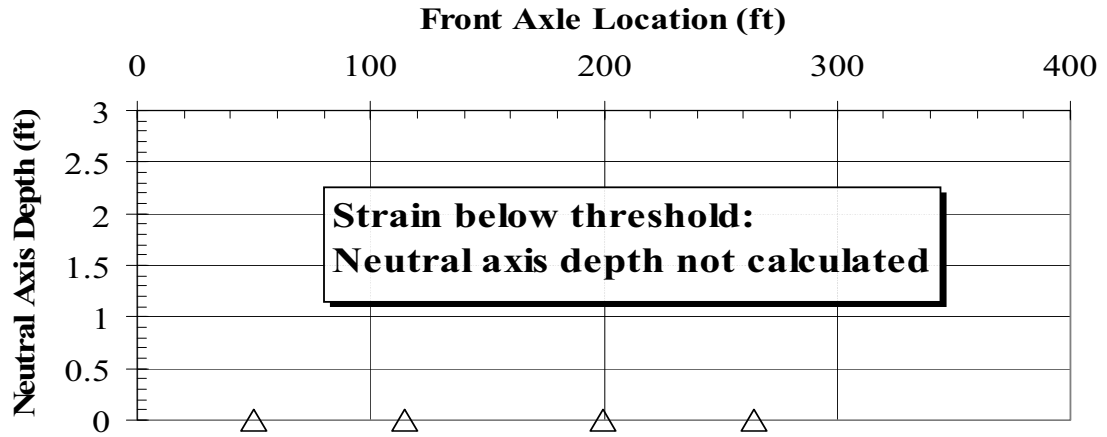


(b) Load Trucks in Lane 2

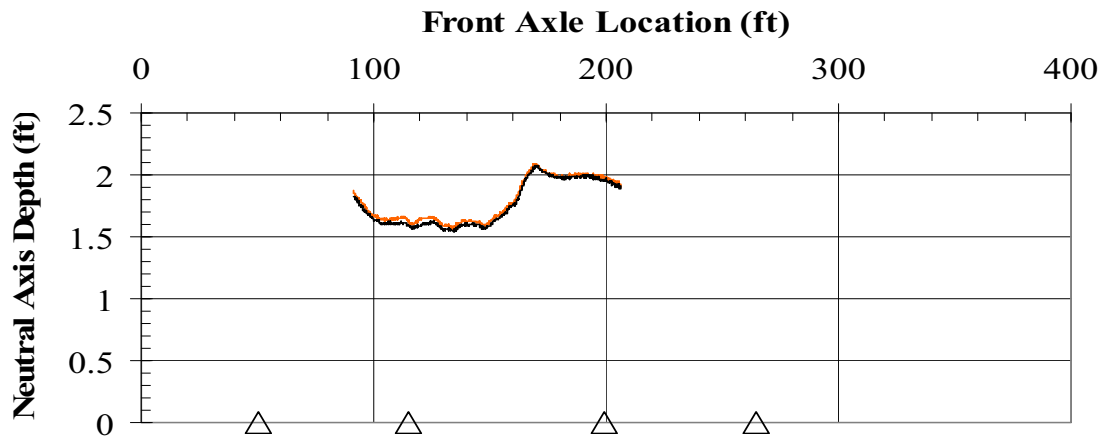


(c) Load Trucks in Lane 3

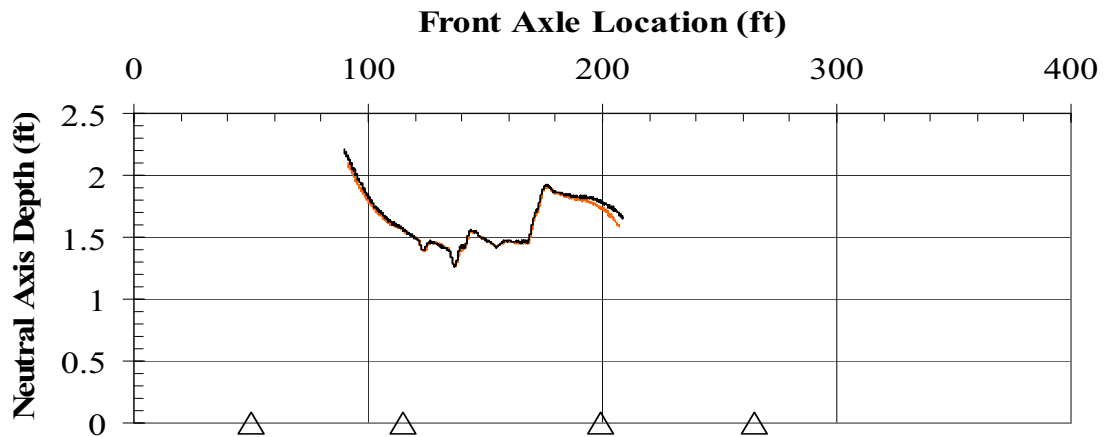
Figure 6.58: Neutral Axis Depth in Cross Section 7 Beam III



(a) Load Trucks in Lane 1

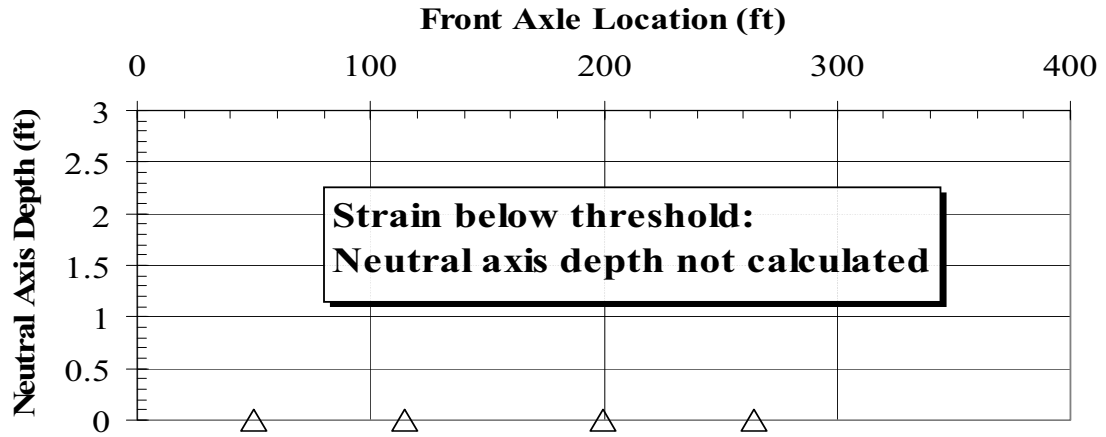


(b) Load Trucks in Lane 2

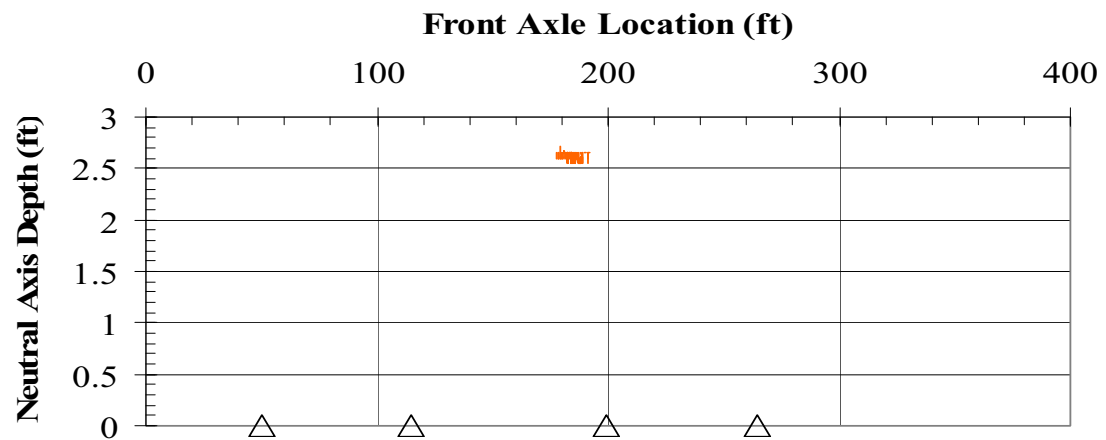


(c) Load Trucks in Lane 3

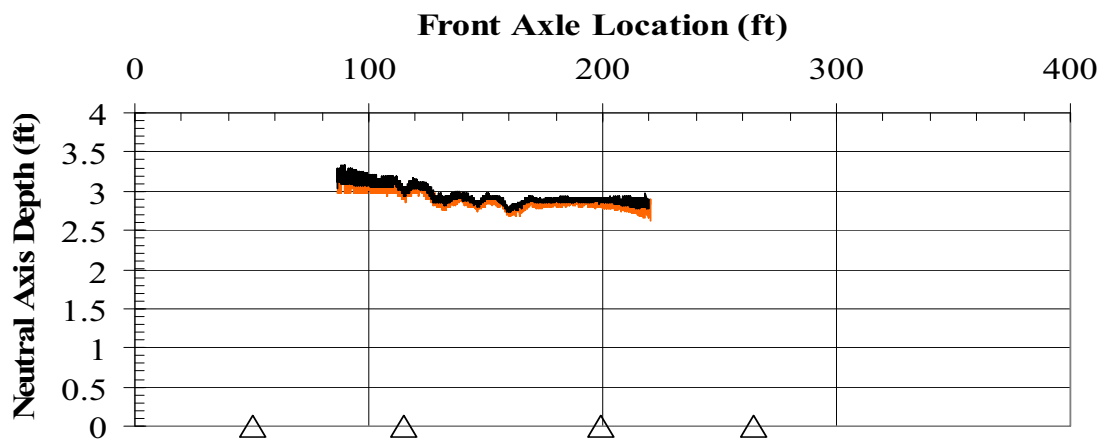
Figure 6.59: Neutral Axis Depth in Cross Section 7 Beam IV



(a) Load Trucks in Lane 1



(b) Load Trucks in Lane 2



(c) Load Trucks in Lane 3

Figure 6.60: Neutral Axis Depth in Cross Section 7 Beam V

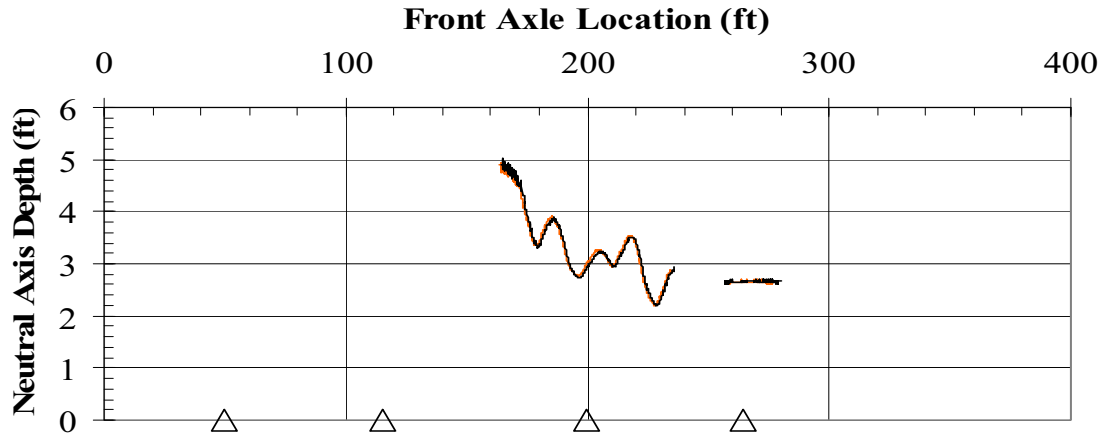
6.2.4.3 Neutral Axis Depth at Damaged Sections

The neutral axis depths calculated at locations where girders were damaged by truck impact are plotted in Figure 6.61 to Figure 6.66 with results summarized in Table 6.20. Most of the neutral axis depths fell within the range of 24 to 36 in (609 to 914 mm), similar to undamaged sections at mid-span. Spikes in the calculated neutral axis depths occurred in strain histories where the lower gauge strain approached $20 \mu\varepsilon$.

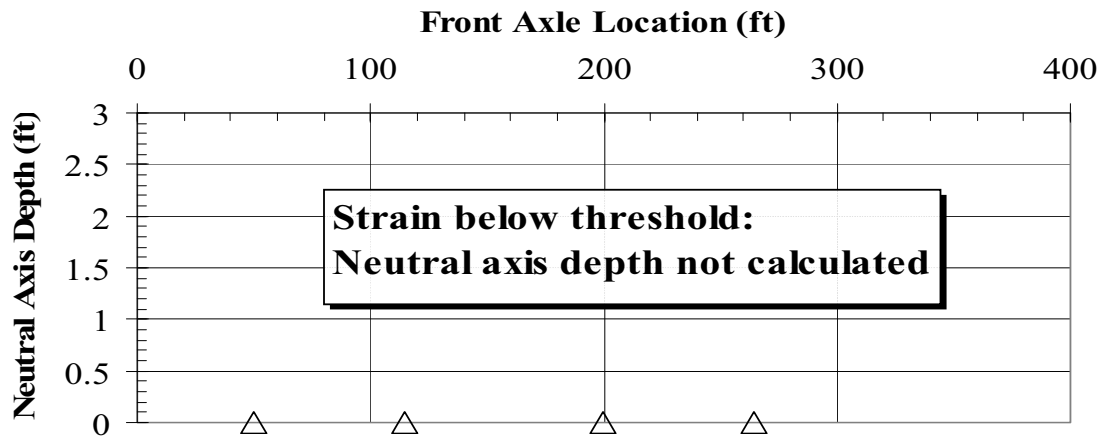
The maximum range of neutral axis depths at damaged sections was found in beam I of cross section 3 with variation from a minimum of 20.3 in (516 mm) to maximum of 58.9 in (1496 mm) with a range of 32.2 in (32.2). Overall the range of depths calculated is greater than mid-span and pier support locations. It is unclear, however, if the damage to the girders is the cause of the variation in measured strains.

Table 6.20: Neutral Axis Depth at Damaged Cross Section

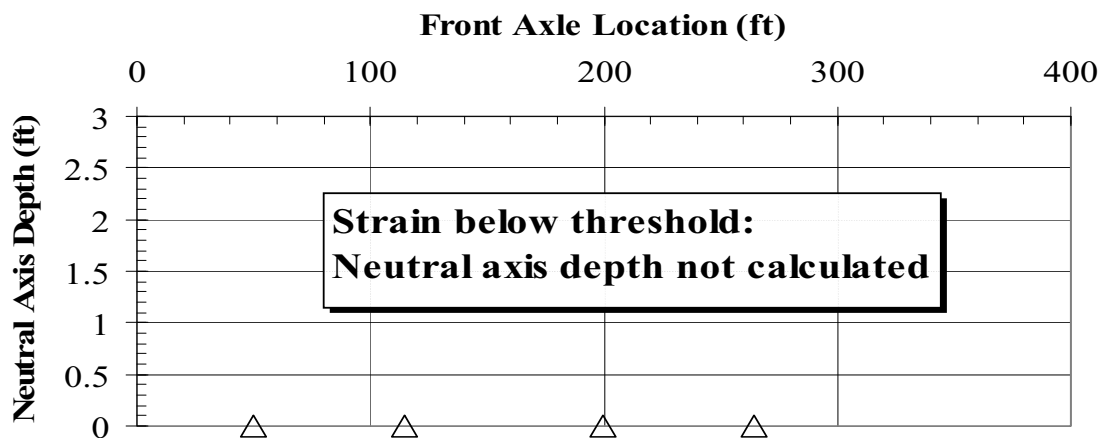
Cross Section	Beam	Lane	Minimum (in)	Maximum (in)	Range (in)
3	I	1	26.5	58.8	32.3
		2	*	*	
		3	*	*	
	II	1	23.4	48.0	24.6
		2	28.0	43.7	15.7
		3	*	*	
	IV	1	24.5	26.0	1.6
		2	26.2	35.5	9.4
		3	29.0	49.6	20.5
5	I	1	33.2	53.3	20.0
		2	31.3	32.3	1.0
		3	*	*	
	II	1	20.3	43.3	23.0
		2	23.0	29.3	6.2
		3	26.6	29.5	2.9
	IV	1	29.5	32.9	3.4
		2	23.5	37.3	13.8
		3	23.3	51.7	28.4



(a) Load Trucks in Lane 1

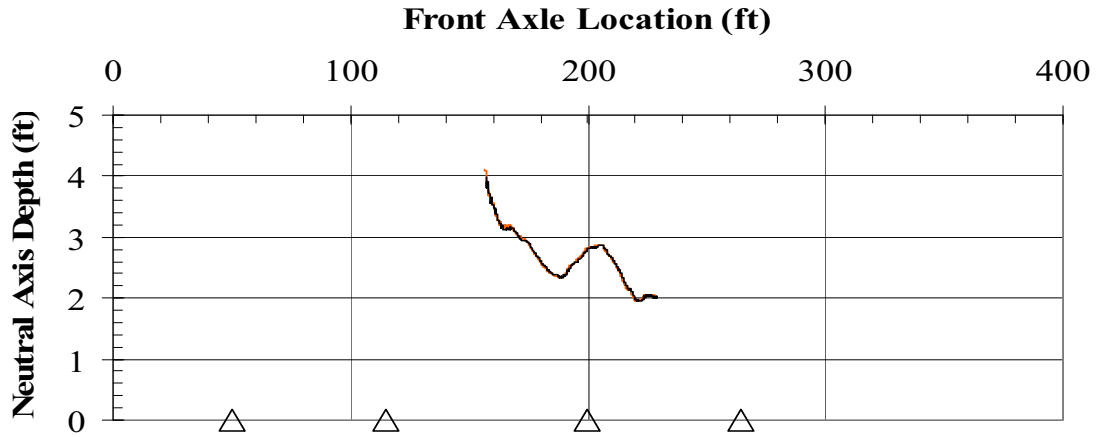


(b) Load Trucks in Lane 2

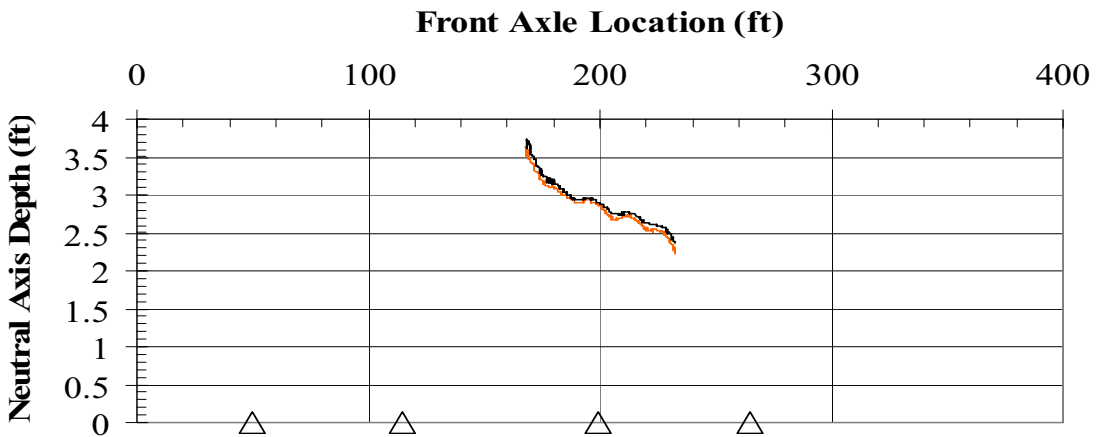


(c) Load Trucks in Lane 3

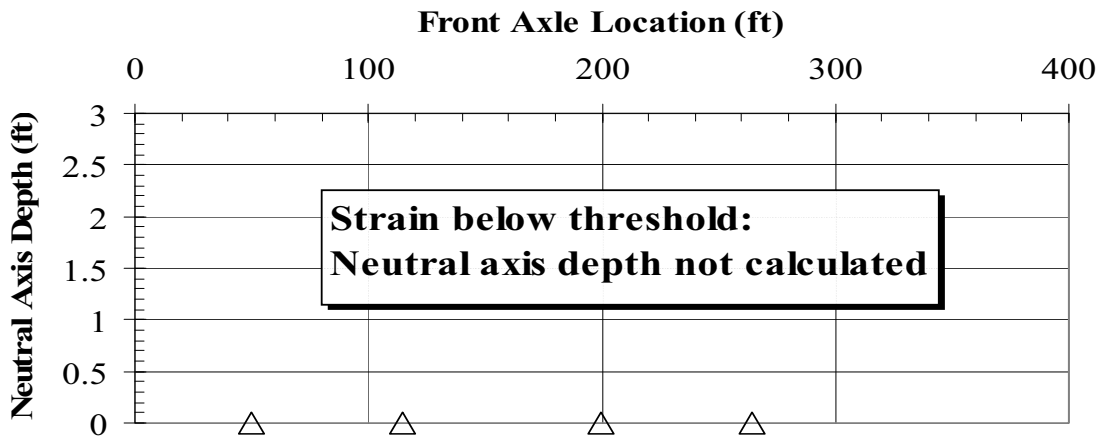
Figure 6.61: Neutral Axis Depth in Cross Section 3 Beam I



(a) Load Trucks in Lane 1

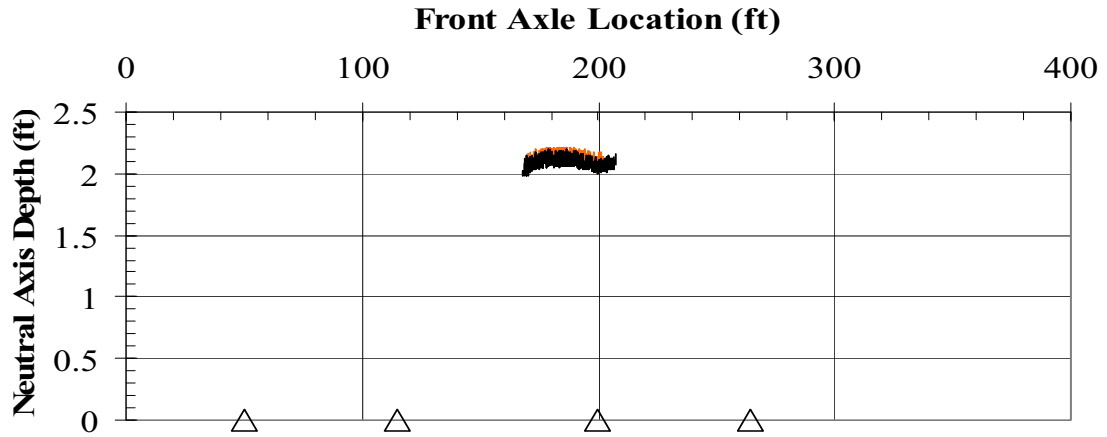


(b) Load Trucks in Lane 2

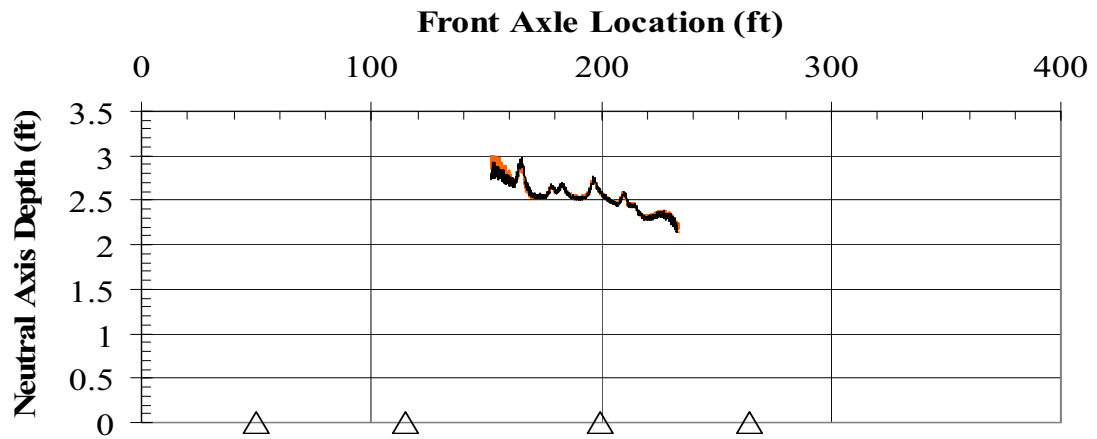


(c) Load Trucks in Lane 3

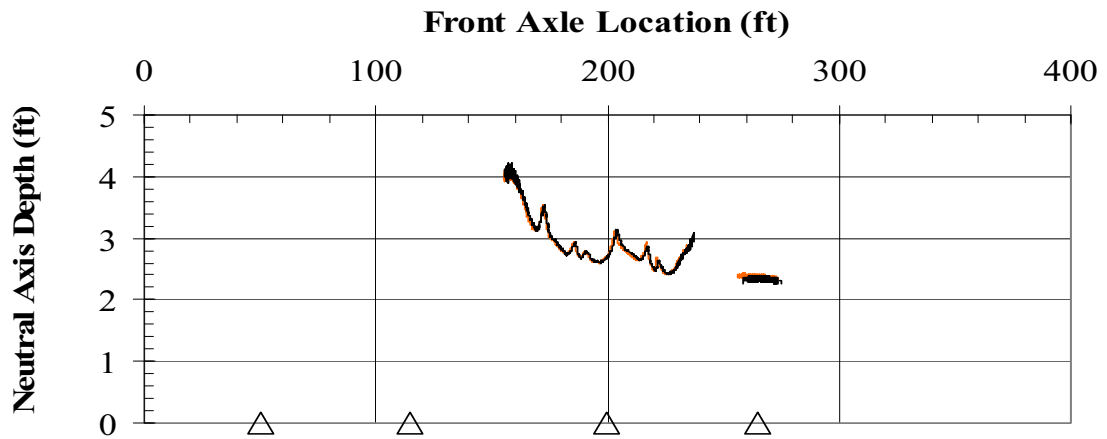
Figure 6.62: Neutral Axis Depth in Cross Section 3 Beam II



(a) Load Trucks in Lane 1

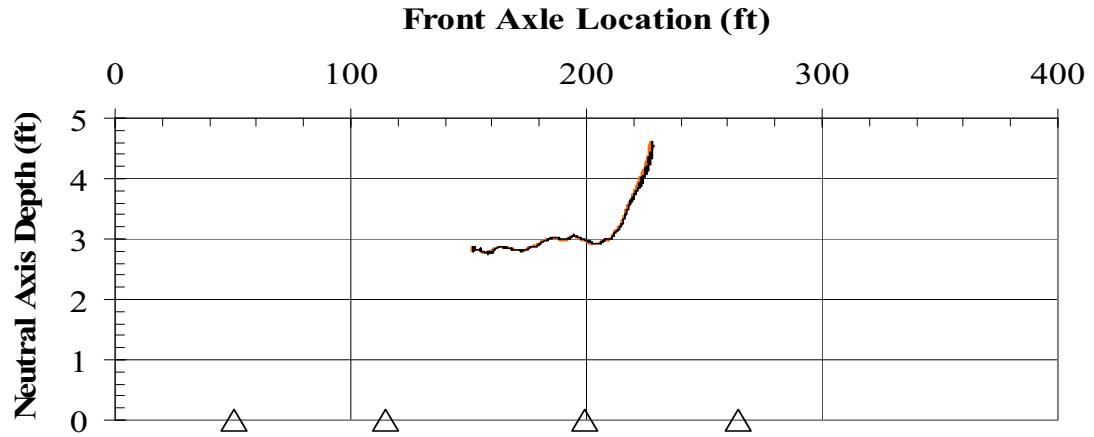


(b) Load Trucks in Lane 2

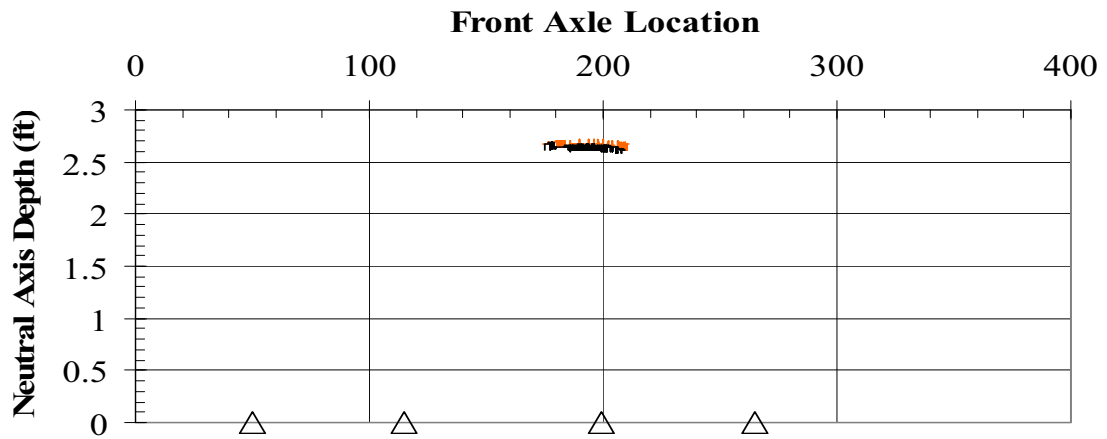


(c) Load Trucks in Lane 3

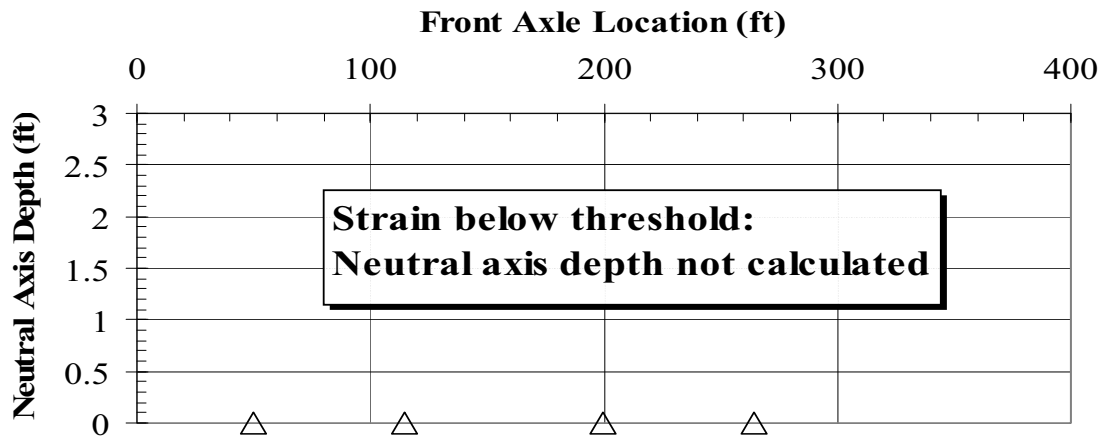
Figure 6.63: Neutral Axis Depth in Cross Section 3 Beam IV



(a) Load Trucks in Lane 1

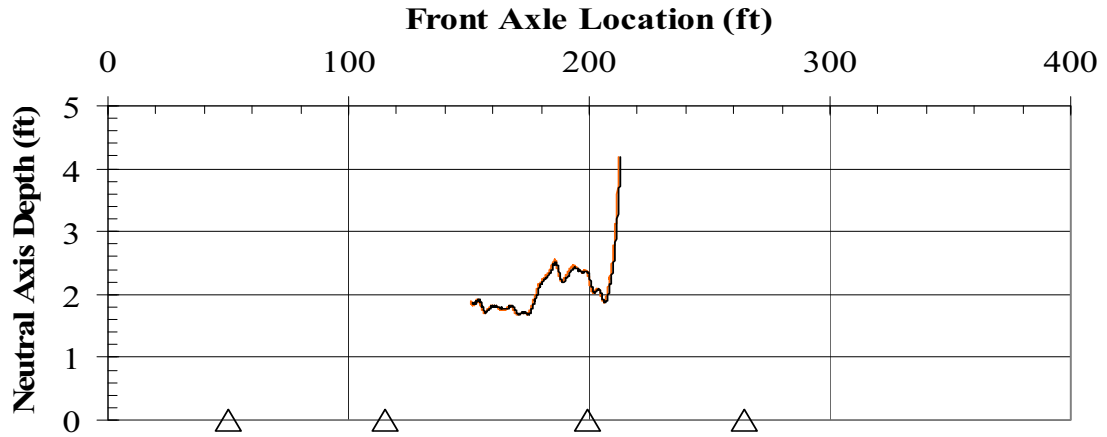


(b) Load Trucks in Lane 2

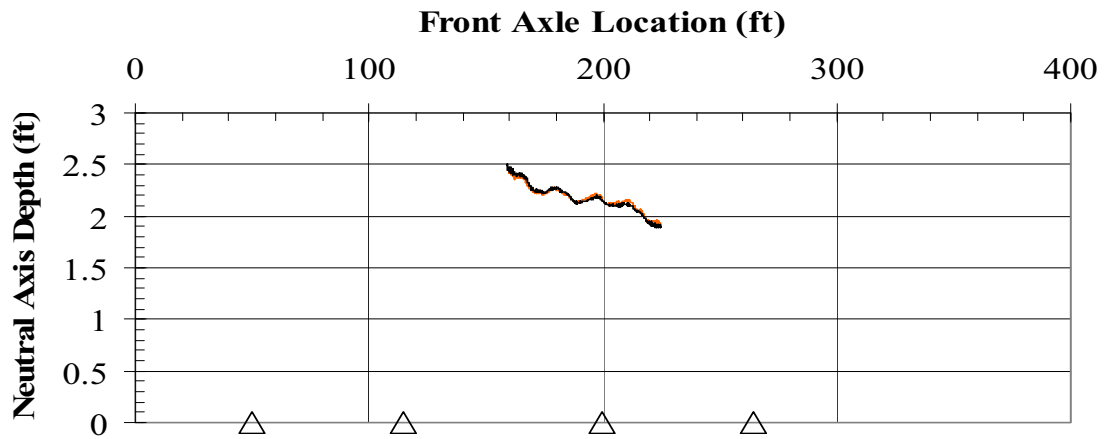


(c) Load Trucks in Lane 3

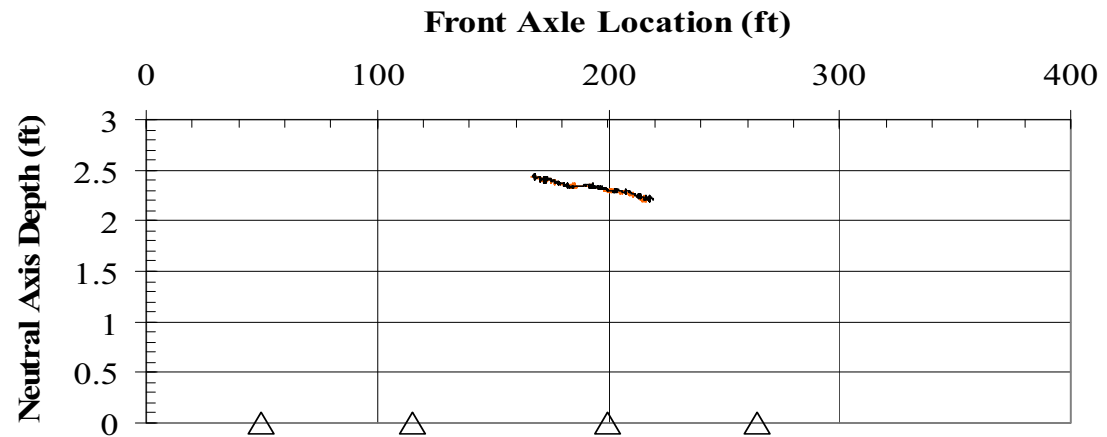
Figure 6.64: Neutral Axis Depth in Cross Section 5 Beam I



(a) Load Trucks in Lane 1

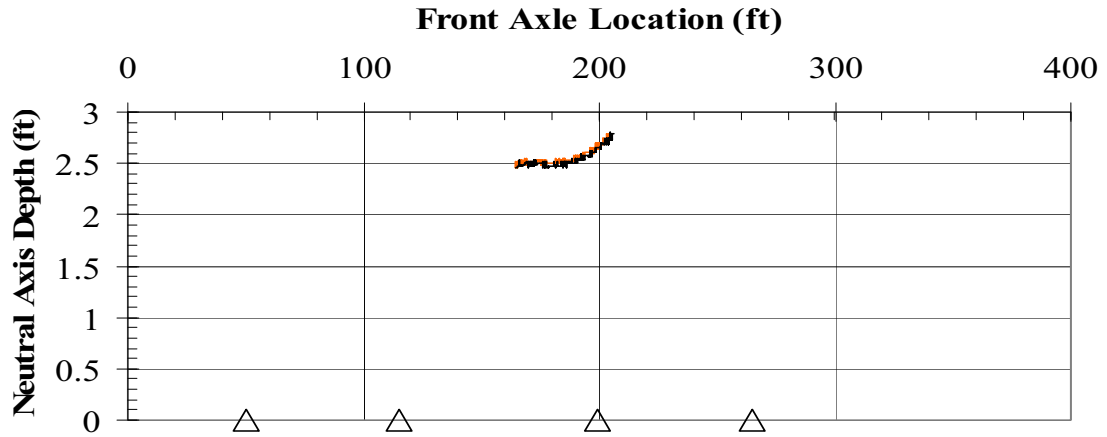


(b) Load Trucks in Lane 2

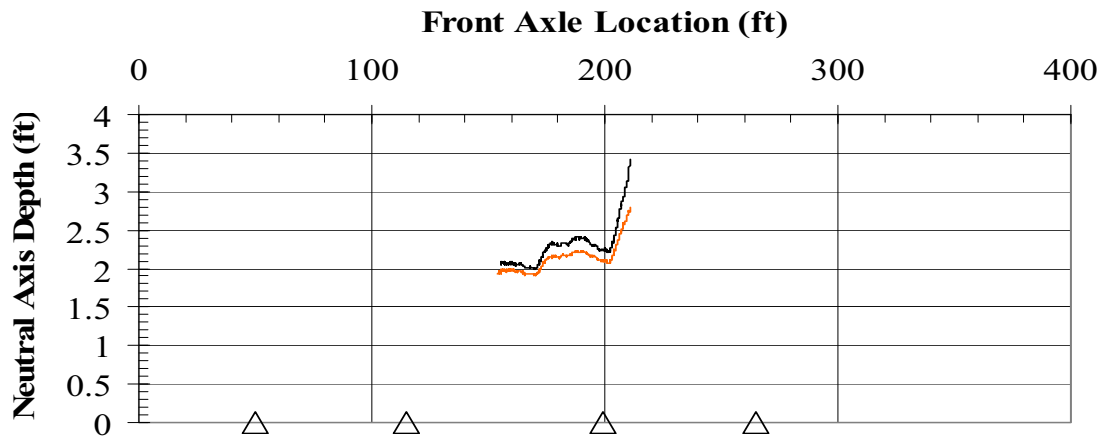


(c) Load Trucks in Lane 3

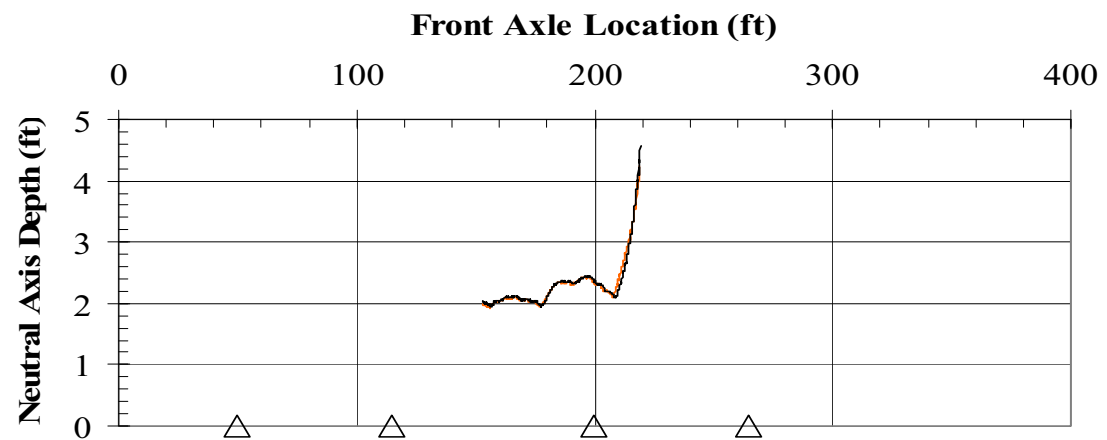
Figure 6.65: Neutral Axis Depth in Cross Section 5 Beam II



(a) Load Trucks in Lane 1



(b) Load Trucks in Lane 2



(c) Load Trucks in Lane 3

Figure 6.66: Neutral Axis Depth in Cross Section 5 Beam IV

6.2.5 Transverse Moment Distribution

The transverse distribution of moment is an important indicator of the load distribution among girders across the bridge deck and the efficiency of transverse diaphragms. Following the geometry of the bridge, girders were instrumented parallel to the bridge skew, such that each instrumented section was located the same distance away from the piers.

Moments were calculated using the measured strain history in this section as long as the lower strain gauge reading exceeded $21 \mu\varepsilon$ in the positive moment region and $8 \mu\varepsilon$ in the negative moment region, using the equations developed in Section 5.3.6. A lower strain threshold was used to compute moments near pier supports in the negative moment region because measured strains in the bottom strain gauges were very low in many of the girders in these cross sections. Based on the results of neutral axis depth in positive moment regions (Section 6.2.4.1), it was assumed that the concrete deck and steel girders acted compositely. It is recognized that full composite action may not be present in the bridge but the full composite action assumption was followed for simplicity.

6.2.5.1 Positive Moment Transverse Distribution

Positive moments were analyzed at mid-span of the bridge in cross section 4, corresponding to the section of maximum positive moment in the bridge. Positive moments were also recorded in cross sections 3 and 5. However, because gauges in these sections were aligned based on the location of damaged sections due to truck impact rather than at sections of calculated maximum moment, transverse moment plots were not created.

After examining the strain histories of all gauges in the cross section, a loading truck position of 190 ft (57.9 m) was selected because it generated the largest response in most girders. Plots from the three loaded lanes with the truck positioned at 190 ft were created (Figure 6.67) to compare the total moment across the bridge section with the loading truck located in each lane at the same distance from its starting point.

Girder I was not instrumented at mid-span in cross section 4. However, even without a moment data point at this exterior girder, several trends can be observed. All girders are engaged under loading; with some girders developing less moment than others, regardless of which lane is loaded. As expected, girders directly below the loaded lane have the highest moments, which is consistent with observations of lower gauge strain data (Section 6.2.2).

It is also apparent that moment generated in girders II and IV is smaller than moment in girder III. In Figure 6.67c, girder IV is closest to a loading axle; however, the generated moment is higher in adjacent girders. One explanation for this behavior is that diaphragms orthogonally connecting the skewed girders, were capable of distributing load to adjacent girders and resulted in higher generated moments in these girders.

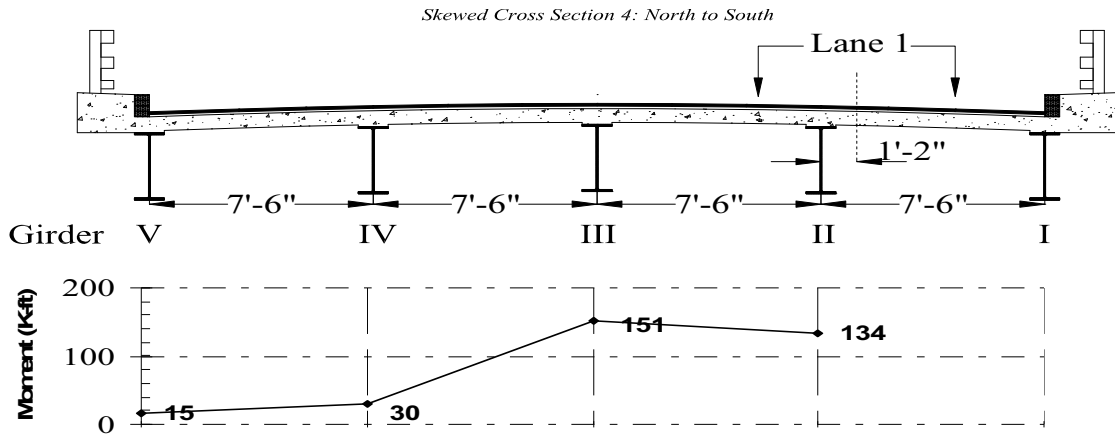
The measured transverse cross sectional moments are summarized in Table 6.21. Since girder I was not instrumented, an estimate of the moment in this girder was taken directly from a finite element analysis of this cross section as discussed in chapter 7. Using this estimate for moment in girder I, the total cross sectional moment varies by 145 K-ft or 30 percent, between lanes with the same truck position.

Table 6.21: Calculated Positive Moment in Cross Section 4 from Field Measurement

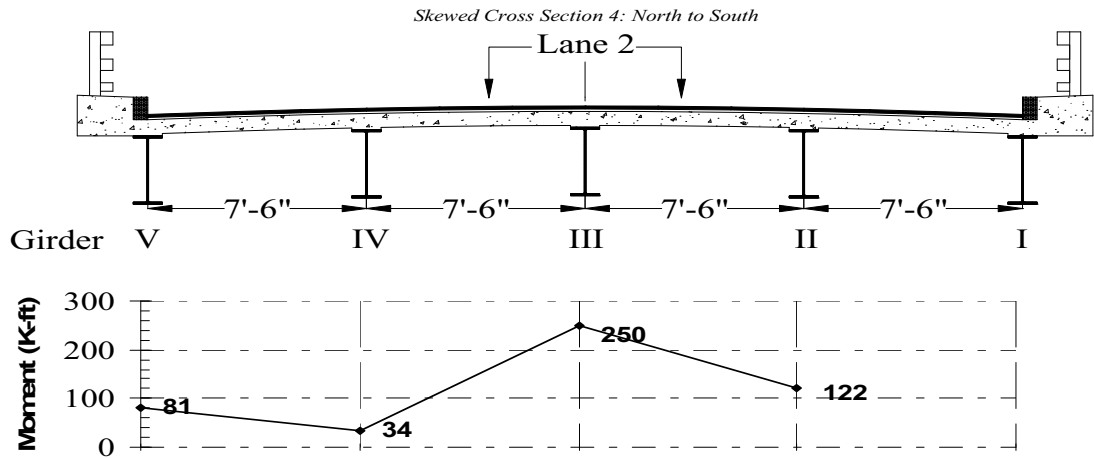
Cross Section	Lane	Figure	Load Truck Location (ft)	Moment Girders II-V Bridge (K-ft)	Estimate of Girder I Moment† (K-ft)	Total Moment (K-ft)
4	1	Figure 6.67a	190	330	144	474
	2	Figure 6.67b		487	56	543
	3	Figure 6.67c		613	6	619

†Girder I moment estimated from finite element analysis (Figure 7.4).

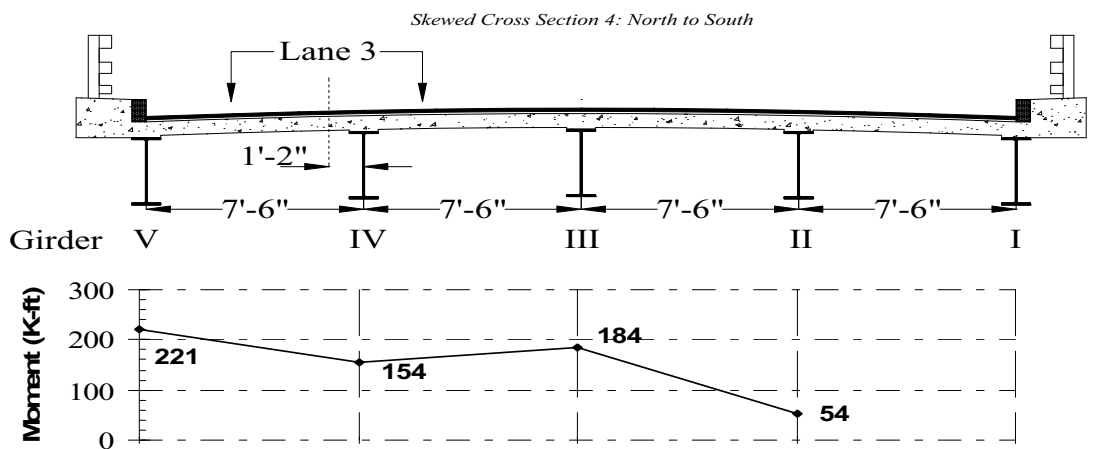
Note: Girder I was not instrumented in this cross section.



(a) Load Truck in Lane 1 (190 ft)



(b) Load Truck in Lane 2 (190 ft)



(c) Load Truck in Lane 3 (190 ft)

Figure 6.67: Calculated Moment in Cross Section 4

6.2.5.2 Negative Moment Transverse Distribution

Plots of moment distribution across the bridge in cross sections 1 and 7 were created to compare measured and calculated moments at locations of largest negative moments. Data was only recorded at these cross sections when the loading trucks traveled in the southbound direction.

Loading truck positions of 178 and 189 ft (54.3 and 57.6 m) were selected for analysis of moments near the north pier and south pier, respectively, because they produced the largest strain response in the girders during the tests. Figure 6.68 and Figure 6.69 plot the transverse moment distribution among girders when the loading trucks traveled in each of the three lanes and the front axle of the loading train was positioned at 178 and 189 ft (54.3 and 57.6 m), respectively.

From these plots, some of the exterior girders are observed to have zero moment, indicating that the measured strain in the lower gauge was below $8 \mu\epsilon$. With the loading trucks in lanes 1 or 3, the calculated moment is approximately zero in the exterior girder farthest from the loaded lane in most plots as would be expected. Occasionally, positive moments were also generated (Figure 6.68a) in the exterior girder farthest from the loaded lane.

While a positive moment is surprising in the negative moment region, it follows a trend in the data. The obtuse corners of the span produce moments that are more positive than would be expected for a non-skewed bridge. With the load truck in lane 2, moments in the acute corners (girder I of Figure 6.68b and girder V Figure 6.69b) are clearly negative, while moments in the opposite exterior girders of the same figures are positive or approximately zero.

In girders directly below a loaded lane, the moment in the exterior girder is smaller in the obtuse corner (Figure 6.68c and Figure 6.69a) than it is in girders located on the side corresponding to the acute corner of the bridge (Figure 6.68a and Figure 6.69c). Since this effect was observed when the loading trucks were in either lane 1 or 3, it is likely not caused by minor differences in weight from the left to right side of the loading trucks. The total cross-sectional moment with the loading trucks traveling along exterior lanes 1 or 3 was greater than when the loading trucks traveled along lane 2 (Table 6.22), even though the opposite exterior girders have higher positive moments.

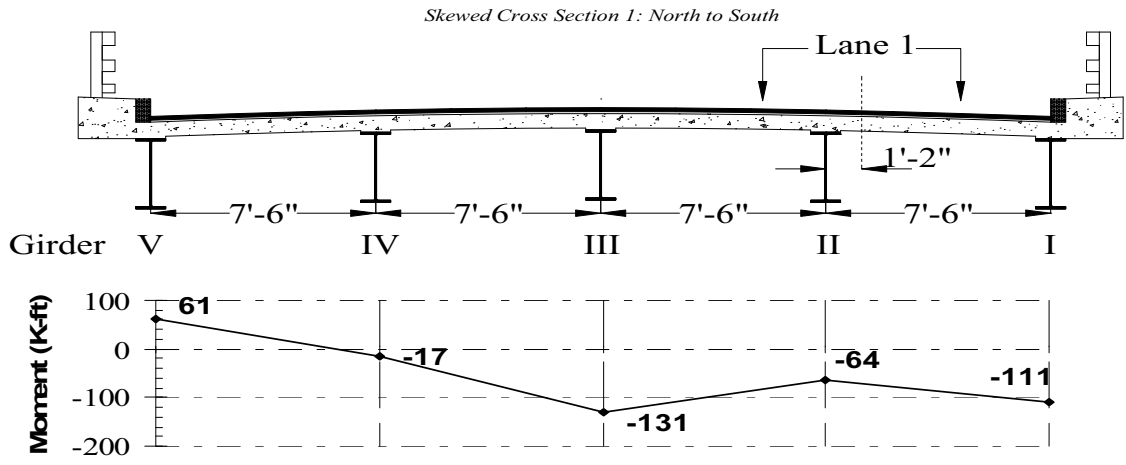
It can also be observed that moment is generated in fewer girders when compared to the mid-span cross section. At pier supports, diaphragms connect the girders following the skew of the piers. These diaphragms appear to have less of an affect on transverse moment distribution than diaphragms near mid-span. The higher bending stiffness caused by the proximity of these sections to the supporting piers is likely to have contributed to a faster transverse moment drop.

The total moment in each cross section is computed in Table 6.22. The differences observed in total cross sectional moment with a variation of loaded lane is surprising. For the same load placed in different lanes, the same bridge cross section moment would have been anticipated. This result may be related to the lower strain gauge threshold of $8 \mu\epsilon$ used to create the transverse moment plots. As described in Section A.4, small strain values can lead to higher error when moment is calculated. In

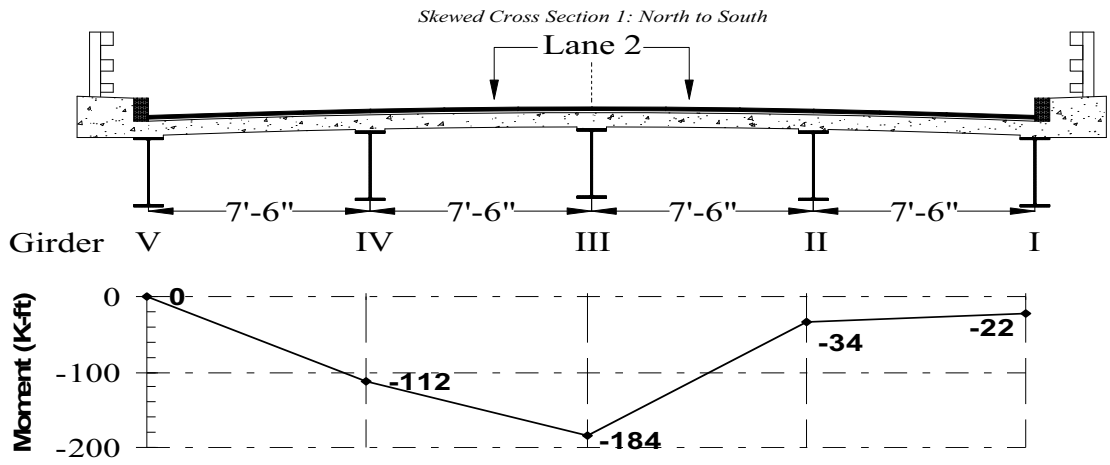
all other sections of this study a lower gauge strain threshold of $21 \mu\varepsilon$ has been used in calculations to produce satisfactory results. To compute moments for profiles in Figure 6.68 and Figure 6.69, 2 or 3 of the 5 girders had lower gauge strain measuring less than $21 \mu\varepsilon$.

Table 6.22: Calculated Negative Moments at Pier Locations from Field Measurement

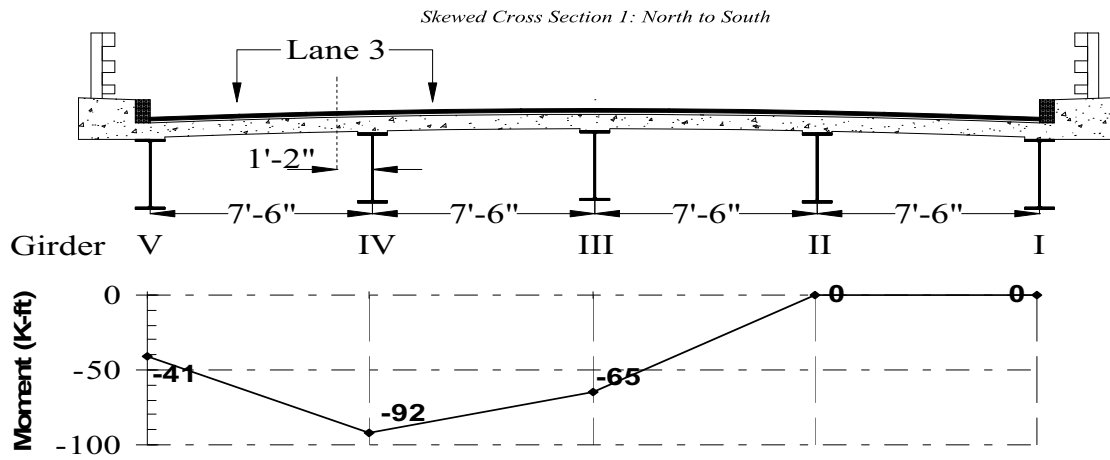
Cross Section	Lane	Figure	Load Truck Location (ft)	Calculated Moment (K-ft)	Number of Girders with Strain Less than $21 \mu\varepsilon$
1	1	Figure 6.68a	189	-262	2
	2	Figure 6.68b		-352	2
	3	Figure 6.68c		-198	2
7	1	Figure 6.69a	178	-351	2
	2	Figure 6.69b		-202	3
	3	Figure 6.69c		-260	3



(a) Load Truck in Lane 1 (189 ft)

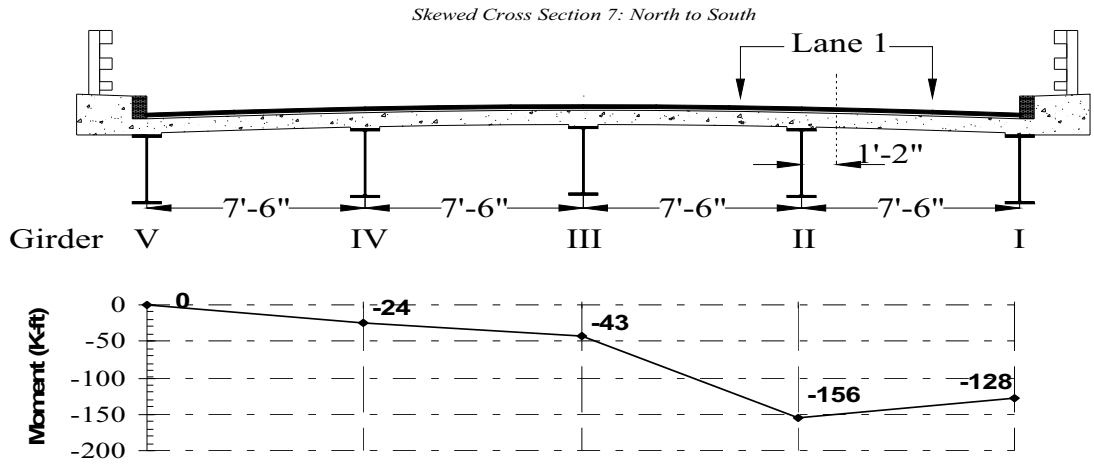


(b) Load Truck in Lane 2 (189 ft)

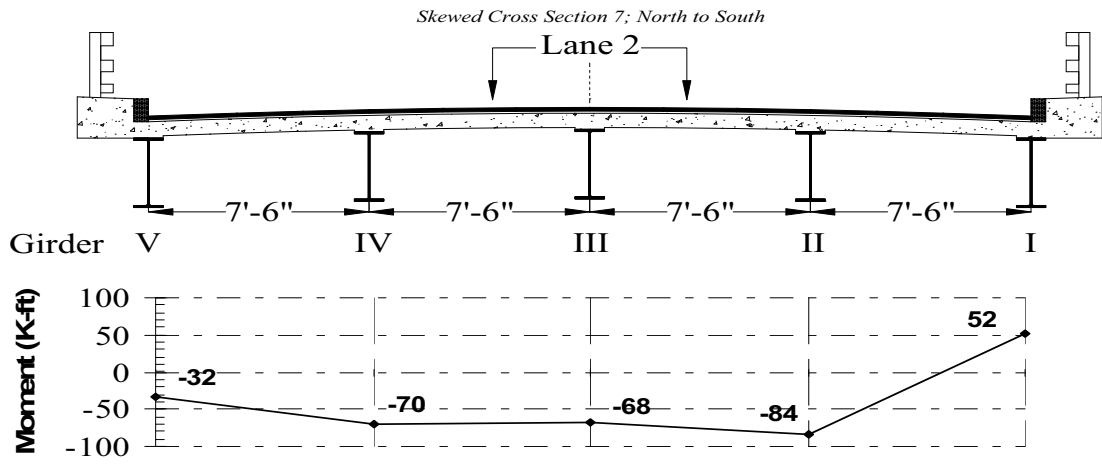


(c) Load Truck in Lane 3 (189 ft)

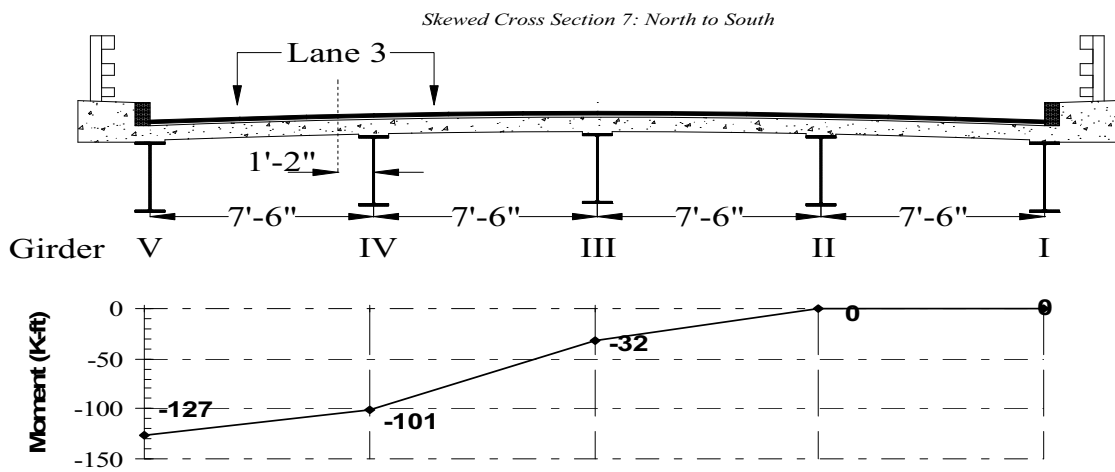
Figure 6.68: Calculated Moment in Cross Section 1



(a) Load Truck in Lane 1 (178 ft)



(b) Load Truck in Lane 2 (178 ft)



(c) Load Truck in Lane 3 (178 ft)

Figure 6.69: Calculated Moment in Cross Section 7

6.2.6 Beam Line Analysis

A beam line analysis was performed for the Weathersfield Bridge as was done for the Royalton Bridge to compare the total bridge moments generated at mid-span with that calculated using a simple model. It was first assumed that the beam line analysis could be used to represent the total moment in the cross section of the bridge. However, it was quickly determined that a beam line analysis had two fundamental flaws as it relates to the anticipated behavior of this type of bridge. The first is that girders at each cross section may not have been instrumented, making an exact comparison of results impossible. The second is that the beam line analysis does not account for effects of skew angle in the bridge.

Using a beam line model, the maximum positive live load moment calculated using the measured weight of the loading truck axles was found to be 881 K-ft (1,194 kN-m) in span 2, which occurs with the front axle of the loading trucks positioned at 178 ft (54.3 m) while traveling in the southbound direction. At mid-span, the maximum moment was 875 K-ft (1,186 kN-m) with the load truck at 176 ft (53.6 m). To compare with field results, the positive moment was calculated with the load truck at 190 ft to be 843 K-ft (1,142 kN-m). From a comparison in Table 6.23, it can be observed that the calculated positive moments using a beam line model grossly overestimated the measured moments during the field tests.

Similarly, the maximum live load negative moment in instrumented sections in span 2 is 700 K-ft (949 kN-m) from the north pier and 693 K-ft (940 kN-m) from the south pier, calculated with southbound load truck positions of 178 and 189 ft (54.3 and 57.6 m), respectively. As for the positive moment comparisons, these moments are much higher than those determined from the load tests (see Table 6.23).

Since the beam line analysis resulted in very poor correlation with moment data determined from the field tests, a three-dimensional finite element model was constructed to analyze the Weathersfield Bridge as described in Chapter 7.

Table 6.23: Beam Line Analysis Moment Comparison

Cross Section	Lane	Truck Position (ft)	Beam Line Analysis (K-ft)	Calculated Moment from Field Data (K-ft)	Percent Difference (%)
1	1	189	-693	-262	165
	2			-352	97
	3			-198	250
4	1	190	843	474	78
	2			543	55
	3			619	36
7	1	178	-700	-351	99
	2			-202	247
	3			-260	169

Note: Shaded areas indicate that not all girders were instrumented in cross-section; moment was estimated in girder I. (see Section 6.2.5.1)

6.2.7 AASHTO Distribution Factor Comparison

The live load distribution factors used by AASHTO in bridge design for one loaded lane can be compared with the transverse distribution of moments measured during the load tests. The distribution factor for interior girders can be calculated using Equation [6.19a] from AASHTO LRFD Table 4.6.2.2.2b-1, which includes multiple presence factors (*AASHTO LRFD Bridge Design Specifications*). The distribution factor for exterior girders (AASHTO Table 4.6.2.2.2.1-1) was calculated using the lever rule, and multiplied by a multiple presence factor of 1.2 for one lane loaded. For comparison purposes, wheel load distribution factors included in the AASHTO Standard Specification (AASHTO

For bridges with a skew angle greater than 10 degrees AASHTO table 4.6.2.2.2e-1 permits a reduction in moment distribution factor with a reduction factor found using Equation [6.22]. The Weathersfield skew reduction factors are equal to 0.94 and 0.93 for positive and negative moments, respectively, for a bridge skew angle of 41.91°. Calculated distribution factors (g) for moments induced by one or two loaded lanes in the Weathersfield Bridge using the *AASHTO LRFD Specification* (2007), including the skew reduction factor, and *AASHTO Standard Specifications* (2002), are listed in Table 6.24. The wheel load distribution factors in the *AASHTO Standard Specification* are equal to $S/7.0$ or $S/5.5$ for one or two traffic lanes, respectively (S , the girder spacing in feet, is 7.5). Wheel load moments are obtained dividing the beam-line model moments (obtained using the test truck) by two.

$$g_{\text{int-1}} = 0.06 + \left(\frac{S}{14}\right)^{0.4} \left(\frac{S}{L}\right)^{0.3} \left(\frac{K_g}{12.0 \cdot L \cdot t_s^3}\right)^{0.1} \quad [6.19a]$$

$$g_{\text{int-2}} = 0.075 + \left(\frac{S}{9.5}\right)^{0.6} \left(\frac{S}{L}\right)^{0.2} \left(\frac{K_g}{12.0 \cdot L \cdot t_s^3}\right)^{0.1} \quad [6.20b]$$

$$K_g = \frac{E_B}{E_D} (I_g + A \cdot e_g^2) \quad [6.21]$$

$$1 - c_1 (\tan \theta)^{1.5} \quad [6.22]$$

$$c_1 = 0.25 \left(\frac{K_g}{12.0 \cdot L \cdot t_s^3}\right)^{0.25} \left(\frac{S}{L}\right)^{0.5} \quad [6.23]$$

Where:

A = Area of beam (in²)

E_B = Modulus of elasticity of beam material (ksi)

E_D = Modulus of elasticity of deck material (ksi)

e_g = Distance between centers of gravity of the basic beam and deck (in)

g_{int-1} = Distribution factor for interior girder, one loaded lane

g_{int-2} = Distribution factor for interior girder, two or more loaded lanes

I_g = Moment of inertia of the beam (in⁴)

K_g = Longitudinal stiffness parameter (in⁴)

L = Span length (ft)

S = Beam spacing (ft)

t_s = Depth of concrete slab (in)

θ = Skew angle (degrees)

Maximum moments of 875 and 700 K-ft (1,184 and 949 kN-m) were calculated from the beam line analysis (Section 6.2.6) for positive moment near mid-span and negative moments at pier supports, respectively. AASHTO design moments for interior and exterior girders using AASHTO distribution factors are listed in Table 6.24. Moments calculated on the *AASHTO Standard Specification* are more conservative than those used in *AASHTO LRFD Specification*.

Table 6.24: AASHTO Distribution Factors and Design Moment for Weathersfield Bridge Girders

Moment	Beam Line Analysis Moment (K-ft)	Girder Location	No. of Loaded Lanes	g LRFD	AASHTO LRFD Moment (K-ft)	g STD Spec	AASHTO STD Spec Moment (K-ft)
Positive	875	Interior	1	0.40	350	1.07	468
			2	0.56	490	1.36	595
		Exterior	1	0.39	341	—	—
Negative	-700	Interior	1	0.42	-294	1.07	375
			2	0.58	-406	1.36	476
		Exterior	1	0.39	-273	—	—

The maximum field positive and negative moments in both interior and exterior girders were then compared with design moments from *AASHTO LRFD Specification*, assuming that the trucks used for the load tests were the design vehicles. Values shown in Figure 6.67 and Figure 6.69 indicate moments in interior and exterior girders corresponding to sections 4 and 7 for positive and negative moments, respectively. For positive moment (Figure 6.67), values in girder III were the highest observed in the field. Similarly, values in girder II (Figure 6.69) were the highest values corresponding to negative moment. To compare results with AASHTO moments for more than one loaded lane, the two highest moments obtained in the critical girder (girder III for positive moment or girder II for negative moment) for different loaded lanes were added.

The maximum measured positive moment in exterior girders was 221 K-ft (300 kN-m) at mid-span with the loading vehicle in lane 3. It should be noted that only one of the exterior girders was instrumented near the positive moment region. Had the other girder been instrumented, it is possible a higher moment could have been observed. The maximum negative moment for exterior beams was found to be 195 K-ft (264 kN-m) in girder V at the north pier with the load vehicle at 197 ft (60.0 m) in lane 3.

As listed in Table 6.25, moments calculated using the *AASHTO LRFD* distribution factors for interior girders in positive and negative moment regions are conservative. Field negative moments, in particular, are more conservative than those obtained for positive moment in span 2.

Table 6.25: Comparison of Measured Moment to AASHTO LRFD Moment

Moment	No. of loaded lanes	Field Moment	AASHTO LRFD Moment	Field Moment/ AASHTO LRFD Moment
		(K-ft)	(K-ft)	(%)
Positive	1 lane	250	350	71
	2 lanes	434	490	89
Negative	1 lane	-156	-294	53
	2 lanes	-240	-406	59

CHAPTER 7 - BRIDGE MODELING

7.1 Model Description

A 3-dimensional linear-elastic finite element model of the Weathersfield Bridge was created using SAP2000 version 11.0.6. The model was created after the limitations of a beam line analysis were observed when results were compared with moments measured in the field tests (Section 6.2.6). The geometry including member lengths and locations as well as the skew angle were taken from bridge plans (Section 3.2.2).

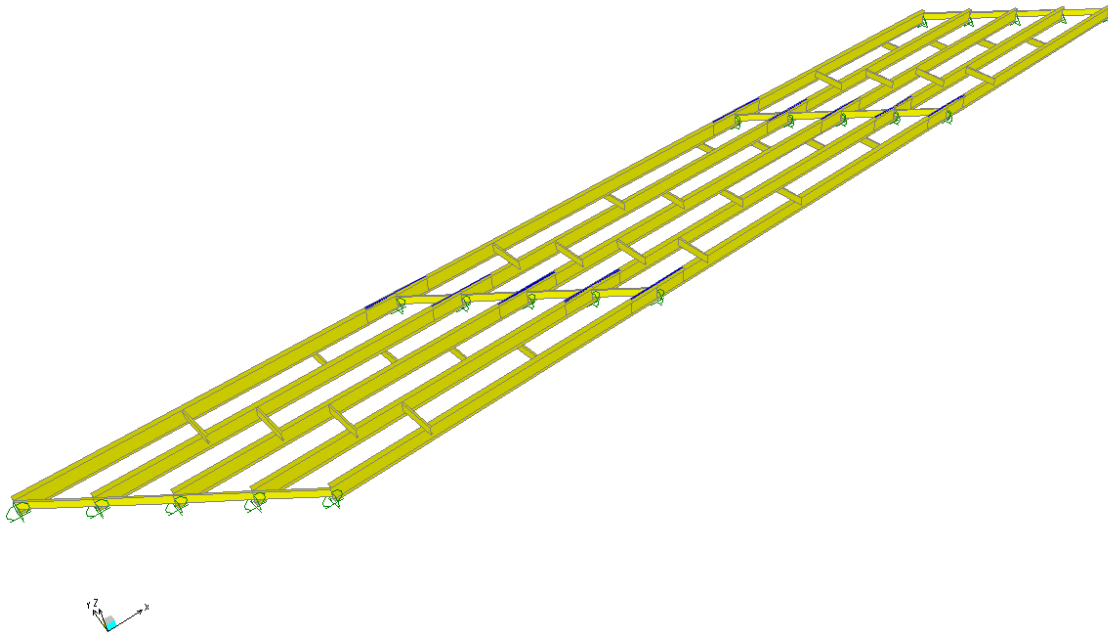
7.1.1 Elements

Two-node frame elements with six degrees of freedom at each node were used to model the steel girders in the superstructure. Four-node shell elements with six degrees of freedom at each node were used to model the concrete deck. The frame elements consisting of W36x170 girders and C18x42.5 diaphragm steel shapes used to model the steel elements part of the bridge superstructure were specified using program default beam element shapes (Figure 7.1a). Sections with top and bottom cover plates near interior supports were created using custom build-up member properties.

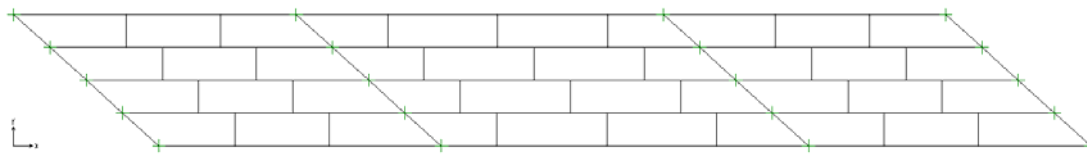
Frame elements used to model the bridge girders were fully continuous (all degrees of freedom) at joints between elements to allow moment transfer. Frame elements used to model diaphragms between girders, were modeled as pin-connected elements at each end, consistent with the connections observed in the field (shear tabs).

Thin shell elements were used to model the concrete bridge deck (Figure 7.1c) assuming un-cracked section properties. Thin-shell elements were used because they are capable of translational and rotational degrees of freedom, and support force and moment calculation. A slab depth consistent with bridge plans of 7.5 in (191 mm) was specified for bending.

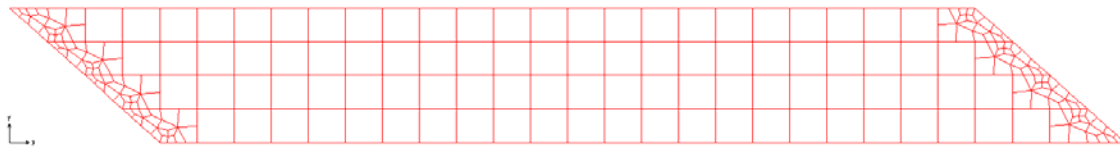
The shells used in the middle portion of the bridge model (away from supports) were discretized into rectangular shapes with approximate dimensions of 8.23 ft (2.51 m) longitudinally and 7.5 ft (2.28 m) transversely. The shells near abutments were irregular pentagon shapes, and were automatically meshed by the program. The longitudinal discretization is approximately 1/10 of the span length for the center span. While the use of rectangular shells is preferred for this type of finite element model, the areas discretized into non-rectangular shapes are near abutments walls, which are far away from the center-span area of interest. Therefore, the use of non-rectangular shell elements to account for the skew is not anticipated to adversely affect the finite element results.



(a) Beam Elements (3 Dimensional View)



(b) Beam Elements (Plan View)



(c) Shell Elements (Plan View)

Figure 7.1 Geometry of Elements used in Finite Element model of Weathersfield Bridge

7.1.2 Material Properties

Material properties assumed in the finite element model (listed in Table 7.1) are consistent with commonly accepted values whenever little or no information about the actual material properties is available. These properties were also consistent with those used when calculating moments from field data (Section 5.3.6).

Table 7.1: Element Material Properties

	W36x170 Girders	W36x170 Girders With Cover Plates	C18x42.5 Diaphragms	Deck
Element Type	Frame	Frame	Frame	Thin Shell
Material Type	A36 Steel	A36 Steel	A36 Steel	Concrete
Poisson's Ratio	0.3	0.3	0.3	0.2
Modulus of Elasticity (ksi)	29,000	29,000	29,000	3,605
Depth (in)	36.2	37.2	18	7.5
Moment of Inertia (x-x axis) (in ⁴)	10,500	13,867	554	
Moment of Inertia (y-y axis) (in ⁴)	320	403	14.3	
Cross Sectional Area (in ²)	50.1	60.1	12.6	

7.1.3 Support Conditions

The Weathersfield Bridge is supported at four locations along each girder: north abutment, north pier, south pier, and south abutment. The north abutment and both piers (Figure 3.21b and c) are modeled with rollers that fix translation in the gravity directions and have free rotation. The south abutment support (Figure 3.21a) is modeled as a pin with fixed translation in all directions but has free rotation. These support conditions are consistent with the supports observed at the bridge during the field tests.

7.1.4 Rigid Links

Rigid links were used to connect the thin shell deck to girder frame elements. The links allow connection between girder nodes and deck nodes, which are not located at the same spatial location in the model. The vertical difference between the girder centerline and the center of the concrete slab that physically exists in the bridge is captured by connecting the girder nodes and shell (deck) nodes through the use of rigid

links. The links had all degrees of freedom constrained to the actual element nodes, thereby enforcing composite action between the deck and girder as was assumed for interpretation of field test results.

Rigid links are 22.85 in (581 mm) long and are spaced 8.23 ft (2.51 m) longitudinally along each girder, located at the corners of shell elements. Each link on interior girders is connected to 4 shells, and links on exterior girders are connected to 2 shells. Deformation and rotation in all directions of the link are fixed.

7.1.5 Lane Definition

Three lanes were defined from layout lines across the bridge transversely, corresponding to measured lane locations in the field test (Figure 7.2). Live loads from the test truck were applied to shell elements lying below each loaded lane. The lanes were defined to be 10 ft (3.05 m) wide, and have an initial station located 50 ft (15.24 m) from the edge of the bridge, where the left front tire of the loading truck was positioned during the load test. By defining lanes in this manner, stations in the model correspond exactly to loading truck positions used in evaluation of field test results. The ending station of each lane extended beyond the bridge end to ensure that the rear axle of the rear loading truck was completely off the bridge at the last load step.

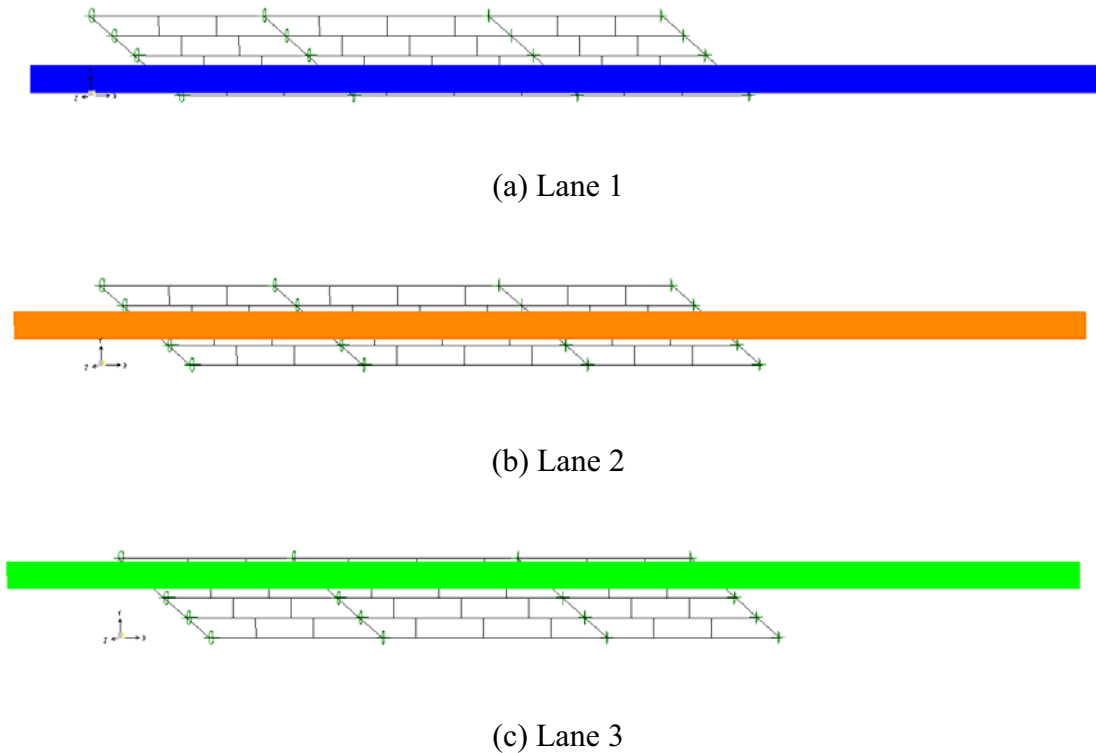


Figure 7.2: Truck Load Lanes in Model (Southbound - Left to Right)

7.1.6 Truck Configuration and Loading

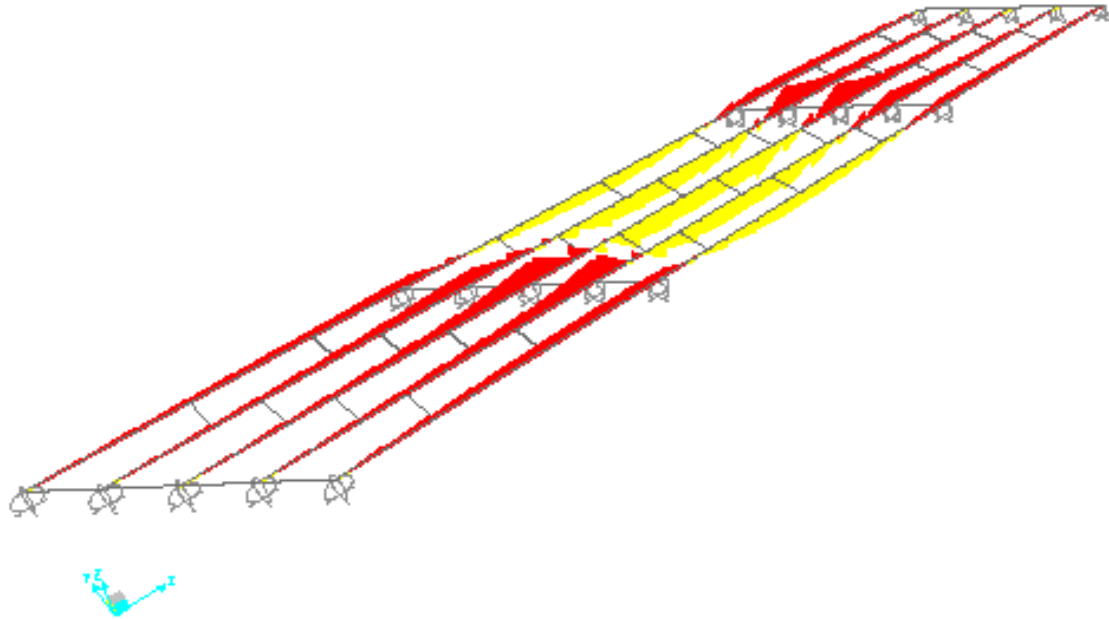
Axle dimensions and spacing of both load trucks were input to SAP2000 using actual measurements of the loading trucks taken in the field prior to testing (Figure 4.12). Point loads were defined at each tire location with a magnitude equal to half the total axle load. The truck loading in the model was chosen to start 50 ft (15.24 m) before the northbound abutment and proceeded forward toward the south abutment (southbound).

Bridge response was calculated at each load step consisting of truck positions placed at 1 ft (305 mm) increments, with the step corresponding to the location of the front axle. This refinement was chosen to correspond with the load steps calculated from field results. From the model, forces in the frame and shell elements were determined at each increment.

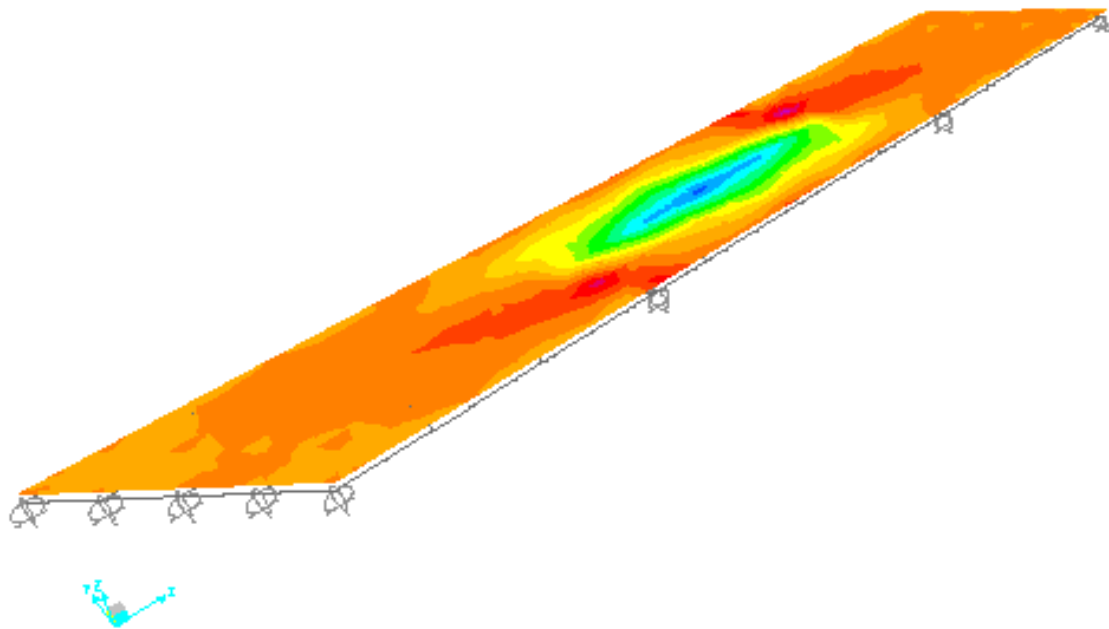
7.1.7 Moments

Moments in the finite element model can be viewed at any location in frame elements corresponding to a load step increment of 1 ft (305 mm). Moment envelopes along the beam elements can also be plotted to find the maximum and minimum moment at any location. For comparison with field results, moments are selected at instrumented cross sections at the load steps equal to the truck position. Moment diagrams for all beam elements in the bridge at each location of interest (Figure 7.3a) were created from the model to represent positive and negative bending.

Moments in the shell elements within the assumed effective bending width (Section 5.3.6.2) were included with the total moment at girder cross sections. From the model (Figure 7.3b), moments were computed per foot of width in the shell element. Using an average moment at each cross section in the shell, the total moment in the cross section was determined. Consideration of shell elements moments to the total cross sectional moment was found to impact moments by up to 8 percent (Table 7.2).



(a) Moments in Beam Elements



(b) Moments in Shell Elements

Figure 7.3: Captured Images of Moments Finite Element Model (Truck at 189 feet in lane 2)

Table 7.2: Effect of Including Shell Moments in Finite Element Model

Cross Section	Lane	Figure	Truck Position (ft)	Moment in Girder (K-ft)	Moment in Shell (K-ft)	Shell Moment/Girder Moment (%)
1	1	a	189	-323	-30	-8
	2	b		-302	-7	-2
	3	c		-313	9	3
4	1	a	190	369	18	5
	2	b		351	31	8
	3	c		381	1	0
7	1	a	178	-300	7	2
	2	b		-290	-18	-6
	3	c		-311	-22	-7

7.2 Finite Element Model Comparison with Beam Line Analysis

The beam line analysis (Section 6.2.6) can also be compared with finite element analysis results. The beam line moments are 96 to 138 percent greater than the finite element model (Table 7.3). As a result the finite element model more closely correlates with results of the field testing, and is preferred over the beam line analysis for bridges with an irregular geometry such as the Weathersfield Bridge.

Table 7.3: Comparison of Beam Line Analysis to Finite Element Model Moment

Cross Section	Lane	Truck Position (ft)	Beam Line Analysis (K-ft)	Finite Element Model Moment (K-ft)	Percent Difference (%)
1	1	189	-693	-353	96
	2			-309	124
	3			-304	128
4	1	190	843	387	118
	2			382	121
	3			384	120
7	1	178	-700	-294	138
	2			-308	127
	3			-333	110

7.3 Model Comparison with Field Results

Moments from the finite element model and the field test data at each girder location were plotted for comparison. Unlike the beam line analysis which can only be used directly to compare moment for an entire cross section, individual moment in each girder can be directly compared with the finite element model.

The general shape of transverse distribution of girder moments from the finite element analysis was found to compare favorably with field test results. The magnitude of the moments from the finite element model, however, over estimated field results in some locations and under estimated girder moments in others. These comparisons are presented and discussed in the following sections.

7.3.1 Positive Moment Comparison with Field Results

Moments in the positive moment region of the finite element model (lighter lines and boxed numbers) are plotted with moments measured from field results (darker lines) in Figure 7.4. The finite element model predicts a smooth, multi-linear distribution among girders in each cross section. Moments are highest under the loaded lane and gradually decrease away from applied loads as would be expected.

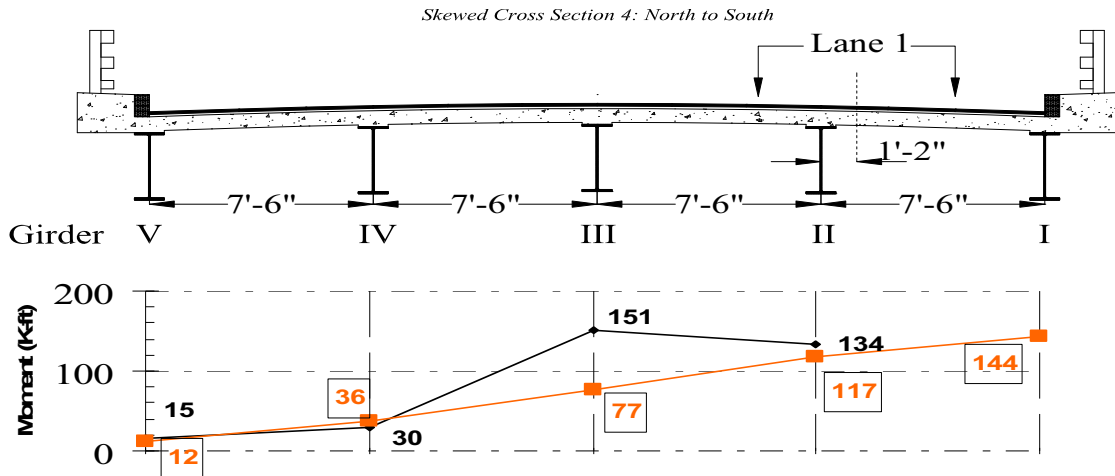
The total moment for both the finite element model and field moments are compared in Table 7.4, only including girders II through V, since girder I was not instrumented. The percent difference between the model and field results were calculated to vary between 17 and 37 percent for the different loaded lanes.

In Figure 7.4 the moment plot in the model matches closely with results from the field tests, with the exception of girder III in which a larger field moment was measured. In Figure 7.4b, the finite element model results show a nearly symmetrical moment distribution among girders about the center girder (girder III). Field moments were found to be higher in girder II, III and V but lower in girder IV. The finite element model moments were also lower than measured in the field for all instrumented girders as shown in Figure 7.4c.

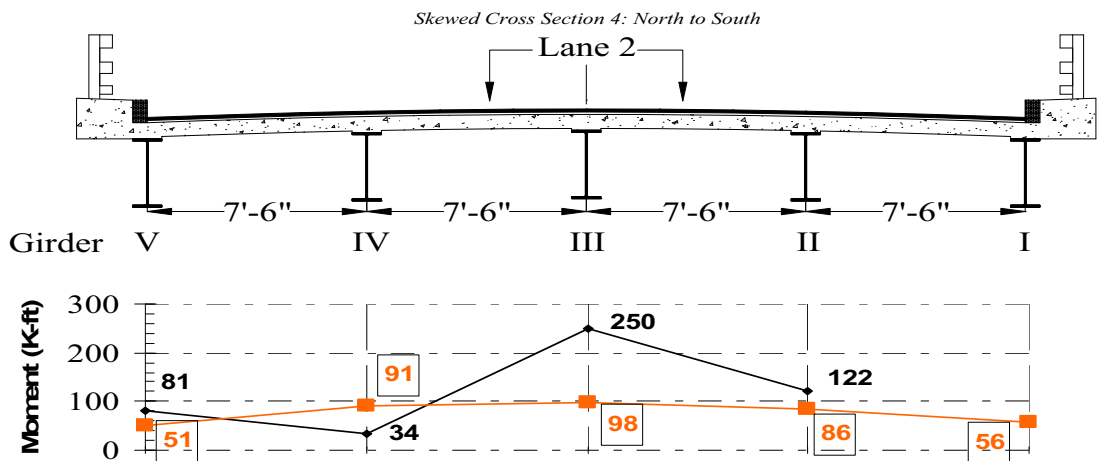
Table 7.4: Comparison of Finite Element and Field Moments in Positive Moment Region (Girders II-V)

Cross Section	Lane	Figure	Truck Position (ft)	Finite Element Calculated Moment (K-ft)	Moments Calculated From Field Test Data (K-ft)	Percent Difference (%)
4	1	Figure 7.4a	190	387	330	17
	2	Figure 7.4b		382	487	-22
	3	Figure 7.4c		384	613	-37

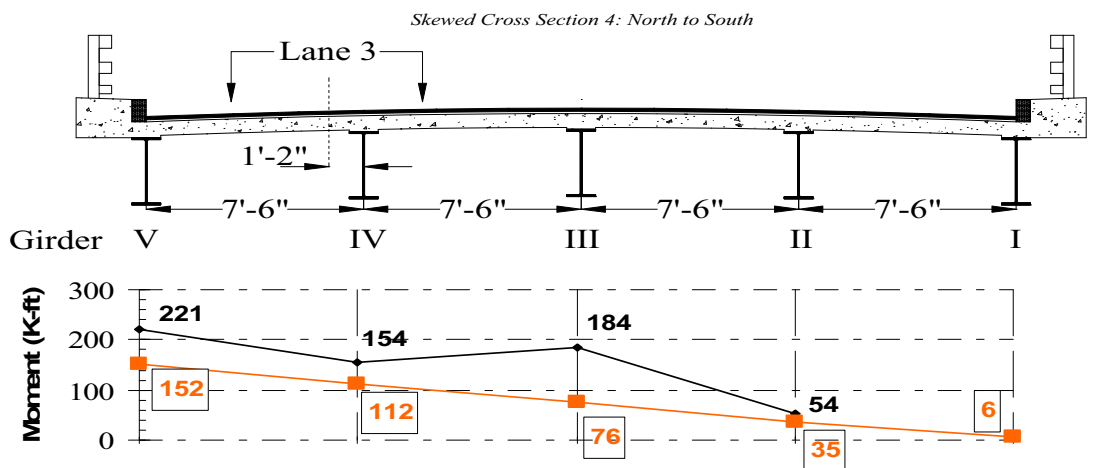
Note: Girder V moments not considered in finite element or field results



(a) Load Truck in Lane 1 (190 ft)



(b) Load Truck in Lane 2 (190 ft)



(c) Load Truck in Lane 3 (190 ft)

Figure 7.4: Comparison between Measured and Calculated Moments in Cross Section 4

7.3.2 Negative Moment Comparison with Field Results

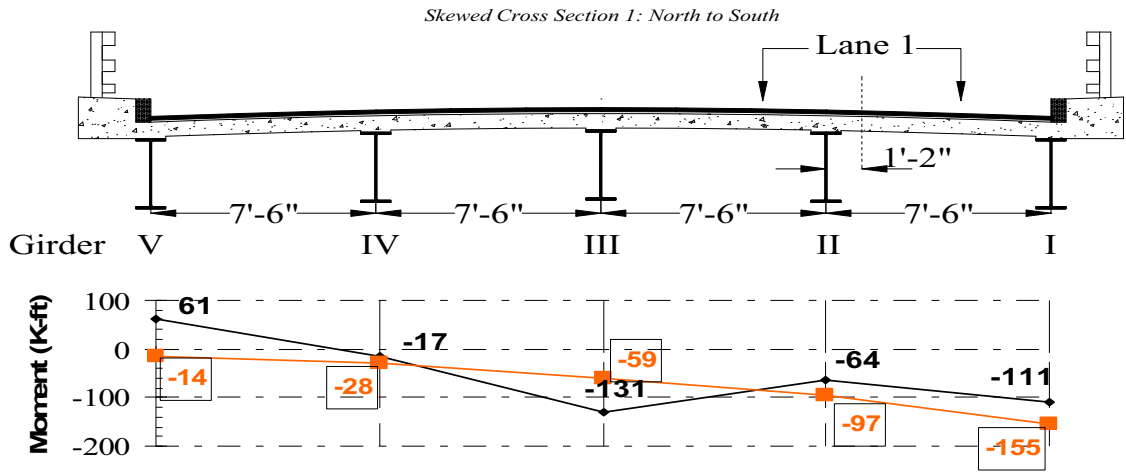
The moments in the negative moment region near pier supports are plotted in Figure 7.5 and Figure 7.6 for the south and north piers, respectively. The general shape of the transverse moment distribution calculated by the finite element model, approximately followed the measured field results. The difference of total cross sectional moment in the negative moment region varied between 12 and 58 percent between the finite element model and field moments (Figure 7.4). While this difference is greater than mid-span percentages, the magnitude of negative moments at piers is smaller than at mid-span, which results in more error in the measurements.

Moments from the finite element model analysis were higher than field results with the trucks in lane 1 and 3 of cross section 1 (Figure 7.5a and c). With loading positioned in lane 2 (Figure 7.5b), the model under predicted field results in interior girders and over predicted moment in exterior girders.

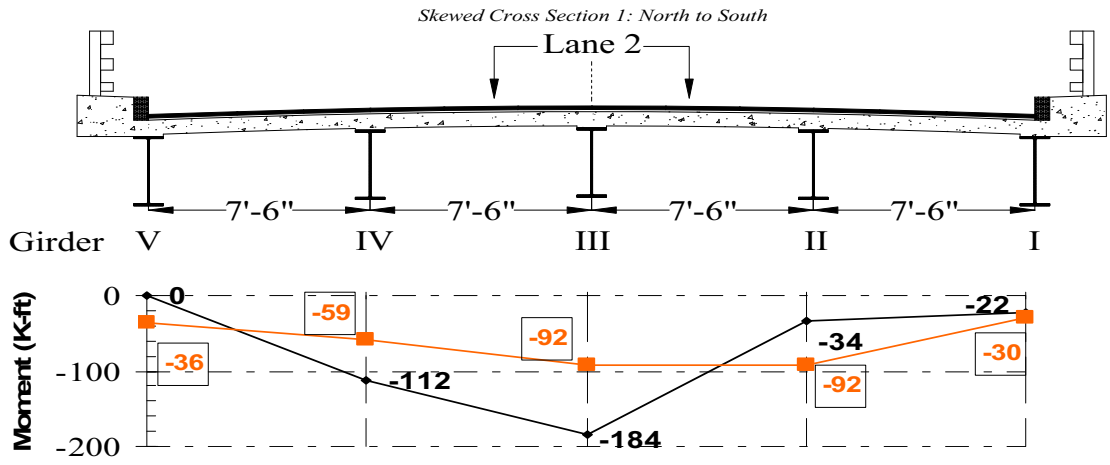
The model results in cross section 7 (Figure 7.6) over estimated the total cross sectional moment with the load truck in lane 2 and 3, and under estimated field moment in lane 1. The shape of the moment distribution from each plot closely matched the field results, including an exact match in girder V with the truck position in lane 2.

Table 7.5: Comparison Finite Element and Field Moments in Negative Moment Region

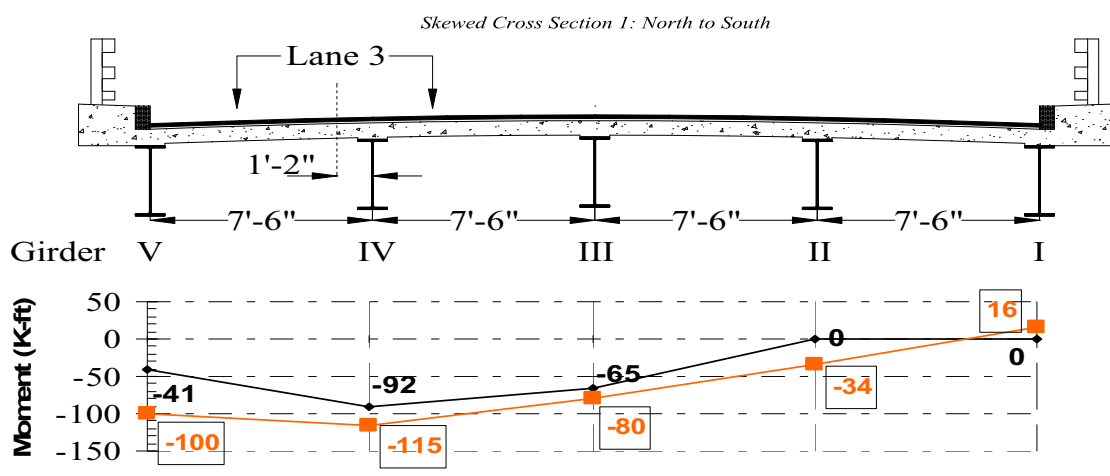
Cross Section	Lane	Figure	Truck Position (ft)	Finite Element Calculated Moment (K-ft)	Moments Calculated From Field Test Data (K-ft)	Percent Difference From Field Measurement (%)
1	1	Figure 7.5a	189	-353	-262	35
	2	Figure 7.5b		-309	-352	-12
	3	Figure 7.5c		-304	-198	54
7	1	Figure 7.6a	178	-294	-351	-16
	2	Figure 7.6b		-308	-202	52
	3	Figure 7.6c		-333	-260	28



(a) Load Truck in Lane 1 (189 ft)

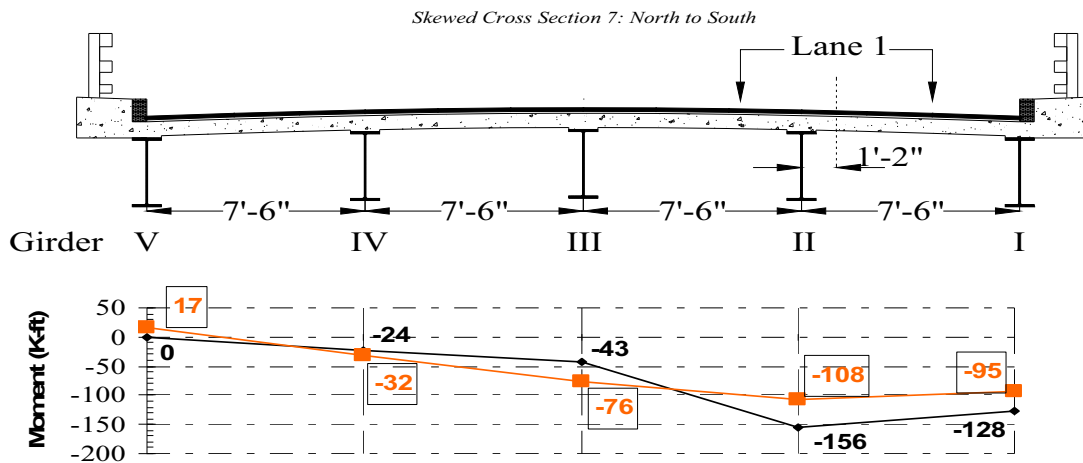


(b) Load Truck in Lane 2 (189 ft)

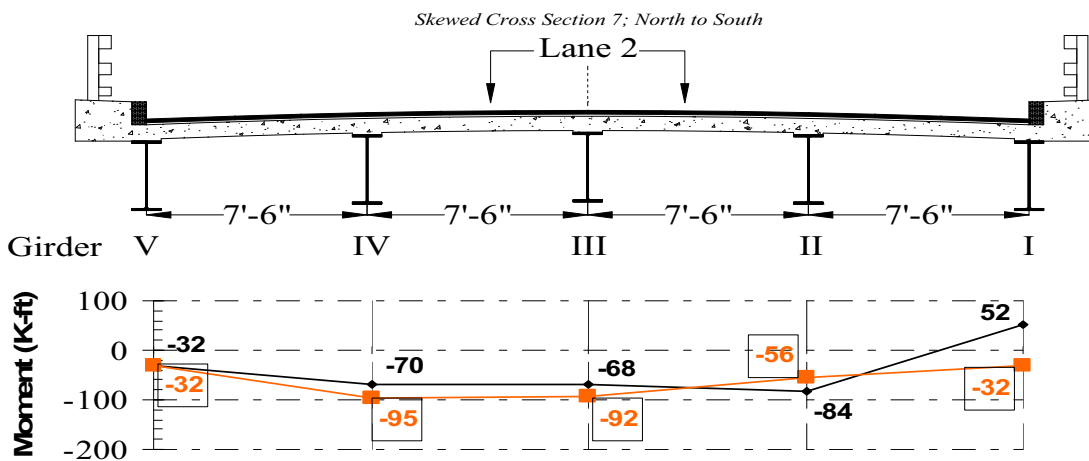


(c) Load Truck in Lane 3 (189 ft)

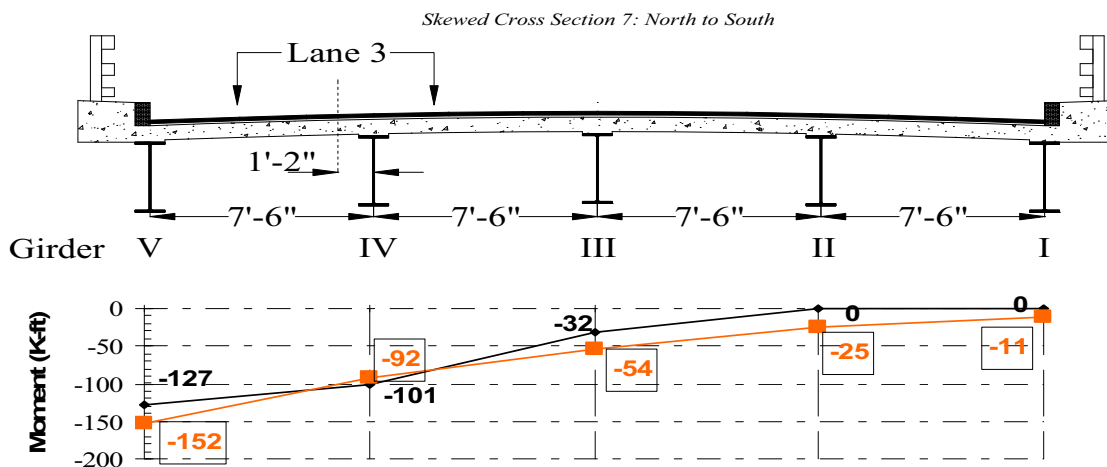
Figure 7.5: Comparison of Measured and Calculated Moments in Cross Section 1



(a) Load Truck in Lane 1 (178 ft)



(b) Load Truck in Lane 2 (178 ft)



(c) Load Truck in Lane 3 (178 ft)

Figure 7.6: Comparison of Measured and Calculated Moments in Cross Section 7

7.4 Summary of Finite Element Modeling

The finite element modeling approach has several advantages to more simplistic analytical methods, such as the beam line analysis, for bridges with irregular geometry or variable material properties. Finite element models would also be useful if the goal of the diagnostic test is to permit crossing of an overload vehicle with unusual axle configuration. The drawback of creating a model is the additional time required to create the model.

Common engineering assumptions of material properties and support conditions were used to create the Weathersfield Bridge model. Without calibration, this model reasonably predicts the calculated behavior from the field-testing with minor differences in magnitude.

CHAPTER 8 – BRIDGE LOAD RATING

8.1 Background

One of the goals of the research project was to provide load rating values for the two bridges tested in this project supported on the diagnostic load test results. These load rating values would then be compared with recent load ratings of these bridges conducted by VTrans engineers in recent years. Because strains and stresses measured during field tests are expected to be representative of actual field conditions and include effects of variables not normally considered in models used for load rating, the load rating values based on field tests are believed to represent more accurately bridge behavior. A characteristic of diagnostic bridge load tests like the ones performed in this research is that stresses induced in the bridges during the load test should not exceed the limit of linear material behavior nor induce damage to bridge components. Because of this, extrapolating bridge load rating values to conditions that are significantly different from those used during the load test is not recommended. Results should not be extrapolated, in particular, to cases where the load rating vehicle is much heavier than the test trucks or if it is anticipated that the imposed live loads would cause higher response of the bridge than that measured during the diagnostic load tests. This chapter discusses the procedure used to calculate load rating values for both bridges tested in this research and compares these values with rating values obtained using traditional load rating techniques.

8.2 Description of Load Rating Procedure

The field load rating procedure adopted for this research is based primarily on the *Manual for Bridge Rating through Load Testing* (Manual 1998). In this manual, the suggested rating factor based on load tests is given by:

$$RF_T = RF_c(K) \quad (8.1)$$

Where RF_T is the rating factor based on load test results; RF_c is the rating factor calculated based on an assumed model; and K is an adjustment factor resulting from comparison of results from the load tests with those from the appropriate analytical model. The value of K will depend on the assumed analytical model so a model that is reflective of actual bridge behavior should be chosen. The diagnostic bridge load tests can be used to assess the validity of specific analytical models. Comparison of measured parameters (such as strains or estimated moments) with calculated values can be used as a means to evaluate the adequacy of a model. The analytical models that were used to calculate RF_c for this project will be discussed in a subsequent section.

The calculated rating factor, RF_c , can be estimated using the traditional load rating equation contained in the *Manual for Condition Evaluation of Bridges* (AASHTO

1994). For this project, a load and resistance factor rating (LRFR) method was selected for consistency with current load rating techniques. The basic load rating equation is:

$$RF_c = \frac{C - A_1 D}{A_2 L (1 + I)} \quad (8.2)$$

where C represents the capacity of the critical member that gives the lowest load rating factor; D is the dead load effect on that member; L is the live load effect; I is an impact coefficient; A_1 is the dead load factor, equal to 1.30; and A_2 is the live load factor, equal to 1.30 for operating level or 2.17 for inventory level rating. When using the LRFR technique, the factored (reduced) strength of a member is used to represent its capacity C . In the case of the two bridges tested in this research, bending moment was the governing action limiting load rating of the bridges. Therefore the flexural capacity was used for C , and dead and live-load moments were used for D and L , respectively.

The test-to-calculated rating adjustment factor, K , provides the connection between results from a load test and those estimated using an analytical model for a given action. Because strains are measured directly in most field tests, strain is the recommended parameter to relate load test results to model results (Manual 1998). The recommended value for K in the *Manual for Bridge Rating through Load Testing* is:

$$K = 1 + K_a K_b \quad (8.3)$$

where K_a and K_b can be estimated using:

$$K_a = \frac{\varepsilon_C}{\varepsilon_T} - 1 \quad (8.4)$$

and

$$K_b = K_{b1} K_{b2} K_{b3} \quad (8.5)$$

K_a accounts for the benefit of the load test by calculating $\varepsilon_C/\varepsilon_T$, the ratio between calculated strain from a model at a given bridge section and the corresponding strain at the same cross section measured during the diagnostic field test. The strain ε_C is calculated using results from the analytical model selected for rating. Model output is typically a force-based quantity (axial force, shear force, bending moment, stresses) so strain is calculated using fundamental mechanics principles and assuming linear material behavior. If bending moment governs the rating of a bridge as was the case in the two bridges tested during this project, bending strains are calculated by dividing moment (M) by the section modulus of the cross section (S) and the modulus of elasticity (E) of the material ($\varepsilon_C = M/SE$). In a concrete deck on steel girder bridge, the assumption of composite or non-composite behavior influences the value of S used to determine ε_C . In a reinforced concrete tee-beam bridge, section modulus is affected by assumptions related to cracking of the cross-section and effective flange contribution

of the deck. The section behavior assumptions made for each of the two bridges are indicated in the section corresponding to rating of each of the two bridges.

The factor K_b is calculated by multiplying three different factors related to the ability of extrapolating results from the bridge testing to other loading conditions (K_{b1}), the anticipated frequency and detail of future bridge inspection (K_{b2}), and the presence of bridge characteristics (desirable or undesirable) that affect bridge performance (K_{b3}). These factors are determined somewhat subjectively but guidance is provided in the *Manual for Bridge Rating through Load Testing* for their estimation. For the case of the two bridges tested in this project, the proposed factors are listed in Table 8.1.

Table 8.1: Selection of Bridge Parameters for Load Rating

Bridge	K_{b1}	K_{b2}	K_{b3}	K_b
Royalton	0.8	0.8	1.0	0.64
Weathersfield	0.8	0.8	1.0	0.64

8.3 Analysis and Rating Trucks

Different analytical models were used to produce a load rating for each of the bridges. Results from the analysis were used to calculate moments induced by different rating trucks and the trucks used during load testing in interior girders. Load rating in the two bridges was governed by flexural strength, so only moments were used to produce load rating values. The moments generated by the loading vehicles were used to calculate strains in interior girders and compare those to the measured values to come up with values for K_a . The calculated moments depend on the type of analytical model used for each bridge. A description of the analytical model used in each of the two bridges is provided in the following section.

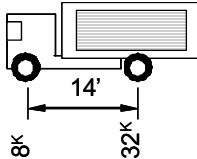
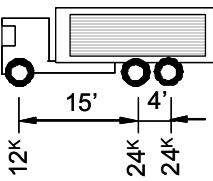
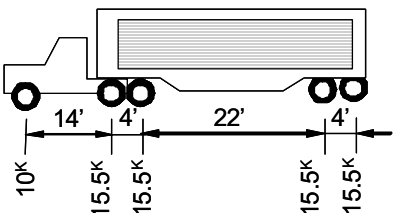
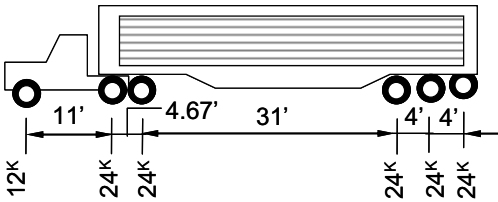
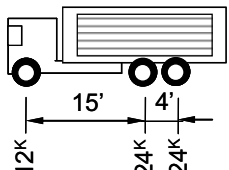
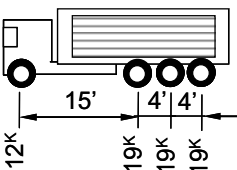
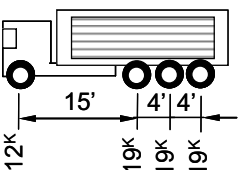
The rating trucks used to produce load rating values for the two bridges are shown in Table 8.2. These trucks correspond to those used commonly by VTrans for load rating and posting of bridges. Loading from these trucks was applied to the bridge models as a moving load combination to generate maximum live-load moment envelopes in interior girders. Using these envelopes, the critical moment values at different sections of the bridges were used to compute rating factors for each section and determine the section of each bridge governing the load rating number. A live-load transverse distribution factor was used to determine moments in girders when 2-dimensional modeling techniques were used (beam-line models). For 3-dimensional finite element models, the moments in girders were determined directly. An impact factor of 30% was used in all cases.

8.4 Royalton Bridge Rating

8.4.1 Selected Bridge Model

The Royalton Bridge was modeled using a beam-line analysis because of symmetry and simple support conditions. It was earlier pointed out that moments calculated from field strains resulted in reasonably similar values of moments determined from a beam line model. For interior girders, the strains determined in the field were generally lower than those computed from the beam line model. This was attributed to larger contribution from the edge girders to the overall moment carrying capacity of the entire bridge cross section as discussed before.

Table 8.2: Rating Trucks

<p>Truck 1: H20 Truck (40,000 lb)</p> 	<p>Truck 2: HS20 Truck (72,000 lb)</p> 
<p>Truck 3: 3S2 Truck (72,000 lb)</p> 	<p>Truck 4: 6 Axle Trailer Truck (132,000 lb)</p> 
<p>Truck 5: 3 Axle Straight Truck (60,000 lb)</p> 	<p>Truck 6: 4 Axle Straight Truck (69,000 lb)</p> 
<p>Truck 7: 5 Axle Semi-trailer (76,000 lb)</p> 	

Because little to no continuity was observed from span to span during the load tests, each span was considered simply supported as assumed during the original design of the bridge. The second span (37 ft long) governed the load rating in the 3-span simply supported Royalton Bridge. Dead loads consisted of interior girder self weights and a superimposed dead load of 167 lb/ft that accounted for weight of the guardrails in each interior girder. This superimposed load was consistent with assumptions used in past load ratings of the bridge by VTrans personnel.

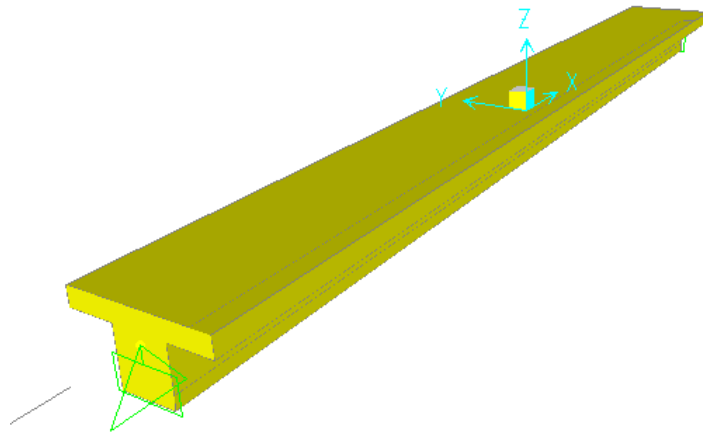


Figure 8.1: Model used for Royalton Bridge Rating Calculations (Span 2)

Live-load moments in a typical interior girder were determined by dividing the moment from each rating truck or loading truck by two to convert to wheel loading. A transverse distribution factor for live-load moments induced by wheel loads equal to $S/6.0$, where S is the spacing between T-beams (equal to 4.5 ft), was used to determine the moment in interior girders. This value was selected for consistency with rating calculations performed previously in the bridge. These wheel load moments in interior girders were then affected by an impact factor of 30%. In the case of moments induced by the loading trucks on the bridge, no impact factor was considered because loads were applied slowly. Dead and live load moments (excluding impact) for a typical interior girder are listed in Table 8.3.

8.4.2 Flexural Strength Assumptions

Flexural strength of interior girders was determined using common assumptions of reinforced concrete design. Only positive moment strength was considered for load rating calculations because of the lack of continuity between spans. A 54-in. effective slab width, equal to the center to center spacing between girders, was considered for moment calculations. Because the bridge had suffered deterioration over years in

service (primarily concrete cracking and corrosion of main longitudinal reinforcement), the design longitudinal reinforcement was decreased by 10% to account for section loss due to corrosion.

The typical cross section at midspan for Span 2 is shown in Figure 8.2. Because the yield strength of the longitudinal reinforcement was unknown, a value of 33 ksi was assumed in accordance with recommendations in the *Manual for Condition Evaluation of Bridges* (AASHTO 2000). Concrete was assumed to carry compression only. The concrete compressive strength f'_c was assumed equal to 6000 psi. This value was determined reasonable due to aging of concrete in the field and was consistent with values found during non-destructive tests using impact hammer sampling of the concrete in the field during the day of field testing. The resulting flexural strength at midspan for typical interior girders was 631 kip-ft.

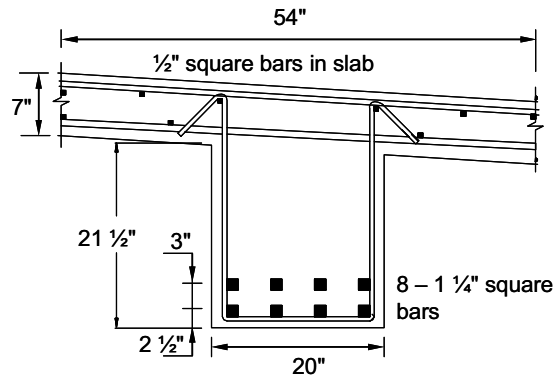


Figure 8.2: Typical Midspan Cross Section for Span 2

Table 8.3: Interior Girder Dead and Live-Load Moments (Impact factor not included) Calculated Using Beam Line Model

Moment location	M_D (kip-ft)	Vehicle type						
		H20	HS20	3S2	6 Axle	3 Axle	4 Axle	5 Axle
		Vehicle weight (ton)						
		20	36	36	66	30	34.5	38
Live-load Moments, M_L (kip-ft)								
Girders II to V	200	118	147	110	214	156	169	119

8.4.3 Royalton Bridge Rating based on Diagnostic Field Tests

Rating results for the Royalton Bridge are summarized in Table 8.4 to Table 8.8. Results from calculation of the test-to-calculated rating adjustment factor, K , are shown in Table 8.4. Live-load moments generated by the loading truck applied to the beam-line model were used to estimate theoretical strains in typical interior girders. These

strains were calculated at a depth corresponding to the depth where strain gauges were placed on the girders using $\varepsilon_c = M_{calc} / S_{bott} E_c$. The section modulus S_{bott} was determined assuming an uncracked cross-section. The modulus of concrete E_c was calculated based on an assumption of a concrete compressive strength of 6000 psi. The values listed for K_a and K were calculated using equations 8.3 and 8.4, respectively, using the value of K_b listed in Table 8.2.

Table 8.4: Ratio of Test to Calculated Rating Factor (K) Based on Non-composite Section Bottom Strains

Girder number	S_{bott} (in ³)	Strains computed using SAP2000 (ε_c)	Field strains (ε_T)	K_a	K
II	5534	8.17E-05	2.50E-05	2.27	2.45
III	5534	8.17E-05	4.43E-05	0.84	1.54
IV	5534	—	—	—	—
V	5534	8.17E-05	3.76E-05	1.17	1.75

The minimum value of K was selected to produce rating values based on diagnostic field testing of the Royalton Bridge. Calculated rating factors and rating (tons) of the bridge using the different rating vehicles in Table 8.2 are listed in Table 8.5, Table 8.6, and Table 8.7 for operating, inventory, and posting purposes, respectively. Since not all rating vehicles are used for the different rating and posting levels, a summary of the applicable values for each vehicle is provided in Table 8.8. The K factor was used to scale the calculated rating results to produce a field test-based rating of the bridge as indicated in the bottom two rows for each corresponding table.

Table 8.5: Operating Rating Based on Uncracked Section Properties ($f_y = 33$ ksi)

Operating Rating							
M_c^+ =	631	kip-ft [Uncracked behavior; $f_y = 33$ ksi]					
A_1 =	1.3						
A_2 =	1.3						
I =	0.3						
$RF_c = \frac{C - A_1 D}{A_2 L(1 + I)}$							
Vehicle weight (ton) and rating vehicle type							
	20	36	36	66	30	34.5	38
	H20	HS20	3S2	6 Axle	3 Axle	4 Axle	5 Axle
Capacity, M_c (kip-ft)	Calculated rating factor, RF_c						
631	1.86	1.92	2.36	1.35	1.33	1.49	2.04
Minimum RF_c	1.86	1.92	2.36	1.35	1.33	1.49	2.04
Rating (tons)	37.3	69.0	85.1	89.1	40.0	51.6	77.4
Rating factor from field tests, RF_T							
$RF_T = RF_c(K)$							
Minimum RF_T	2.87	2.29	3.07	1.58	2.16	2.00	2.83

Rating (tons)	57.4	82.6	110.7	104.4	64.9	68.9	107.7
---------------	------	------	-------	-------	------	------	-------

Table 8.6: Inventory Rating Based on Uncracked Section Properties ($f_y = 33$ ksi)

Inventory Rating							
$M_c^+ =$	631	kip-ft [Uncracked behavior; $f_y = 33$ ksi]					
$A_1 =$	1.3	$RF_c = \frac{C - A_1 D}{A_2 L(1 + I)}$					
$A_2 =$	2.17						
$I =$	0.3						
Vehicle weight (ton) and rating vehicle type							
	20	36	36	66	30	34.5	38
	H20	HS20	3S2	6 Axle	3 Axle	4 Axle	5 Axle
Capacity, M_C (kip-ft)	Calculated rating factor, RF_C						
631	1.12	0.89	1.20	0.62	0.84	0.78	1.10
Minimum RF_C	1.12	0.89	1.20	0.62	0.84	0.78	1.10
Rating (tons)	22.3	32.1	43.1	40.6	25.2	26.8	41.9
Rating factor from field tests, RF_T $RF_T = RF_C (K)$							
Minimum RF_T	1.72	1.37	1.84	0.95	1.30	1.20	1.70
Rating (tons)	34.4	49.5	66.3	62.5	38.9	41.3	64.5

Table 8.7: Posting Values Based on Uncracked Section Properties ($f_y = 33$ ksi)

Posting							
$M_c^+ =$	631	kip-ft [Uncracked behavior; $f_y = 33$ ksi]					
$A_1 =$	1.3	$RF_c = \frac{C - A_1 D}{A_2 L(1 + I)}$					
$A_2 =$	1.55						
$I =$	0.3						
Vehicle weight (ton) and rating vehicle type							
	20	36	36	66	30	34.5	38
	H20	HS20	3S2	6 Axle	3 Axle	4 Axle	5 Axle
Capacity, M_C (kip-ft)	Calculated rating factor, RF_C						
631	1.56	1.25	1.67	0.86	1.18	1.09	1.54
Minimum RF_C	1.56	1.25	1.67	0.86	1.18	1.09	1.54
Rating (tons)	31.3	45.0	60.3	56.9	35.3	37.5	58.6
Rating factor from field tests, RF_T $RF_T = RF_C (K)$							
Minimum RF_T	2.41	1.92	2.58	1.33	1.81	1.68	2.38
Rating (tons)	48.2	69.3	92.8	87.5	54.4	57.8	90.3

Table 8.8: Rating Based on Load Testing: Royalton Bridge (tons)*

	H20	HS20	3S2	6 Axle	3 Axle Truck	4 Axle Truck	5 Axle Semi
Inventory	34.4	49.5	66.3	62.5	38.9	41.3	64.5
Posting	48.2	69.3	92.8	87.5	54.4	57.8	90.3
Operating	57.4	82.6	110.7	104.4	64.9	68.9	107.7

*Values in shaded cells are not used for the corresponding rating or posting category.

Table 8.9: Rating Conducted by VTrans: Royalton Bridge (tons)

	H20	HS20	3S2	6 Axle	3 Axle Truck	4 Axle Truck	5 Axle Semi
Inventory		30					
Posting	30		58		34	36	56
Operating	35	51	69	65	40		

8.5 Weathersfield Bridge Rating

8.5.1 Selected Bridge Model

An important component in providing an accurate rating value for this bridge was in the selection of the bridge analytical model. The inability of a beam-line model to capture the measured moment response of the Weathersfield bridge was discussed in detail in Section 6.2.6, which required development of a refined analytical model that better represented bridge behavior. A three-dimensional (3D) finite element model of the bridge was constructed to capture the response of the bridge more accurately and to provide, therefore, a reliable value of bridge rating based on the diagnostic field test results.

The bridge analytical model was constructed using commercially available structural analysis software (SAP2000-Bridge Modeler). Slight modifications to the model presented in Chapter 7 were done to allow effective application of dead load on the bridge deck and creation of influence lines and moment envelopes generated by the different rating vehicles used. A detailed description of the characteristics of the analytical model were provided in Chapter 7, so only a brief discussion of the major features of the model are included in this section.

The deck was modeled using 4-node shell elements with 6 degrees of freedom per node. Girder elements were modeled using 2-node frame elements with 6 degrees of freedom per node. Deck and girder elements were connected using a body constraint, a feature enabling degrees of freedom between deck and girders to be constrained as if belonging to the same rigid body. This constraint effectively limits the slip between deck and girders, which was considered a reasonable assumption to determine moments on the bridge cross-section. The girder insertion point, the point

where section properties are calculated in the model, was selected at the top-middle of each girder (connection between top flange and web of girder). Nodes located at girder insertion points and bottom of girder were connected using a rigid link. This was done to apply the boundary conditions at bridge abutments and interior bents on the bottom joint of each girder (Figure 8.3). The girder cross-section was modified near interior bents to account for the presence of top and bottom cover plates extending 6.5 and 8.0 ft into the exterior and interior spans, respectively (Figure 8.4 and Figure 8.6). A bottom view of the finite element model is shown in Figure 8.5.

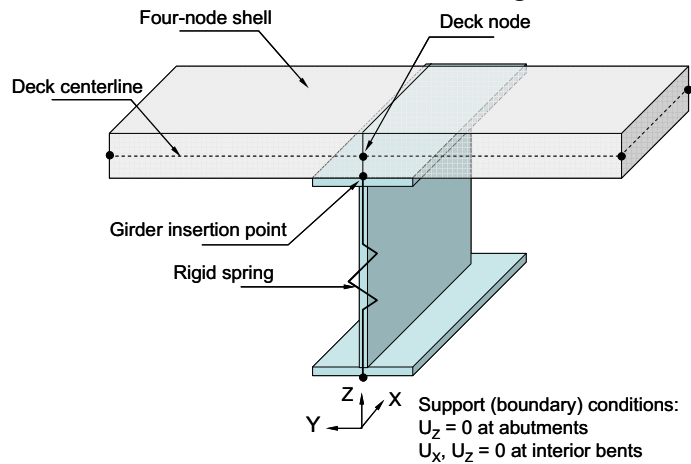


Figure 8.3: Detail of Connection Between Deck and Girders and Application of Support Conditions

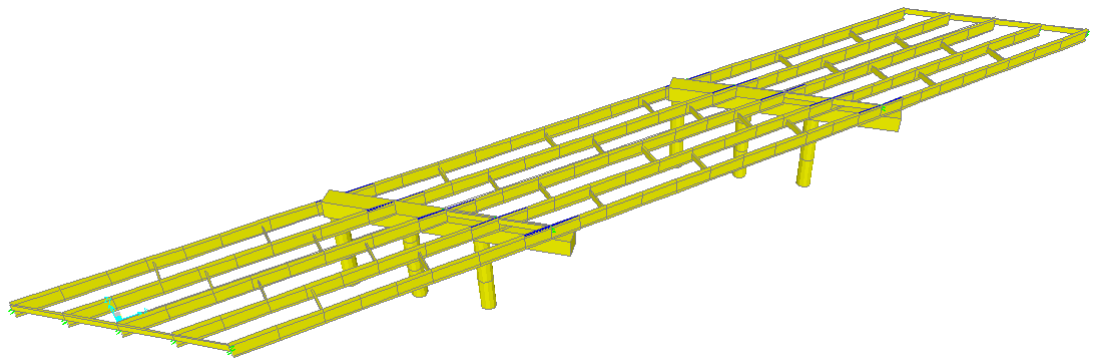


Figure 8.4: General View of 3D Model of Weathersfield without Deck Elements

Supports were placed under each girder at the abutments and on the interior bridge bents. At the abutments only vertical displacement was restrained, whereas vertical and longitudinal displacements were restrained at interior bents. Beam diaphragms were modeled using 2-node frame elements with 6 degrees of freedom per node. These element nodes had all rotational degrees of freedom released (zero moment was transmitted to bridge girders) because of the flexibility of the connection between diaphragms and girders.

Sustained loading consisted of self-weight of deck (7.5-in. thickness), self-weight of steel girders (W36x170 sections), self-weight of riding surface (2-in. thick bituminous concrete), and allowance for curb weight (4.83-ft wide by 10-in. thick) distributed equally to all girders on the bridge. Live loads consisted of the 7 different trucks used for load rating purposes by VTrans (Table 8.2) applied individually on one, two, or three lanes defined for the bridge, and the trucks used during load tests applied in each of the three lanes defined on the bridge. Although the bridge has only two traffic lanes, three design lanes were used because of the total width of the bridge. A multiple presence factor of 0.9 was used when rating trucks were applied simultaneously on the three design lanes.

During diagnostic field tests some level of composite action was detected between steel girders and concrete deck. For the purpose of load rating, however, a non-composite behavior was assumed in order to provide a conservative value that would be reliable in case of overload in the bridge.

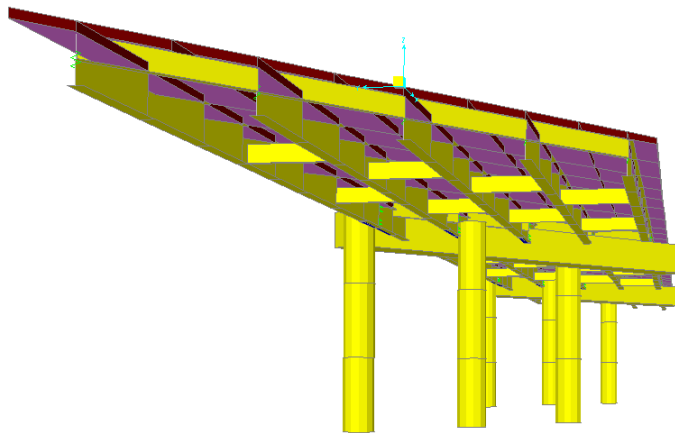


Figure 8.5: Underside View of 3D-Finite Element Model of Weathersfield Bridge

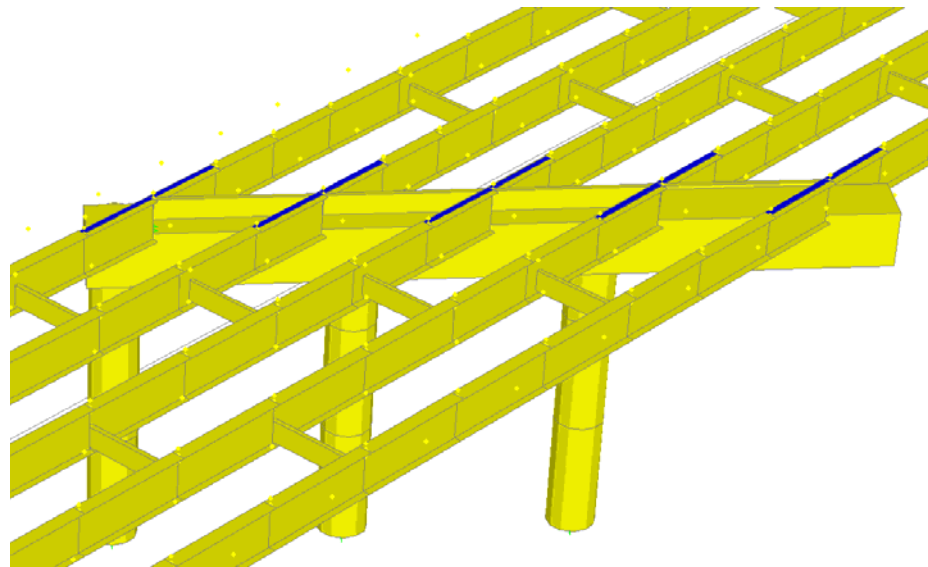


Figure 8.6: Detail of Cover Steel Girders over Interior Support in Weathersfield Bridge Model

Results from application of unfactored dead and live loads to the bridge model are presented in Table 8.10 for the critical interior girder. Moments were calculated at midspan in each of the three bridge spans and over interior supports. The live-load moment values listed in the table do not include the 30% impact factor considered for load rating. The impact factor along with load factors required to load rate the bridge were applied separately.

Table 8.10: Dead and Live-Load Moments Calculated Using 3D-FEM Model

Moment location	M_D (kip-ft)	Vehicle type						
		H20	HS20	3S2	6 Axle	3 Axle	4 Axle	5 Axle
		Vehicle weight (ton)						
		20	36	36	66	30	34.5	38
Live-load Moments, M_L (kip-ft)								
M^+ span 1	329	415	595	460	776	570	640	552
M^+ span 2	346	433	626	500	830	602	660	577
M^+ span 3	307	420	600	467	775	585	645	554
M^- supp 1	700	270	460	405	760	396	450	460
M^- supp 2	700	270	460	400	760	396	450	455

8.5.2 Weathersfield Bridge Rating based on Diagnostic Field Tests

Rating results for the Weathersfield Bridge are summarized in Table 8.11 to Table 8.15. Results from calculation of the test-to-calculated rating adjustment factor, K , are shown in Table 8.11. Three separate calculations were conducted to determine the critical K factor because calculated (ϵ_C) and measured (ϵ_T) strains varied depending on the loaded lane. Live-load moments generated by the loading truck applied on each of the defined lanes were used to estimate the maximum value of ϵ_C in interior girders for each lane. These strains were calculated at the bottom flange of the girders in accordance with the position of the strain gauge used during the diagnostic field test using the flexure formula $\epsilon_C = M_{calc} / S_{bott} E_s$. The section modulus S_{bott} was determined assuming non-composite behavior of the girder, and the modulus of steel E_s was assumed equal to 29,000 ksi. The values listed for K_a and K were calculated using equations 8.3 and 8.4, respectively, using the value of K_b listed in Table 8.1.

The smallest value of K calculated for each individual lane was selected as the critical value for use in producing the load rating values based on field testing. Calculated rating factors for the different rating trucks are presented in Table 8.12 to Table 8.15. The calculated rating factor (RF_C) is the minimum rating factor obtained for the different sections investigated along the bridge. The rating factor corresponding to field load testing (RF_T) was calculated as the minimum value of the products of

rating factors at individual sections times corresponding K factors for each of the rating vehicles. Finally, a summary of rating values (tons) for operating, inventory rating, and load posting is provided in Table 8.15 for the Weathersfield Bridge.

Table 8.11: Ratio of Test to Calculated Rating Factor (K) Based on Non-composite Section Bottom Strains

Moment location	Section modulus (in ³)	Lane 1			Lane 2			Lane 3					
		SAP2000 strains (ϵ_C)	Field strains (ϵ_T)	K_a	K	SAP2000 strains (ϵ_C)	Field strains (ϵ_T)	K_a	K	SAP2000 strains (ϵ_C)	Field strains (ϵ_T)	K_a	K
M ⁺ span 1	580	2.32E-04	—	—	—	2.19E-04	—	—	—	2.26E-04	—	—	—
M ⁺ span 2	580	2.47E-04	9.43E-05	1.62	2.04	2.26E-04	8.09E-05	1.8	2.15	2.42E-04	9.43E-05	1.56	2.00
M ⁺ span 3	580	2.32E-04	—	—	—	2.19E-04	—	—	—	2.33E-04	—	—	—
M ⁻ supp 1	766	1.57E-04	4.93E-05	2.18	2.39	1.57E-04	5.90E-05	1.66	2.06	1.55E-04	9.24E-05	0.68	1.43
M ⁻ supp 2	766	1.59E-04	1.18E-04	0.35	1.22	1.54E-04	7.14E-05	1.16	1.74	1.62E-04	1.18E-04	0.37	1.24

Table 8.12: Operating Rating Based on Non-composite Section Properties

Operating Rating							
M_c^+ =	2,004	kip-ft	[Non-composite behavior for M ⁺]				
M_c^- =	2,560	kip-ft	[Non-composite behavior for M ⁻]				
A_1 =	1.3		$RF_c = \frac{C - A_1 D}{A_2 L(1 + I)}$				
A_2 =	1.3						
I =	0.3						
Vehicle weight (ton) and rating vehicle type							
	20	36	36	66	30	34.5	38
	H20	HS20	3S2	6 Axle	3 Axle	4 Axle	5 Axle
Capacity, M_c (kip-ft)	Calculated rating factor, RF_c						
2004	2.25	1.57	2.03	1.20	1.64	1.46	1.69
2004	2.12	1.47	1.84	1.11	1.53	1.39	1.59
2004	2.26	1.58	2.03	1.23	1.62	1.47	1.71
2560	3.62	2.12	2.41	1.28	2.47	2.17	2.12
2560	3.62	2.12	2.44	1.28	2.47	2.17	2.15
Minimum RF_c	2.12	1.47	1.84	1.11	1.53	1.39	1.59
Rating (tons)	42.5	52.9	66.2	73.1	45.8	48.1	60.6
Rating factor from field tests, RF_T							
	$RF_T = RF_c(K)$						
Minimum RF_T	4.25	2.60	2.99	1.57	3.02	2.66	2.63
Rating (tons)	85.0	93.5	107.6	103.8	90.6	91.6	99.8

Table 8.13: Inventory Rating Based on Non-composite Section Properties

Inventory Rating							
M_c^+ =	2,004	kip-ft	[Non-composite behavior for M^+]				
M_c^- =	2,560	kip-ft	[Non-composite behavior for M^-]				
A_1 =	1.3		$RF_c = \frac{C - A_1 D}{A_2 L(1 + I)}$				
A_2 =	2.17						
I =	0.3						
Vehicle weight (ton) and rating vehicle type							
	20	36	36	66	30	34.5	38
	H20	HS20	3S2	6 Axle	3 Axle	4 Axle	5 Axle
Capacity, M_C (kip-ft)	Calculated rating factor, RF_C						
2004	1.35	0.94	1.21	0.72	0.98	0.87	1.01
2004	1.27	0.88	1.10	0.66	0.92	0.83	0.95
2004	1.35	0.95	1.22	0.73	0.97	0.88	1.03
2560	2.17	1.27	1.44	0.77	1.48	1.30	1.27
2560	2.17	1.27	1.46	0.77	1.48	1.30	1.29
Minimum RF_C	1.27	0.88	1.10	0.66	0.92	0.83	0.95
Rating (tons)	25.4	31.7	39.7	43.8	27.5	28.8	36.3
Rating factor from field tests, RF_T $RF_T = RF_C(K)$							
Minimum RF_T	2.55	1.56	1.79	0.94	1.81	1.59	1.57
Rating (tons)	50.9	56.0	64.4	62.2	54.3	54.9	59.8

Table 8.14: Posting Values Based on Non-composite Section Properties

Posting								
$M_c^\dagger =$	2,004	kip-ft	[Non-composite behavior for M^\dagger]					
$M_c =$	2,560	kip-ft	[Non-composite behavior for M]					
$A_1 =$	1.3		$RF_c = \frac{C - A_1 D}{A_2 L(1 + I)}$					
$A_2 =$	1.55							
$I =$	0.3							
Vehicle weight (ton) and rating vehicle type								
	20	36	36	66	30	34.5	38	
	H20	HS20	3S2	6 Axle	3 Axle	4 Axle	5 Axle	
Capacity, M_C (kip-ft)	Calculated rating factor, RF_C							
2004	1.89	1.31	1.70	1.01	1.37	1.22	1.42	
2004	1.78	1.23	1.54	0.93	1.28	1.17	1.34	
2004	1.90	1.33	1.71	1.03	1.36	1.23	1.44	
2560	3.03	1.78	2.02	1.08	2.07	1.82	1.78	
2560	3.03	1.78	2.05	1.08	2.07	1.82	1.80	
Minimum RF_C	1.78	1.23	1.54	0.93	1.28	1.17	1.34	
Rating (tons)	35.6	44.4	55.5	61.3	38.4	40.3	50.8	
Rating factor from field tests, RF_T $RF_T = RF_C(K)$								
Minimum RF_T	3.57	2.18	2.51	1.32	2.53	2.23	2.20	
Rating (tons)	71.3	78.5	90.2	87.1	76.0	76.9	83.7	

Table 8.15: Rating Based on Load Testing: Weathersfield Bridge (tons)*

	H20	HS20	3S2	6 Axle	3 Axle Truck	4 Axle Truck	5 Axle Semi
Inventory	50.9	56.0	64.4	62.2	54.3	54.9	59.8
Posting	71.3	78.5	90.2	87.1	76.0	76.9	83.7
Operating	85.0	93.5	107.6	103.8	90.6	91.6	99.8

*Values in shaded cells are not used for the corresponding rating or posting category.

Table 8.16: Rating Conducted by VTrans: Weathersfield Bridge (tons)

	H20	HS20	3S2	6 Axle	3 Axle Truck	4 Axle Truck	5 Axle Semi
Inventory		35					
Posting	40		60		43	44	55
Operating	48	58	72	86	52		

CHAPTER 9 - SUMMARY AND CONCLUSIONS

The main observations are summarized in this chapter along with conclusions on the behavior of the two tested bridges. Additionally, comments on the testing procedure to follow for a typical bridge is outlined and limitations of the testing equipment and software are identified.

9.1 Summary

The objective of this project was to develop a load test methodology and demonstrate it through diagnostic field tests of two bridges in the State of Vermont. The main goal of the field tests was to gain a better understanding of bridge behavior to assist VTrans engineers in future bridge evaluations. These two bridges were selected in coordination with VTrans personnel to achieve specific goals in each test.

The first bridge selected consisted of an old (1920s) 3-span simply supported reinforced concrete T-beam bridge located in Royalton, Vermont. The bridge carries two lanes of traffic on a rural state highway over a river crossing. The second bridge consisted of a 3 span continuous steel girder bridge constructed in the 1965 was designed with a non-composite concrete deck. The bridge carries two southbound lanes of Interstate 91 and is located in Weathersfield, Vermont.

The Royalton Bridge has been rated structurally deficient; spalled concrete and corroded reinforcement were documented in several areas of the bridge on the day of the test. Effects of this deterioration are difficult to quantify by visual inspection and made this bridge ideal for a diagnostic test.

The Royalton Bridge field testing was completed in two days, with one day of preparation and one day of load testing. The main objectives in this test were to determine the contribution the guardrails have to overall bridge behavior, the transverse distribution of moments, and actual restraint at simply supported ends of each span. The first two spans were instrumented at mid-span and at a section close to exterior or interior supports.

The Weathersfield Bridge has load restrictions for overload vehicles based on calculated negative moment strength at interior pier supports. Additionally, several of the main support girders have damage that was caused by impact of an over-height vehicle traveling on the road underneath the bridge. The field test was completed in one day. The main objectives of the load test were to evaluate the assumption of non-composite action between deck and girders used during design and bridge rating, to examine the transverse moment distribution among parallel girders, to calculate negative moments near pier supports, and to investigate detrimental effects of the bridge damage caused by the truck impact. To accomplish these objectives only the center span was instrumented, with gauges placed near pier supports, at mid-span, and near damaged areas.

It is recognized that for this type of testing to be practical, simplistic methods of analysis that yield reasonable results are necessary to check and compare with field results. Common assumptions of material properties were used to determine moments from the strain data. Moments calculated from field data were then compared with moments from analytical models. The Royalton Bridge test results were compared with a beam line analysis, while the Weathersfield Bridge was compared and analyzed with a 3-D finite element model. These results are discussed in detail in chapters 6 and 7.

Presents a summary of results from the moment comparisons conducted for each of the two bridges.

Table 9.1: Comparison of Moments in Critical Interior Girder of Royalton Bridge

Span	No. of loaded lanes	Field Moment	AASHTO LRFD Moment (Beam Line Model)	Field Moment/AASHTO LRFD Moment
		(K-ft)	(K-ft)	(%)
1	1 lane	90	127	71
	2 lanes	129	156	83
2	1 lane	84	150	56
	2 lanes	120	190	63

Table 9.2: Comparison of Moments in Critical Interior Girder of Weathersfield Bridge

Moment	No. of loaded lanes	Field Moment	AASHTO LRFD Moment (Beam Line Model)	Field Moment/AASHTO LRFD Moment	FEM Moment	Field Moment/FEM Moment
		(K-ft)	(K-ft)	(%)	(K-ft)	(%)
Positive	1 lane	250	350	71	117	137
	2 lanes	434	490	89	303	143
Negative	1 lane	-156	-294	53	-108	144
	2 lanes	-240	-406	59	-164	146

Table 9.3: Comparison of Finite Element and Field Moments in Positive Moment Region (Girders II-V)

Cross Section	Lane	Figure	Truck Position (ft)	Finite Element Calculated Moment (K-ft)	Moments Calculated From Field Test Data (K-ft)	Percent Difference (%)
4	1	Figure 7.4a	190	387	330	17
	2	Figure 7.4b		382	487	-22
	3	Figure 7.4c		384	613	-37

Note: Girder V moments not considered in finite element or field results

Table 9.4: Comparison Finite Element and Field Moments in Negative Moment Region

Cross Section	Lane	Figure	Truck Position (ft)	Finite Element Calculated Moment (K-ft)	Moments Calculated From Field Test Data (K-ft)	Percent Difference From Field Measurement (%)
1	1	Figure 7.5a	189	-353	-262	35
	2	Figure 7.5b		-309	-352	-12
	3	Figure 7.5c		-304	-198	54
7	1	Figure 7.6a	178	-294	-351	-16
	2	Figure 7.6b		-308	-202	52
	3	Figure 7.6c		-333	-260	28

9.2 Conclusions

Diagnostic load testing can be used to provide a better understanding of bridge behavior. A diagnostic bridge test can give engineers confidence in their understanding of bridge behavior when faced with a complex bridge geometry or structural deficiency that is difficult to quantify. As described below, behavior in both the Royalton and Weathersfield Bridge tests was observed that was not predicted by approximate design methods. This behavior could be beneficial if considered in a future load rating.

9.2.1 Royalton Bridge

From a visual inspection of strain data plots, the bridge behaved within the linear-elastic range under the load of the truck. Neutral axis depth plots that were

created located the neutral axis depth near the bottom of the concrete slab in most cross sections, close to the theoretical neutral axis position assuming elastic properties of the cross sections. Neutral axis depths were found to be higher in exterior girders due to interaction with concrete guard rails.

As a result of diagnostic testing, a better estimate was made of concrete material properties and assumptions of load distribution among girders. Analysis results indicate that concrete strength is likely much higher (about twice) than assumed in past load ratings. To confirm this observation, concrete core samples from the bridge should be used to verify these results before any future load ratings using this estimate.

To verify field results, a beam line analytical model was created for the bridge. Using loads measured from the load truck and axle configuration, moments from this model were compared with results from field tests.

The transverse moment distribution of live load moments were only compared in the positive moment region with AASHTO guidelines, since negative moments were not significant. It was found that AASHTO transverse distribution factors resulted in higher moments in girders than those determined from the field tests (conservative). Some factors in the bridge that might have caused lower moments include the contribution from guardrails and some rotational restraint at beam ends. An analysis of guardrail strains measured during the tests indicated that they have a significant contribution to the strength and stiffness exterior T-beams at mid-span.

Although the bridge was designed assuming simply supported spans, small negative moments were recorded at instrumented cross sections near the pier and abutment supports. This indicates that there is a small amount of fixity at beam-ends, perhaps caused by debris accumulation or restraint from overlays applied throughout the lifetime of the bridge. End partial restraint reduces the positive moments at mid-span, but in the case of the Royalton Bridge this effect was found to be negligible. Small moments are also transferred into the piers and abutments. The third span was not instrumented during the test. However, the bridge is symmetrical and similar behavior in spans 1 and 3 can reasonably be expected.

9.2.2 Weathersfield Bridge

From the strain data plots, linear elastic behavior was inferred from all gauge pairs during loading. The neutral axis depths were determined at cross sections where measured strain was high enough (in absolute value) to prevent excessive errors. The calculated neutral axis locations gave indication that the bridge sections near mid-span, including those damaged by the truck impact, were acting compositely for positive bending moment. All of the neutral axis locations at mid-span in the positive moment region lied above girder mid-height, indicating composite behavior.

Bridge sections near pier supports exhibited partially-composite behavior for negative bending moment. In this region most of the girders act compositely, with neutral axis depths well above mid-height. However, some neutral axis depths were calculated to be at mid-height or slightly below mid height of the girders indicating non-composite behavior during the load tests

The Weathersfield Bridge response could not be captured with a reasonable level of accuracy with a beam line analysis because of the skewed geometry. Therefore, the bridge was analyzed using a finite element model, created using common engineering assumptions of material properties and behavior. Although finite element models are more time consuming to construct and analyze than a beam line models, more realistic behavior can be obtained particularly for bridges that have complex geometries that require consideration of three dimensional effects.

The finite element model of the Weathersfield Bridge was not calibrated to observed field results. This was purposely done to investigate how accurately the response could be simulated by using common engineering assumptions. Although girder moments from the model did not match exactly the values measured during the tests, the shape of transverse moment distribution among girders in the model was remarkably similar to the shapes of moments inferred from field results. With model calibration, performed by refining assumptions of material properties or support fixity, the model would perhaps be able to match the numeric results of the field tests better.

A fully calibrated model could more accurately match field test data, and be used to predict bridge behavior for any load configuration. Without this calibration, the finite element model was a useful tool to compare moments in individual girders and compare trends in the data. It was also found that AASHTO guidelines for live load distribution factors for moment yielded conservative values for both positive and negative moment regions.

9.3 Methodology for instrumentation and data reduction on site specific bridges

The experience gained from testing the two bridges described in this research report served to identify particular needs of specific types of bridges and tested the flexibility of the load testing equipment for varied field conditions. A proposed methodology to test future bridges based on the experience gained through these tests is outlined below. Testing is divided into three broad categories: test planning, test execution, data reduction, and analysis. The steps in each of the categories are outlined below. Further details on some of the steps are given in Appendix C.

1. Planning

- a. Conduct site visit
 - i. Identify bridge condition.
 - ii. Document damage.
 - iii. Identify bridge accessibility for instrumentation.
- b. Collect available information (drawings, load rating, inspection reports).
- c. Conduct preliminary analysis to identify and select instrumentation goals
- d. Map location of instrumented sections to achieve each of the test goals.
Depending on site conditions, four to five different test setups may be conducted during one day with the available instrumentation on this date (20 strain gage channels).

- e. Determine the number of lanes to be used during testing.
 - f. Select loading vehicle and contact district engineer for availability of vehicles on test day. Arrange for location of vehicle weighing on the morning of the day of testing.
 - g. Contact traffic engineer to identify traffic control strategy and schedule for test day.
 - h. Determine if man lifts or other equipment is required to provide access for instrumentation. Equipment should already be on-site on the day of testing.
 - i. Plan number of test runs to conduct for each testing configuration.
2. Test Execution
- a. Arrive at site at least 1.5 to 2 hours before testing to place gauges for initial test setup. Gauge serial numbers should be clearly identified and related to position on bridge for each test setup. Longitudinal position along girders or other structural members, and precise location on the cross section should be documented. This information is fundamental for data reduction.
 - b. Connect all gages to data acquisition system.
 - c. Select loading truck wheel that will be instrumented using the truck position indicator.
 - d. Measure the distance travelled by the truck for a given number of revolutions that the instrumented wheel undergoes. Repeat this measurement.
 - e. Mark truck starting position on pavement approximately 40 ft outside of the first bridge expansion joint. This allows the trucks to accelerate to constant speed prior to reaching the bridge.
 - f. Mark the starting position of the loading truck for each lane. Refer starting position to one of the wheels (e.g. front-left) in the truck.
 - g. Conduct loading runs for the first lane as planned in phase 1. Repeat each truck run for repeatability of results.
 - h. After all runs for a given test configuration, remove gauges and position in the next testing configuration. Conduct truck runs as before.
3. Data Reduction
- a. Organize strain gauge data by pairs (top and bottom) for reduction. This can be done using the Excel macro written for this project (see Appendix D).
 - b. Gauge pair data at a specific section for repeat test runs is averaged by the Excel macro.
 - c. Calculate the observed neutral axis depth assuming linear variation of strains with depth. Geometry of structural elements obtained from the as-built drawings and verified in the field should be used for this calculation. This can also be done using an Excel macro developed for this research project.
4. Analysis of Test Results
- a. Calculate moments (or other internal action) from strains measured during load tests. Calculate these actions for each of the loaded lanes.

- b. Construct simple or more involved analytical models to relate test results with predictions. For
- c. Conduct load-rating following recommendations from the *Manual for Bridge Rating Through Load Testing* (NCHRP 1998).

Limitations on use of equipment and software

The equipment used for the load tests in this project consists of 20 strain gauges that can be attached to steel or concrete elements. Gauge boxes placed at selected locations along the bridge collect wires from four gauges at a time. All boxes are connected in series and a single cable is connected to the STS system box. The STS system box connects to a laptop computer that contains the software that controls acquisition rate and saves all test data. In addition, the system contains a vehicle location device (auto-clicker), which allows determining the exact position of the loading vehicle and provides reference points of its position relative to the measured data. A brief description of the functions of each of the testing system component is listed below:

Strain Gauge: Full wheatstone bridge strain gauge with 20 ft wire (20 gauges)

Strain Gauge Box: Up to 4 strain gauges connect to each box, which connect in series to STS II

STS II: (Structural Testing System) Powers and measures voltage of strain gauges

Field Laptop: Software controls STSII and records data after each tests

AutoClicker: Used to monitor load truck position

In its current configuration, the equipment limitations lie primarily in the number of instrumented sections that can be used for individual setups. If two gauges are required at each section, for example, to determine neutral axis location and moment, then the number of instrumented sections for each test configuration is only ten. However, the system is expandable easily by purchasing additional strain gauges and boxes. The STS box automatically recognizes the number of gauges connected to the system and the software is easily configured to acquire readings from these gauges.

The software purchased as part of the system is used to control the tests primarily. It also contains features to plot the raw data in strain vs. truck position format, but can not be used to calculate neutral axis location or moment in a section. For this last purpose, a computer spreadsheet (Excel) was used to organize the acquired data into strain gauge pairs, calculate neutral axis position, and determine moment at instrumented positions as a function of truck position along the bridge. The spreadsheets, however, were set up for 20 gauges as is the case for the current system. They could be modified to accommodate and calculate a larger number of gauges if more are purchased in the future.

APPENDIX A - TESTING OF FIELD EQUIPMENT

Before the strain gauges were used in the field, they were tested using a four-point load setup in the load frame of the structural engineering laboratory at the University of Massachusetts Amherst (Figure A.1). The objective of these tests was to verify the behavior of BDI gauges and testing equipment, compare results with a standard laboratory strain gauge, compare measured strains with theoretical strains, and evaluate strain gauge attachment methods (bonded or clamped). Evaluation of different techniques for strain gauge attachment is presented in Appendix B.

A W12x30 beam, 90.5 inches (2.30 m) in length was supported by rollers on each end and loaded using a 3-foot (914 mm) load beam, centered on the top flange (Figure A.2). A single load piston applied force to the top of the load beam symmetrically at mid-span. This setup was created to produce a region of constant moment in the center of the W12x30 beam between the two load points.

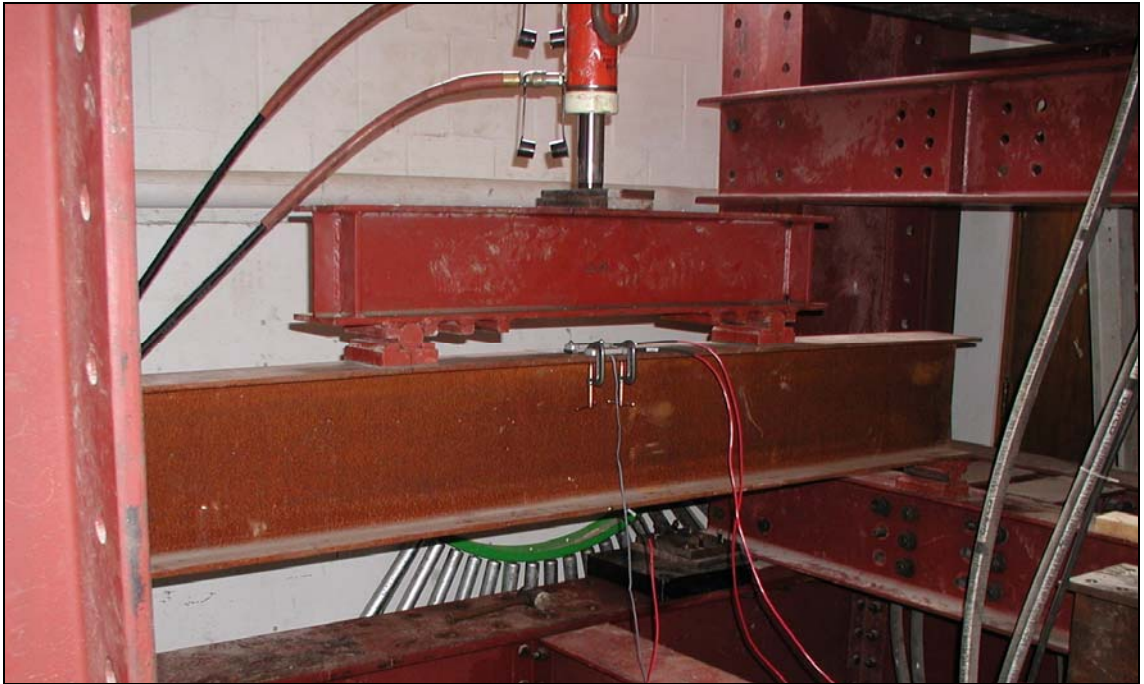


Figure A.1: Photograph of Beam in Four Point Load Test

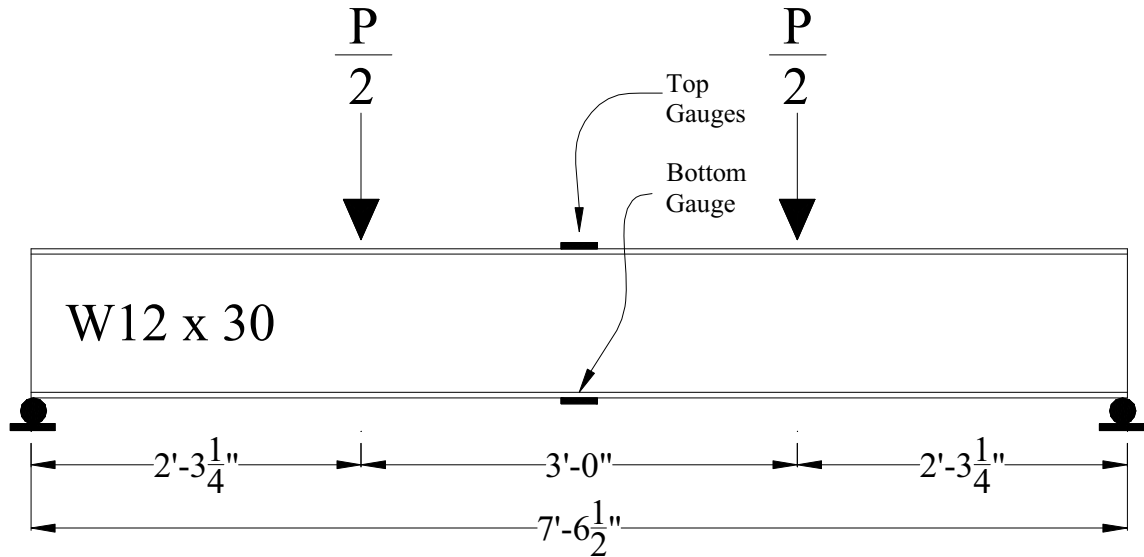


Figure A.2: Drawing of Test Setup

A.1 Testing Procedure

Each of the 22 BDI strain gauges purchased with the equipment was tested in a series of eight tests, with three gauges attached during each test. Additionally, an electrical resistance strain gauge was bonded to the beam and remained in place for all test loadings to provide a baseline for strain reading comparison. With gauges attached to the beam, the strain history of each gauge was recorded as a load was applied to the beam.

All of the strain gauges were attached mid-span to the W12x30 beam in the region of constant moment. Before attaching the laboratory gauge, the area under the gauge was sanded with heavy grit sandpaper, then cleaned with acid and neutralizer. The surface was then sanded again with lighter grit sandpaper and cleaned once more with the acid and neutralizer. The gauge was then centered on the top flange of beam to measure strain in the longitudinal direction and secured using the recommended adhesive for this application.

During each test, three BDI gauges were simultaneously tested. The first gauge was attached to the top flange of the W12x30 beam centered above the laboratory gauge (Figure A.3). The low profile of the lab gauge and the clearance below the BDI gauge spacing allowed this configuration. The second BDI gauge was clamped to the outside edge of the top flange. The third BDI gauge was attached to the bottom flange, centered at mid-span using tabs and adhesive.



Figure A.3: 2 BDI Gauges and Laboratory Gauge Attached to Top Flange

The gauges that used tabs were adhered to the steel surface using Loctite Black Toughened Instant Adhesive and Loctite Accelerator Metered Mist. Tabs were first secured to the strain gauge using a BDI tab jib to align tabs while the nuts were tightened. The beam was cleaned using a power grinder to remove surface rusting in locations the tabs would contact the beam.

After each test was complete, the BDI gauges were removed and the lab gauge was left in place to be re-used for subsequent tests. To remove a BDI gauge, the tab was held in place with an adjustable wrench while the nut was loosened. This prevented the tab from popping off the steel and damaging the gauge during removal. A new gauge was then attached by first securing the tab with a wrench before tightening the nut. Using this method the tabs remained adhered to the beam in the same location for all tests, and were used to attach multiple gauges.

A.2 Load and Strain Measurement

A hydraulic piston applied load to the center of the 3-foot load beam. The load beam was symmetrically supported by the W12x30 beam with rollers at each end. With this setup, half the force of the piston was applied to each load point on the W12x30 beam shown in Figure A.2.

Loading was controlled using a hand pump that pressurized the piston with hydraulic fluid. A pressure gauge was used to monitor the hydraulic fluid pressure during the test. The pressure is correlated to an applied force on the to the load beam using Equation [A.1] and the effective cylinder area of the piston of 5.15 in^2 (645 mm^2),

provided by the piston manufacturer. For reference and comparison of data, loading was temporarily stopped at 1000, 2000, and 3000 psi (6.89, 13.79, and 20.68 MPa) with corresponding forces calculated in Table A.1. Strain data was recorded for each gauge at a 1-Hz acquisition rate (1 data point/sec).

$$P = (\text{Gauge Pressure}) \cdot (\text{Effective Cylinder Area}) \quad [\text{A.1}]$$

A.3 Analysis and Test Results

A graphical comparison of readings was then created for each test similar to Figure A.4, with tensile strain plotted as positive and compression strain negative. The identifiers shown at the bottom of the figure are used for each group of data points, and correspond to the gauge number. The performance of each strain gauge included in these tests was determined by simple analysis of strain data history plots. Plateaus in the data occur when the loading was briefly stopped and held constant at the reference loads in Table A.1. The strains measured using BDI gauges on the top flange were averaged to produce the values listed in this table.

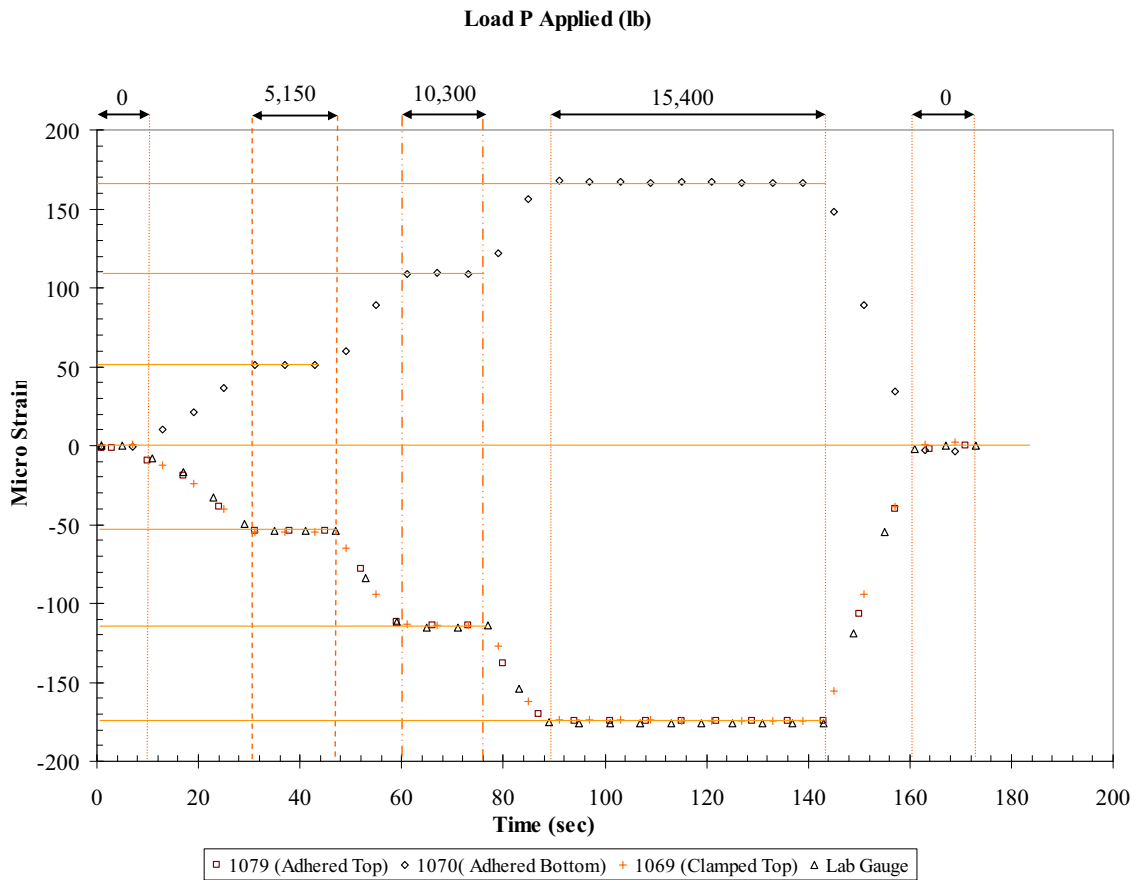


Figure A.4: Record of Strain History Tested In Load Frame

Table A.1: Reference Loads Applied to Beam

Load Point #	Hydraulic Pressure (psi)	Piston Force (lb)	Top Micro Strain	Bottom Micro Strain
1	1000	5,150	54	-51
2	2000	10,300	114	-110
3	3000	15,450	175	-167

The location of the neutral axis of bending could first be verified by comparing the strain measured during load holds (Figure A.5). From the strain history of top and bottom gauges, the strains of equal magnitude but opposite sign indicate the neutral axis of bending was measured to be within 3% of the theoretical location at mid-depth in the W12x30 beam.

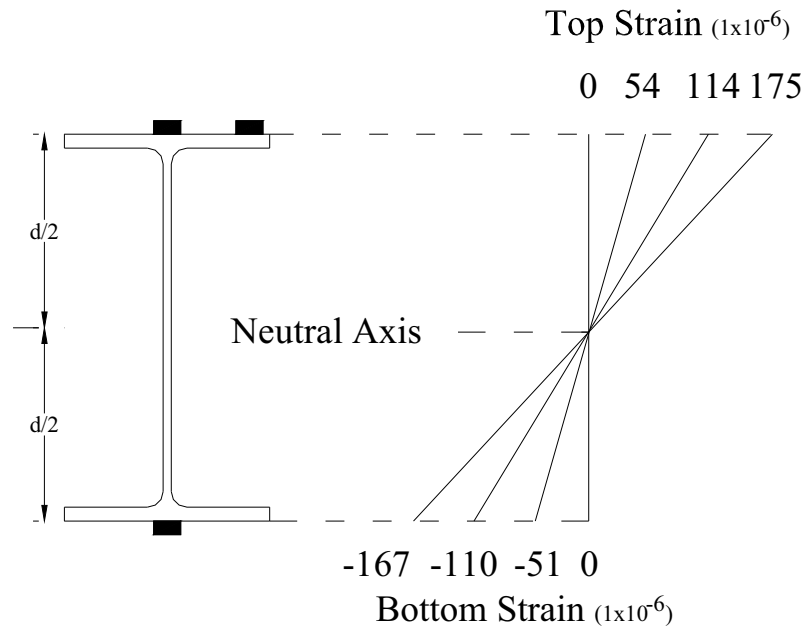


Figure A.5: Neutral Axis of Bending Calculation

The plot of strain history for the two top BDI gauges was compared with the laboratory gauge in each test. As illustrated by Figure A.4, the magnitude and shape of strain history of the laboratory gauge corresponds with both of the BDI gauges attached to the top flange. This comparison assures the performance of gauges to be used in the field, as the strain measurements were recorded using gauges and equipment from two manufacturers.

Comparisons between the two BDI gauges attached to the top flange of the beam shows gauges have identical strain histories. This indicates that the attaching method (either tabs with adhesive or clamps) does not appear to affect results. Additionally, the placement of a gauge on the steel beam flange either centered or near edge does not appear to significantly influence strain measurements. These

observations are important because placement of gauges at the center of the beam would be impossible for the field tests because of the presence of the bridge deck.

The strain history plot also demonstrates linear-elastic behavior of the W12x30 beam, as strain readings returned to zero when the load was removed. Therefore, at the conclusion of each test, no residual strain was measured in the beam or gauges.

A.4 Strain Calculation

The measured strains were also compared with the calculated strain expected in the top and bottom flange for the three levels of applied load (Equations [A.2] and [A.3]). The theoretical strain was calculated for each reference load and compared with measured strain in the test setup in Table A.2.

$$\sigma = \frac{M \cdot C}{I} = \frac{0.5 \cdot P \cdot a \cdot \frac{h}{2}}{I} \quad [\text{A.2}]$$

$$\varepsilon = \frac{\sigma}{E} = \frac{0.25 \cdot P \cdot a \cdot h}{E \cdot I} \quad [\text{A.3}]$$

$$\varepsilon = \frac{(0.352 \cdot P)}{29,000,000} \quad [\text{A.4}]$$

Where:

- σ = Stress (psi)
- a = Shear span (27-¼ in)
- C = Distance from neutral axis to extreme fiber (in)
- E = Modulus of elasticity of steel = 29x10⁶ (psi)
- h = Beam depth = 12.3 (in)
- I = Moment of inertia of W12x30 shape = 238 (in⁴)
- M = Moment = (Force P/2) (27-¼ in) (lb-in)
- P = Applied load (lb)
- ε = Calculated strain (in/in)

Table A.2: Comparison of Theoretical Calculated and Measured Strain

Reference Force (lb)	Calculated Strain (x10 ⁻⁶)	Measured Strain (Top) (x10 ⁻⁶)	Difference %
5,150	63	54	13.6
10,300	125	114	8.8
15,450	188	175	6.7

The test results show that the percent difference between calculated and measured strain in Table A.2 decreased with higher loading. Higher percent in

experimental error at low loads is common; therefore, these results are not surprising. The percent difference between calculated and measured strains is useful to provide an idea of the expected level of accuracy in the field tests depending on the magnitude of applied strains. Since strains are used to determine neutral axis locations, it is anticipated that neutral axis depth determined from field measurements can vary by as much as 10%.

APPENDIX B- TESTING OF GAUGE EXTENSIONS

Laboratory testing was conducted on the use of strain gauge extensions with the four-point beam loading setup described in Appendix A, in the Structural Engineering Laboratory of the University of Massachusetts Amherst. Extensions are aluminum channels sections with pre-drilled holes that can be attached to BDI gauges, to create an effective gauge length between 6 and 24 inches (152 and 610 mm). The objective of these tests was to investigate whether any measurable error occurs with the use of strain gauge extensions.

The manufacturer of the gauges and extensions typically recommends a correction factor of 1.11 for strain data recorded by any gauge with an attached extension. The correction factor accounts for strain developed along the metal extension and bolted connection between the gauge and extension.

B.1 Testing Procedure

Following the procedure outlined in the BDI literature, a setup was created to load the beam and create an area of constant moment (Figure A.2). Strain gauges with extensions that created an effective gauge length of 18 in (457 mm) were attached at mid-span on the W12x30 beam on both top and bottom flanges. The extension and gauge were adhered to the steel section using Loctite Adhesive and tabs. The tabs were adhered 9 in (229 mm) on either side of the beam centerline, such that the center of the effective gauge length was at mid-span (Figure B.1).

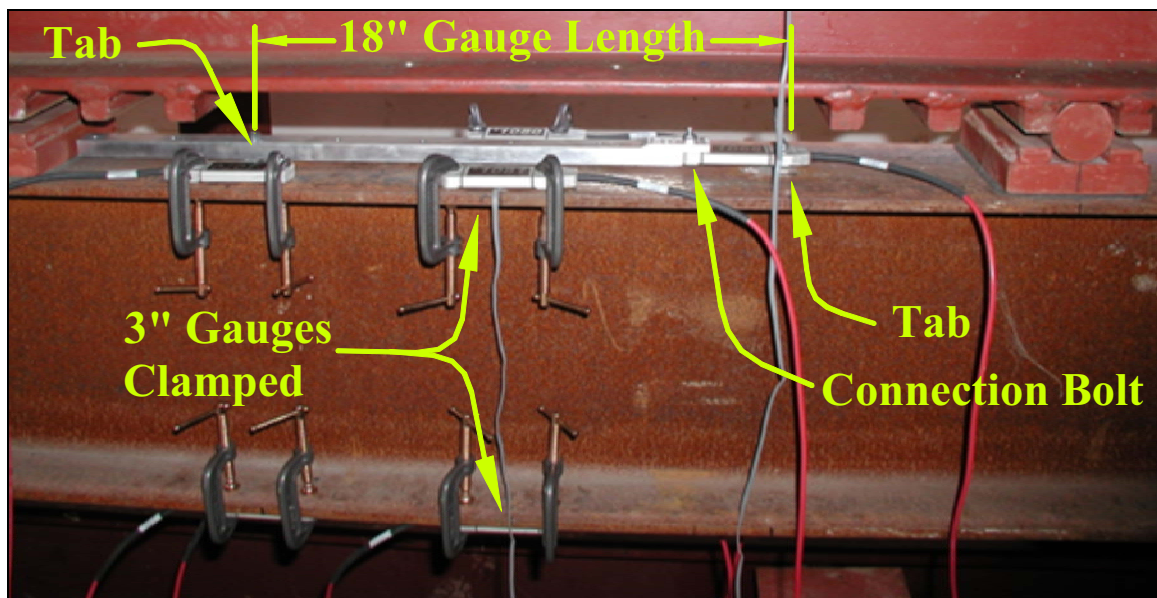


Figure B.1: Photograph of Gauges Attached to W12x30 Beam

Standard 3-in (76 mm) BDI gauges without extensions were also attached to the outer edge of both top and bottom flanges using 2-in (51 mm) clamps for comparison.

Two gauges without extensions were also placed at mid-span and two at the end of the extension. The beam was loaded using a hydraulic hand pump as described in Appendix A. A pressure gauge was used to track the loading, which was paused at three reference loadings of 1000, 2000, and 3000 psi (6.89, 13.79, and 20.68 MPa) during the test, following procedures described in Appendix A.

B.2 Analysis and Test Results

Raw data measured in these tests was plotted as shown in Figure B.2. The strain data recorded with extensions is then divided by six (6) for comparison with the raw data measured using 3-in (76 mm) gauges (Figure B.3). As the gauges with extensions were attached to the same flange as the gauges without extensions, it was expected that both strain readings should be identical.

It was observed that strains measured using gauges with extensions were consistently lower than those measured using gauges with no extensions. Using the recommended correction factor of 1.11, the strain history of both extended gauges and standard 3-in (76 mm) gauges is nearly identical (Figure B.4). These results indicate that a correction factor of 1.11 should be applied to data with the use of strain gauge extensions.

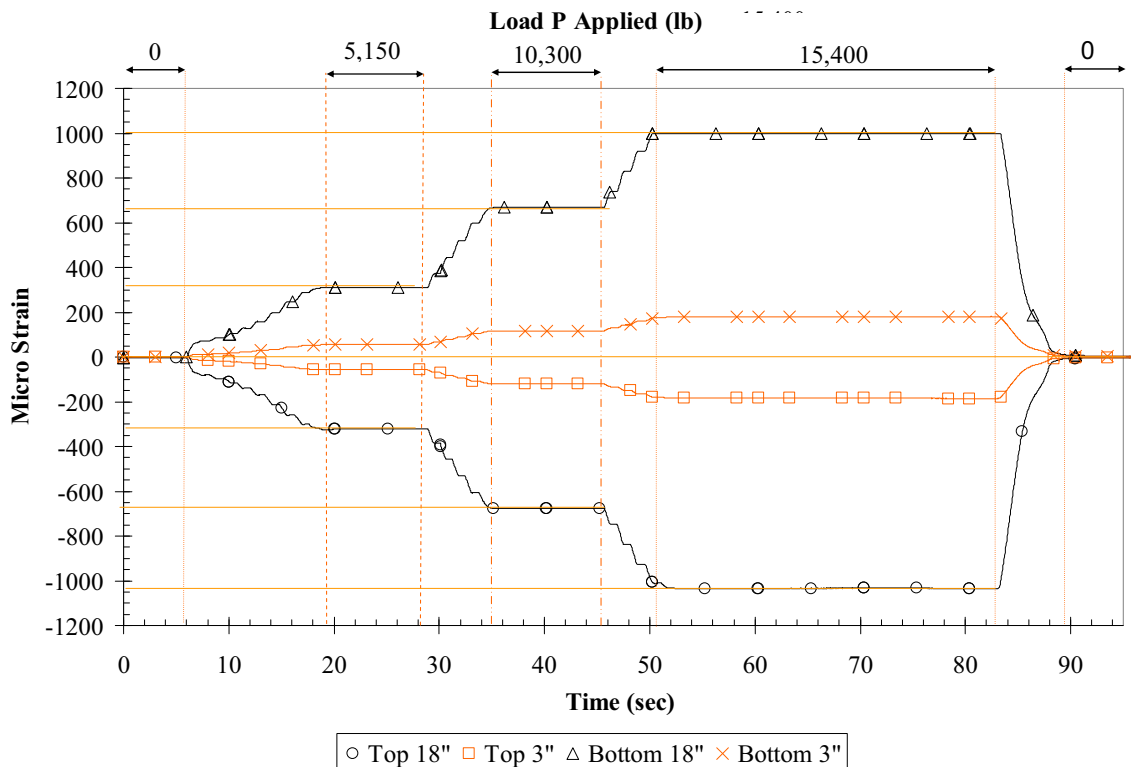


Figure B.2: Raw Strain Data

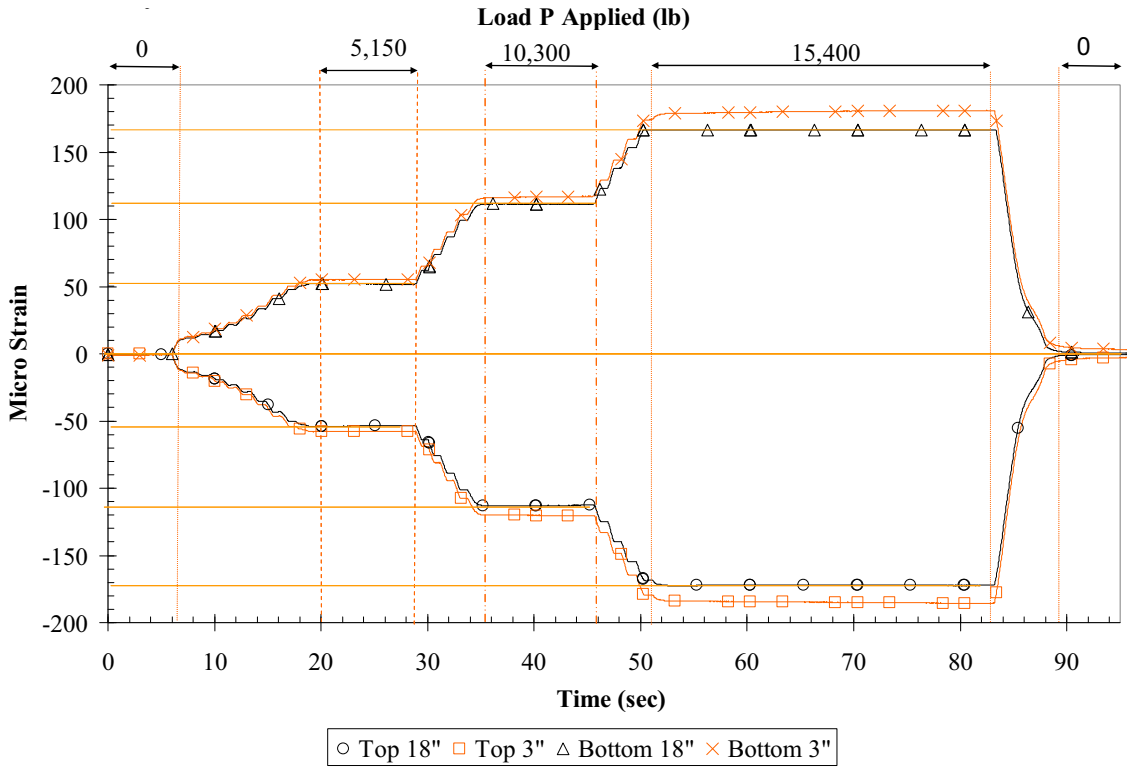


Figure B.3: Raw 3-in Gauge Strain and One-Sixth of 18-in Extension Strain

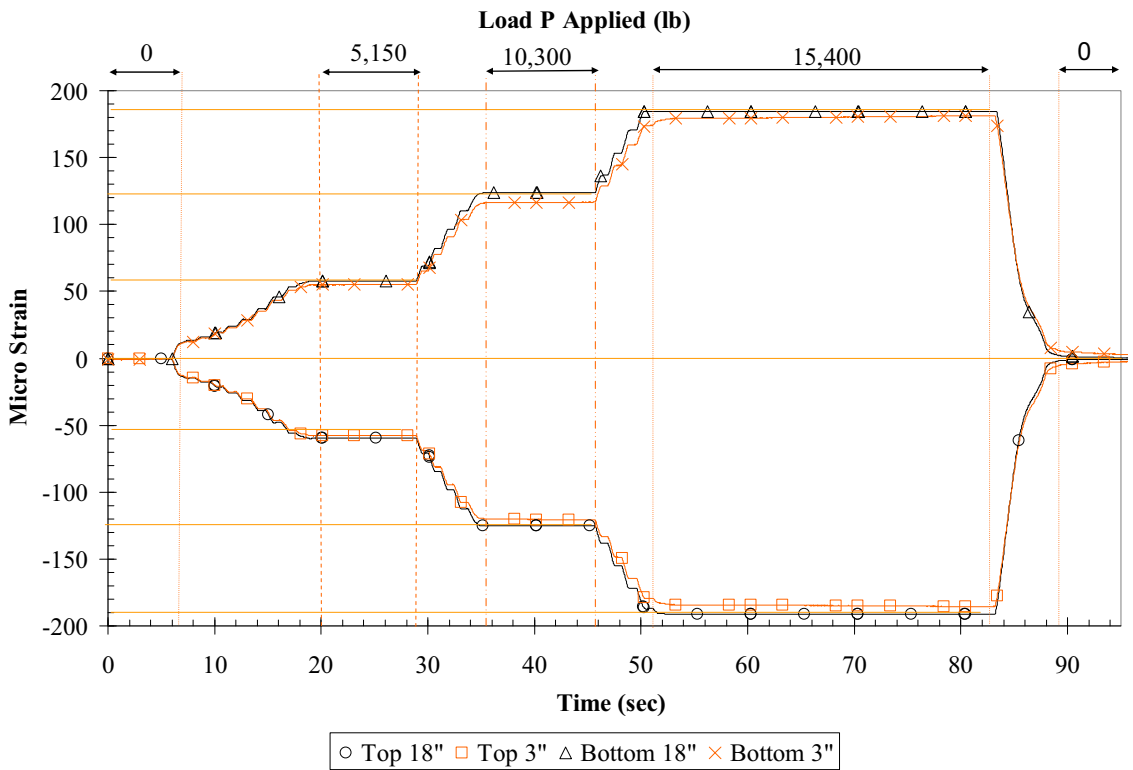


Figure B.4: Raw 3-in Gauge Strain and Corrected 18-in Extension Strain

APPENDIX C- GUIDE FOR CONDUCTING LOAD TESTS

This appendix is included to serve as a guide for conducting future load tests. It highlights general procedures and practices learned from conducting both the Royalton and Weathersfield tests. Methods described are based on the use of equipment manufactured by BDI described in Chapter 4.

C.1 Pre-Inspection Planning

Before setting foot into the field, the goal of the test must be determined to prioritize the focus of the investigation. Due to the necessary coordination and resources required to run a single test, the instrumentation and loading of a bridge may have to take place in a single day. Planning the location of each strain gauge is critical; they must be placed in select locations where the most useful data can be obtained to accomplish the goals of the test.

As-built drawings of the bridge and a field pre-inspection of the bridge condition are useful to help determine strain gauge placement. In both tests conducted for this project gauge pairs were placed at mid-span and at beam-ends to determine the shape of moment diagrams and record maximum moments. When creating instrumentation plans, it is important to keep in mind constraints in the field that may control the placement of gauges such as access to the structure, traffic control during installation, and the cable length available to connect all gauges to the system.

During the pre-inspection visit, the dimensions of as-built construction drawings should be verified for any inconsistencies. This ensures accurate instrumentation plans can be created prior to arrival in the field.

C.2 Attaching Strain Gauges

Measurements from the instrumentation plan based on as-built drawings or prior field reconnaissance are used to first mark the locations of each gauge. After the location of a gauge has been established, the spot on the bridge must be cleaned and prepared for gauge attachment to ensure a good bond. Loose surface materials such as concrete chips, peeling paint, or rust are not suitable for gauge attachment and must be removed before placing a gauge. For concrete members, grinders powered by a generator can be used to smooth the surface with a stiff brush to clean residual dust. On steel members, grime should be brushed away from the surface in locations where the tabs or clamps will hold the gauges.

If possible, clamps should be used to attach gauges on steel members. From laboratory tests described in Appendix A, clamps give nearly identical results to using tabs and adhesive. The advantage of using clamps is that these gauges will not detach from a structural member during the test, and gauges are attached much rapidly. Clamps are also easier to install and remove and do not require cleaning.

Adhesive can be used to attach gauges to either steel or concrete members with the use of removable tabs that are bolted to the strain gauge. It was found that Loctite Black Toughened Instant Adhesive and Loctite Accelerator Metered Mist provided a good bond to members for the testing, and could be easily removed after tests to switch gauges.

To attach a gauge, a small bead of adhesive is first squeezed onto each tab after it has been secured to the gauge. The tabs are then gently pressed against the structural member in the desired location to mark their exact location on the surface. Next, the gauge and tabs are removed, and adhesive is sprayed with accelerator. The tabs are then quickly pressed back against the desired location of the bridge and held in place. In less than one minute, a proper bond forms that is sufficient to hold the gauge in place for testing.

Gauge pairs located in direct sunlight were found to have noticeable drift in strain readings due to temperature changes with the aluminum gauge and extension. In these conditions, a white sheet can be placed over the gauges to reduce solar heating effects.

After all of the gauges are attached and wired, the serial number of each gauge must be recorded along with their location on the bridge. The testing system identifies the strain data by the serial number of each gauge regardless of the configuration. Sketches illustrating the location of strain gauges as determined during test planning are useful for this purpose. It is important to keep good field notes with the location of the gauge on the bridge for post processing and analysis of data.

After all test runs are performed for a setup, gauges are removed from the bridge. If gauges are attached using the tab and adhesive method, each tab must be removed from the gauge and replaced with a clean tab, since excess adhesive remains on the tab after each test. Cleaning can be performed using acetone. With the use of a jib developed by BDI the tabs can be quickly removed and new ones attached without causing damage to the gauge. During the switching procedure, one person was assigned to clean the adhesive and any concrete from the tabs using acetone, thereby allowing tabs to be re-used for future tests configurations.

C.3 Load Vehicle

The load vehicle selected for testing should be of sufficient weight to generate a moderate bridge response without causing damage. While the test should not load a bridge beyond service limits, loadings well below service limits may not generate a significant response from the bridge, and measurements will have the highest percent of experimental error.

The individual axle weight of the loading vehicle and geometry must be recorded for calibration of a finite element model. In both tests conducted with this project, portable scales were provided by the Department of Motor Vehicles of the Vermont Agency of Transportation to weight individual tire loads.

Longitudinal truck position can be tracked with the use of the AutoClicker, manufactured by BDI. The AutoClicker uses a portable radio to emit a click at each tire revolution, which is recorded by a second radio connected to the laptop computer. To

correlate distance traveled between clicks, this distance must be recorded in the field. The average distance traveled per wheel revolution was determined by measuring the distance that the load truck traveled during five wheel revolutions. This distance was then divided by five to obtain the distance traveled per click registered by the AutoClicker.

Prior to moving the load vehicle on the bridge, traveling lanes should be defined and marked for the driver to follow during the test. Finally, the starting point of the loading truck should be defined away from the bridge abutment and kept constant for each travel lane for consistency throughout testing.

C.4 Use of More Than One Load Vehicle

After determining the goal of a test, it may be advantageous to use more than one load vehicle for the test based on the estimated weight of an available load vehicle. In the Weathersfield Bridge test, it was calculated that having two vehicles traverse the bridge at the same time would generate a moment close to the maximum service moment over interior piers, which was a primary interest of the test.

Using more than one load truck can create a challenge when attempting to track the position of both vehicles during the test. The AutoClicker works well with one truck as long as the travel lane is known. Unfortunately, only one AutoClicker can be connected to the equipment at any time.

To track both load vehicles in the Weathersfield test, two methods were used to determine their position. The first method was used during high-speed runs where drivers were asked to drive side-by-side in parallel travel lanes. Because the AutoClicker could not be used at high speeds, a portable radio was used by an observer to manually “click” when the trucks crossed bridge abutments. However, it was found that drivers had difficulty maintaining the same pace, which resulted in one truck being consistently ahead of the other. Additionally, the observer who manually marks the trucks passing introduced some margin of error.

The methodology used for the remainder of the runs solved both of these problems. A chain was used to connect the trucks back-to-back leaving a specified distance between the trucks. The front truck could tow the rear truck in neutral gear with tension in the chain to maintain a constant spacing (Figure C.1). The AutoClicker was attached to the front truck to monitor the load position.



Figure C.1: Photo of Load Truck Being Pulled With Chain

C.5 Equipment Setup

In addition to strain gauges and wiring, the equipment necessary to run the field test includes an electrical source, power supply unit for strain gauges, and a laptop computer. The electrical source used in the field was a standard deep-cycle battery, connected to an inverter. Both the laptop computer and power supply box for strain gauges were powered from the battery during the day of testing.

The location of the computer and power supply is governed by the bridge site, and the length of cable available to reach from strain gauges attached to the bridge to the power source. Ideally, the computer operator can be positioned to observe the load testing above the bridge. This allows the operator a line of sight to balance strain gauges prior to testing when no vehicles are loading the bridge, and control recording of strain data when the load truck is in position. When the operator does not have a line of sight to the load truck, portable radios on a different frequency from the AutoClicker radio can be used to communicate with persons above the bridge deck. This procedure was used with ease in the Weathersfield Bridge testing where given site constrains the computer operator was located below the bridge.

APPENDIX D- DATA FORMATTING AND VISUAL BASIC

This appendix is included to serve as a guide for formatting raw strain data recorded with BDI load testing equipment. Included is an overview of steps and calculations that were performed prior to data analysis using software developed by BDI and Microsoft Excel. Steps include the import of data to Microsoft Excel, input of test parameters, and running two visual basic macros. The macros were created to organize the raw data file into gauge pairs, and then calculate neutral axis depths and moments.

D.1 Formatting Raw Data

Raw strain data recorded in the field is first opened and formatted with WinGRF software written by BDI, without the initial subtraction option that can be used to modify the data. Next, the clicker override feature is used to override the default clicker spacing. The distance the load vehicle traveled between clicks of the AutoClicker as recorded in field notes is entered as a positive distance in feet next to all clicker times; except the first clicker time is left at zero feet. The file can then be closed without saving, as the process of opening the file and inputting the clicker time has already modified the raw data file.

After launching Microsoft Excel and selecting FILE > OPEN, the modified data file can be opened after selecting “delimited” by comas. The modified data as opened in Microsoft Excel is then copied and pasted directly into a new file with a template and visual basic program written by Andrew Jeffrey and Josh Rubero. The first tab in the file is a master input page for the user. Additional tabs in the template file that are linked to the master input tab are setup for data storage, calculations, and printing graphs.

D.2 Organization of Modified Data

When a modified raw data file is opened with Microsoft Excel, data in the first 21 rows contain information about the test record including a list of strain gauges used in the test by serial number, and the sample frequency that was used to record strain data. Beginning on row 22 (time zero), strain data points are recorded for each strain gauge in subsequent rows, corresponding to a point in time. In tests conducted with a sampling frequency of 33.33 hertz, 33.33 rows of data were created per second for each strain gauge connected to the system.

The rows below strain data in the modified raw data file contain the starting position of the truck before the bridge abutment in feet, the distance the load vehicle travels between each click, the total number of clicks made by the AutoClicker in the record, and the time of each click rounded to the nearest second.

D.3 Main Visual Basic Macro

The main program determines the recording time for each strain data point and corresponding location of the load truck. It then organizes all data by gauge pairs and calculates a neutral axis depth for each gauge pair. The macro is run individually in each tab of Excel that the modified raw data is input. The gauge serial numbers, gauge pair spacing, minimum strains considered, secondary gauge factors, distance interval, and initial data offset are input by the user on the master input tab and are used by the program in calculations.

D.3.1 Load Truck Position and Time

The time between each row of data recorded is calculated using Equation [D.1]. In the test record, the exact position of the load vehicle is known only at the time of each AutoClicker mark. The distance traveled by the load truck between the times of AutoClicker marks must therefore be calculated.

Because the load truck speed is approximately constant during the test, it is assumed that the speed of the truck between clicker times is constant. Therefore, between two clicker times x and y , the distance traveled by the load vehicle between two rows of recorded data are calculated with Equation [D.2]. Using these equations, the macro determines the exact time each row of strain data was recorded as well as the corresponding position of load vehicle.

$$\text{Seconds Between Sequential Rows of Recorded Data} = \frac{1}{F} \quad [\text{D.1}]$$

$$D_T = \frac{D_C}{\left(T_y - T_x\right) \cdot F} \quad [\text{D.2}]$$

Where:

D_C = Clicker distance (ft)

D_T = Distance traveled between sequential rows of data (ft)

F = Sampling Frequency (Hz)

T_x = Time at click mark x in data (sec)

T_y = Time at click mark y in data (sec)

D.3.2 Organization of Data into Gauge Pairs

The modified raw data file lists the strain history of each gauge in columns marked by the serial number of the gauge used to record the data. Because strain gauges connected to the system are randomly listed in columns, the program uses a search algorithm to find each gauge and column then sort the data by gauge pairs. The

user must specify pairs of gauges used in the test at each instrumented section on a master input page by serial numbers. Once the column with a gauge is found by the search algorithm, the strain data in that column is copied and pasted by the macro into a nearby column, and organized by the user specified gauge pairs.

Although the strain gauges were balanced before each load test, small initial strain readings sometimes occur at the start of the test. To correct these readings, a user specified option is included on the master input tab to force the first reading in the strain history to be zero. If the initial subtraction option is selected, the first value of strain data found in row 22 is subtracted from all subsequent rows of data in the strain history when the data is copied by the macro to a nearby column. If the initial subtraction is not selected, the strain data is copied directly to a nearby column without subtraction.

The macro also has the ability to apply a secondary gauge factor to all strain data, with a user input on the master input tab. This option was developed for tests conducted using gauge extensions on reinforced concrete, incorporating the factors described in Appendix B.

D.3.3 Comparing Data From Repeated Test Runs

During the bridge tests, runs were often repeated with the truck traversing the bridge in the same lane for repetition. For this comparison, the two modified raw data files must be copied into different worksheet tabs in the template Excel file. The data between each of these runs is then graphically compared to check for consistency. Because the raw strain data is recorded against time, the distance calculated by the main visual basic macro with Equation [D.2] is used to compare the two strain histories. If it is found that the strain history data is nearly identical for a truck in the same lane, the strain data is averaged.

D.3.4 Calculation of Neutral Axis Depth

The next step of the program is to calculate the neutral axis of bending from the interpolated strain history using Equation [D.3] for each row of strain data. This equation uses the distance between top and bottom gauges input by the user on the master input worksheet tab.

$$\bar{y} = \frac{-\varepsilon_B \cdot D_{\text{Gauge}}}{\varepsilon_T - \varepsilon_B} \quad \text{[D.3]}$$

Where:

\bar{y} = Neutral Axis depth above bottom gauge (ft)

D_{Gauge} = Distance between top and bottom gauges attached at a cross section (ft)

ε_T = Strain in top gauge ($\mu\varepsilon$)

ε_B = Strain in bottom gauge ($\mu\varepsilon$)

The user also has the option of not calculating the neutral axis if strain values are below a defined threshold. As the neutral axis calculation is based on the geometric angle of the strain profile, very small angles introduce a large amount of error in the calculation (Section A.4). The user can input the absolute value of a minimum strain value for either top or bottom gauges, below which the program will not calculate a neutral axis depth.

D.3.5 Strain and Neutral Axis at Incremental Distances

To average the strain values between test runs, common distance points first have to be created in both test records, as the load truck position versus time is not identical in both test runs. An algorithm in the program creates these common distance points at intervals input by the user and interpolates strain from each test at this point.

The user can control the number of calculations by changing the input incremental distance on the master input worksheet tab. The strain values calculated at incremental distances of the two test runs can then be compared. The program uses Equation [D.4] to interpolate strain values in two rows with the closest distance both before and after the incremental distance. The last step of the first macro is to calculate the neutral axis depth at each of the interpolated strain points for each gauge pair using the same procedure described above.

$$\text{Interpolated Strain} = \varepsilon_A - \frac{(\varepsilon_B - \varepsilon_A) \cdot (D_B - D_I)}{(D_B - D_A)} \quad [\text{D.4}]$$

Where:

D_A = Distance point before increment (ft)

D_B = Distance point after increment (ft)

D_I = Increment Distance (ft)

ε_A = Strain corresponding to distance point before increment ($\mu\varepsilon$)

ε_B = Strain corresponding to distance point after increment ($\mu\varepsilon$)

D.4 Moment Visual Basic Macro

The interpolated strain data and neutral axis depth for both test runs is averaged by a linked worksheet tab in the Excel file. A second macro can then be used to calculate the moment at each of these points, using properties of the structural member and bridge deck on the master input page. Separate macros were created to perform moment calculations for the Royalton and Weathersfield Bridges.

D.4.1 Royalton Moment Calculation

Bending moments are calculated for the Royalton Bridge about the calculated neutral axis, considering the dimensions and material properties of each instrumented

beam section. Using the strain profile, stress is determined assuming a modulus of elasticity for each material and that plane sections remain plane with bending. Moment is calculated only where a neutral axis depth was determined by the first macro and the lower strain lower strain exceeds the input minimum value.

Using Equation [D.5] stress is calculated at the centroid of each reinforcing bar layer in tension. Average stress at the centroid of rectangular concrete areas is determined using the stress at the top and bottom of rectangular shapes. The stress at the top of the slab is calculated using Equation [D.6], bottom of slab using Equation [D.7] and bottom of the beam using Equation [D.8].

$$f_s = E_s \cdot \left[\frac{c - (\bar{y} + h_{BG})}{\left[\frac{D_{Gauge}}{\varepsilon_T - \varepsilon_B} \right]} \right] \quad [D.5]$$

$$f_{C \text{ slab top}} = E_c \cdot \left[\frac{h - (\bar{y} + h_{BG})}{\left[\frac{D_{Gauge}}{\varepsilon_T - \varepsilon_B} \right]} \right] \quad [D.6]$$

$$f_{C \text{ slab bottom}} = E_c \cdot \left[\frac{(h - t_s) - (\bar{y} + h_{BG})}{\left[\frac{D_{Gauge}}{\varepsilon_T - \varepsilon_B} \right]} \right] \quad [D.7]$$

$$f_{C \text{ beam bottom}} = E_c \cdot \left[\frac{\bar{y} - h_{BG}}{\left[\frac{D_{Gauge}}{\varepsilon_T - \varepsilon_B} \right]} \right] \quad [D.8]$$

Where:

c = Centroid of rebar layer (in)

D_{Gauge} = Gauge spacing (in)

E_c = Modulus of elasticity of concrete (ksi)

E_s = Modulus of elasticity of steel (ksi)

ε_T = Strain in top gauge (micro-strain)

ε_B = Strain in bottom gauge (micro-strain)

f_s = Stress in steel (ksi)

f_c = Stress in concrete (ksi)

h = Beam height (in)

h_{BG} = Height of bottom gauge above bottom of T-beam (in)

\bar{y} = Neutral axis location above bottom strain gauge (in)

To calculate moments in each section, concrete areas in compression and tension as well as steel rebar in tension are considered. In positive bending, the concrete area above the neutral axis of bending is in compression and the rebar at the bottom of the T-beam is in tension. In negative bending, concrete below the neutral axis is in compression and concrete and rebar above the neutral axis in the slab is in tension.

D.4.1.1 Roylton Positive Moment Calculation with Neutral Axis in T-Beam Stem

When calculating moments, a cross section is considered to be in positive bending when the top of the deck slab ($f_{c \text{ slab top}}$) is in compression and the bottom of the T-beam ($f_{c \text{ beam bottom}}$) is in tension. Cross sectional dimensions and material properties listed in Table D.1 must be entered into the master input page for positive moment calculation.

Table D.1: Input Parameters for Positive Bending Moment Calculation

Deck	Beam
1. Slab depth	1. Total beam height (slab and stem)
2. Effective width	2. Beam width
3. Modulus of elasticity of concrete	3. Steel area for each layer of rebar
	4. Centroid of each steel rebar layer above beam bottom
	5. Modulus of elasticity of steel rebar
	6. Modulus of elasticity of concrete

The neutral axis may be located either below the deck slab (Figure D.1) or in the slab (Figure D.2). If the neutral axis is below the slab, moment (M_1) is determined from the compressive stress in the concrete stem (Area 1) using Equation [6.9] and moment (M_2) from compressive stresses in the slab (Area 2) with Equation [6.10]. Moment (M_3) is determined from tensile stresses in the stem (Area 3) with Equation [D.11]. The moments (M_4 and M_5) from each layer of reinforcement are calculated using Equation [6.11] and [6.12]. The total cross sectional moment is then calculated with Equation [6.14].

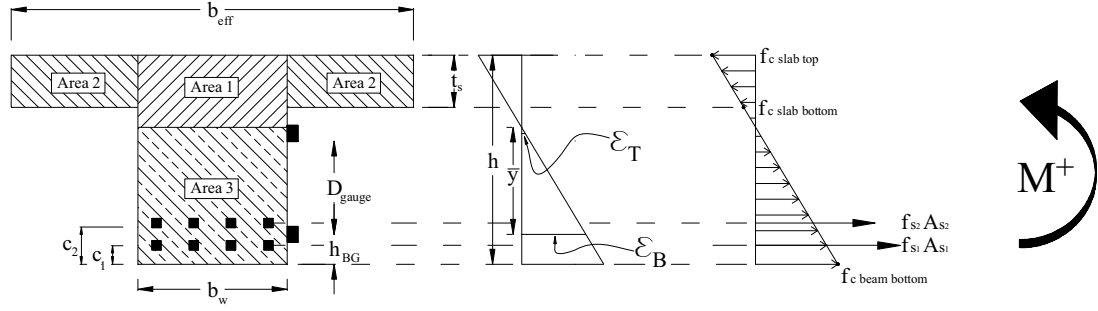


Figure D.1: Cross Section in Positive Bending with Neutral Axis Below Slab

$$M_1 = (h - \bar{y} - h_{BG}) \cdot b_w \cdot \frac{f_{C \text{ slab top}}}{2} \cdot \frac{2}{3} \cdot (h - \bar{y} - h_{BG}) \quad [\text{D.9}]$$

$$M_2 = t_s \cdot (b_{\text{eff}} - b_w) \cdot \left(\frac{f_{C \text{ slab top}} - f_{C \text{ slab bottom}}}{2} \right) \cdot \left(h - \bar{y} - h_{BG} - \frac{t_s}{3} \right) +$$

$$t_s \cdot (b_{\text{eff}} - b_w) \cdot f_{C \text{ slab bottom}} \cdot \left(h - \bar{y} - h_{BG} - \frac{t_s}{2} \right) \quad [\text{D.10}]$$

$$M_3 = (\bar{y} + h_{BG}) \cdot b_w \cdot \frac{f_{C \text{ beam bottom}}}{2} \cdot \frac{2}{3} \cdot (\bar{y} + h_{BG}) \quad [\text{D.11}]$$

$$M_4 = A_{s1} \cdot f_{s1} \cdot (\bar{y} - c_1 + h_{BG}) \quad [\text{D.12}]$$

$$M_5 = A_{s2} \cdot f_{s2} \cdot (\bar{y} - c_2 + h_{BG}) \quad [\text{D.13}]$$

$$M = \frac{1}{12} [|M_1| + |M_2| + |M_3| + |M_4| + |M_5|] \quad [\text{D.14}]$$

Where:

A_s = Area of reinforcing bar steel in layer (in²)

b_w = Beam width (in)

b_{eff} = Effective deck width (in)

M = Moment (k-ft)

t_s = Slab thickness (in)

D.4.1.2 Roylton Positive Moment Calculation with Neutral Axis in T-beam Slab

For the neutral axis within the top slab in positive bending (Figure D.2), the moment (M_5) from compression concrete stresses in Area 1 is calculated with Equation [D.15]. The moment (M_7) from tension concrete stresses in Area 2 are calculated using Equation [D.16]. Moment (M_8) from tension concrete stresses in Area 3 is calculated using Equation [D.17]. The moments (M_9 and M_{10}) of each layer of reinforcement are

calculated using Equation [D.18] and Equation [D.19]. The total moment for this section is calculated using Equation [D.20].

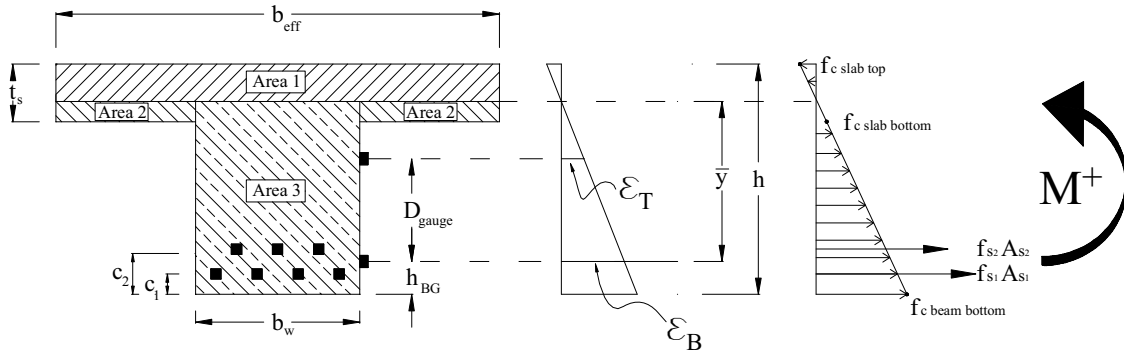


Figure D.2: Cross Section in Positive Bending with Neutral Axis in Slab

$$M_6 = (h - \bar{y} - h_{BG}) \cdot b_{eff} \cdot \frac{f_{C \text{ slab top}}}{2} \cdot \frac{2}{3} \cdot (h - \bar{y} - h_{BG}) \quad [D.15]$$

$$M_7 = [t_s - (h - \bar{y} - h_{BG})] \cdot (b_{eff} - b_w) \cdot \frac{f_{C \text{ bot}}}{2} \cdot \frac{2}{3} \cdot [t_s - (h - \bar{y} - h_{BG})] \quad [D.16]$$

$$M_8 = (\bar{y} + h_{BG}) \cdot b_w \cdot \frac{f_{C \text{ beam bot}}}{2} \cdot \frac{2}{3} \cdot (\bar{y} + h_{BG}) \quad [D.17]$$

$$M_9 = A_{s1} \cdot f_{s1} \cdot (\bar{y} - c_1 + h_{BG}) \quad [D.18]$$

$$M_{10} = A_{s2} \cdot f_{s2} \cdot (\bar{y} - c_2 + h_{BG}) \quad [D.19]$$

$$M = \frac{1}{12} [|M_6| + |M_7| + |M_8| + |M_9| + |M_{10}|] \quad [D.20]$$

D.4.1.3 Roylton Negative Moment Calculation

A cross section is considered to be in negative bending when the top of slab ($f_{C \text{ slab top}}$) is in tension, and the bottom of beam ($f_{C \text{ beam bottom}}$) is in compression (Figure D.3). The areas of concrete in tension and compression as well as tensile reinforcement in the deck slab are considered when calculating the negative moment. Cross sectional dimensions and material properties listed in Table D.2 must be entered into the master input page for negative moment calculation.

Table D.2: Input Parameters for Moment Calculation with Positive bending

Deck	Beam
1. Slab depth	1. Total beam height (slab and stem)
2. Effective width	2. Beam width
3. Steel area for each layer of rebar	3. Modulus of concrete
4. Centroid of each steel rebar layer above beam bottom	
5. Modulus of elasticity of steel rebar	
6. Modulus of elasticity of concrete	

The moment (M_{11}) from concrete stresses in compression in Area 1 are calculated with Equation [D.21]. Moment (M_{12}) from tension stress in concrete in Area 2 is calculated using Equation [D.22]. Moments (M_{13} and M_{14}) from tension stress in concrete in Area 3 are calculated using Equation [D.23] and Equation [D.24]. Contributions to the total moment from the reinforcing bar layers (M_{15} and M_{16}) in the deck slab are calculated using Equation [D.25] and Equation [D.26]. The total moment for this section is calculated using Equation [D.27].

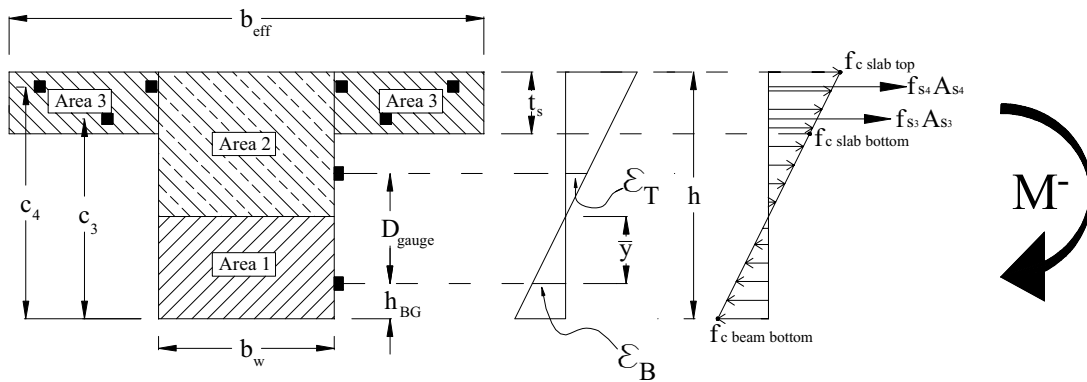


Figure D.3: Cross Section in Negative Bending

$$M_{11} = (\bar{y} + h_{BG}) \cdot b_w \cdot \frac{f_{C \text{ beam bottom}}}{2} \cdot \frac{2}{3} \cdot (\bar{y} + h_{BG}) \quad [\text{D.21}]$$

$$M_{12} = (h - \bar{y} - h_{BG}) \cdot b_w \cdot \frac{f_{C \text{ top}}}{2} \cdot \frac{2}{3} \cdot (h - \bar{y} - h_{BG}) \quad [\text{D.22}]$$

$$M_{13} = t_s (b_{\text{eff}} - b_w) \cdot \frac{f_{C \text{ top}} - f_{C \text{ bot}}}{2} \cdot \left(h - \bar{y} - h_{BG} - \frac{t_s}{3} \right) \quad [\text{D.23}]$$

$$M_{14} = t_s (b_{\text{eff}} - b_w) \cdot f_{C \text{ bot}} \cdot \left(h - \bar{y} - h_{BG} - \frac{t_s}{2} \right) \quad [\text{D.24}]$$

$$M_{15} = A_{s3} \cdot f_{s3} \cdot [c_3 - \bar{y} - h_{BG}] \quad [\text{D.25}]$$

$$M_{16} = A_{s4} \cdot f_{s4} \cdot [c_4 - \bar{y} - h_{BG}] \quad [\text{D.26}]$$

$$M = -\frac{1}{12} [|M_{11}| + |M_{12}| + |M_{13}| + |M_{14}| + |M_{15}| + |M_{16}|] \quad [\text{D.27}]$$

D.4.2 Weathersfield Moment Calculation

Bending moments are calculated for the Weathersfield Bridge about the calculated neutral axis, using calculated section properties of each instrumented beam section. The macro can be used with the assumption of either composite or non-composite behavior of the bridge deck with steel girders.

The user has the option of only entering data for the girder if the deck acts non-compositely or may include properties of the concrete deck for composite behavior. Different deck properties may be entered on the master input page for both positive bending (lower gauge in tension) and negative bending (lower gauge in compression).

D.4.2.1 Positive Bending Moment of Inertia

For bridges with a composite concrete deck and steel girders in positive bending (Figure D.4), the concrete section is transformed into an effective steel area to calculate the total moment of inertia. For these calculations, the parameters listed in Table D.3 must be entered on the master input page for each gauge pair.

The composite calculation ignores any contributions from rebar in the deck and only considers the effective concrete area in compression. The total moment of inertia including both girder sections and a composite slab is calculated using Equations [5.8] and [5.9]. The modulus of elasticity of the concrete deck is calculated on the master input tab using Equation [6.1].

Table D.3: Input Parameters for Composite Sections in Positive bending

Deck	Girder
1. Moment of inertia	1. Moment of inertia
2. Modulus of elasticity of concrete	2. Modulus of elasticity
3. Centroid of deck above lower strain gauge	3. Centroid of beam above lower strain gauge
4. Effective area of concrete	4. Area of beam section

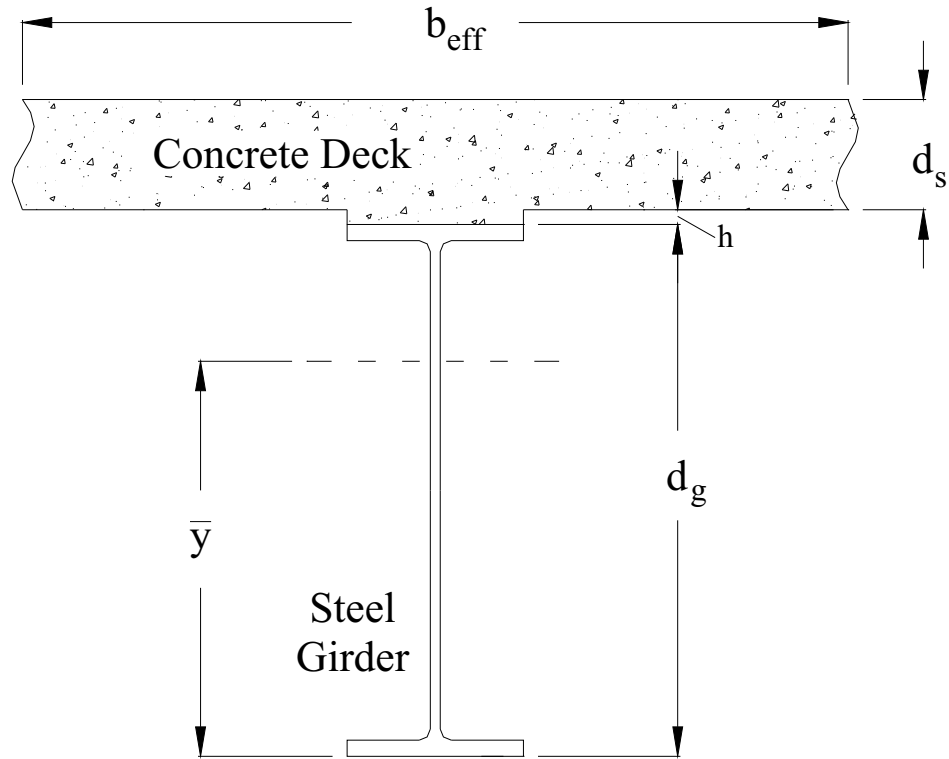


Figure D.4: Cross Section of Typical Composite Section in Positive Bending

$$I_d = \frac{b_{\text{eff}} \cdot (d_s)^3}{12} \quad [\text{D.28}]$$

$$I_{\text{Comp}} = \left[I_g + \left(A_g \cdot \left(\bar{y} - \frac{d_g}{2} \right)^2 \right) \right] + \quad [\text{D.29}]$$

$$\frac{E_d}{E_g} \cdot \left[I_d + (b_{\text{eff}} \cdot d_s) \cdot \left(\left(d_g + h + \frac{d_s}{2} \right) - \bar{y} \right)^2 \right] \quad [\text{D.30}]$$

$$E_d = 57 \sqrt{f'_c}$$

Where:

- A_g = Area of steel girder cross section (in²)
- b_{eff} = Effective width of concrete deck (in)
- d_g = Depth of steel girder (in)
- d_s = Depth of slab (in)
- E_d = Modulus of elasticity of deck material (ksi)
- E_g = Modulus of elasticity of girder material (ksi)
- f'_c = Concrete compressive strength (psi)
- h = Depth of haunch (in)
- I_d = Moment of inertia of deck (in⁴)
- I_g = Moment of inertia of girder (in⁴)
- y = Neutral Axis depth above bottom gauge (in)

D.4.2.2 Negative Bending Moment of Inertia

For bridges with a composite concrete deck and steel girders in negative bending (Figure D.5), reinforcing bars in the deck parallel to girders can be considered to contribute the effective moment of inertia of each girder. Up to two layers of steel reinforcement in the deck can be input for calculation using Equation [5.10]. The parameters listed in Table D.4 must be entered on the master input page for each gauge pair to consider composite behavior.

Table D.4: Input Parameters for Composite Sections in Negative Bending

Deck	Beam
1. Modulus of elasticity of reinforcing bars	1. Moment of inertia
2. Total steel area in each layer (if any)	2. Modulus of elasticity
3. Centroid of each layer of rebar above lower gauge	3. Centroid of beam above lower strain Gauge
	4. Area of beam section

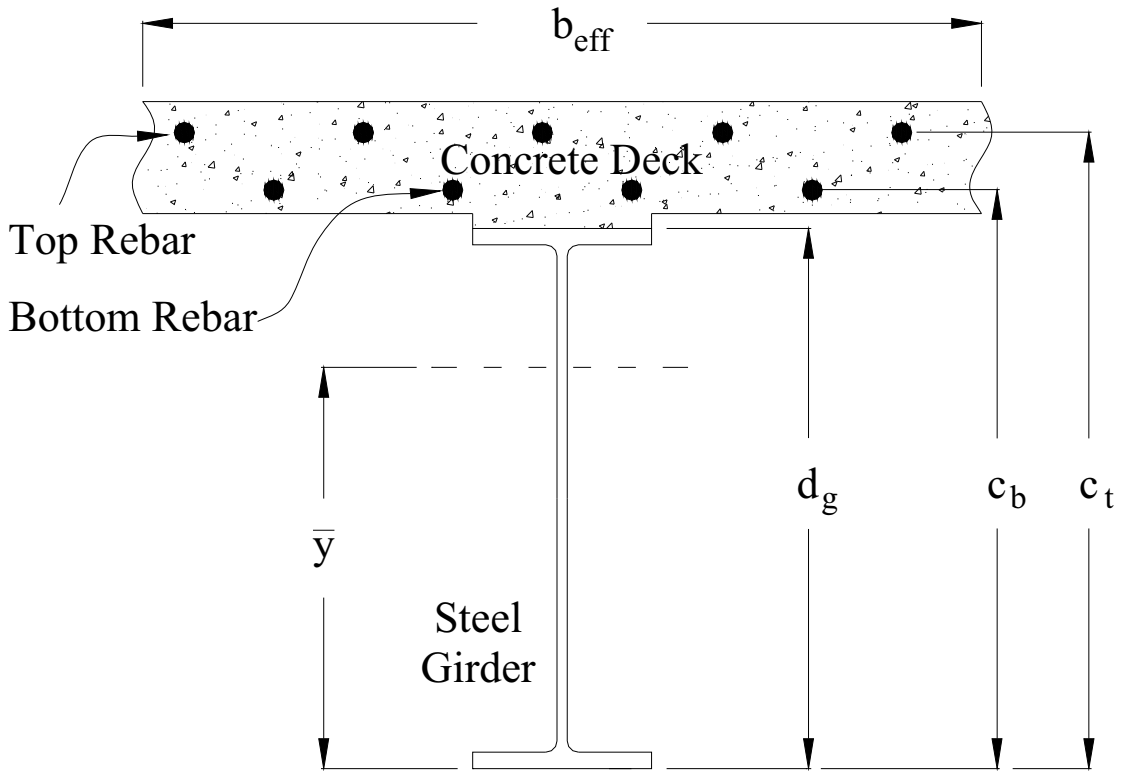


Figure D.5: Cross Section of Typical Composite Section in Negative Bending

$$I_{\text{Comp}} = \left[I_g + \left(A_g \cdot \left(\bar{y} - \frac{d_g}{2} \right)^2 \right) \right] + \frac{E_s}{E_g} \cdot \left[A_{st} \cdot (\bar{y} - c_t)^2 + A_{sb} \cdot (\bar{y} - c_b)^2 \right] \quad [\text{D.31}]$$

Where:

- A_g = Area of steel girder cross section (in²)
- A_{sb} = Area of bottom layer reinforcement (in²)
- A_{st} = Area of top layer reinforcement (in²)
- C_b = Centroid of bottom layer reinforcement above lower strain gauge (in)
- C_t = Centroid of top layer reinforcement above lower strain gauge (in)
- d_g = Depth of steel girder (in)
- E_s = Modulus of elasticity of deck reinforcement (ksi)
- E_g = Modulus of elasticity of girder material (ksi)
- I_g = Moment of inertia of girder (in⁴)
- \bar{y} = Neutral Axis depth above bottom gauge (in)

D.4.2.3 Weathersfield Moment Equations

The moment at the gauge pair versus truck position is calculated using Equation [D.32]. The moment is calculated at each point of strain data where a neutral axis has been calculated as the truck moves across the bridge. Moment is calculated only where a neutral axis depth was determined by the first macro and the lower strain lower strain exceeds the input minimum value (Figure D.6).

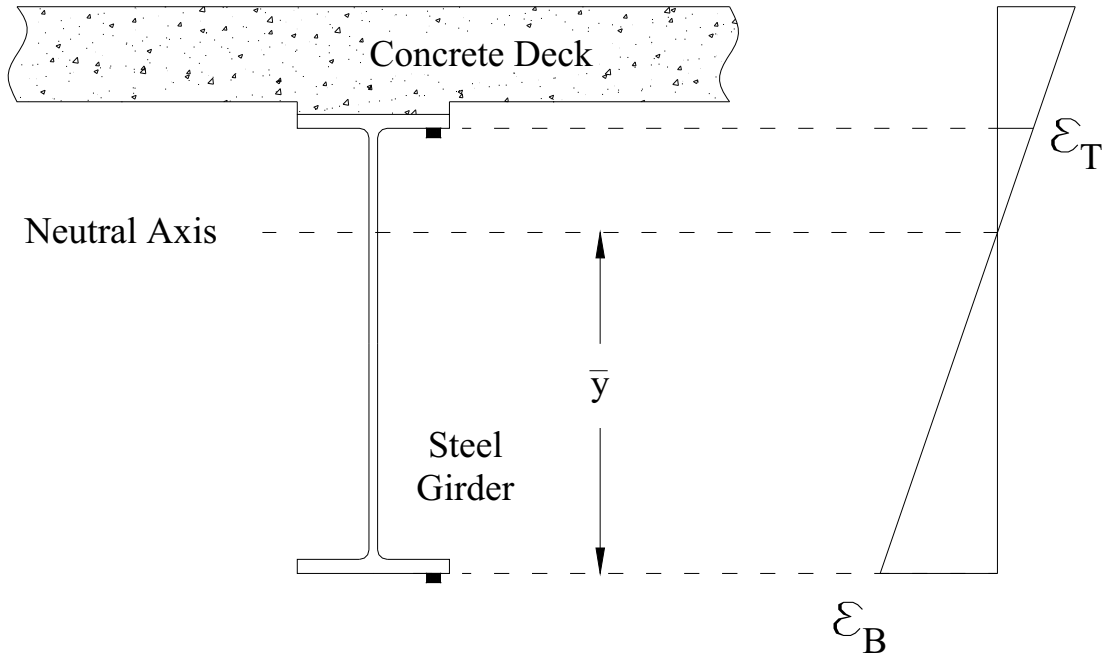


Figure D.6: Strain Profile of Weathersfield Bridge

$$M = \frac{\epsilon_B \cdot E_g \cdot I_{Comp}}{y \cdot (1.44 \times 10^8)} \quad [D.32]$$

Where:

M = Moment (k-ft)

ϵ_B = Strain in bottom gauge ($\mu\epsilon$)

ϵ_T = Strain in top gauge ($\mu\epsilon$)

I_{Comp} = Effective moment of inertia of structural section (in^4)

E_g = Modulus of elasticity of girder material (ksi)

\bar{y} = Neutral Axis Depth (ft)